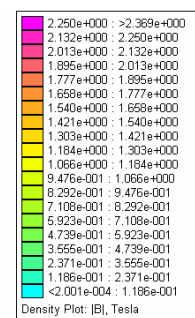
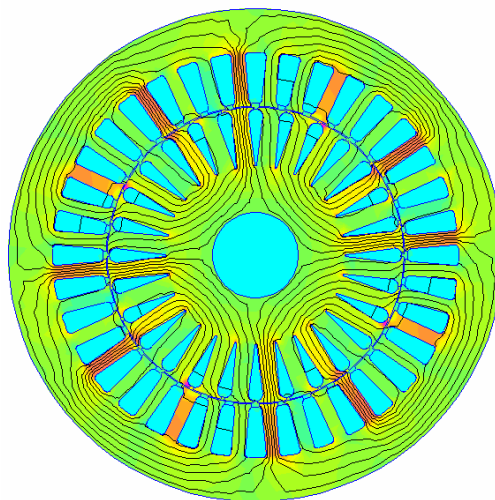
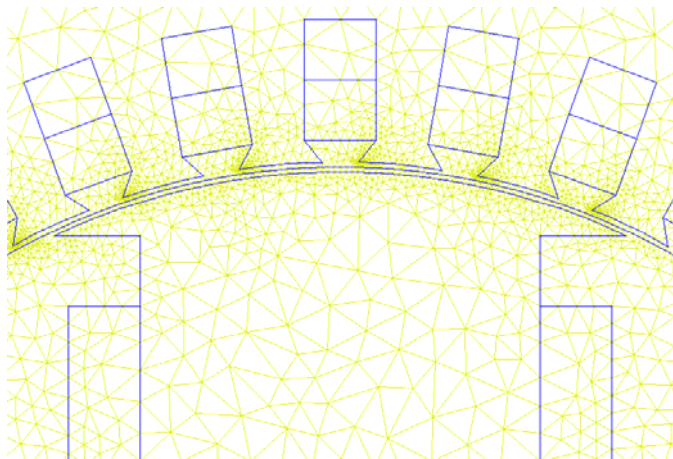
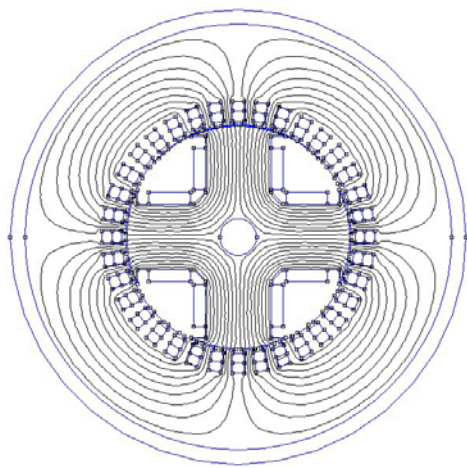
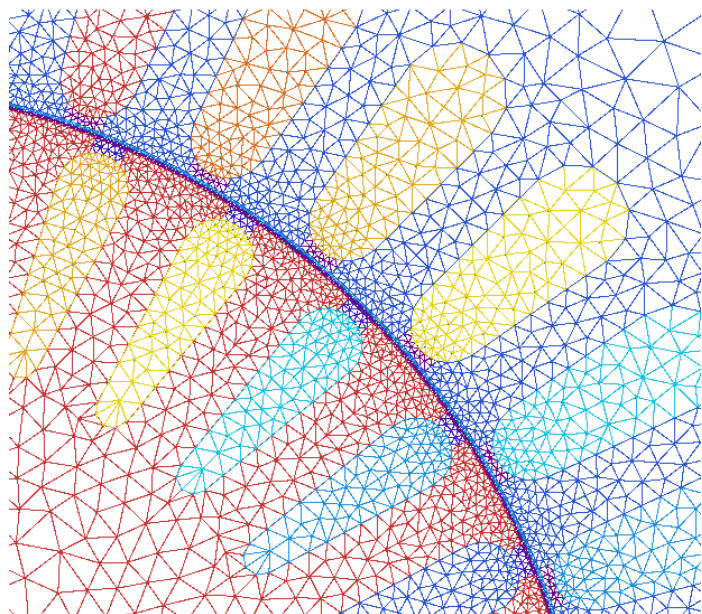
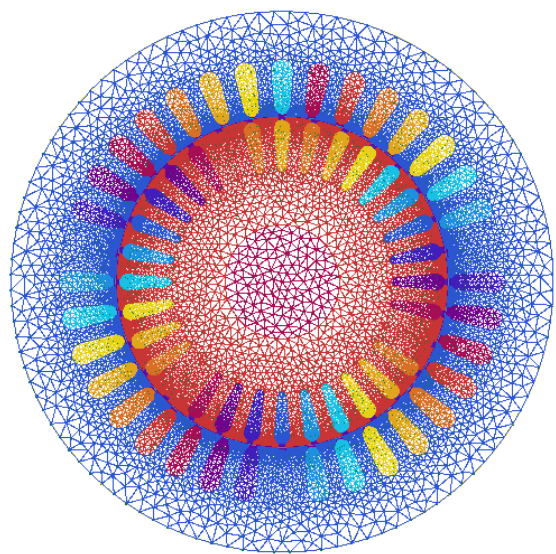
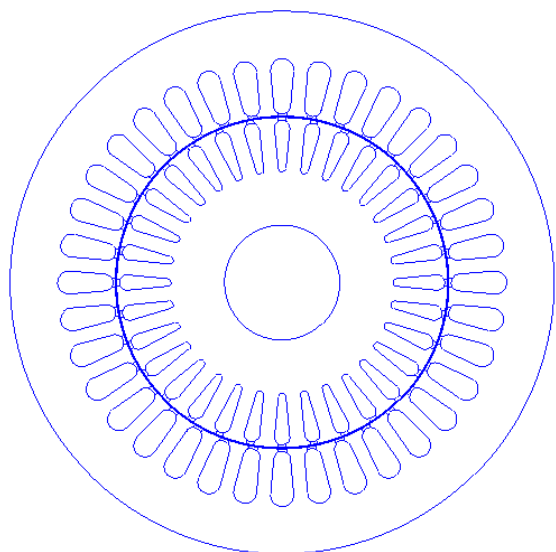




FINITE ELEMENTS FOR ELECTRICAL ENGINEERING





FINITE ELEMENTS METHODS FOR ELECTRICAL ENGINEERING

AIMS

- To put into practice the FE method to analyse and design electrical machines and apparatus.
- To put into practice the 2D formulation.
- To train in some commercial software programs for modelling and analysis of any electric and magnetic element or machine.

ASSESSMENT

- Numerical resolution of some applications is presented. If possible, compare numerical results with analytical or experimental results.

SPECIALIZATION: Drives and electrical machines.

PROGRAM

OVERVIEW

History of FEM & FEA
FEM and FEA at the EUETIB
Application Areas
What's the difference between FEM & FEA ??
Electromagnetics & Related Analyses

INTRODUCTION

Maxwell equations
Constitutive relations
Electrostatic, Magnetostatic and Magnetodynamic Fields
Thermal problems
Boundary conditions
Reduction of a 3D problem to a 2D problem
Materials properties. Linear and Non-linear models
Permanent magnets (PM) modelling.

ANALYTICAL SOLUTION

Some important theorems
Analytical resolution. Separation of variables.
Electric machines modelling
Permanent Magnets
Some examples

NUMERICAL SOLUTION. FUNDAMENTALS AND BASIC METHODS

General concepts
Classification of electromagnetic (EM) problems
Finite Differences
Monte Carlo's method
Approximation techniques

FINITE ELEMENT METHOD**ONE DIMENSIONAL FINITE ELEMENT ANALYSIS**

Discretization and interpolation
Formulation
Assembly of the equations
Boundary conditions

TWO DIMENSIONAL FINITE ELEMENT ANALYSIS

Domain discretization
Interpolation
Variational formulation
Assembly to form the system of equations
Incorporation of the boundary conditions of the third kind
Imposition of the Dirichlet boundary condition
Nonlinear problems
Permanent magnets (PM) modelling

TRANSIENT SOLUTION.

Voltage fed electromagnetic devices
Coupling of field and electrical circuit equations.
Thick conductors. Thin conductors.
Equations for the whole domain.

MOVEMENT MODELLING FOR ELECTRICAL MACHINES**INTEGRAL EQUATION METHOD**

Connection between differential and integral equations
The Moment Method
Boundary Element Method
Comparison of the FE and BE Methods

COMPUTATION OF OTHER QUANTITIES.

Post-processing. Basic quantities. Derived quantities.
Energy Stored in the Magnetic Field. Linked Flux. Inductance
Back emf
Resistance. Joule losses power.
Capacitance.
Eddy current losses
Force and Torque. Maxwell Stresses. Virtual Work method.
Core Losses

GENERAL ARCHITECTURE OF CAD SYSTEM BASED ON THE FINITE ELEMENT METHOD

The data entry module
The solver
The postprocessor
Examples(2D): FEMM, MAXWELL_SV.

APPLICATIONS (2D)

Solved applications.
Applications to solve.

Basic Bibliography

- M.V.K. Chari, S.J. Salon. Numerical methods in electromagnetism. Ed. Academic Press. 2000.
- J.P.A. Bastos, N. Sadowsky. Electromagnetic modelling by finite element methods. Ed. Marcel-Decker. 2003.
- S.J. Salon. Finite element analysis of electrical machines. Ed. Kluwer. 1995.

Complementary Bibliography

- N. Bianchi. Electrical Machine Analysis using Finite Elements. CRC. Taylor&Francis. 2005
- G.R. Buchanan. Finite Element Analysis. Schaum's Outlines. Mc Graw-Hill. 1995.
- P.P. Silvester, R.L. Ferrari. Finite elements for electrical engineers (3rd edition). Cambridge University Press. 1996.
- K. Hameyer, R: Belmans. Numerical modelling and design of electrical machines and devices. Ed. WIT Press. 1999
- A.B.J. Reece, T.W. Preston. Finite element methods in electrical power engineering. Ed. Oxford University Press. 2000.
- M.N.O. Sadiku. Numerical techniques in electromagnetics. Ed. CRC Press.2001
- D. Poljak, C.A. Brebbia. Boundary Element Methods for Electrical Engineers. Wit Press. 2005.
- B. Nogarede. Électrodynamique Appliquée. Bases et principes physiques de l'électrotechnique. Ed. Dunod. 2005.
- Jan K. Sykulski. Computational Magnetism. Chapman&Hall. 1995.
- Les Techniques de l'Ingenieur.

Software's manuals

- D. Meeker. FEMM 4.0 user's manual.
- D. Meeker. MIRAGE 1.0 user's manual.
- Ansoft Corp. Maxwell 2D Student version.
- GRUCAD. EFCAD 6.0. Manual.

Course Organization

- This course will be developed in theory and practice sessions (indicated in the next table).
- Sessions will be held at :
 - EUETIB. 187 Urgell Street.
 - Meeting Room. 0 floor.
 - 15 to 17 h each Thursday. A detailed program is given in final table.
- This course is equivalent to 3 ECTS (1 ECTS is equivalent from 25 to 30 h of student effort). Half of this time is devoted to classes (both theory and practice). The student will devote the rest of his time to personal study, solution of set exercises and develop the final project.
- Each week I will put a documentation related to my next class on a course web page.
 - I would like you read and study this before the class.
 - Dates indicated in the syllabus are subject to change.

Note: If documentation exceeds the web page quota, I will prepare a CD-ROM with ALL of the documentation and the software necessary for this course (with extras)

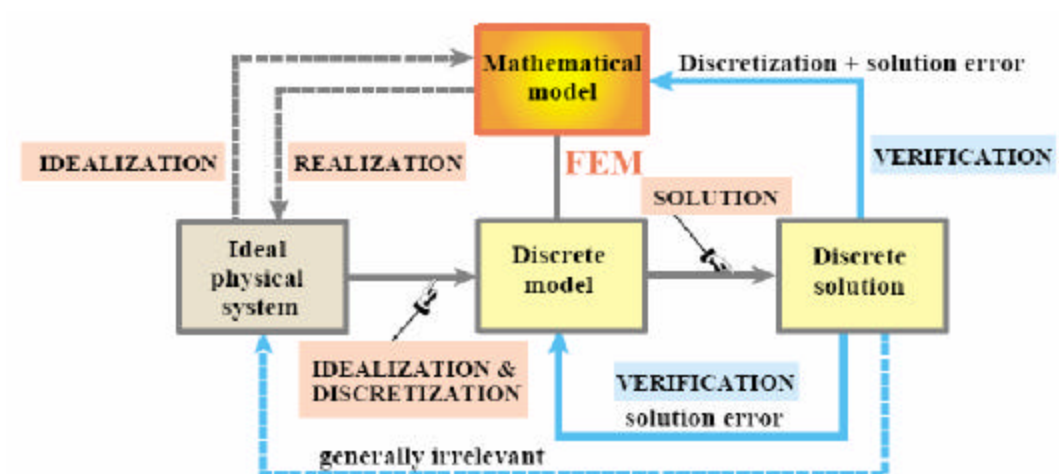
- Normal communication must be carried by e-mail. In some cases telephone or personal communication will be accepted.
- Each week I will present exercises.
 - Some exercises are solved.
 - You must solve the unsolved exercises and return these to me before the final date indicated in the documentation.
- A final project must be completed.
 - You must talk to me about this work.
 - If possible I prefer applications that are interesting for you.
 - If possible, you must obtain experimental results to compare with numerical results.
 - If possible, the project must be developed in a group to encourage the group and interdisciplinary work. Groups may include up to 1 to 3 people. Exceptions must be approved by me.
- The final project presentation must take place in a public session (attendees will be other students of this course, other professors, and, of course, me)
- Projects must contain all of the following items:
 - Problem to solve.
 - Mathematical model of the problem.
 - Drawing of the model.
 - Simplifications and symmetries.
 - Boundary conditions and sources.
 - Mesh used.
 - Graphical maps of flux, potential, etc.
 - Main numerical results obtained.
 - Comparison with analytical and/or experimental results (If possible)
 - Conclusions.
 - Electronic appendix with all of the simulation files.
- All work must be presented in electronic format such as MSWord or PDF files. Please type your work. I don't accept handwritten work or work which has been scanned.

Good luck ☺

SYLLABUS

Week	Class	Lesson
02/03/06	Theory	INTRODUCTION Maxwell equations, Electrostatics, Magnetostatics and Magnetodynamics Fields. Materials property. Boundary conditions.
09/03/06	Theory	INTRODUCTION 3D and 2D models. Linear and Non-linear models. Permanent magnets. Applications. Electric machines modelling. Other: Thermal modelling.
16/03/06	Theory	NUMERICAL SOLUTION : Introduction and basic methods. Finite differences. Montecarlo method. Approximation techniques. Weighted residual methods: point collocation, sub domain collocation, least squares, Galerkin method. Variational principles.
23/03/06	Theory	FINITE ELEMENTS METHOD I ONE DIMENSIONAL FINITE ELEMENT ANALYSIS. Discretization and interpolation. Formulation. Assembly of the equations. Boundary conditions.
30/03/06	Theory	FINITE ELEMENTS METHOD II TWO DIMENSIONAL FINITE ELEMENT ANALYSIS. Domain discretization. Interpolation. Variational formulation. Assembly to form the system of equations. Incorporation of the boundary conditions. Nonlinear problems. Permanent magnets (PM) modelling.
20/04/06	Theory	FINITE ELEMENTS METHOD III TRANSIENT SOLUTION. Voltage fed electromagnetic devices. Coupling of field and electrical circuit equations. Thick conductors. Thin conductors. Equations for the whole domain. MOVEMENT MODELLING FOR ELECTRICAL MACHINES.
27/04/06	Theory	INTEGRAL EQUATION METHOD The Moment Method. Boundary Element Method.
04/05/06	Theory	COMPUTATION OF OTHER QUANTITIES Energy. Flux. Magnetic Losses. Resistance. Inductance. Force. Torque. Other quantities.
11/05/06	Theory	GENERAL ARCHITECTURE OF CAD SYSTEM BASED ON THE FINITE ELEMENT METHOD Data entry module. Solver. Postprocessor. Examples(2D): FEMM, MIRAGE, MAXWELL_SV, EFCAD.
18/05/06	Practice	APPLICATIONS (2D) Electrostatic fields: Dielectric materials. Exercise: High Voltage isolator analysis. Stationary currents: conducting material. Exercise: computation on fuse resistance. Nominal current.
25/05/06	Practice	APPLICATIONS (2D) Magnetic fields: Electric machines. Permanent magnets. Exercise: (a) D.C. machine analysis. Armature reaction. (b) Design of field coil on a series DC motor.
01/06/06	Practice	APPLICATIONS (2D) Eddy currents. Exercise: Study to frequency variation and shape of the rotor slot in the rotoric impedance (asynchronous machine)
08/06/06	Practice	APPLICATIONS (2D) Computation of losses. Resistances. Inductances. Force. Torque. Exercise: (a) equivalent circuit of induction machine. (b) Torque calculation of induction machine. (c) Main inductance calculation on salient pole machine.
15/06/06	Practice	APPLICATIONS (2D) Transients. Exercise: Heating and Cooling of a Slot of an Electric Machine.

OVERVIEW



OVERVIEW

The field of Electrical Engineering (or Electromagnetism) can be subdivided into three major areas:

- Theoretical Electricity (Electromagnetism)
- Applied Electricity (Electromagnetism)
- Computacional Electromagnetism

Theoretical electricity deals with fundamental laws and principles of electromagnetism studied for their intrinsic scientific value. Applied electricity transfers this theoretical knowledge to scientific and engineering applications, especially as regards the construction of mathematical models of physical phenomena. Computational electromagnetism solves specific problems by simulation through numerical methods implemented on digital computers.

Paraphrasing an old joke about mathematicians, one may define a computational electrician as a person who searches for solutions to given problems, an applied electrician as a person who searches for problems that fit given solutions, and a theoretical electrician as a person who can prove the existence of problems and solutions.

Analysis and design of electrical equipment is a difficult task due to some aspects:

- Complex geometry
- Mixed set of materials involved. Some of these have non-linear characteristics.
- Mixed phenomena are present:
 - Electromagnetic field.
 - Thermal aspects
 - Mechanical aspects.
- Dynamical aspects (dependence on time. Only in a few simple cases can we find on time analytical solutions. Numerical solution is the only available method to find answers to many problems of electrical equipment design.

The first step of analysis is the selection of what aspects are considered in our case. Other aspects are neglected or ignored. This step is named **MODELING**. This aspect is the concern of the Theoretical Engineer.

Related to this modelling is the definition of the universe of analysis; for example if we need to determine the distribution of temperature in a room, we neglect the variation of the exterior temperature (this is considered a constant)

Another aspect is the level of detail in the analysis, for example:

- We can consider all of the conductors into a slot separately or together.
- We can consider a discrete distribution of currents (discrete number of slots) or a continuous approximation of this (sheet of current).
- Static or dynamic analysis (consideration or not of the time variations)
- Etc.

The second step of analysis is the selection of a numerical method to solve the problem. This process is named **DISCRETISATION** of the problem. There are some methods for this process:

- Finite Element (FEM)
- Boundary Element (BEM)
- Finite Difference (FDM)
- Moments method (MM)
- Montecarlo method (MCM)

FDM is adequate for linear problems with regular geometry and time-dependent problems. BE is used in some cases without meshing the complete geometry. The mathematical aspects of this limits its application to linear problems. MM and MCM are used only in linear cases and simple geometries. FEM is the most used method to linear and nonlinear problems without restrictions on the geometry.

This aspect is the concern of Computational Engineer.

What Does a Discretisation Look Like?

The concept of discretisation will be partly illustrated through a truly ancient problem: find the perimeter L of a circle of diameter d . Since $L = \pi d$, this is equivalent to obtaining a numerical value for π .

Draw a circle of radius r and diameter $d = 2 \cdot r$ as in next figure (a).

Then inscribe a regular polygon of n sides, where $n = 8$ in Figure (b).

Rename polygon sides as **elements** and vertices as **nodes**.

Label nodes with integers 1, . . . 8.

Extract a typical element, say that joining nodes 4–5, as shown in Figure (c). This is an instance of the **generic element $i-j$** pictured in Figure (d).

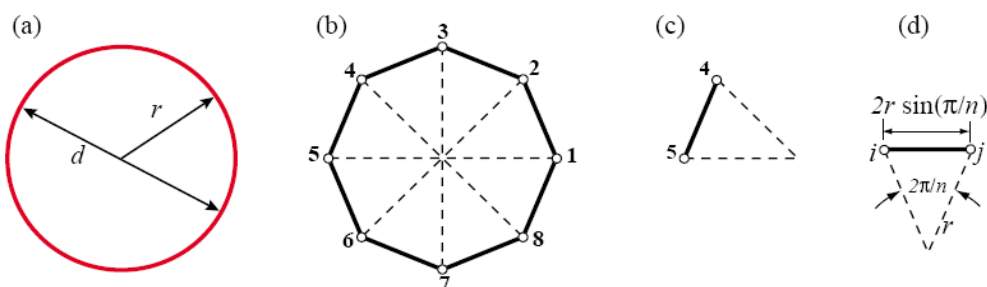
The element length is $L_{ij} = 2 \cdot r \cdot \sin(\frac{\pi}{n})$.

Since all elements have the same length, the polygon perimeter is

$$L_n = n \cdot L_{ij}$$

then the approximation to π is

$$\pi_n = \frac{L_n}{d} = n \cdot \sin(\frac{\pi}{n})$$



Values of π_n obtained for $n = 1, 2, 4, \dots, 65536$ are listed in the second column of the following table. As can be seen the convergence to π is fairly slow. The use of the power of 2 is adequate to avoid the use of sinusoidal function:

If we start with $n = 2$, considering that $\sin(\frac{\pi}{2}) = 1$, and

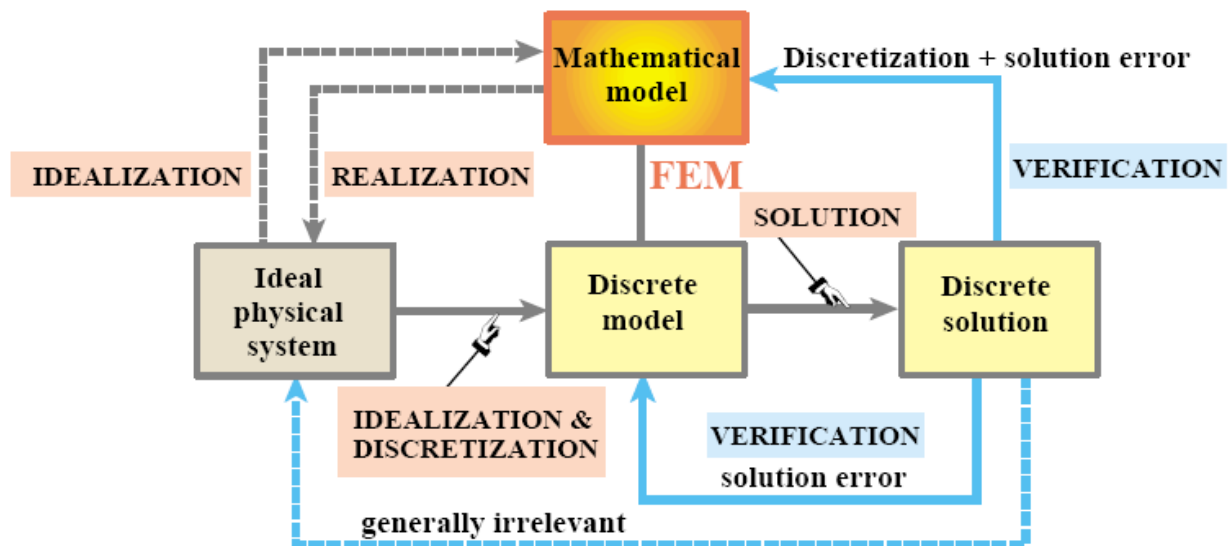
$$\sin(\alpha) = \frac{1}{\sqrt{2}} \cdot \sqrt{1 - \sqrt{1 - \sin(2 \cdot \alpha)^2}}$$

we can calculate any of the values as in the following table.

n	pi	error
2	2.0000000000	-1.141592654
4	2.8284271247	-0.313165529
8	3.0614674589	-0.080125195
16	3.1214451523	-0.020147501
32	3.1365484905	-0.005044163
64	3.1403311570	-0.001261497
128	3.1412772509	-0.000315403
256	3.1415138011	-7.88524E-05
512	3.1415729404	-1.97132E-05
1024	3.1415877253	-4.92831E-06
2048	3.1415914215	-1.23209E-06
4096	3.1415923456	-3.07979E-07
8192	3.1415925765	-7.70448E-08
16384	3.1415926335	-2.01265E-08
32768	3.1415926548	1.2178E-09
65536	3.1415926453	-8.26858E-09

Some key ideas behind the FEM (and other discretization methods) can be identified in this example. The circle, viewed as a *source mathematical object*, is replaced by polygons. These are **discrete approximations** of the circle. The sides, renamed as **elements**, are specified by their end **nodes**. Elements can be separated by disconnecting nodes, a process called **disassembly** in the FEM. Upon disassembly a **generic element** can be defined, **independently of the original circle**, by the segment that connects two nodes i and j . The relevant element property: side length L_{ij} , can be computed in the generic element independently of the others, a property called **local support** in the FEM. The target property: the polygon perimeter, is obtained by **reconnecting** n elements and adding up their length; the corresponding steps in the FEM being **assembly** and **solution**, respectively.

The third (and final) step of analysis is computation of additional results and analysis of the solution. If the results aren't the desired or wished results the analysis must be repeated.



This aspect is the concern of Applied Engineer.

History of FEM & FEA

- 1851 Schellbach avoided the differential equations by replacing them with an approximate set of algebraic equations.
- 1942 R. Courant used a piecewise continuous function defined over a triangle.
- 1956 Turner, Martin, Topp established a broader definition of numerical analysis.
- 1960 Clough used for the first time the term of Finite Element Method.
- Early 70's FEM was limited to expensive mainframe computers owned by the aeronautics, automotive, defense, nuclear industries and, in general sense, heavy industry.
- 70's FEM further enhanced by Zienkiewicz & Cheung – variational approach: Laplace and Poisson's equations. Mathematicians developed better solutions: Galerkin, Ritz emerged as optimum solutions for certain categories of general problems. Modeling and solution of non-linear problems.
- 1995 more than 3800 published papers about Finite Element Analysis.

Finite Element Analysis (FEA) was first developed in 1942 by R. Courant, who utilized the Ritz method of numerical analysis and minimization of variational calculus to obtain approximate solutions for vibration systems. Shortly thereafter, a paper published in 1956 by Turner, Clough, Martin, & Topp established a broader definition of numerical analysis. This paper centered on the "stiffness and deflection of complex structures".

By the early 70's, FEA used only on expensive mainframe computers generally owned by the aeronautics, automotive, defense, and nuclear industries, and the scope of analyses was considerably limited. Finite Element technology was further enhanced during the 70's by such people as Zeinkiewicz & Cheung, when they applied the technology to general problems described by Laplace & Poisson's equations. Mathematicians were developing better solution algorithms, the Galerkin, Ritz & Rayleigh-Ritz methods emerged as the optimum solutions for certain categories of general type problems. Later, considerable research was carried out into the modeling & solution of non-linear problems, Hinton & Crisfield being major contributors.

While considerable strides were made in the development of the finite element method, other areas did not remain static. Very powerful mesh generation algorithms have been developed. Commercial generators have the capability of meshing all but the most difficult geometry. Superior CAE concepts have also emerged, it is not unusual to have a single CAD model for producing engineering drawings, carrying out kinematic & assembly analysis, as well as being used for finite element modelling.

Due to the rapid decline in the cost of computers and the phenomenal increase in computing power, present day desktop computers are capable of producing accurate results for all kinds of parameters (standard PC's are over 10 times more powerful than the best supercomputers of the early 90's).

The finite element method now has its roots in many disciplines, the end result is a technology that is so advanced that it is almost indistinguishable from magic. The vast catalog of capability that comprises FEA, will no doubt grow considerably larger in the future. CAE is here to stay, but in order to harness its true power, the user must be familiar with many concepts, including the mechanics of the problem being modelled. All analyses require time, experience & most importantly, careful planning.

FEM and FEA at the EUETIB

- 1983. First FEM course, taught by J.C. Sabonadiere (ENSIEG, Grenoble, France)
- 1983. Some professors visited ENP de Grenoble (France). Software FLUX-2D at its earlier releases.
- 1985. Doctoral dissertation of J. Llaverías "Exact determination of earth potentials in big transformation areas". By the use of the moment's method.
- 1990. First contact with C. Lemos Antunes (Coimbra University, Portugal).
- 1990. Generalized Least Squares Method to modelization of earth structure (two-layer model)
- 1992. R. Bargallo visited the Coimbra University for trained at "CADdyMAG" software, developed by C.L. Antunes. The Electrotechnical Department bought this software.
- 1994. Electrotechnical Department organized the first course about "The FEM applied to Electrical Engineering". This course was taught by M. Bonet, R. Bargalló, J. Morón and with the collaboration of C.L. Antunes (Coimbra University)
- 1994-2000. CADdyMAG software is used in the regular courses (Design of Electrical Machines)
- 2000-2005. FEMM software is used in the regular courses (Design of Electrical Machines, Energy Systems and other)
- 2002. A. de Blas started its doctoral dissertation about hysteresis modelling and its application to the electrical machines design.

Application Areas

In essence, the finite element is a mathematical method for solving ordinary & partial differential equations. Because it is a numerical method, it has the ability to solve complex problems that can be represented in differential equation form. As these types of equations occur naturally in virtually all fields of the physical sciences, the applications of the finite element method are limitless as regards to the solution of practical design problems.

Due to the high cost of computing power of years gone by, FEA has a history of being used to solve complex & cost critical problems. Classical methods alone usually cannot provide adequate information to determine the safe working limits of a major civil engineering construction. If a tall building, a large suspension bridge or a nuclear reactor failed catastrophically, the economic & social costs would be unacceptably high.

In recent years, FEA has been used almost universally to solve structural engineering problems. One discipline that has relied heavily on the technology is the aerospace industry. Due to the extreme demands for faster, stronger, lighter & more efficient aircraft, manufacturers have to rely on the technique to stay competitive. But more importantly, due to safety, high manufacturing costs of components & the high media coverage that the industry is exposed to, aircraft companies need to ensure that none of their components fail, that is to cease providing the service that the design intended.

FEA has been used routinely in high volume production & manufacturing industries for many years, as to get a product design wrong would be detrimental. For example, if a large manufacturer had to recall one model alone due to a piston design fault, they would end up having to replace up to 10 million pistons. Similarly, if an oil platform had to shut down due to one of the major components failing (platform frame, turrets, etc..), the cost of lost revenue is far greater than the cost of fixing or replacing the components, not to mention the huge environmental & safety costs that such an incident could incur. The finite element method is a very important tool for those involved in engineering design, it is now used routinely to solve problems in the following areas:

- Structural strength design
- Structural interaction with fluid flows
- Analysis of Shock (underwater & in materials)
- Acoustics
- **Thermal analysis**
- Vibrations
- Crash simulations
- Fluid flows
- **Electrical analyses**
- Mass diffusion
- Buckling problems
- Dynamic analyses
- **Electromagnetic evaluations**
- Metal forming
- Coupled analyses

Nowadays, even the most simple of products rely on the finite element method for design evaluation. This is because contemporary design problems usually cannot be solved as accurately & cheaply using any other method that is currently available. Physical testing was the norm in years gone by, but now it is simply too expensive.

What's the difference between FEM & FEA ??

The terms '**finite element method**' & '**finite element analysis**' seem to be used interchangeably in most documentation, so the question arises is there a difference between FEM & FEA ?

The answer is yes, there is a difference, albeit a subtle one that is not really important enough to lose sleep over.

The **finite element method** is a **mathematical method for solving ordinary & elliptic partial differential equations** via a piecewise polynomial interpolation scheme. Put simply, FEM evaluates a differential equation curve by using a number of polynomial curves to follow the shape of the underlying & more complex differential equation curve.

Each polynomial in the solution can be represented by a number of points and so FEM evaluates the solution at the points only. A linear polynomial requires 2 points, while a quadratic requires 3. The points are known as node points or nodes. There are essentially three mathematical ways that FEM can evaluate the values at the nodes, there is the non-variational method (Ritz), the residual method (Galerkin) & the variational method (Rayleigh-Ritz).

The **finite element analysis** is an **implementation of FEM to solve a certain type of problem**. For example, if we were intending to solve a 2D stress problem. For the FEM mathematical solution, we would probably use the minimum potential energy principle, which is a variational solution. As part of this, we need to generate a suitable element for our analysis. We may choose a plane stress, plane strain or an axisymmetric type formulation, with linear or higher order polynomials. Using a piecewise polynomial solution to solve the underlying differential equation is FEM, while applying the specifics of element formulation is FEA, e.g. a plane strain triangular quadratic element.

Electromagnetics & Related Analyses

Many kinds of electromagnetic phenomenon can be modeled, from the propagation of microwaves to the torque in an electric motor. Analysis of electrostatic and magnetic fields passing through and around a structure provides insight into the response, and hence a means for regulating these fields to attain specific responses.

FEA can be used to analyse the linear electric or magnetic behaviour of devices. Analyses typically involve the evaluation of magnetic, electric and thermal fields. Further applications include the analysis of shape-memory materials & piezoelectric effects. An analysis can be static, harmonic or transient state in nature. Due to the complexity of the practical applications of the technique, it is not unusual to have magnetic, dielectric and thermal couplings in a single model. Such complex analyses generally make realistic modelling an arduous task.

Application Areas

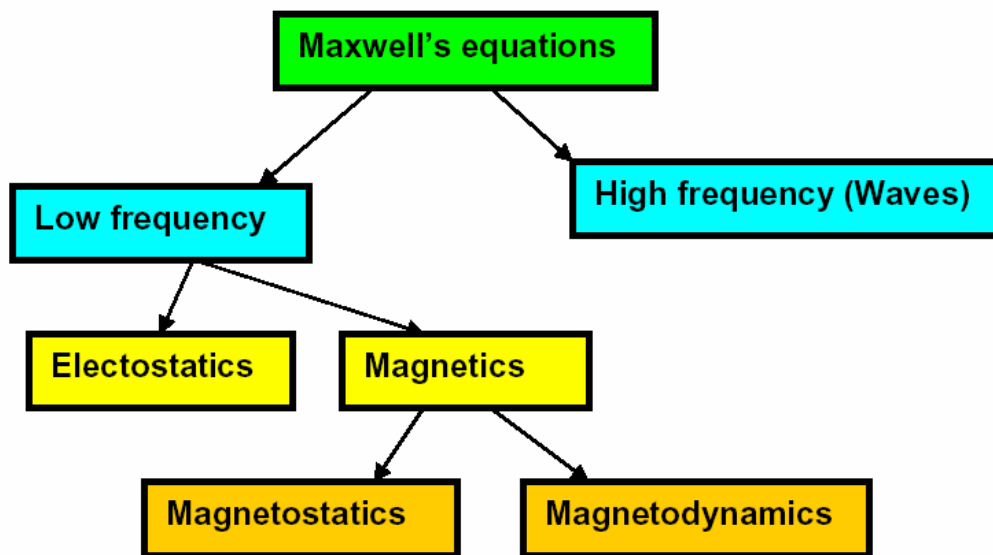
The application areas include, but are not limited to the design of:

- Rotating machines (DC motors, synchronous machines, induction motors, stepper motors, coupling devices, brushless motors, switched reluctance motors, PM motors, generators)
- Energy transfer and conversion modules (transformers, cables, high voltage devices, insulators, connectors & fuses).
- Electrical actuators (linear motors, electromagnetic brakes, contactors, magnetic bearings, fuel injectors, electromagnetic launchers).
- Sensors (capacitive and inductive, speed, eddy currents non destructive testing, magnetoscopy, resolvers, electric meters).
- Field generators (mass spectrometers, magnetic recording, polarisation fields, magnetisation devices).

Analysis Types

- **Magnetostatic Analysis.** Magnetic analysis is used to design or analyze a variety of devices such as solenoids, electric motors, magnetic shields, permanent magnets, magnetic disk drives, and so forth. Generally the quantities of interest in magnetostatic analysis are magnetic flux density, field intensity, forces, torques, inductance, and flux linkage.
- **Transient Electromagnetic Analysis.** Transient magnetics allows performing transient or steady state AC analysis designing for a variety of DC or AC devices such as electric motors, transformers, and so forth. Generally the quantities of interest in transient magnetics analysis are time functions of magnetic flux density, field intensity, external, induced and total current densities, forces, torques, inductance, and flux linkage.
- **Time-Harmonic Electromagnetic Analysis.** Time-harmonic electromagnetic analysis is used to analyze magnetic fields caused by alternating currents and, vice versa, electric currents induced by alternating magnetic fields (eddy currents). This kind of analysis is useful with different inductor devices, solenoids, electric motors, and so forth. Generally the quantities of interest in harmonic magnetic analysis are electric current (and its source and induced component), voltage, generated Joule heat, magnetic flux density, field intensity, forces, torques, impedance and inductance.
- **Electrostatic Analysis.** Electrostatic analysis is used to design or analyze a variety of capacitive systems such as fuses, transmission lines and so forth. Generally the quantities of interest in electrostatic analysis are voltages, electric fields, capacitances, and electric forces.
- **Current Flow Analysis.** Current flow analysis is used to analyze a variety of conductive systems. Generally the quantities of interest in current flow analysis are voltages, current densities, electric power losses (Joule heat).
- **Thermal Analysis.** Thermal analysis plays an important role in the design of many different mechanical and electrical systems. Generally the quantities of interest in thermal analysis are temperature distribution, thermal gradients, and heat losses. Transient analysis allows you to simulate transition of heat distribution between two heating states of a system.
- **Stress Analysis.** Stress analysis plays an important role in design of many different mechanical and electrical components. Generally the quantities of interest in stress analysis are displacements, strains and different components of stresses.

INTRODUCTION



INTRODUCTION

The operation of electrical systems designed to perform certain engineering tasks depends, at least in part, on electrical, electromechanical, or electrochemical phenomena. The electrical aspects of these applications are described by **Maxwell's equations**.

The theory of Electromagnetics (EM) took a long time to be established. It can be understood by the fact that the EM quantities can not be “seen” or “touched” (contrarily to others, such as mechanical and thermal quantities).

Actually, the majority of the EM phenomena were established by other scientists before Maxwell (1831 – 1879):

- Ampere (1775 -1836)
- Gauss (1777 -1855)
- Faraday (1791 – 1867)
- Lenz (1804 – 1865)

among others (Coulomb, Lorentz, Laplace).

Maxwell, introducing an additional term (in 1862) to Ampere's law, could synthesize the EM in **four** equations. The physical possibility of this group of equations (along with **constitutive relations**) is so high that very different phenomena (e.g. microwaves and permanent magnet fields) can be **precisely** described by it. Additionally, these equations survived the formulation of relativity and were instrumental in shaping it; thus they also survived the introduction of quantum theory!

While the formalism and the basic concepts of the EM are *relatively simple*, realistic problems can be very complicated and difficult to solve. Some examples of these complications are:

- Complicated geometry.
- Materials non-linearity.
- Non-static field sources.

It is impossible to find analytical solutions for many problems and that is the main reason why numerical methods have become widely used tools in Electrical Engineering today.

Maxwell equations

Faraday introduced a new concept in which he envisioned the space between interacting charges to be filled with **fields**. From Faraday's point of view, electric and magnetic fields are defined at a point **r** even when there is no charge present there. The fields are defined in terms of the force that would be exerted on a test charge **q** if it were introduced at **r** moving at a speed **v** at the time of interest. The force is summarized in terms of the **electric field intensity E** and **magnetic flux density B** by the **Lorentz force law**:

$$f = q \cdot (E + v \times B)$$

Gauss's law

Gauss's law describes how the electric field intensity is related to its source. The net charge within an arbitrary volume **V** that is enclosed by a surface **S** is related to the net electric flux through that surface by

$$\oint_S \epsilon \cdot E \cdot dS = \iiint_V \rho \cdot dV \Rightarrow D = \epsilon \cdot E$$

$$\oint_S D \cdot dS = \iiint_V \rho \cdot dV$$

D is the electric displacement flux density and ρ is the charge density. If different materials are present, Gauss's integral law requires that

$$n \cdot (\epsilon_a \cdot E_a - \epsilon_b \cdot E_b) = \sigma_s$$

in the interface of different materials. σ_s is the surface charge density and **n** denotes the normal component of **E**.

Ampere's integral law

The law relating the magnetic field intensity **H** to its source, the current density **J**, is:

$$\oint_C H \cdot dl = \iint_S J \cdot dS + \frac{d}{dt} \iint_S D \cdot dS$$

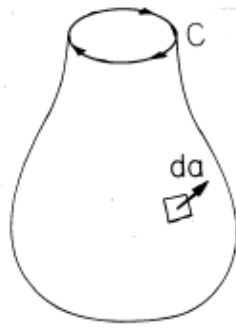
A surface current density in a surface **S** causes a discontinuity of the magnetic field intensity. Ampere's law requires that

$$n \cdot (H_a - H_b) = K$$

in the interface of a surface. **K** is the surface current density and **n** denotes the normal component of **H**.

Charge conservation law

Embedded in the laws of Gauss and Ampere is a relationship between the charge and current densities. Apply Ampere's law to a closed surface, If the contour C is regarded as the "drawstring" and S as the "bag," then this limit is one in which the "string" is drawn tight so that the contour shrinks to zero. thus the contour integral vanishes:



$$\oint_C \mathbf{H} \cdot d\mathbf{l} = 0 = \iint_S \mathbf{J} \cdot d\mathbf{S} + \frac{d}{dt} \iint_S \mathbf{D} \cdot d\mathbf{S}$$

After, the surface integral of the electric displacement can be replaced by the total charge enclosed:

$$\iint_S \mathbf{J} \cdot d\mathbf{S} + \frac{d}{dt} \iiint_V \rho \cdot dV = 0$$

This is the law of charge conservation. This equation shows that the net current out of the volume requires that the net charge enclosed be decreasing with time. The continuity condition associated with charge conservation is

$$\nabla \cdot (\mathbf{J}_a - \mathbf{J}_b) + \frac{d\sigma_s}{dt} = 0$$

Implicit in this condition is the assumption that J is finite. Thus, the condition does not include the possibility of a surface current.

Faraday's integral law.

The laws of Gauss and Ampere relate **fields to sources**. The statement of charge conservation implied by these two laws relates these sources. New integral laws are introduced that do not involve the charge and current densities.

Faraday's integral law states that the circulation of E around a contour C is determined by the time rate of change of the magnetic flux linking the surface enclosed by that contour:

$$\oint_C E \cdot dl = -\frac{d}{dt} \iint_S B \cdot dS$$

The continuity condition associated with Faraday's law is

$$n \cdot (E_a - E_b) = 0$$

Gauss's integral law of magnetic flux

The net magnetic flux out of any region enclosed by a surface S must be zero:

$$\oiint_S B \cdot dS = 0$$

The continuity condition associated with Gauss's integral law of magnetic flux is:

$$n \cdot (B_a - B_b) = 0$$

SUMMARY OF MAXWELL'S INTEGRAL LAWS

Name	Integral law
Gauss's law	$\oiint_S \varepsilon \cdot E \cdot dS = \iiint_V \rho \cdot dV \Rightarrow D = \varepsilon \cdot E$ $\oiint_S D \cdot dS = \iiint_V \rho \cdot dV$
Ampere's law	$\oint_C H \cdot dl = \iint_S J \cdot dS + \frac{d}{dt} \iint_S D \cdot dS$
Faraday's law	$\oint_C E \cdot dl = -\frac{d}{dt} \iint_S B \cdot dS$
Magnetic flux continuity	$\oiint_S B \cdot dS = 0$
Charge conservation	$\iint_S J \cdot dS + \frac{d}{dt} \iiint_V \rho \cdot dV = 0$

SUMMARY OF CONTINUITY CONDITIONS

	Name	Continuity condition
1	Gauss's law	$n \cdot (\varepsilon_a \cdot E_a - \varepsilon_b \cdot E_b) = \sigma_s$
2	Ampere's law	$n \cdot (H_a - H_b) = K$
3	Faraday's law	$n \cdot (E_a - E_b) = 0$
4	Magnetic flux continuity	$n \cdot (B_a - B_b) = 0$
5	Charge conservation	$n \cdot (J_a - J_b) + \frac{d\sigma_s}{dt} = 0$

Divergence theorem

The divergence of a vector A is defined in terms of the limit of a surface integral:

$$\operatorname{div} A = \lim_{\Delta V \rightarrow 0} \frac{1}{\Delta V} \cdot \oiint_S A \cdot dS$$

In Cartesian coordinates, the divergence operator is

$$\operatorname{div} A = \frac{\partial A_x}{\partial x} + \frac{\partial A_y}{\partial y} + \frac{\partial A_z}{\partial z}$$

This results suggests an alternative notation. The delta operator is defined as:

$$\nabla \equiv i \frac{\partial}{\partial x} + j \frac{\partial}{\partial y} + k \frac{\partial}{\partial z}$$

where i , j and k are unitary vectors. So that $\operatorname{div} A$ can be written as (dot product)

$$\operatorname{div} A = \nabla \cdot A$$

The following table shows the divergence operator in some common coordinate systems.

Cartesian coordinates	$\frac{\partial A_x}{\partial x} + \frac{\partial A_y}{\partial y} + \frac{\partial A_z}{\partial z}$
Cylindrical coordinates	$\frac{1}{r} \cdot \frac{\partial(r \cdot A_r)}{\partial r} + \frac{1}{r} \cdot \frac{\partial A_\phi}{\partial \phi} + \frac{\partial A_z}{\partial z}$
Spherical coordinates	$\frac{1}{r^2} \cdot \frac{\partial(r^2 \cdot A_r)}{\partial r} + \frac{1}{r \cdot \sin(\theta)} \cdot \frac{\partial(A_\theta \cdot \sin(\theta))}{\partial \theta} + \frac{1}{r \cdot \sin(\theta)} \cdot \frac{\partial A_\phi}{\partial \phi}$

Divergence theorem shows meaning to replace the integration over the volume to integration around the contour:

$$\oiint_S A \cdot dS = \iiint_V \nabla \cdot A \cdot dV$$

The div notation suggests that this combination of derivatives describes the outflow of A from the neighbourhood of the point of evaluation.

Curl operator

The curl of a vector A is defined in terms of the limit of a contour integral:

$$\text{curl} A = \lim_{\Delta S \rightarrow 0} \frac{1}{\Delta S} \cdot \oint_C A \cdot dl$$

In Cartesian coordinates, the curl operator is

$$\text{curl} A = \left(\frac{\partial A_z}{\partial y} - \frac{\partial A_y}{\partial z} \right) \cdot i + \left(\frac{\partial A_x}{\partial z} - \frac{\partial A_z}{\partial x} \right) \cdot j + \left(\frac{\partial A_y}{\partial x} - \frac{\partial A_x}{\partial y} \right) \cdot k$$

So that $\text{curl} A$ can be written as (vector product)

$$\text{curl} A = \nabla \times A$$

Thus in Cartesian coordinates:

$$\nabla \times A = \begin{vmatrix} i & j & k \\ \frac{\partial}{\partial x} & \frac{\partial}{\partial y} & \frac{\partial}{\partial z} \\ A_x & A_y & A_z \end{vmatrix}$$

The following table shows the curl operator in some common coordinate systems.

Cartesian coordinates	$\left(\frac{\partial A_z}{\partial y} - \frac{\partial A_y}{\partial z} \right) \cdot i + \left(\frac{\partial A_x}{\partial z} - \frac{\partial A_z}{\partial x} \right) \cdot j + \left(\frac{\partial A_y}{\partial x} - \frac{\partial A_x}{\partial y} \right) \cdot k$
Cylindrical coordinates	$\left(\frac{1}{r} \cdot \frac{\partial A_z}{\partial \phi} - \frac{\partial A_\phi}{\partial z} \right) \cdot a_r + \left(\frac{\partial A_r}{\partial z} - \frac{\partial A_z}{\partial r} \right) \cdot a_\phi + \frac{1}{r} \cdot \left(\frac{\partial(r \cdot A_\phi)}{\partial r} - \frac{\partial A_r}{\partial \phi} \right) \cdot a_z$
Spherical coordinates	$\frac{1}{r \cdot \sin(\theta)} \cdot \left(\frac{\partial(A_\phi \cdot \sin(\theta))}{\partial \phi} \theta - \frac{\partial A_\phi}{\partial \phi} \right) \cdot a_r + \frac{1}{r} \cdot \left(\frac{1}{\sin(\theta)} \cdot \frac{\partial A_r}{\partial \phi} - \frac{\partial(r \cdot A_\phi)}{\partial r} \right) \cdot a_\theta + \frac{1}{r} \cdot \left(\frac{\partial(r \cdot A_\theta)}{\partial r} - \frac{\partial A_r}{\partial \theta} \right) \cdot a_\phi$

Stokes's (curl) theorem shows meaning to replace the integration over the surface to integration around the contour:

$$\oint_C A \cdot dl = \iint_S \nabla \times A \cdot dS$$

A non-zero curl implies that the corresponding vector field has a rotational property. One way to look for a curl is to imagine that the vector field corresponds to the flow of water. If we place a small paddle wheel in the field then the presence of a non-zero curl suggests that the wheel will rotate.

If A has no divergence, a field is said to be **solenoidal**. If it has no curl, it is **irrotational**.

Gradient operator

Differential of a scalar function A is

$$dA = \frac{\partial A}{\partial x} \cdot dx + \frac{\partial A}{\partial y} \cdot dy + \frac{\partial A}{\partial z} \cdot dz$$

In vector notation this can be showed how:

$$dA = \left(i \frac{\partial A}{\partial x} + j \frac{\partial A}{\partial y} + k \frac{\partial A}{\partial z} \right) \cdot (i \cdot dx + j \cdot dy + k \cdot dz)$$

The gradient of a scalar function A is defined as (in Cartesian coordinates)

$$\text{grad}A = \nabla A = \left(i \frac{\partial A}{\partial x} + j \frac{\partial A}{\partial y} + k \frac{\partial A}{\partial z} \right)$$

gradA is a vector, perpendicular to a surface on which A is constant and pointing in the direction of increasing A. We also note that gradA points to the direction of maximum change in A.

Applying the above theorems (Stokes and divergence) we can obtain the **differential forms of Maxwell's equations**:

Gauss's law

$$\left. \begin{aligned} \oint_S \varepsilon \cdot E \cdot dS &= \iiint_V \rho \cdot dV \\ \oint_S \varepsilon \cdot E \cdot dS &= \iiint_V \nabla \cdot (\varepsilon \cdot E) \cdot dV \end{aligned} \right\} \iiint_V \nabla \cdot (\varepsilon \cdot E) \cdot dV = \iiint_V \rho \cdot dV \Rightarrow \nabla \cdot (\varepsilon \cdot E) = \rho$$

Ampere's law

$$\left. \begin{aligned} \oint_C H \cdot dl &= \iint_S J \cdot dS + \frac{d}{dt} \iint_S D \cdot dS \\ \oint_C H \cdot dl &= \iint_S \nabla \times H \cdot dS \end{aligned} \right\}$$

$$\iint_S \nabla \times H \cdot dS = \iint_S J \cdot dS + \frac{d}{dt} \iint_S D \cdot dS \Rightarrow \nabla \times H = J + \frac{dD}{dt}$$

Faraday's law

$$\left. \begin{aligned} \oint_C E \cdot dl &= -\frac{d}{dt} \iint_S B \cdot dS \\ \oint_C E \cdot dl &= \iint_S \nabla \times E \cdot dS \end{aligned} \right\} \iint_S \nabla \times E \cdot dS = -\frac{d}{dt} \iint_S B \cdot dS \Rightarrow \nabla \times E = -\frac{dB}{dt}$$

Magnetic flux continuity

$$\left. \begin{aligned} \oint_S B \cdot dS &= 0 \\ \oint_S B \cdot dS &= \iiint_V \nabla \cdot (B) \cdot dV \end{aligned} \right\} \iiint_V \nabla \cdot (B) \cdot dV = 0 \Rightarrow \nabla \cdot B = 0$$

Charge conservation

$$\left. \begin{aligned} \oint_S J \cdot dS + \frac{d}{dt} \iiint_V \rho \cdot dV &= 0 \\ \oint_S J \cdot dS &= \iiint_V \nabla \cdot (J) \cdot dV \end{aligned} \right\}$$

$$\iiint_V \nabla \cdot (J) \cdot dV + \frac{d}{dt} \iiint_V \rho \cdot dV = 0 \Rightarrow \nabla \cdot (J) + \frac{d\rho}{dt} = 0$$

SUMMARY OF MAXWELL'S DIFFERENTIAL LAWS

	Name	Integral law
1	Gauss's law	$\nabla \cdot (\varepsilon \cdot E) = \rho$
2	Ampere's law	$\nabla \times H = J + \frac{dD}{dt}$
3	Faraday's law	$\nabla \times E = -\frac{dB}{dt}$
4	Magnetic flux continuity	$\nabla \cdot B = 0$
5	Charge conservation	$\nabla \cdot (J) + \frac{d\rho}{dt} = 0$

Differential forms are better than integral forms. Integrals forms are dependents on volume and the surface of integration. Differential forms are independent of these.

Constitutive relations

The field vectors D and E and also B and H are related by the properties of the materials at any point in the field region. These are often referred to as the **constitutive properties** of the material and are given by:

(a)	$D = \varepsilon \cdot E$
(b)	$B = \mu \cdot H$
(c)	$J = \sigma \cdot E$

ε is the permittivity of the material, μ is the magnetic permeability of the material and σ is the conductivity of the material. In some cases these values can be indicated in relative form:

$$\varepsilon = \varepsilon_0 \cdot \varepsilon_r$$

$$\mu = \mu_0 \cdot \mu_r$$

ε_0 , μ_0 are the values for free space and ε_r , μ_r are the relative values of the material.

Equations (1) to (4) and relations (a) to (c) are the well known Maxwell's equations.

With the addition of the **continuity conditions** we can solve any electromagnetic problem.

Maxwell's equations do not make a distinction between low and high frequency applications, but for practical applications it is possible to adapt them to these two situations.

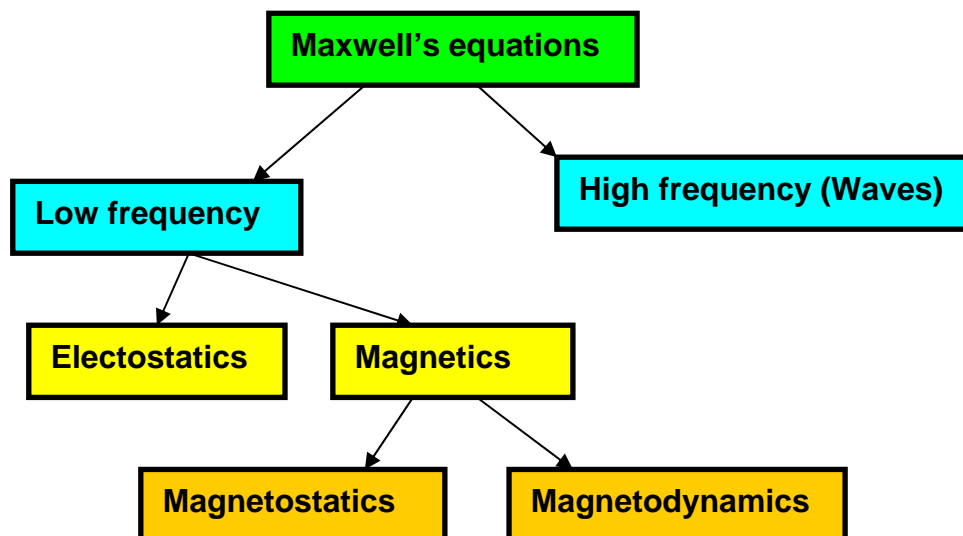
We will be interested in **low-frequency** phenomena. When describing low frequency problems the Maxwell's equations can be divided into two groups:

- **Electrostatics and**
- **Magnetostatics.**

And, an important point:

These can be treated independently!

The following pages will be devoted to this approach.



Second order operators. Laplace operator.

It is possible to combine two vector operators on scalar functions and vector functions. One of these is the Laplace operator (called in short, the Laplacian), this is the div of grad of a scalar function U:

$$\operatorname{div}(\operatorname{grad}(U)) = \nabla^2 U = \left(i \frac{\partial}{\partial x} + j \frac{\partial}{\partial y} + k \frac{\partial}{\partial z} \right) \cdot \operatorname{grad}(U)$$

Following table shows the Laplace operator in some common coordinate systems.

Cartesian coordinates	$\frac{\partial^2 U}{\partial x^2} + \frac{\partial^2 U}{\partial y^2} + \frac{\partial^2 U}{\partial z^2}$
Cylindrical coordinates	$\frac{1}{r} \cdot \frac{\partial}{\partial r} \left(r \cdot \frac{\partial U}{\partial r} \right) + \frac{1}{r^2} \cdot \frac{\partial^2 U}{\partial \phi^2} + \frac{\partial^2 U}{\partial z^2}$
Spherical coordinates	$\frac{1}{r^2} \cdot \frac{\partial}{\partial r} \left(r^2 \cdot \frac{\partial U}{\partial r} \right) + \frac{1}{r^2 \cdot \sin(\theta)} \cdot \frac{\partial}{\partial \theta} \left(\sin(\theta) \cdot \frac{\partial U}{\partial \theta} \right) + \frac{1}{r^2 \cdot \sin^2(\theta)} \cdot \frac{\partial^2 U}{\partial \phi^2}$

If A is a vector function, we can demonstrate that:

$$\nabla^2 A = \operatorname{grad}(\operatorname{div}(A)) - \operatorname{curl}(\operatorname{curl}(A))$$

where $\nabla^2 A$ is called the “vector Laplacian” of A. This is written as (in Cartesian coordinates)

$$\nabla^2 A = i \cdot \nabla^2 A_x + j \cdot \nabla^2 A_y + k \cdot \nabla^2 A_z$$

where, for example, the component in the Ox direction is:

$$\nabla^2 A_x = \frac{\partial^2 A_x}{\partial x^2} + \frac{\partial^2 A_x}{\partial y^2} + \frac{\partial^2 A_x}{\partial z^2}$$

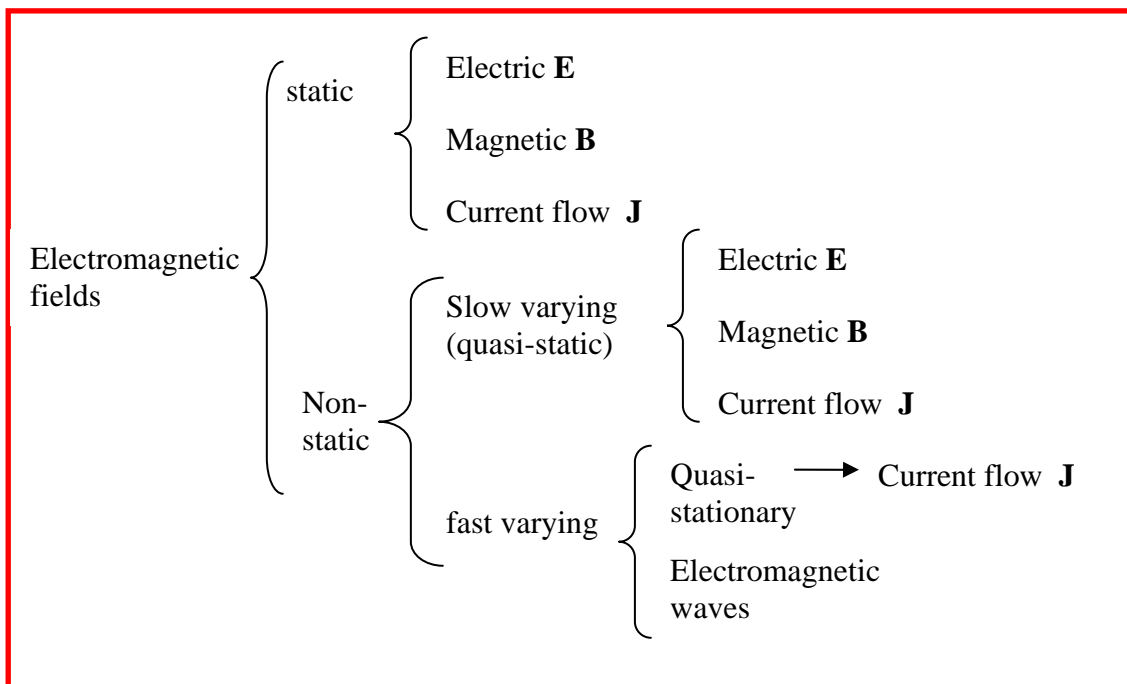
Electrostatic, Magnetostatic and Magnetodynamic Fields

In general, there are two classes of electromagnetic fields can be described:

- The time independent static and
- Time varying fields.

They can be scalar and vector fields. A typical scalar field for example is the electrostatic potential distribution $V(x,y,z)$ between charged electrodes; and the magnetic field intensity $H(x,y,z)$ surrounding a current carrying conductor is a typical vector field.

We have to distinguish between the slow and fast varying electrical current flow field with regard to the geometrical dimensions of the current carrying conductor.



The **slow varying fields** are understood to be fields not leading to current redistributions. This means that there are no **eddy current effects** as the dimensions of the current carrying conductor are smaller than the penetration depth of the field. The currents at those frequencies are distributed as in the DC case, uniformly over the whole surface of the conductor. Eddy current effects are considered in the fields with fast varying time dependence, due to the low frequency being treated as quasi-stationary. High frequency fields, as focussed on antenna problems and leading to the electromagnetic waves, are not considered in this course.

Most of the physical issues in energy engineering can be described by **quasi-static phenomena**. Slowly varying and periodic fields up to 10 kHz are considered to be quasi-stationary. Electrical energy devices such as motors, actuators, induction furnaces and high voltage transmission lines are operated at low frequency.

Typical examples of quasi-static fields are the fields excited by coils in rotating electrical machines and transformers. Inside these conductors the displacement current is negligible and the magnetic field H outside the coil is exclusively excited by the free current density J . For those quasi-static fields, Ampere's law is applicable:

$$\nabla \times H = J$$

Deciding whether the displacement current can be neglected or not, depends on the wavelength λ of the problem considered in the frequency domain. If it is large compared to the physical dimensions of the problem L , the displacement current is negligible.

In general if

$$\lambda \approx (5 \dots 10)L$$

the field problem can be considered as quasi-static. For this class of problem, the interesting fields vary slowly and can be periodic. So, three categories of problems are distinguished:

- Static
- Slowly varying transient
- Time-harmonic eddy current

In time-harmonic problems sinusoidal varying field quantities is assumed. In theory, a time-harmonic solution is only valid for linear systems as a sinusoidal excitation does not yield a single frequency response in the non-linear case.

Electrostatic fields

The two fundamental laws governing these electrostatic fields are Gauss's law and Faraday's law, and the constitutive relation between D and E

Gauss's law	$\nabla \cdot (D) = \rho$	1
Faraday's law	$\nabla \times E = 0$	2
Constitutive relation	$D = \varepsilon \cdot E$	3

In terms of the **electric (scalar) potential V** , E is expressed as

$$E = -\nabla V$$

or

$$V = -\int E \cdot dl$$

Combining 1, 3 and the above relation, gives **Poisson's equation**:

$$\nabla \cdot \varepsilon \nabla V = -\rho$$

or, if ε is constant:

$$\nabla^2 V = -\frac{\rho}{\varepsilon}$$

When $\rho = 0$, this equation becomes **Laplace's equation**:

$$\nabla^2 V = 0$$

Laplace's equation of the Electric field for conductive media

Here we use the charge conservation equation (4) and constitutive relation (5). This is usually referred to as point form of **Ohm's law**.

Charge conservation	$\nabla \cdot (J) = 0$	4
Constitutive relation	$J = \sigma \cdot E$	5

Although this expression comes from an equation linked to magnetic cases, it deals with electrostatic fields and that is the reason why it is presented here.

Using the constitutive relation (5) and $E = -\nabla V$ we have

$$\nabla \cdot J = \nabla \cdot \sigma (-\nabla V) = 0$$

or, if σ is constant:

$$\nabla^2 V = 0$$

which is Laplace's equation.

Magnetostatic fields

The basic laws of magnetostatic fields are Ampere's law, and the law of conservation of magnetic flux

Ampere's law	$\nabla \times H = J$	6
Magnetic flux continuity	$\nabla \cdot B = 0$	7
Constitutive relation	$B = \mu \cdot H$	8

In terms of the **magnetic (vector) potential A**

$$B = \nabla \times A$$

Applying the vector identity

$$\nabla \times \nabla \times F = \nabla(\nabla \cdot F) - \nabla^2 F$$

to the equations (6) and 8, substituting $B = \nabla \times A$, and assuming **Coulomb gauge condition** ($\nabla \cdot A = 0$) leads to **Poisson's equation** for magnetostatic fields:

$$\nabla^2 A = -\mu \cdot J$$

When $J=0$, this equation becomes **Laplace's equation**:

$$\nabla^2 A = 0$$

The electric vector potential

In analogy to the magnetic vector potential A , we can define the **electric vector potential** T which is related to the current density J by

$$J = \nabla \times T$$

assuming E to be time independent, $\nabla \times E = 0$ and, with $E = J/\sigma$, we now have:

$$\nabla \times \left(\frac{1}{\sigma} \cdot \nabla \times T \right) = 0$$

Comparing this with the formulation presented in the previous paragraph the following equivalent relationships can be written:

A	T
B	J
H	E
$B = \mu \cdot H$	$J = \sigma \cdot E$

Laplace's equation for this problem is similar to $\nabla^2 A = 0$:

$$\nabla^2 T = 0$$

Magnetodynamic fields (low frequency quasi-stationary fields)

The basic laws of magnetodynamic fields are Ampere's law, **without consideration of time variation of electric displacement flux density D** ($\partial D / \partial t \approx 0$), Faraday's law, Magnetic flux continuity and the constitutive relations.

Ampere's law	$\nabla \times H = J$	1
Faraday's law	$\nabla \times E = -\frac{dB}{dt}$	2
Magnetic flux continuity	$\nabla \cdot B = 0$	3
	$B = \mu \cdot H$	4
	$J = \sigma \cdot E$	5

In terms of the **magnetic (vector) potential A**

$$B = \nabla \times A$$

and substituting in Faraday's law, we can obtain:

$$\nabla \times E = -\frac{dB}{dt} = -\frac{\partial}{\partial t} \nabla \times A$$

Now employing Ohm's law to calculate the eddy currents J_e yields:

$$J_e = \sigma \cdot E = -\sigma \cdot \frac{\partial A}{\partial t}$$

Ampere's law can now be rewritten, yielding the A-formulation for the **quasi-stationary magnetic field in the time domain**:

$$\nabla \times \left(\frac{1}{\mu} \cdot \nabla \times A \right) + \sigma \cdot \frac{\partial A}{\partial t} = J$$

Substituting again

$$\nabla \times \nabla \times A = \nabla(\nabla \cdot A) - \nabla^2 A$$

and assuming the Coulomb gauge condition ($\nabla \cdot A = 0$) leads to

$$\nabla^2 A - \mu \cdot \sigma \cdot \frac{\partial A}{\partial t} = -\mu \cdot J$$

Assuming sinusoidal excitation currents with an angular frequency ω and thus substituting

$$\frac{\partial A}{\partial t} = j \cdot \omega \cdot A$$

yields the A-formulation in the frequency domain to solve **eddy current problems**:

$$\nabla^2 A - j \cdot \omega \cdot \mu \cdot \sigma \cdot A = -\mu \cdot J$$

We can develop other equations to B, E, H, and J, in similar way. The following table shows these equations.

$\nabla^2 H - \mu \cdot \sigma \cdot \frac{\partial H}{\partial t} = 0$
$\nabla^2 B - \mu \cdot \sigma \cdot \frac{\partial B}{\partial t} = 0$
$\nabla^2 E - \mu \cdot \sigma \cdot \frac{\partial E}{\partial t} = 0$
$\nabla^2 J - \mu \cdot \sigma \cdot \frac{\partial J}{\partial t} = 0$

These equations are named as **diffusion equations**.

Magnetodynamic fields (waves)

The basic law of magnetodynamic fields are Ampere's law, Faraday's law, Gauss's law and the constitutive relations.

Ampere's law	$\nabla \times H = J + \frac{dD}{dt}$	1
Faraday's law	$\nabla \times E = -\frac{dB}{dt}$	2
Gauss's law	$\nabla \cdot (D) = \rho$	3
	$D = \varepsilon \cdot E$	4
	$B = \mu \cdot H$	5
	$J = \sigma \cdot E$	6

$$\nu = \frac{1}{\mu}$$

Substituting in Ampere's law with use of potential vector A: $B = \nabla \times A$

$$\nabla \wedge H = \nu(\nabla \wedge \nabla \wedge A) = J + \varepsilon \frac{\partial E}{\partial t}$$

$$\nabla \wedge \nabla \wedge A = \mu J + \mu \varepsilon \frac{\partial E}{\partial t}$$

$$\nabla \cdot (\nabla \cdot A) - \nabla^2 A = \mu J + \mu \varepsilon \frac{\partial E}{\partial t} = \mu J - \mu \varepsilon \nabla \frac{\partial V}{\partial t} - \mu \varepsilon \frac{\partial^2 A}{\partial t^2}$$

and assuming the Lorentz condition

$$\nabla \cdot A = -\mu \varepsilon \frac{\partial V}{\partial t}$$

leads to

$$-\mu \varepsilon \nabla \frac{\partial V}{\partial t} - \nabla^2 A = \mu J - \mu \varepsilon \nabla \frac{\partial V}{\partial t} - \mu \varepsilon \frac{\partial^2 A}{\partial t^2}$$

$$\nabla^2 A - \mu \varepsilon \frac{\partial^2 A}{\partial t^2} = -\mu J$$

for slow varying fields $\frac{\partial D}{\partial t} \approx 0$, and we obtain:

$$\nabla \wedge H = J$$

$$\nabla^2 A = -\mu J$$

Poisson's equation for magnetostatic fields!

Using a scalar potential V defined as:

$$\nabla V = -E - \frac{\partial A}{\partial t}$$

And substituting in Gauss equation gives:

$$\nabla \cdot E = \frac{\rho}{\varepsilon} = -\nabla^2 V - \frac{\partial(\nabla \cdot A)}{\partial t}$$

using Lorentz condition once results in:

$$\nabla^2 V - \mu \cdot \varepsilon \cdot \frac{\partial^2 V}{\partial t^2} = -\frac{\rho}{\varepsilon}$$

These two equations are named **non-homogeneous wave equations**. The following table shows these. These two equations with the addition of Lorentz conditions are equivalent to the four Maxwell equations. These equations are valid anywhere.

MAXWELL EQUATIONS AS A FUNCTION OF POTENTIAL

$\nabla^2 A - \mu\epsilon \frac{\partial^2 A}{\partial t^2} = -\mu J$
$\nabla^2 V - \mu \cdot \epsilon \cdot \frac{\partial^2 V}{\partial t^2} = -\frac{\rho}{\epsilon}$
$\nabla \cdot A = -\mu\epsilon \frac{\partial V}{\partial t}$

The applications of these equations not will be considered in this course.

Thermal problems

Heating is a very frequent phenomenon on electromagnetic devices and, in many situations, the evaluation of temperature is necessary to avoid over-heating in structures. In our area, there are different sources of heat such as, Joule effects by eddy and conducting currents, magnetic hysteresis and also mechanical friction.

Now, we will present briefly some topics on heat transmission, but for more detailed presentation, specialized references may be consulted.

There are three different ways of that heat is transmitted:

- Conduction
- Radiation
- Convection

Thermal conduction

Conduction is a process where the heat is transmitted inside a body or between different bodies having physical contact. The basic equation describing thermal conduction is (**Fourier's equation**)

$$c \cdot \frac{\partial T}{\partial t} + \nabla \cdot (-\lambda \cdot \nabla T) = Q$$

where:

- c is the thermal capability ($J/(m^3 \cdot ^\circ C)$)
- λ is the thermal conductivity ($W/(m \cdot ^\circ C)$)

- T is the temperature ($^{\circ}\text{C}$)
- Q is the thermal source volumetric density (W / m^3)

If λ is independent of the temperature or position, the above equation can be rewritten as:

$$\nabla^2 T - \frac{c}{\lambda} \cdot \frac{\partial T}{\partial t} = -\frac{Q}{\lambda}$$

This equation is similar to

$$\nabla^2 A - \mu \cdot \sigma \cdot \frac{\partial A}{\partial t} = -\mu \cdot J$$

and can be solved in similar way.

For instance, Q can be defined as the Joule's effect source by:

$$Q = \frac{J^2}{\sigma}$$

where J is the current density (for both, eddy or conducting currents, depending on the studied case)

Convection transmission

Convection occurs when a fluid has contact with a heated solid body. There will be a constant movement where the heated particles will be replaced by cooler ones. The main effect, heat is transmitted from the body to the fluid by the following equation (**Newton's equation**):

$$\lambda \cdot \frac{dT}{ds} \cdot \vec{n} = -h \cdot (T - T_a)$$

where

- h is the coefficient of heat transfer by convention ($\text{W} / (\text{m}^2 \cdot ^{\circ}\text{C})$)
- λ is the thermal conductivity ($\text{W} / (\text{m} \cdot ^{\circ}\text{C})$)
- T is the temperature at the heated wall ($^{\circ}\text{C}$)
- T_a is the temperature of the fluid at a point far from the wall ($^{\circ}\text{C}$)

The quantity h depends on the fluid properties, velocity and geometry. In practical applications, h is difficult to evaluate and it is normally determined experimentally.

Radiation

As seen before, normally for convection and conduction, at least two materials must be present in the system. This is not the case for radiation. A body emits electromagnetic waves. This radiation can reach another body. Part of these waves will be reflected and part will be absorbed by this second body. This last portion will be transformed into thermal energy.

A body at temperature T radiates energy to another at temperature T_a , involving it, according to the following expression

$$\lambda \cdot \frac{dT}{ds} \cdot \vec{n} = \varepsilon \cdot \gamma \cdot (T^4 - T_a^4)$$

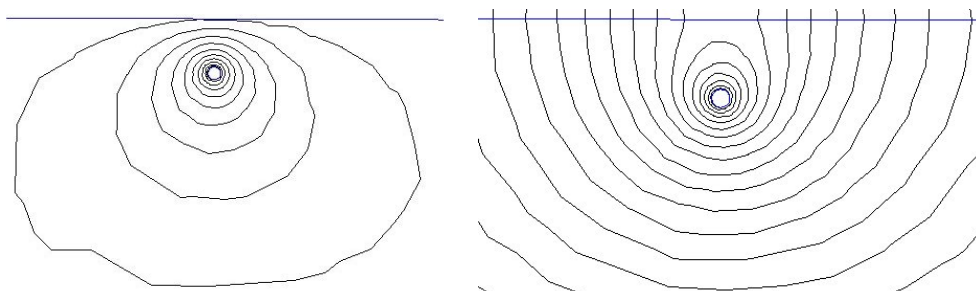
where

- γ is the Stefan-Boltzmann constant
- ε is the emittivity of the body

This class of heat transmission is sometimes not considered.

Boundary conditions

Our problem consists of finding the unknown function Φ of a PDE. In addition to the fact that Φ satisfies equation $L\Phi = g$ within a prescribed solution region R , must satisfy certain conditions on S , the boundary of R . The choice of the boundary conditions not only influences the final solution, but can further reduce the analysis domain.



Different field solutions with different boundary conditions.

Left: Dirichlet boundary condition

Right: Neumann boundary condition

The boundary conditions that can be imposed form three main groups:

- Dirichlet condition: this condition is assigning by fixing a determined value of the potential on a given boundary curve. In this way, this curve is characterised by a constant value of the potential, then the equipotential

lines result tangential to such a boundary. In other words, no line crosses that boundary.

The Dirichlet condition can be expressed as

$$\Phi(r) = f(r) \quad r \text{ on } S.$$

If $f(r) = 0$ this condition is named **homogeneous condition**; if $f(r) \neq 0$ is known as **inhomogeneous condition**.

- Neumann condition: this condition is assigned by fixing the normal derivative of the potential on a given boundary curve. In other words, the lines cross the boundary in a known way.

The Neumann condition can be expressed as

$$\frac{\partial \Phi(r)}{\partial n} = g(r) \quad r \text{ on } S$$

If $g(r) = 0$ this condition is named **homogeneous condition**; if $g(r) \neq 0$ is known as **inhomogeneous condition**.

- Mixed boundary condition

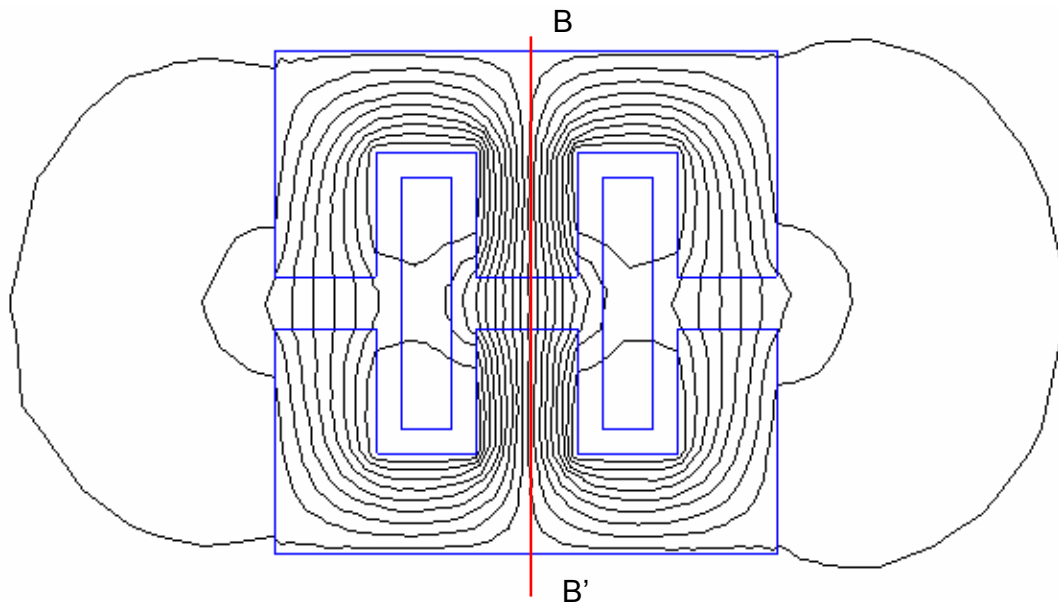
$$\frac{\partial \Phi(r)}{\partial n} + h(r) \cdot \Phi(r) = w(r) \quad r \text{ on } S$$

where $h(r)$ and $w(r)$ are explicit known functions on the boundary S .

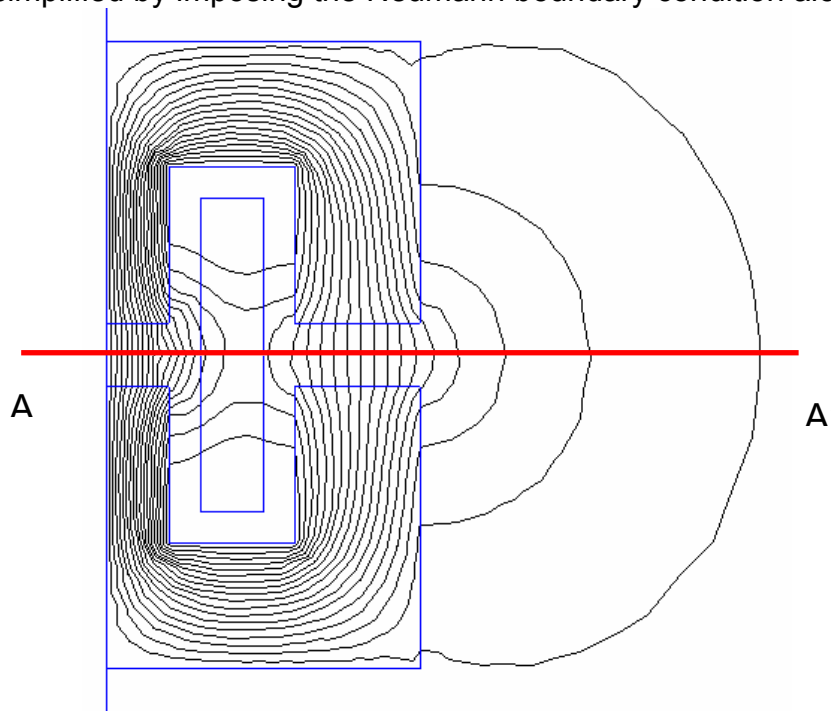
Reduction of the analysis domain by means of assignment of suitable Dirichlet and Neumann boundary conditions.

These boundary conditions are particularly useful in structures characterised by one or more symmetry axes. The analysis is accomplished only on a part of the total structure, imposing the Dirichlet or the Neumann conditions on the symmetry axis itself.

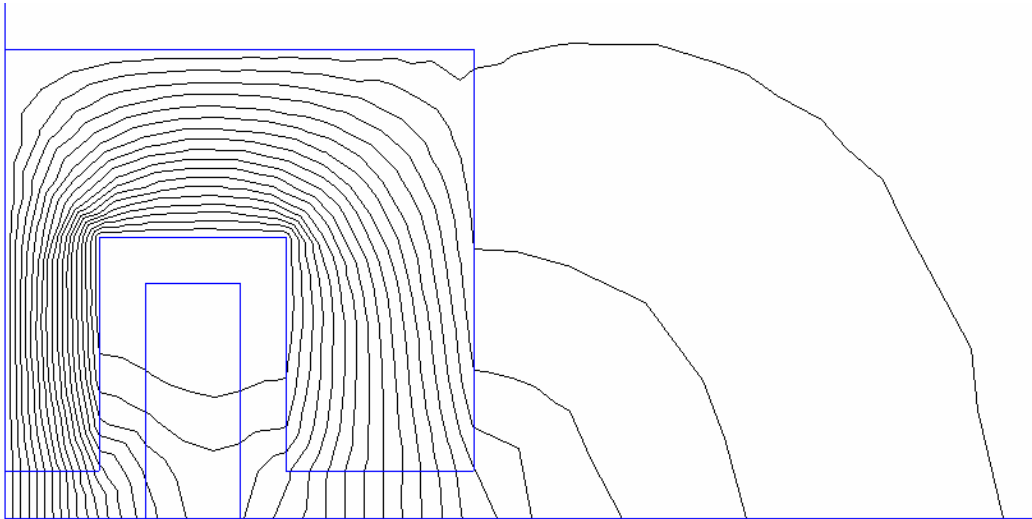
Consider, for example, the three column single-phase reactance. The flux density vectors are tangent to the axis BB' . The structure can be simplified by imposing the Dirichlet boundary condition along the BB' line.



Also, the flux density vectors are normals to the axis AA' . The structure can also be simplified by imposing the Neumann boundary condition along the AA' line.



Here we have reduced the complete structure to $\frac{1}{4}$ of its size. The study on the reduced structure will be simpler and faster.



Reduction of the domain by means of the periodic conditions

In multi-pole rotating machines the field analysis can be reduced to an even number of poles by employing **periodic boundary conditions**. Let p be the number of pole pairs and using the polar coordinates, the periodic boundary conditions are:

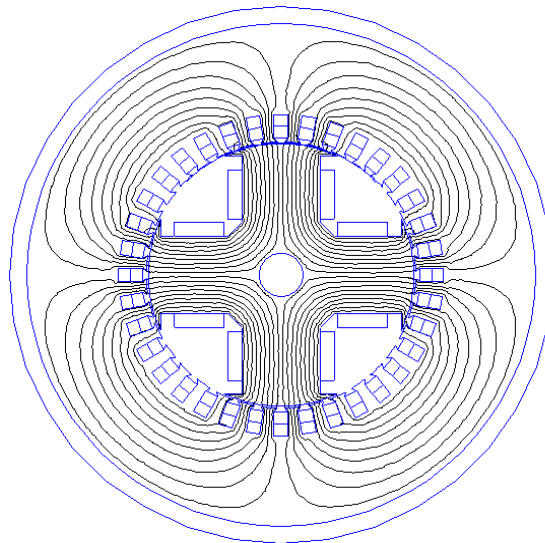
$$A(r, \theta) = A\left(r, \theta + 2 \cdot k \cdot \frac{\pi}{p}\right)$$

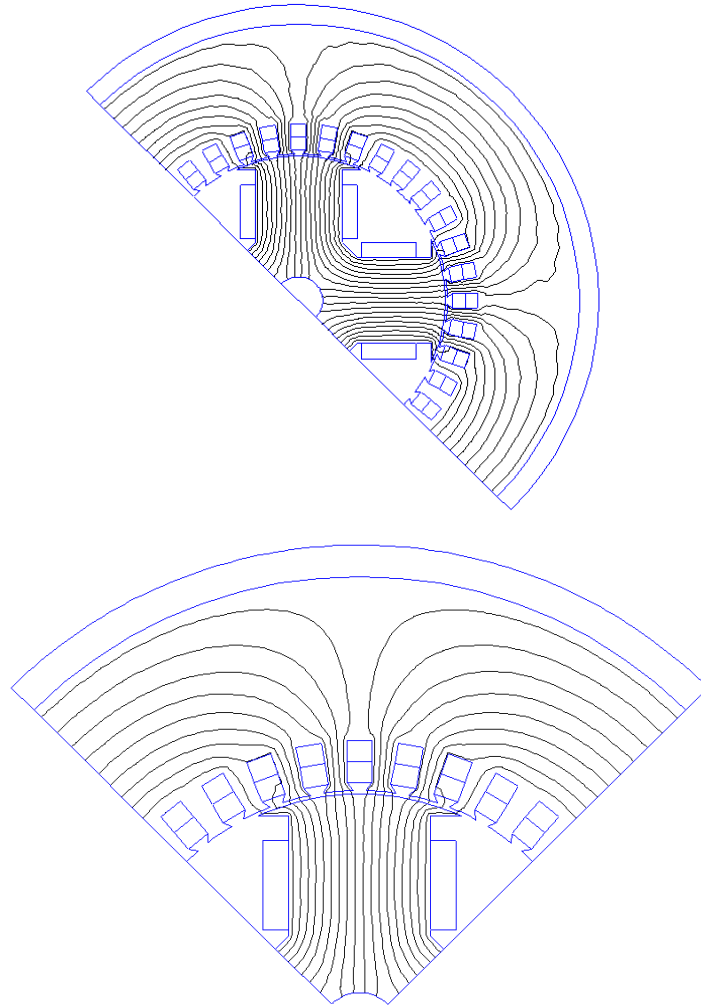
$$k = 1, 2, 3, \dots$$

The analysis can be reduced to an odd number of poles by employing **anti-periodic boundary conditions**:

$$A(r, \theta) = -A\left(r, \theta + (2 \cdot k - 1) \cdot \frac{\pi}{p}\right)$$

$$k = 1, 2, 3, \dots$$





If the symmetry or periodicity boundaries are individuated, the study of a complex structure is reduced to a study only one of its parts. This yields the double advantage:

- The reduction of the domain to be analysed, with the resultant reduction of calculation time.
- The possibility of a more accurate analysis of the remaining part.

Open Boundary Problems

Typically, finite element methods are best suited to problems with well-defined, closed solution regions. However, a large number of problems that one might like to address have no natural outer boundary. A prime example is a solenoid in air. The boundary condition that one would *like* to apply is $A = 0$ at $r = \infty$. However, finite element methods, by nature, imply a finite domain. Fortunately, there are methods that can be applied to get solutions that closely approximate the “open boundary” solution using finite element methods.

Truncation of Outer Boundaries

The simplest, but least accurate, way to proceed is to pick an arbitrary boundary “far enough” away from the area of interest and declare either $A = 0$ or $\partial A/\partial n = 0$ on this boundary. A rule of thumb is that the distance from the center of the problem to the outer boundary should be at least five times the distance from the center to the outside of the objects of interest. Truncation is the method employed by most magnetic finite element programs, because it requires no additional effort to implement. The down side to truncation is that to get an accurate solution in the region of interest, a volume of air much larger than the region of interest must also be modeled. Usually, this large region exterior to the area of interest can be modeled with a relatively coarse mesh to keep solution times to a minimum. However, some extra time and space is still required to solve for a region in which one has little interest.

Asymptotic Boundary Conditions

The simple way to approximate an “open” boundary (other than truncation) is to use asymptotic boundary conditions. The result is that by carefully specifying the parameters for the “mixed” boundary condition, and then applying this boundary condition to a circular outer boundary, the unbounded solution can be closely approximated. Consider a 2-D planar problem in polar coordinates. The domain is a circular shell of radius r_o in an unbounded region. As $r \rightarrow \infty$, vector potential A goes to zero. On the surface of the circle, the vector is a prescribed function of θ . This problem has an analytical solution, which is:

$$A(r, \theta) = \sum_{m=1}^{\infty} \frac{a_m}{r^m} \cdot \cos(m \cdot \theta + \alpha_m)$$

where the a_m and α_m parameters are chosen so that the solution matches the prescribed potential on the surface of the circle.

One could think of this solution as describing the solution exterior to a finite element problem with a circular outer boundary. The solution is described inside the circle via a finite element solution. The trick is to knit together the analytical solution outside the circle to the finite element solution inside the circle.

From inspection, one can see that the higher-numbered harmonic, the faster the magnitude of the harmonic decays with respect to increasing r . After only a short distance, the higher numbered harmonics decay to the extent that almost all of the open-space solution is described by only the leading harmonic. If n is the number of the leading harmonic, the open-field solution for large, but not infinite, r is closely described by:

$$A(r, \theta) \approx \frac{a_n}{r^n} \cdot \cos(n \cdot \theta + \alpha_n)$$

Differentiating with respect to r yields:

$$\frac{\partial A}{\partial r} = -m \cdot \frac{a_m}{r^{m+1}} \cdot \cos(m \cdot \theta + \alpha_m)$$

If the above equation is solved for a_m and substituted into the complete solution, the result is:

$$\frac{\partial A}{\partial r} + \frac{m}{r} \cdot A = 0$$

Now, this equation is a very useful result. This is the same form as the mixed boundary condition. If the outer edge of the solution domain is circular, and the outer finite element boundary is somewhat removed from the area of primary interest, the open domain solution can be closely approximated by applying the above equation to the circular boundary.

Some care must be used in applying this boundary condition. Most of the time, it is sufficient to take $n = 1$ (i.e the objects in the solution region look like a dipole when viewed from a large distance). However, there are other cases (e.g. a 4-pole Halbach permanent magnet array) in which the leading harmonic is something other than $n = 1$. You need to use your insight into your specific problem to pick the appropriate n for the leading harmonic. You also must put the objects of interest roughly in the center of the circular finite element domain to minimize the magnitude of higher-order field components at the outer boundary.

Although the application of this boundary condition requires some thought on the part of the user, the results can be quite good. The following figure represents the field produced by an air-cored coil in free space. The asymptotic boundary condition has been applied to the circular outer boundary. Inspecting the solution, flux lines appear to cross the circular boundary as if the solution domain were truly unbounded.

To apply the Asymptotic Boundary Condition, define a new, mixed-type boundary condition.

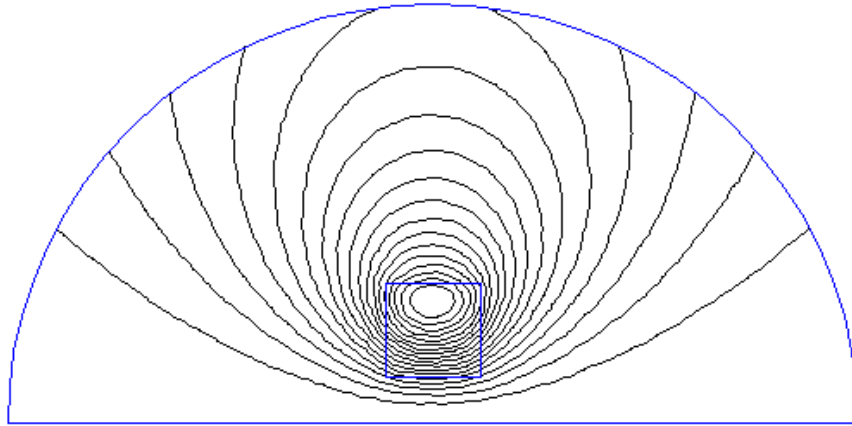
$$\frac{\partial \Phi(r)}{\partial n} + h(r) \cdot \Phi(r) = w(r) \quad r \text{ on } S$$

Then, pick the parameters so that:

$$h(r) = \frac{n}{\mu_0 \cdot r_0} \quad \text{or} \quad \frac{\varepsilon_0 \cdot n}{r_0}$$

$$w(r) = 0$$

where r_0 is the outer radius of the region in meters (regardless of the working length units).



Kelvin Transformation

A particularly good approach to “open boundary” problems is the Kelvin Transformation, a technique first discussed in the context of computational magnetics. The strengths of this technique are:

- the effects of the exterior region are, in theory, exactly modeled by this approach;
- a sparse matrix representation of the problem is retained (unlike FEM-BEM methods, which give the same “exact solution” but densely couples together the boundary nodes).
- requires no “special” features in the finite element solver to implement the technique, other than the ability to apply periodic boundary conditions.

Derivation

In the “far field” region, the material is typically homogeneous (*e.g. air* and free of sources) In this case, the differential equation that describes vector potential A is the Laplace equation:

$$\nabla^2 A = 0$$

If we write the above equation in polar notation, A is described by (2D analysis):

$$\frac{1}{r} \cdot \frac{\partial}{\partial r} \left(r \cdot \frac{\partial A}{\partial r} \right) + \frac{1}{r^2} \cdot \frac{\partial^2 A}{\partial \phi^2} = 0$$

Assume that the “near field” region of the problem can be contained in a circle of radius r_0 centred at the origin. The far-field region is then everything outside the circle. One approach to unbounded problems is to attempt to map the unbounded region onto a bounded region, wherein problems can more easily be solved. Specifically, we desire a way to transform the unbounded region outside the circle into a bounded region. One simple way to make such a mapping is to define another variable, R , that is related to r by:

$$R = \frac{r_0^2}{r}$$

By inspecting the above transformation it can be seen that this relationship maps the exterior region onto a circle of radius r_0 .

The next step is to transform the differential equation that the field must satisfy, into the mapped space. That is, the Laplace equation must be written in terms of R and θ rather than r and θ . We can evaluate derivatives in terms of R instead of r by employing the chain rule:

$$\frac{\partial}{\partial r} = \frac{\partial r}{\partial R} \left(\frac{\partial}{\partial r} \right) = - \frac{\partial}{\partial R} \left(\frac{R}{r_0} \right)$$

Now, we can note that at $r = R = r_0$,

$$\frac{\partial A}{\partial r} = - \frac{\partial A}{\partial R}$$

and after some algebraic manipulation we must obtain:

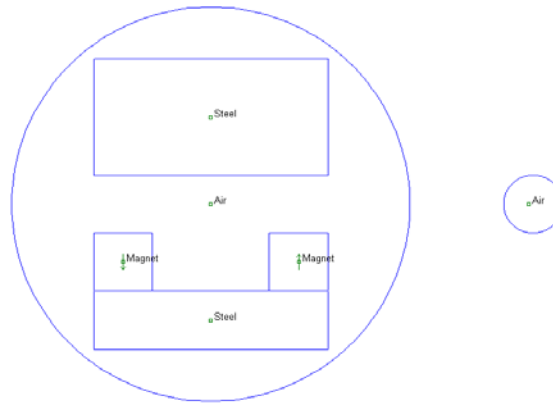
$$\frac{1}{R} \cdot \frac{\partial}{\partial R} \left(R \cdot \frac{\partial A}{\partial R} \right) + \frac{1}{R^2} \cdot \frac{\partial^2 A}{\partial \phi^2} = 0$$

The transformed equation for the outer region, has exactly the same form as that for the inner region, only in terms of R rather than r . The implication is that for the 2-D planar problem, the exterior can be modelled simply by creating a problem domain consisting of two circular regions:

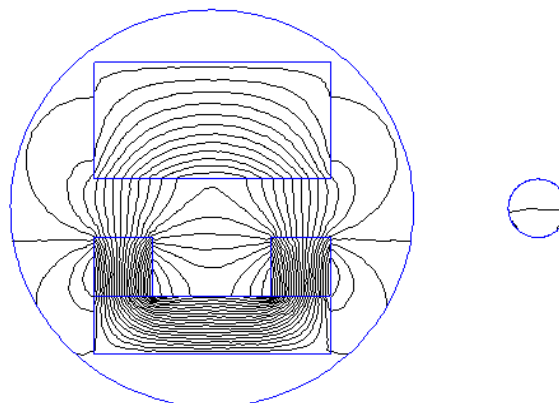
- one circular region containing the items of interest, and an additional circular region to represent the “far field.” Then, periodic boundary conditions must be applied to corresponding edges of the circle to enforce the continuity of A at the edges of the two regions. They is the continuity of A at the boundary between the exterior and interior regions.
- The second circular region exactly models the infinite space solution, but does it on a bounded domain—one could always back out the field for any point in space by applying the inverse of $R = \frac{r_0^2}{r}$.

As an example, consider an E-core lamination stack with a winding around it. Suppose that the objective is to determine the field around the E-core in the absence of any flux return path (*i.e.* when the magnetic circuit is open). In this case, the flux is not constrained to flow in a path that is *a priori* well defined, because the laminations that complete the flux path have been removed.

The geometry was chosen arbitrarily, the purpose here being more the procedure than the actual problem. The material for the core is linear with a relative permeability of 2500. The coil carries a bulk current density of 2 MA/m². The input geometry is shown in the following figure. Here the core is placed within a circular region, and a second circular region is drawn next to the region containing the core. Periodic boundary conditions are applied to the arcs that define the boundaries as shown in the figure.



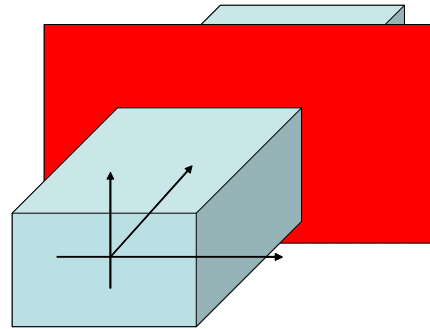
Also notice that a point has been drawn in the center of the exterior region. A point property has been applied to this point that specifies that $A = 0$ at this reference point. The center of the circle maps to infinity in the analogous open problem, so it makes sense to define, in effect, $A = 0$ at infinity. If no reference point is defined, it is fairly easy to see that the solution is only unique to within a constant. The situation is analogous to a situation where Neumann boundary conditions have been defined on all boundaries, resulting in a non-unique solution for A . The resulting solution is shown in the following figure. As is the intention, the flux lines appear to cross out of the of the region containing the core as if unaffected by the presence of the boundary. The flux lines reappear in the domain representing the exterior region, completing their flux paths through the exterior region.



Reduction of a 3D problem to a 2D problem

The **3D problem is reduced** considering the symmetry of the system. The symmetries can be of two kinds:

- **Plane symmetry.** The electromagnetic phenomena are supposed to be identical on each plane perpendicular to an axis, called a symmetry axis. The field is identical on each section of the element normal to the z-axis, if we suppose an infinite length of the system and neglecting the end effects.



The analysis is then given on the (x,y) plane. The solution is very simply and easily obtained. For example on the magnetostatic problem, we can obtain the following conditions:

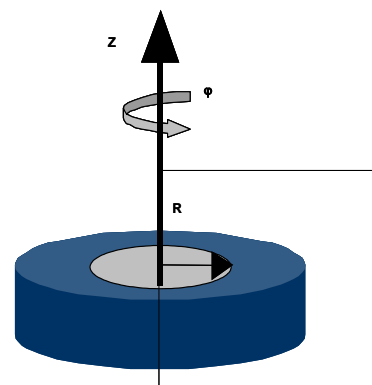
- The current density vector J has the z axis component $J = (0, 0, J_z)$, only. This component can be a function of the x and y coordinates, i.e. $J_z = J_z(x, y)$.
- The magnetic vector potential A has a component parallel to vector J only, that is the z axis component, $A = (0, 0, A_z)$. This component is a function of the x and y coordinates, i.e. $A_z = A_z(x, y)$.
- The flux density vector B has components only on the (x,y) plane, as obtained from:

$$B = \nabla \times A$$

That is:

$$B = \left(\frac{\partial A_z}{\partial y} \quad -\frac{\partial A_z}{\partial x} \quad 0 \right)$$

- **Axial symmetry.** The electromagnetic phenomena are supposed as identical on each semi-plane obtained by rotation through a fixed axis.



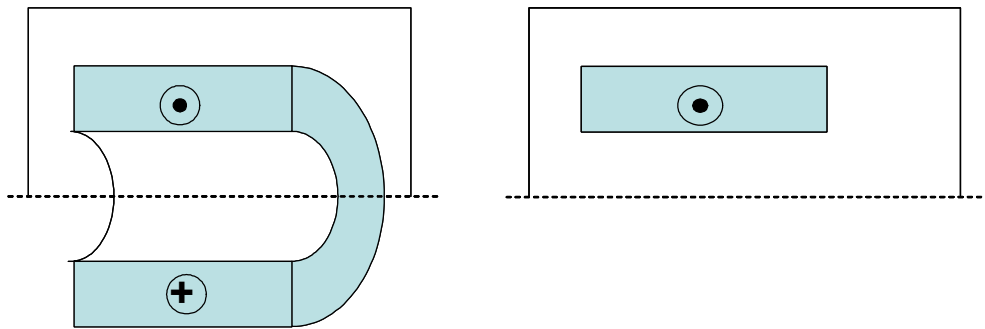
The analysis is then given on the (r,z) plane. The solution is very simple and easy. For example on the magnetostatic problem, we can obtain the following conditions:

- The current density vector J has θ axis component $J = (0, J_\theta, 0)$, only. This component can be a function of the r and z coordinates, i.e. $J_\theta = J_\theta(r, z)$.
- The magnetic vector potential A has component parallel to vector J only, that is θ axis component, $A = (0, A_\theta, 0)$. This component is a function of the r and θ coordinates, i.e. $A_\theta = A_\theta(r, z)$.
- The flux density vector B has components only on the (r, θ) plane, as obtained from:

$$B = \nabla \times A$$

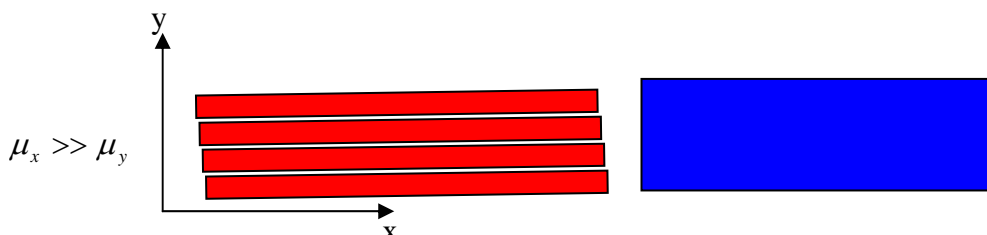
That is:

$$B = \left(\frac{\partial A_\theta}{\partial z} \quad 0 \quad \frac{1}{r} \frac{\partial}{\partial r} (r \cdot A_\theta) \right)$$



Materials properties. Linear and Non-linear models

It is possible to apply Maxwell's equations in various situations and in combinations of different materials. For this purpose it is necessary to introduce the concept of magnetic anisotropy. Consider a material whose magnetic permeability is dominant in a certain direction. One such material is a sheet of iron with grain-oriented structure or thin plates made of sheet metal which form, for example, the core of a transformer, as in the following figure.



It is reasonable to assume that in both cases, the magnetic flux flows more easily in the direction Ox . In the first case, this is due to the orientation of the grains and in the second due to the presence of small gaps between the layers

of sheet metal. Assuming a field intensity H whose components H_x and H_y are equal to H and if μ_x and μ_y are the permeabilities in the direction Ox and Oy respectively, we have:

$$B_x = \mu_x \cdot H_x$$

$$B_y = \mu_y \cdot H_y$$

We note that B_x is larger than B_y . We conclude that the relation

$$B = \mu \cdot H$$

where μ is a scalar, is not general since it does not satisfy the cases above mentioned. Because of this, we introduce the concept of **permeability tensor** denoted by $\|\mu\|$. In general form, the relation between B and H can be written as:

$$\begin{bmatrix} B_x \\ B_y \\ B_z \end{bmatrix} = \begin{bmatrix} \mu_x & \mu_{xy} & \mu_{xz} \\ \mu_{xy} & \mu_y & \mu_{yz} \\ \mu_{xz} & \mu_{yz} & \mu_z \end{bmatrix} \cdot \begin{bmatrix} H_x \\ H_y \\ H_z \end{bmatrix}$$

$$B = \|\mu\| \cdot H$$

In general applications we can write similar relations to other characteristics, such as the conductivity or permittivity:

$$E = \|\varepsilon\| \cdot D$$

$$J = \|\sigma\| \cdot E$$

Besides the concept of anisotropy, which complicates the study of magnetic and electric materials, we introduce another phenomenon, frequently encountered in electromagnetic devices. In these devices, the magnetic permeability is not constant but depends on the particular value of H in the magnetic material in question. This phenomenon is called **non-linearity** or **saturation**. The general relation between B and H is now:

$$B = \|\mu(H)\| \cdot H$$

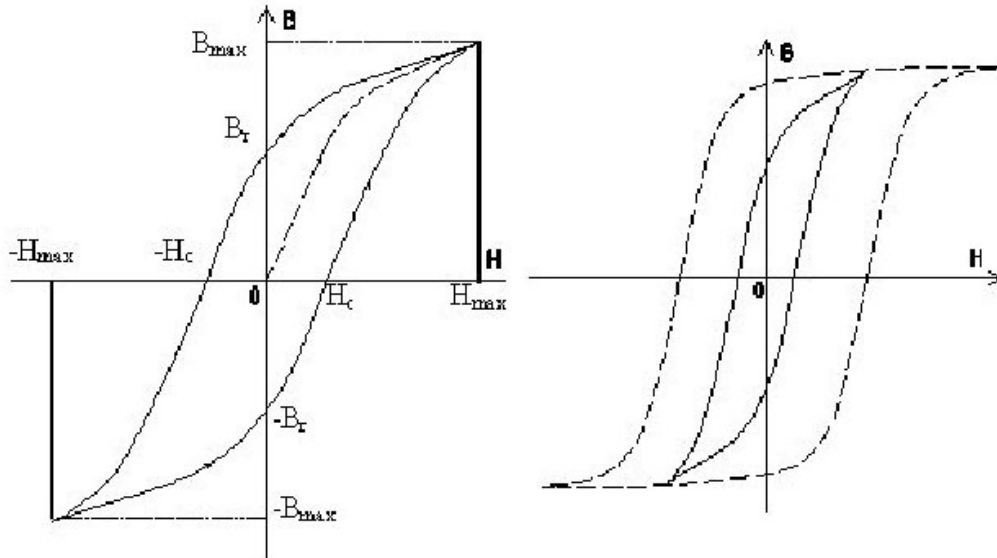
In some cases the better option, for numerical calculation, is to use the inverse of μ . This is called **magnetic reluctivity** ν :

$$\nu = \frac{1}{\mu} = \nu(B)$$

To avoid the use of negative values of B , we can use a modified relation between ν and B^2 .

$$\nu = \nu(B^2)$$

For numerical stability this function must be continuous and differentiable. A number of approximations are possible from polynomials to exponentials. A popular selection is the cubic spline. This method gives piecewise cubic polynomials that are continuous with continuous derivatives.



The above figure shows the hysteresis loop for a magnetic material. The discontinuous line shows the named **normal magnetisation curve**. For soft magnetic materials, the hysteresis loop is narrow and this line is a good approximation. For hard magnetic materials (permanent magnets) the treatment is slightly different. The next section is dedicated to the modelling of permanent magnets.

Permanent magnets (PM) modelling.

The development of high energy permanent magnet materials such as SmCo and NdFeB has led to increased interest in the use of permanent magnet material in electrical machines and actuators. As mentioned in the last section, ferromagnetic materials are characterised by a narrow hysteresis loop. In contrast, hard magnetic materials such as PM exhibit wide loops. It is often acceptable to consider the magnetic characteristic of a PM by a straight line in the second quadrant of the hysteresis loop. The intersection of the hysteresis loop with the ordinate is called the residual or remanence flux density B_r . The intersection of the abscissa and the loop is called the coercitive force H_c . There are two possibilities for the modelling of a PM material:

- Magnetisation model
- Current sheet approach

Although these two methods have a different starting point, they both result in the same set of equations. Assuming a straight line as the characteristic of the PM material, there are only two parameters required to define the characteristic:

- The slope of the line μ_m
- The y-axis intercept B_r

Magnetic vector model

The demagnetisation characteristic is defined by

$$B = \mu_0 \cdot ((1 + \chi_m) \cdot H + M)$$

where χ_m is the magnetic susceptibility, M the magnetisation vector and H the field strength at the operating point. In terms of the remanent flux density

$$B_r = \mu_0 \cdot M$$

The incremental permeability, the slope of the demagnetisation characteristic is

$$\frac{\partial |B|}{\partial |H|} = \mu_0 \cdot (1 + \chi_m)$$

χ_m is a very small positive number so that the apparent permeability of the magnet is only slightly larger than that of the free space. The reluctivity is defined as

$$\nu = \frac{1}{\mu_0 \cdot (1 + \chi_m)}$$

and applying this to the demagnetisation characteristic, yields

$$H = \nu \cdot (B - \mu_0 \cdot M)$$

using the Maxwell equation for a magnetostatic problem:

$$\nabla \times H = J$$

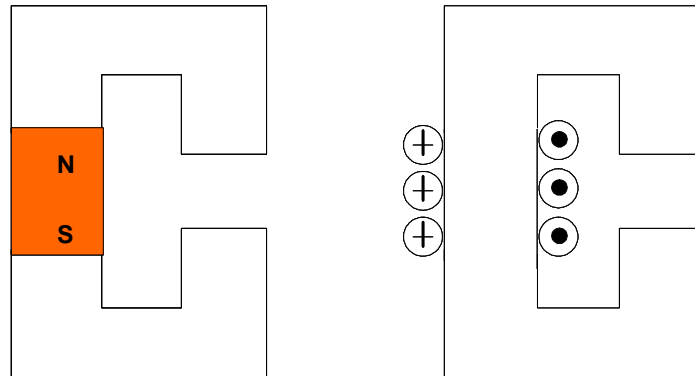
yields

$$\nabla \times (\nu \cdot B) = J + \nabla \times (\nu \cdot \mu_0 \cdot M)$$

The second term, the magnetic vector, on the right-hand side represents a source term and can be identified as an equivalent magnetic current.

Current sheet approach

The use of an equivalent current sheet representing the PM material is an easy way to introduce the materials properties.



Taking the permeability of the iron core in the above figure to be infinite, Ampere's law yields

$$H_m \cdot l_m + H_a \cdot \delta = 0$$

Ignoring fringing and corner effects, the flux density B is uniform and:

$$B = -\mu_0 \cdot \frac{l_m}{\delta} \cdot H_m$$

The intersection between the air gap characteristic, the load line, and the demagnetisation curve represents the operating point of the system. For a lineal magnet we have:

$$B_m = B_r \cdot \left(1 + \frac{H_m}{H_c}\right) = B_r + \mu_0 \cdot (1 + \chi_m) \cdot H$$

$$B_m = B_r + \mu \cdot H$$

The PM can be represented by a **current sheet** with total ampere-turns

$$N \cdot I = H_c \cdot l_m$$

and a material of equivalent permeability

$$\mu = \frac{B_r}{H_c}$$

Again assuming an infinite permeability of the iron parts of the material core,

$$H_m \cdot l_m + H_a \cdot \delta = H_c \cdot l_m$$

This yields

$$\frac{H_c}{B_r} \cdot B + \nu_0 \cdot \frac{\delta}{l_m} \cdot B = H_c$$

All magnetic quantities outside the PM remain the same as in the case of the magnetic vector, but are shifted to the first quadrant of the magnetisation characteristic. This method is easy to implement for rectangular magnets with a magnetisation parallel to two sides of the rectangle:

- Replace the magnet by a material of permeability $\mu = \frac{B_r}{H_c}$
- Add a thin current sheet along the two sides of the magnet to produce a field in the direction of the magnetization. The linear current density (A/m) must be equal to H_c , the coercitive force.

These ideas can be transferred to PM with an arbitrary shape. The current in the sheet is given by:

$$I_{ab} = -H_c \cdot \vec{l}_{ab} \cdot \vec{n}_{cd}$$

where \vec{l}_{ab} is a vector pointing in the direction of sheet current and whose magnitude is the length of the edge. \vec{n}_{cd} is a unity vector pointing in the direction of magnetization.

ANALYTICAL SOLUTION

$$\frac{\partial^2 \Phi}{\partial x^2} + k_x^2 \cdot X(x) = 0$$

$$\frac{\partial^2 \Phi}{\partial y^2} + k_y^2 \cdot Y(y) = 0$$

$$\frac{\partial^2 \Phi}{\partial z^2} + k_z^2 \cdot Z(z) = 0$$

Analytical solution

Some important theorems

Two theorems are of fundamental importance in solving EM problems. These are:

- **Superposition principle.** If each member of a set of functions Φ_n , $n = 1, 2, \dots, N$, is a solution to the PDE $L\Phi = g$ with some prescribed boundary conditions, then a linear combination

$$\Phi = \Phi_0 + \sum_{n=1}^N a_n \cdot \Phi_n$$

also satisfies $L\Phi = g$. Also we can divide the complex problem into a set of reduced problems, which are easier to solve than the original problem. The solution to the original problem is given by:

$$\Phi = \sum_{n=0}^N \Phi_n$$

- **Uniqueness theorem.** This theorem guarantees that the solution obtained for a PDE with some prescribed boundary conditions is the only one possible. In a general way, a solution of $\nabla^2 U = 0$ is uniquely determined by specifying either the value of U or the normal component of ∇U (in the case of scalar potential) or the tangential component of $\nabla \times U$ (in the case of potential vector) at **each point of the boundary surface**.

Analytical resolution. Separation of variables.

The method of separation of variables (sometimes called the Fourier's method) is a conventional method for solving a partial differential equation. Basically, it entails seeking a solution which breaks down into a product of functions, each of which involves only one of the variables. For example, if we are seeking a solution $\Phi(x, y, z, t)$ to some PDE, we require that it has the product form:

$$\Phi(x, y, z, t) = X(x) \cdot Y(y) \cdot Z(z) \cdot T(t)$$

A solution of the form in the above equation is said to be separable in x , y , z , and t .

We begin the application of separation of variables by finding the product solution of the homogeneous scalar wave equation

$$\nabla^2 \Phi - \frac{1}{c^2} \cdot \frac{\partial^2 \Phi}{\partial t^2} = 0$$

Solution to Laplace's equation can be derived as a special case of the wave equation. Diffusion and heat equations can be handled in the same manner as we will treat wave equation. To solve this equation, it is expedient that we first separate the time dependence. We let

$$\Phi(\mathbf{r}, t) = \Phi(\mathbf{r}) \cdot T(t)$$

Substituting this in the above equation:

$$T \cdot \nabla^2 U - \frac{1}{c^2} \cdot U \cdot T'' = 0$$

dividing by $U \cdot T$ gives:

$$\frac{\nabla^2 U}{U} = \frac{T''}{c^2 \cdot T}$$

the left side is independent of T , while the right side is independent of \mathbf{r} ; the equality can be true only if each side is independent of both variables. If we let an arbitrary constant $-k^2$ be the common value of the both sides, the equation reduces to

$$\nabla^2 U + k^2 \cdot U = 0$$

$$T'' + c^2 \cdot k^2 \cdot T = 0$$

Thus we have been able to separate the space variable \mathbf{r} from the time variable t . The arbitrary constant introduced in the course of the separation of variables is called the **separation constant**. We shall see that in general the total number of independent separation constants in a given problem is one less than the number of independent variables involved. The second equation is an ordinary differential equation with the general solution

$$T(t) = a_1 \cdot e^{j \cdot c \cdot k \cdot t} + a_2 \cdot e^{-j \cdot c \cdot k \cdot t}$$

Since the time dependence does not change with a coordinate system, the time dependence expressed in the above equation is the same for all coordinate systems. Therefore, we shall henceforth restrict our effort to seeking solution to the first equation. Notice that if $k = 0$, the time dependence disappears and this equation becomes Laplace's equation.

To outline the method consider the Laplace's equation in Cartesian coordinates

$$\frac{\partial^2 \Phi}{\partial x^2} + \frac{\partial^2 \Phi}{\partial y^2} + \frac{\partial^2 \Phi}{\partial z^2} = 0$$

The solution can be written as the product of three separate solutions:

$$\Phi(x, y, z) = X(x) \cdot Y(y) \cdot Z(z)$$

where $X(x)$ is only dependent on the x variable, $Y(y)$ on the y variable and $Z(z)$ on the z variable. Substitution of the general solution into the original PDE and dividing by $X(x) \cdot Y(y) \cdot Z(z)$ gives

$$\frac{1}{X(x)} \cdot \frac{\partial^2 \Phi}{\partial x^2} + \frac{1}{Y(y)} \cdot \frac{\partial^2 \Phi}{\partial y^2} + \frac{1}{Z(z)} \cdot \frac{\partial^2 \Phi}{\partial z^2} = 0$$

In this form, each term depends on a single variable and, therefore, can be separated. For the separation to be valid, each term must be equal to a constant to be determined. The equation can be written as

$$\frac{1}{X(x)} \cdot \frac{\partial^2 \Phi}{\partial x^2} = -k_x^2$$

$$\frac{1}{Y(y)} \cdot \frac{\partial^2 \Phi}{\partial y^2} = -k_y^2$$

$$\frac{1}{Z(z)} \cdot \frac{\partial^2 \Phi}{\partial z^2} = -k_z^2$$

where the three constants must satisfy

$$k_x^2 + k_y^2 + k_z^2 = 0$$

The following three differential equations are obtained:

$$\frac{\partial^2 \Phi}{\partial x^2} + k_x^2 \cdot X(x) = 0$$

$$\frac{\partial^2 \Phi}{\partial y^2} + k_y^2 \cdot Y(y) = 0$$

$$\frac{\partial^2 \Phi}{\partial z^2} + k_z^2 \cdot Z(z) = 0$$

Now, the three equations are completely independent and can be solved separately. Any combination of constants can be chosen, if the above equation is satisfied. These constants must be selected for specific applications. For example, we can assume that

$$k_x^2 > 0; k_y^2 > 0 \text{ and } k_z^2 = -(k_x^2 + k_y^2)$$

The general solutions for $X(x)$ and $Y(y)$ are

$$X(x) = a_1 \cdot e^{j \cdot k_x \cdot x} + a_2 \cdot e^{-j \cdot k_x \cdot x}$$

$$Y(y) = a_3 \cdot e^{j \cdot k_y \cdot y} + a_4 \cdot e^{-j \cdot k_y \cdot y}$$

Therefore, because $k_z^2 = -(k_x^2 + k_y^2) < 0$ the general solution for $Z(z)$ is:

$$Z(z) = a_5 \cdot e^{|k_z| \cdot y} + a_6 \cdot e^{-|k_z| \cdot y}$$

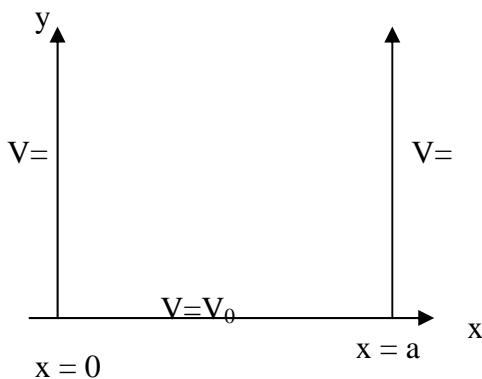
where the constants a_1 to a_6 must be evaluated to obtain a particular solution. These are evaluated from the boundary conditions of the problem. Any of the constants a_i can be zero, depending on the boundary conditions of the problem. Finally, although the solution appears in terms of nine unknowns (a_1 to a_6 , k_x , k_y , k_z), only six unknowns are independent.

For example, consider a two-dimensional box defined by two parallel surfaces, both semi-infinite in extent and both at zero potential. The lower surface is at potential V_0 . Also, the potential at infinity is zero. Calculate the potential everywhere in the channel so defined. For two dimensional analysis, we can show that:

$$k_y^2 = -k_x^2 = -k^2$$

The general solution is:

$$V(x, y) = (a_1 \cdot \sin(k \cdot x) + a_2 \cdot \cos(k \cdot x)) \cdot (b_1 \cdot e^{k \cdot y} + b_2 \cdot e^{-k \cdot y})$$



For the solution in the y direction, we use the exponential form. This is because we anticipate using values of y that tend to infinity. For such values, exponential forms are more convenient than the hyperbolic forms. To satisfy the boundary conditions, we write:

$$\text{At } x = 0 \quad V(0, y) = (a_2) \cdot (b_1 \cdot e^{k \cdot y} + b_2 \cdot e^{-k \cdot y}) = 0 \Rightarrow a_2 = 0$$

At $x = a$

$$V(a, y) = (a_1 \cdot \sin(k \cdot a)) \cdot (b_1 \cdot e^{k \cdot y} + b_2 \cdot e^{-k \cdot y}) = 0 \Rightarrow a_1 \cdot \sin(k \cdot a) = 0$$

This gives:

$$k \cdot a = m \cdot \pi \Rightarrow k = \frac{m \cdot \pi}{a}$$

where m is any integer, including zero. We will, however, exclude m=0 from the solution because it leads to k = 0 and a linear solution of the form

$$Ax + b$$

Similarly, the negative values of m need not be considered because negative m will only change the sign of the solution. The general solution at this stage looks like:

$$V(x, y) = \left(a_1 \cdot \sin\left(\frac{m \cdot \pi}{a} \cdot x\right) \right) \cdot \left(b_1 \cdot e^{\frac{m \cdot \pi}{a} \cdot y} + b_2 \cdot e^{-\frac{m \cdot \pi}{a} \cdot y} \right)$$

$$\text{At } y = \infty \Rightarrow V(x, \infty) = \left(a_1 \cdot \sin\left(\frac{m \cdot \pi}{a} \cdot x\right) \right) \cdot \left(b_1 \cdot e^{\frac{m \cdot \pi}{a} \cdot \infty} \right) = 0 \Rightarrow b_1 = 0$$

The solution at this stage is:

$$V(x, y) = C \cdot \left(\sin\left(\frac{m \cdot \pi}{a} \cdot x\right) \right) \cdot \left(e^{-\frac{m \cdot \pi}{a} \cdot y} \right)$$

$$C = a_1 \cdot b_2$$

At y = 0 V(x,0) = V₀; to satisfy this condition, we cannot simply substitute y = 0 in the general solution. If we did, the solution would be sinusoidal in the x direction and no constant C can satisfy the boundary condition. However, the solution may also be written as a superposition of solutions of the above form. We write

$$V(x, y) = \sum_{m=1}^{m=\infty} C_m \cdot e^{-\frac{m \cdot \pi}{a} \cdot y} \cdot \sin\left(\frac{m \cdot \pi}{a} \cdot x\right)$$

Now, we substitute y = 0:

$$V(x, 0) = V_0 = \sum_{m=1}^{m=\infty} C_m \cdot \sin\left(\frac{m \cdot \pi}{a} \cdot x\right)$$

The latter form is a Fourier sin series which, in effect, approximates the pulse V(x,0) = V₀, 0 ≤ x ≤ a, by an infinite series. In this sense, C_m, are the amplitude of the coefficients of the series. To obtain C_m, we multiply both sides by

$\sin\left(\frac{p \cdot \pi \cdot x}{a}\right)$, where p is an integer, and integrate both sides from zero to a . This is a general technique we will use again and was developed by Fourier himself:

$$\begin{aligned} \int_0^a V_0 \cdot \sin\left(\frac{p \cdot \pi \cdot x}{a}\right) \cdot dx &= \int_0^a \sum_{m=1}^{m=\infty} C_m \cdot \sin\left(\frac{m \cdot \pi}{a} \cdot x\right) \cdot \sin\left(\frac{p \cdot \pi \cdot x}{a}\right) \cdot dx = \\ &= \sum_{m=1}^{m=\infty} \int_0^a C_m \cdot \sin\left(\frac{m \cdot \pi}{a} \cdot x\right) \cdot \sin\left(\frac{p \cdot \pi \cdot x}{a}\right) \cdot dx \end{aligned}$$

where the integration and the sum are interchanged. Each side of the relation is integrated separately. The left hand side gives

$$\int_0^a V_0 \cdot \sin\left(\frac{p \cdot \pi \cdot x}{a}\right) \cdot dx = \begin{cases} \frac{2 \cdot a \cdot V_0}{p \cdot \pi} & \text{for } p = m \\ 0 & \text{for } p \neq m \end{cases}$$

For the right hand side, we integrate each integral in the sum. For any value of m , we get

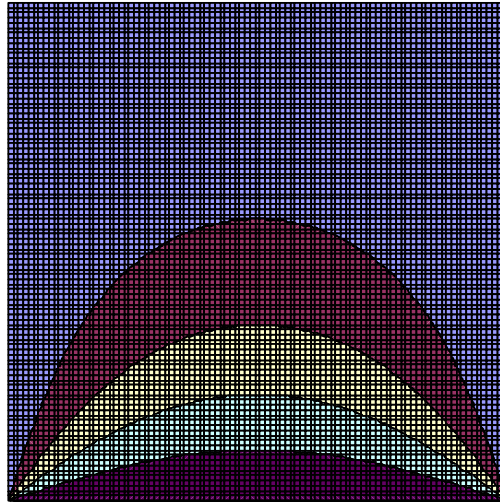
$$\int_0^a C_m \cdot \sin\left(\frac{m \cdot \pi}{a} \cdot x\right) \cdot \sin\left(\frac{p \cdot \pi \cdot x}{a}\right) \cdot dx = \begin{cases} \frac{a \cdot C_m}{2} & \text{for } p = m \\ 0 & \text{for } p \neq m \end{cases}$$

To satisfy both conditions above, m must be odd and $p = m$. Any other value yields zero. Thus:

$$C_m = \frac{4 \cdot V_0}{m \cdot \pi}; \quad m = 1, 3, 5, \dots$$

If we substitute this in the general solution, we obtain the general solution inside the box:

$$V(x, y) = \frac{4 \cdot V_0}{\pi} \cdot \sum_{m=1,3,5,\dots}^{m=\infty} \frac{1}{m} \cdot e^{-\frac{m \cdot \pi}{a} \cdot y} \cdot \sin\left(\frac{m \cdot \pi}{a} \cdot x\right)$$



The following tables resumes the general solutions of Laplace's equation in different coordinate systems.

Cartesian coordinates	$\frac{\partial^2 U}{\partial x^2} + \frac{\partial^2 U}{\partial y^2} + \frac{\partial^2 U}{\partial z^2} = 0$
X(x)=	$\begin{cases} a_1 \cdot e^{j \cdot k_x \cdot x} + a_2 \cdot e^{-j \cdot k_x \cdot x} = a'_1 \cdot \text{sen}(k_x \cdot x) + a'_2 \cdot \text{cos}(k_x \cdot x) & k_x \neq 0 \\ a_1 \cdot x + a_2 & k_x = 0 \end{cases}$
Y(y)=	$\begin{cases} b_1 \cdot e^{j \cdot k_y \cdot y} + b_2 \cdot e^{-j \cdot k_y \cdot y} = b'_1 \cdot \text{sen}(k_y \cdot y) + b'_2 \cdot \text{cos}(k_y \cdot y) & k_y \neq 0 \\ b_1 \cdot y + b_2 & k_y = 0 \end{cases}$
Z(z)=	$\begin{cases} c_1 \cdot e^{k_z \cdot z} + c_2 \cdot e^{-k_z \cdot z} = c'_1 \cdot \text{senh}(k_z \cdot z) + c'_2 \cdot \text{cosh}(k_z \cdot z) & k_z \neq 0 \\ c_1 \cdot z + c_2 & k_z = 0 \end{cases}$

Cylindrical coordinates	$\frac{1}{r} \cdot \frac{\partial}{\partial r} \left(r \cdot \frac{\partial U}{\partial r} \right) + \frac{1}{r^2} \cdot \frac{\partial^2 U}{\partial \phi^2} + \frac{\partial^2 U}{\partial z^2} = 0$
Z(z)=	$\begin{cases} c_1 \cdot e^{k_z \cdot z} + c_2 \cdot e^{-k_z \cdot z} = c'_1 \cdot \text{senh}(k_z \cdot z) + c'_2 \cdot \text{cosh}(k_z \cdot z) & k \neq 0 \\ c_1 \cdot z + c_2 & k = 0 \end{cases}$
$\Phi(\phi) =$	$\begin{cases} b_1 \cdot \text{sen}(n \cdot \phi) + b_2 \cdot \text{cos}(n \cdot \phi) & n \neq 0 \\ b_1 \cdot \phi + b_2 & n = 0 \end{cases}$
R(r) =	$\begin{cases} c_1 \cdot J_n(k \cdot r) + c_2 \cdot Y_n(k \cdot r) & k \neq 0 \\ c_1 \cdot r^n + c_2 \cdot r^{-n} & k = 0 \text{ and } n \neq 0 \\ c_1 \cdot \ln(r) + c_2 & k = 0 \text{ and } n = 0 \end{cases}$

Spherical coordinates	$\frac{1}{r^2} \cdot \frac{\partial}{\partial r} \left(r^2 \cdot \frac{\partial U}{\partial r} \right) + \frac{1}{r^2 \cdot \sin(\theta)} \cdot \frac{\partial}{\partial \theta} \left(\sin(\theta) \cdot \frac{\partial U}{\partial \theta} \right) + \frac{1}{r^2 \cdot \sin^2(\theta)} \cdot \frac{\partial^2 U}{\partial \phi^2} = 0$
$R(r) =$	$c_1 \cdot r^n + c_2 \cdot r^{-(n+1)} \quad n = 0, 1, 2, \dots$
$\Phi(\theta) =$	$b_1 \cdot P_n(\cos(\theta)) + b_2 \cdot Q_n(\cos(\theta))$

Other examples

Consider the skin effect on a solid cylindrical conductor. The current density distribution within a good conducting wire obeys the diffusion equation

$$\nabla^2 J = \mu \cdot \sigma \cdot \frac{\partial J}{\partial t}$$

We want to solve this equation for a long conducting wire of radius a . Assume harmonic field, i.e. $J = A(r, \phi, z) \cdot e^{j\omega t}$, thus

$$\nabla^2 \mathbf{J} = j \cdot \mu \cdot \sigma \cdot \mathbf{J}$$

For infinitely long wire, the above equation reduces to a one dimensional problem in cylindrical coordinates:

$$\frac{1}{r} \cdot \frac{\partial}{\partial r} \left(r \cdot \frac{\partial \mathbf{J}}{\partial r} \right) = j \cdot \mu \cdot \sigma \cdot \mathbf{J}$$

This equation is a modified Bessel equation of zero order. Hence the solution is

$$\mathbf{J} = c_1 \cdot I_0(\lambda \cdot r) + c_2 \cdot K_0(\lambda \cdot r)$$

where

$$\lambda = \sqrt{j \cdot \omega \cdot \sigma \cdot \mu} = \sqrt{j} \cdot \frac{\sqrt{2}}{\delta}$$

$$\delta = \sqrt{\frac{2}{\omega \cdot \sigma \cdot \mu}}$$

δ is the skin depth. Constant c_2 must vanish if \mathbf{J} is to be finite at $r = 0$. At $r = a$

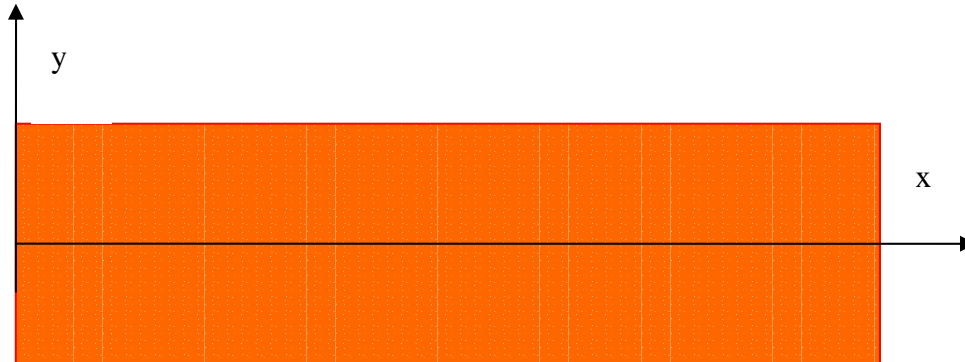
$$\mathbf{J}(a) = c_1 \cdot I_0(\lambda \cdot a) \Rightarrow c_1 = \frac{\mathbf{J}(a)}{I_0(\lambda \cdot a)}$$

Thus

$$\mathbf{J}(r) = \frac{\mathbf{J}(a)}{I_0(\lambda \cdot a)} \cdot I_0(\lambda \cdot r)$$

Skin effect on a plane infinite conductor

We can suppose a plane conductor inside of a magnetic field. This field has periodic and sinusoidal. This conductor is rectilinear and is extends to infinity in x coordinate. The Maxwell's equations for this case are:



$$\nabla \times \vec{H} = \vec{J}$$

$$\nabla \times \vec{E} = -\frac{\partial \vec{B}}{\partial t}$$

and with the constitutive relations:

$$\vec{B} = \mu \cdot \vec{H}$$

$$\vec{J} = \sigma \cdot \vec{E}$$

The solutions are:

$$\vec{H}(x,t) = \vec{H}(t) \cdot e^{j\omega t}$$

$$\vec{J}(x,t) = \vec{J}(t) \cdot e^{j\omega t}$$

Applying the curl operator:

$$\nabla \times \nabla \times \vec{H} = \nabla \times \vec{J}$$

and substituting Ohm's law:

$$\nabla \times \nabla \times \vec{H} = \nabla \times (\sigma \cdot \vec{E})$$

and applying the following vector identity, and Gauss's theorem:

$$\nabla \times \nabla \times \vec{H} = \nabla(\nabla \cdot \vec{H}) - \nabla^2 \vec{H}$$

$$\nabla \cdot \vec{B} = 0; \nabla(\mu \cdot \vec{H}) = \mu \cdot \nabla(\vec{H}) = 0$$

we can obtain:

$$\nabla^2 H = -\nabla \times (\sigma \cdot E) = \sigma \cdot \frac{\partial B}{\partial t}$$

$$\nabla^2 H = \sigma \cdot \mu \cdot \frac{\partial H}{\partial t}$$

In this case, only the x dimension is considered

$$\frac{d^2 \vec{H}}{dx^2} - j \cdot \sigma \cdot \omega \cdot \mu \cdot \vec{H} = 0$$

The general solution is:

$$H(x, t) = H_0 \cdot e^{\left(\frac{1+j}{\delta} \cdot x\right)} \cdot e^{j\omega t}$$

or

$$H(x, t) = H_0 \cdot e^{\left(\frac{x}{\delta}\right)} \cdot e^{j\left(\omega t - \frac{x}{\delta}\right)}$$

- $e^{\left(\frac{x}{\delta}\right)}$, is an attenuation term; The field decreases with x. For $x = \delta$ the field is reduced by a factor e^{-1} .
- $e^{j\left(\omega t - \frac{x}{\delta}\right)}$, is a propagation factor.

We can obtain a similar expression for the density of current in the conductor

$$\frac{d^2 \vec{J}}{dx^2} - j \cdot \sigma \cdot \omega \cdot \mu \cdot \vec{J} = 0$$

$$J(x, t) = J_0 \cdot e^{\left(\frac{x}{\delta}\right)} \cdot e^{j\left(\omega t - \frac{x}{\delta}\right)}$$

with

$$J_0 = \frac{1+j}{\delta} \cdot H_0$$

The current density is greater on the surface of conductor than inside the conductor. For example in a copper conductor in a 50 Hz field the skin depth is ($\sigma = 56 \cdot 10^6 \text{ S}\cdot\text{m}$):

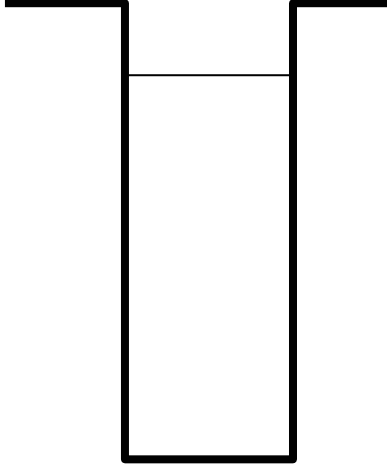
$$\delta = \sqrt{\frac{2}{\mu \cdot \sigma \cdot \omega}} = \sqrt{\frac{2}{4 \cdot \pi \cdot 10^{-7} \cdot 56 \cdot 10^6 \cdot 2 \cdot \pi \cdot 50}} = 9.51 \cdot 10^{-3} \text{ m} \approx 9.5 \text{ mm}$$

near to 1 cm.

Open Rectangular slot. Full conductor

The following figure shows an open rectangular slot with a one piece conductor. This slot has a height of h (m) and a width of b (m). We consider that $b \ll h$.

The general solution is



$$\vec{H} = \frac{I}{b} \cdot \frac{sh(\gamma \cdot y)}{sh(\gamma \cdot h)}$$

$$\vec{J} = I \cdot \frac{\gamma}{b} \cdot \frac{ch(\gamma \cdot y)}{sh(\gamma \cdot h)}$$

$$\gamma = \sqrt{\frac{j \cdot \mu_0 \cdot \omega}{\rho}}$$

To calculate the electric resistance and inductance we first determine the voltage drop along the bar.

To begin with, we calculate the difference of electric potential along the bar:

$$V_R = \int_0^L E \cdot dl = \int_0^L \rho \cdot J \cdot dl = \rho \cdot I \cdot \frac{\gamma}{b} \cdot L \cdot \frac{ch(\gamma \cdot y)}{sh(\gamma \cdot h)}$$

Second, we calculate the e.m.f. due to the time variation of linked flux. The flux linked at the “ y ” coordinate is:

$$\begin{aligned} \Phi(y) &= \int_0^L \int_y^h B \cdot dy \cdot dz = \int_0^L \int_y^h \mu_0 \cdot H \cdot dy \cdot dz = \int_0^L \int_y^h \mu_0 \cdot \frac{I}{b} \cdot \frac{sh(\gamma \cdot y)}{sh(\gamma \cdot h)} \cdot dy \cdot dz = \\ \Phi(y) &= \mu_0 \cdot \frac{I}{\gamma \cdot b} \cdot L \cdot \frac{ch(\gamma \cdot h) - ch(\gamma \cdot y)}{sh(\gamma \cdot h)} \end{aligned}$$

The e.m.f. is:

$$\begin{aligned} V_L &= \frac{\partial \Phi(y)}{\partial t} \\ V_L &= j \cdot \omega \cdot \Phi(y) \\ V_L &= j \cdot \omega \cdot \mu_0 \cdot \frac{I}{\gamma \cdot b} \cdot L \cdot \frac{ch(\gamma \cdot h) - ch(\gamma \cdot y)}{sh(\gamma \cdot h)} \end{aligned}$$

The total voltage drop is:

$$V_{bar} = V_r + V_L$$

$$V_{bar} = \rho \cdot I \cdot \frac{\gamma}{b} \cdot L \cdot \frac{ch(\gamma \cdot y)}{sh(\gamma \cdot h)} + j \cdot \omega \cdot \mu_0 \cdot \frac{I}{\gamma \cdot b} \cdot L \cdot \frac{ch(\gamma \cdot h) - ch(\gamma \cdot y)}{sh(\gamma \cdot h)}$$

and using:

$$\frac{j \cdot \omega \cdot \mu_0}{\gamma} = \frac{j \cdot \omega \cdot \mu_0}{\sqrt{\frac{j \cdot \mu_0 \cdot \omega}{\rho}}} = \rho \cdot \sqrt{\frac{j \cdot \mu_0 \cdot \omega}{\rho}} = \rho \cdot \gamma$$

we can obtain

$$V_{bar} = \rho \cdot I \cdot \frac{\gamma}{b} \cdot L \cdot \frac{ch(\gamma \cdot h)}{sh(\gamma \cdot h)}$$

The impedance of a slot-bar is determined as

$$Z_{barra} = \frac{V_{barra}}{I} = \rho \cdot \frac{\gamma}{b} \cdot L \cdot \frac{ch(\gamma \cdot h)}{sh(\gamma \cdot h)}$$

The D.C. resistance is simply:

$$R_{DC} = \rho \cdot \frac{L}{b \cdot h}$$

and

$$Z_{bar} = R_{DC} \cdot (\gamma \cdot h) \cdot \frac{ch(\gamma \cdot h)}{sh(\gamma \cdot h)}$$

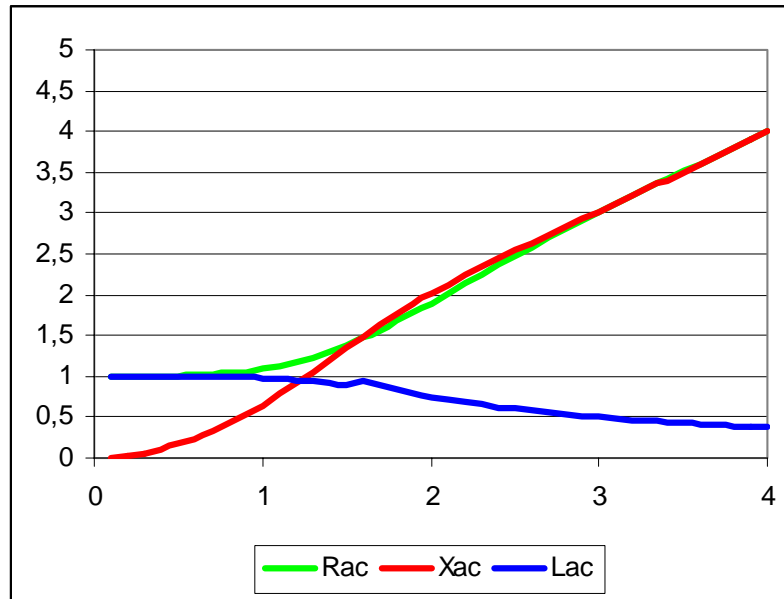
Expanding real and imaginary parts we can write:

$$R_{AC} = R_{DC} \cdot \frac{h}{\delta} \cdot \frac{sh(2 \cdot \frac{h}{d}) + sen(2 \cdot \frac{h}{d})}{ch(2 \cdot \frac{h}{d}) - cos(2 \cdot \frac{h}{d})}$$

$$X_{AC} = R_{DC} \cdot \left(\frac{h}{\delta}\right) \cdot \frac{sh(2 \cdot \frac{h}{d}) - sen(2 \cdot \frac{h}{d})}{ch(2 \cdot \frac{h}{d}) + cos(2 \cdot \frac{h}{d})}$$

the following figure shows the resistance, inductance and reactance variation as a function of the a dimensional parameter $\frac{h}{\delta}$

- Resistance grows with the frequency.
- Inductance decays with the frequency.



Some useful approximations

a) If $\frac{h}{\delta} < 1.5$ we can write:

$$R_{AC} = R_{DC} \cdot \left[1 + \frac{4}{45} \cdot \left(\frac{h}{\delta} \right)^4 - \frac{16}{4725} \cdot \left(\frac{h}{\delta} \right)^8 + \dots \right]$$

$$X_{AC} = \frac{2}{3} \cdot \left(\frac{h}{\delta} \right)^2 \cdot R_{DC} \cdot \left[1 - \frac{8}{315} \cdot \left(\frac{h}{\delta} \right)^4 + \frac{32}{31185} \cdot \left(\frac{h}{\delta} \right)^8 + \dots \right]$$

and

$$\frac{2}{3} \cdot \left(\frac{h}{\delta} \right)^2 \cdot R_{DC} = \frac{2}{3} \cdot \left(\sqrt{\frac{\mu \cdot \omega}{2 \cdot \rho}} \cdot h \right)^2 \cdot \rho \cdot \frac{L}{b \cdot h} = \omega \cdot \frac{\mu_0}{3} \cdot \frac{h \cdot L}{b} = \omega \cdot L_{DC}$$

$$L_{DC} = \frac{\mu_0}{3} \cdot \frac{h \cdot L}{b}$$

$$X_{AC} = \omega \cdot L_{DC} \cdot \left[1 - \frac{8}{315} \cdot \left(\frac{h}{\delta} \right)^4 + \frac{32}{31185} \cdot \left(\frac{h}{\delta} \right)^8 + \dots \right]$$

b) If $\frac{h}{\delta} \gg \gg$

$$R_{AC} = R_{DC} \cdot \frac{h}{\delta}$$

$$X_{AC} = R_{DC} \cdot \frac{h}{\delta} = \frac{3}{2} \cdot \omega \cdot \frac{\delta}{h} \cdot L_{DC}$$

Electric machines modelling

Field Description of Energy Flow: Poynting's Theorem

Start with Faraday's and Ampere laws:

$$\begin{aligned}\nabla \times E &= -\frac{\partial B}{\partial t} \\ \nabla \times H &= J\end{aligned}$$

multiplying the first of these by H and the second by E and taking the difference:

$$\begin{aligned}H \cdot \nabla \times E - E \cdot \nabla \times H &= \nabla \cdot (E \times H) = -H \cdot \frac{\partial B}{\partial t} - J \cdot E \\ \nabla \times H &= J\end{aligned}$$

On the left of this expression is the divergence of electromagnetic energy flow:

$$S = E \times H$$

Here, S is the celebrated Poynting flow which describes power in an electromagnetic field system. (The unit of this quantity is watts per square meter in the International System). On the right hand side are two terms:

$$-H \cdot \frac{\partial B}{\partial t} - J \cdot E$$

The first term is the rate of change of magnetic stored energy. The second term, represents like power dissipation. We will discuss each of these in more detail. For the moment, however, note that the divergence theorem of vector calculus yields:

$$\iiint_{Vol} \nabla \cdot S \cdot dV = \iint S \cdot \vec{n} \cdot dA$$

that is, the volume integral of the divergence of the Poynting energy flow is the same as the Poynting energy flow over the surface of the volume in question. This integral becomes:

$$\iint S \cdot \vec{n} \cdot dA = -\iiint_{Vol} \left(H \cdot \frac{\partial B}{\partial t} + J \cdot E \right) \cdot dV$$

which is simply a realization that the total energy flow into a region of space is the same as the volume integral over that region of the rate of change of energy stored plus the term that looks like dissipation. Before we close this, note that, if there is motion of any material within the system, we can use the empirical

expression for transformation of electric field between observers moving with respect to each other. Here the 'primed' frame is moving with respect to the 'unprimed' frame with the velocity v :

$$E' = E + v \times B$$

This transformation describes, for example, the motion of a charged particle such as an electron under the influence of both electric and magnetic fields. Now, if we assume that there is material motion in the system we are observing and if we assign v to be the velocity of that material, so that E' is measured in a frame in which there is no material motion (that is the frame of the material itself), the product of electric field and current density becomes:

$$J \cdot E = (E' - v \times B) \cdot J = E' \cdot J - v \times B \cdot J = E' \cdot J + v \cdot J \times B$$

In the last step we used the fact that in a scalar triple product the order of the scalar (dot) and vector (cross) products can be interchanged and that reversing the order of terms in a vector (cross) product simply changes the sign of that product. Now we have a ready interpretation for what we have calculated:

If the 'primed' coordinate system is actually the frame of material motion,

$$E' \cdot J = \frac{1}{\sigma} \cdot J^2$$

which is easily seen to be dissipation and is positively defined if material conductivity σ is positive. The last term is obviously conversion of energy from electromagnetic to mechanical form:

$$v \cdot J \times B = v \cdot F$$

where we have now identified force density to be:

$$F = J \times B$$

This is the Lorentz Force Law, which describes the interaction of current with magnetic field to produce force. It is not, however, the complete story of force production in electromechanical systems. As we learned earlier, changes in geometry which affect magnetic stored energy can also produce force. Fortunately, a complete description of electromechanical force is possible using only magnetic fields and that is the topic of our next section.

Field Description of Forces: Maxwell Stress Tensor

Forces of electromagnetic origin, because they are transferred by electric and magnetic fields, are the result of those fields and may be calculated once the fields are known. In fact, if a surface can be established that fully encases a

material body, the force on that body can be shown to be the integral of force density, or traction over that surface. The traction τ derived by taking the cross product of surface current density and flux density on the air-gap surface of a machine (above) actually makes sense in view of the empirically derived Lorentz Force Law:

Substituting the Maxwell's equations in the Lorentz force expression:

$$\nabla \times H = J \Rightarrow \frac{1}{\mu} \nabla \times B = \nu \nabla \times B = J$$

we obtain:

$$f = (\nu \nabla \times B) \times B$$

Developing this equation, we obtain the following equation (we only show the equation for X – component):

$$f_x = \nu \left(B_z \frac{\partial B_x}{\partial z} - B_z \frac{\partial B_z}{\partial x} - B_y \frac{\partial B_y}{\partial x} + B_y \frac{\partial B_x}{\partial y} \right)$$

If a term $\nu B_x \frac{\partial B_x}{\partial x}$ is added and subtracted from the above equation, and the identity

$$\frac{\partial}{\partial x} (B_x^2) = 2 B_x \frac{\partial B_x}{\partial x}$$

is used, then the force component becomes:

$$f_x = \nu \left(\frac{1}{2} \frac{\partial}{\partial x} (B_x^2) + B_z \frac{\partial B_x}{\partial z} + B_y \frac{\partial B_x}{\partial y} - \frac{1}{2} \frac{\partial}{\partial x} (B_x^2 + B_y^2 + B_z^2) \right)$$

Some further manipulations gives:

$$f_x = \nu \left(\frac{\partial}{\partial x} \left(B_x^2 - \frac{1}{2} |B|^2 \right) + \frac{\partial (B_x B_z)}{\partial z} + \frac{\partial (B_x B_y)}{\partial y} - B_x \nabla \cdot B \right) \Rightarrow (\nabla \cdot B = 0)$$

$$f_x = \nu \left(\frac{\partial}{\partial x} \left(B_x^2 - \frac{1}{2} |B|^2 \right) + \frac{\partial (B_x B_z)}{\partial z} + \frac{\partial (B_x B_y)}{\partial y} \right)$$

The remaining expression may be recognized as the divergence of a vector f_x , whose components are:

$$\nabla \cdot T_x = \begin{cases} \frac{\partial T_x}{\partial x} = f_{xx} = \nu \left(B_x^2 - \frac{1}{2} |B|^2 \right) \\ \frac{\partial T_x}{\partial y} = f_{xy} = \nu (B_x B_z) \\ \frac{\partial T_x}{\partial z} = f_{xz} = \nu (B_x B_y) \end{cases}$$

A similar development holds for each of the other force components (f_y and f_z). Thus these vectors can be combined into a Tensor T:

$$T = \nu \begin{pmatrix} \left(B_x^2 - \frac{1}{2} |B|^2 \right) & (B_x B_y) & (B_x B_z) \\ (B_y B_x) & \left(B_y^2 - \frac{1}{2} |B|^2 \right) & (B_y B_z) \\ (B_z B_x) & (B_z B_y) & \left(B_z^2 - \frac{1}{2} |B|^2 \right) \end{pmatrix}$$

The force density can now be written as the divergence of this tensor:

$$f = \nabla \cdot T$$

The total force can be found by integration over the volume:

$$F = \iiint_V f dV = \iiint_V \nabla \cdot T dV$$

Using the divergence theorem, this volume integral may be reduced to a surface integral:

$$F = \iiint_V \nabla \cdot T dV = \oint_S T dS$$

We limit the following development to two dimensional geometry, so that the surface of integration is a line (we consider a unit depth). The unit normal and tangential vectors to the surface are:

$$\begin{aligned} \vec{a}_t &= s_x \vec{a}_x + s_y \vec{a}_y \\ \vec{a}_n &= s_x \vec{a}_y - s_y \vec{a}_x \end{aligned}$$

The incremental integration path is then: $ds = \vec{a}_n dl$ where dl is a differential length along the integration path. The incremental force is now:

$$f = T \cdot ds$$

$$f = \nu \begin{pmatrix} \left(B_x^2 - \frac{1}{2} |B|^2 \right) & (B_x B_y) \\ (B_y B_x) & \left(B_y^2 - \frac{1}{2} |B|^2 \right) \end{pmatrix} \begin{pmatrix} -s_y \\ s_x \end{pmatrix} dl$$

The tangential and normal component are:

$$f_t = f \cdot \vec{a}_t = \nu \cdot dl \left((B_x B_y) (s_x^2 - s_y^2) + s_x s_y (B_y^2 - B_x^2) \right)$$

$$f_n = f \cdot \vec{a}_n = \nu \cdot dl \left(B_x^2 s_y^2 + B_y^2 s_x^2 - \frac{1}{2} |B|^2 - 2 B_x B_y s_x s_y \right)$$

The tangential and normal components of the flux density are:

$$\vec{B}_t = B_x s_x + B_y s_y$$

$$\vec{B}_n = -B_x s_y + B_y s_x$$

Substituting and some after algebraic manipulations, we can write:

$$f_t = \nu (B_n B_t) dl$$

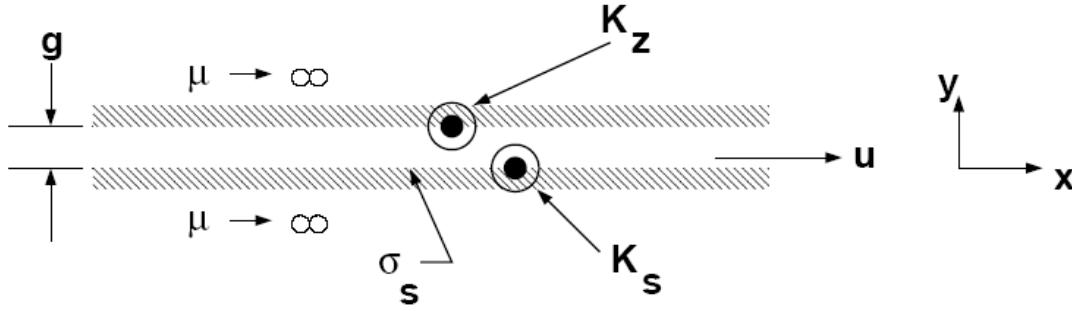
$$f_n = \frac{1}{2} \nu (B_n^2 - B_t^2) dl$$

The torque on an arc of radius r is given by:

$$M = \nu \int B_n B_t r \cdot dl$$

Example: Linear Induction Machine

The following figure shows a highly simplified picture of a single sided linear induction motor. This is not how most linear induction machines are actually built, but it is possible to show through symmetry arguments that the analysis we can carry out here is actually valid for other machines of this class. This machine consists of a stator (the upper surface) which is represented as a surface current on the surface of a highly permeable region. The moving element consists of a thin layer of conducting material on the surface of a highly permeable region.



The moving element (or 'shuttle') has a velocity u with respect to the stator and that motion is in the x direction. The stator surface current density is assumed to be:

$$K_z = \text{Re}(\underline{K_z} \cdot e^{j(\omega t - kx)})$$

Note that we are ignoring some important effects, such as those arising from finite length of the stator and of the shuttle. Such effects can be quite important, but we will leave those until later, as they are what make linear motors interesting. Viewed from the shuttle for which the dimension in the direction of motion is $x' = x - ut'$, the relative frequency is:

$$\omega t - kx = (\omega - ku)t - kx' = \omega_s t - kx'$$

Now, since the shuttle surface can support a surface current and is excited by magnetic fields which are in turn excited by the stator currents, it is reasonable to assume that the form of the rotor current is the same as that of the stator:

$$K_s = \text{Re}(\underline{K_s} \cdot e^{j(\omega_s t - kx')})$$

Ampere's Law is, in this situation:

$$g \cdot \frac{\partial H_y}{\partial x} = K_z + K_s$$

which is, in complex amplitudes:

$$\underline{H_y} = \frac{\underline{K_z} + \underline{K_s}}{-j \cdot k \cdot g}$$

The y - component of Faraday's Law is as follows, assuming the problem is uniform in the z - direction:

$$-j \cdot \omega_s \cdot B_y = j \cdot k \cdot E'$$

$$E' = -\frac{\omega_s}{k} \cdot \mu \cdot H_y$$

A bit of algebraic manipulation yields expressions for the complex amplitudes of rotor surface current and gap magnetic field:

$$\underline{K}_s = \frac{\frac{-j \cdot \mu_0 \cdot \omega_s \cdot \sigma_s}{k^2 \cdot g}}{1 + \frac{j \cdot \mu_0 \cdot \omega_s \cdot \sigma_s}{k^2 \cdot g}} \cdot \underline{K}_z$$

$$\underline{H}_y = \frac{\frac{j}{k \cdot g}}{1 + \frac{j \cdot \mu_0 \cdot \omega_s \cdot \sigma_s}{k^2 \cdot g}} \cdot \underline{K}_z$$

To find surface traction, the Maxwell Stress Tensor can be evaluated at a surface just below the stator (on this surface the x- directed magnetic field is simply $H_x = K_z$. Thus the traction is

$$\tau_x = T_{xy} = \mu_0 \cdot H_x \cdot H_y$$

and the average of this is:

$$\langle \tau_x \rangle = \frac{\mu_0}{2} \text{Re}(\underline{H}_x \cdot \underline{H}_y^*)$$

That is:

$$\langle \tau_x \rangle = \frac{\mu_0}{2} \cdot \frac{1}{k \cdot g} \cdot \frac{\frac{\mu_0 \cdot \omega_s \cdot \sigma_s}{k^2 \cdot g}}{1 + \left(\frac{\mu_0 \cdot \omega_s \cdot \sigma_s}{k^2 \cdot g} \right)^2} \cdot |K_z|^2$$

Now, if we consider electromagnetic power flow (Poynting's Theorem): in the y-direction:

$$S_y = E_z \cdot H_x$$

And since in the frame of the shuttle $\underline{E}_z' = -\frac{\omega_s}{k} \cdot \mu_0 \cdot \underline{H}_y$

$$\langle S_y' \rangle = -\frac{1}{2} \cdot \frac{\omega_s}{k} \cdot \frac{\mu_0}{k \cdot g} \cdot \frac{\frac{\mu_0 \cdot \omega_s \cdot \sigma_s}{k^2 \cdot g}}{1 + \left(\frac{\mu_0 \cdot \omega_s \cdot \sigma_s}{k^2 \cdot g} \right)^2} \cdot |K_z|^2 = -\frac{\omega_s}{k} \cdot \langle \tau_x \rangle$$

Similarly, evaluated in the frame of the stator:

$$\langle S_y \rangle = -\frac{\omega}{k} \cdot \langle \tau_x \rangle$$

This shows what we already suspected: the electromagnetic power flow from the stator is the force density on the shuttle times the wave velocity. The electromagnetic power flow into the shuttle is the same force density times the 'slip' velocity. The difference between these two is the power converted to mechanical form and it is the force density times the shuttle velocity.

Rotating Machines

The use of this formulation in rotating machines is a bit tricky because, at least formally, directional vectors must have constant identity if an integral of forces is to become a total force. In cylindrical coordinates, of course, the directional vectors are not of constant identity. However, with care and understanding of the direction of traction and how it is integrated we can make use of the Maxwell Stress Tensor (MST) approach in rotating electric machines. Now, if we go back to the case of a circular cylinder and are interested in torque, it is pretty clear that we can compute the circumferential force by noting that the normal vector to the cylinder is just the radial unit vector, and then the circumferential traction must simply be:

$$\tau_\phi = \mu_0 \cdot H_r \cdot H_\phi$$

Assuming that there are no fluxes inside the surface of the rotor, simply integrating this over the surface gives azimuthal force. In principal this is the same as surrounding the surface of the rotor by a continuum of infinitely small boxes, one surface just outside the rotor and with a normal facing outward, the other surface just inside with normal facing inward. (Of course the MST is zero on this inner surface). Then multiplying by radius (moment arm) gives torque. The last step is to note that, if the rotor is made of highly permeable material, the azimuthal magnetic field just outside the rotor is equal to surface current density.

Generalization to Continuous Media

Now, consider a system with not just a multiplicity of circuits but a continuum of current-carrying paths. In that case we could identify the co-energy as:

$$W_m' = \int \int_{area} \lambda(a) \cdot dJ \cdot da$$

where that area is chosen to cut all of the current carrying conductors. This area can be picked to be perpendicular to each of the current filaments since the divergence of current is zero. The flux λ is calculated over a path that coincides

with each current filament (such paths exist since current has zero divergence). Then the flux is:

$$\lambda(a) = \iint B \cdot d\vec{n}$$

Now, if we use the vector potential, the flux linked by any one of the current filaments is:

$$\lambda(a) = \oint A \cdot dl$$

where dl is the path around the current filament. This implies directly that the co-energy is:

$$W_m' = \int \oint_{area J} A \cdot dl \cdot dJ \cdot da$$

Now: it is possible to make dl coincide with da and be parallel to the current filaments, so that:

$$W_m' = \iiint_{vol} A \cdot dJ \cdot dV$$

For linear continuous media we can write:

$$W_m = W_m' = \frac{1}{2} \iiint_{Vol} A \cdot J \cdot dV$$

Permanent Magnets

Permanent magnets are becoming an even more important element in electric machine systems. Often systems with permanent magnets are approached in a relatively ad-hoc way and made equivalent to a current that produces the same MMF as the magnet itself. The constitutive relationship for a permanent magnet relates the magnetic flux density B to magnetic field H and the property of the magnet itself, the magnetization M,

$$B = \mu_0 \cdot (H + M)$$

Now, the effect of the magnetization is to act as if there were a current with density:

$$J^* = \nabla \times M$$

Note that this current "acts" just like ordinary current in making magnetic flux density. Magnetic co-energy is:

$$W_m' = \iiint_{vol} A \cdot \nabla \times dM \cdot dV$$

Next note the vector identity:

$$\nabla \cdot (C \times D) = D \cdot (\nabla \times C) - C \cdot (\nabla \times D)$$

Now,

$$\begin{aligned} W_m' &= \iiint_{vol} -\nabla \cdot (A \times dM) dV + \iiint_{vol} (\nabla \times A) \cdot dM dV = \\ &= -\oint (A \times dM) \cdot dS + \iiint_{vol} B \cdot dM dV \end{aligned}$$

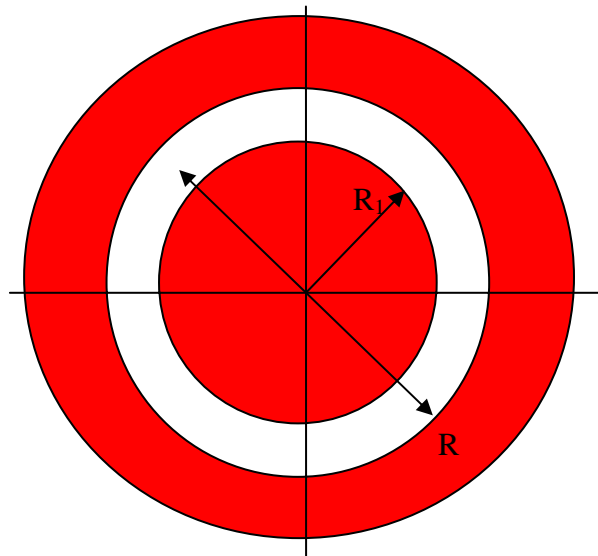
The first of these integrals (closed surface) vanishes if it is taken over a surface just outside the magnet, where M is zero. Thus the magnetic co-energy in a system with only a permanent magnet source is

$$W_m' = \iiint_{vol} B \cdot dM dV$$

Adding current carrying coils to such a system is done in the obvious way.

Some examples

Application. Consider the following picture. The 'machine' consists of a cylindrical rotor and a cylindrical stator which are coaxial and which have sinusoidal current distributions on their surfaces: the outer surface of the rotor and the inner surface of the stator.



The 'rotor' and 'stator' bodies are made of highly permeable material (we approximate this as being infinite for the time being, but this is something that needs to be looked at carefully later). We also assume that the rotor and stator have current distributions that are axially (z) directed and sinusoidal:

$$K_z^S = K_s \cdot \cos(p\phi)$$

$$K_z^R = K_r \cdot \cos(n(\phi - \alpha))$$

Here, the angle ϕ is the physical angle of the rotor. Due to the symmetry, the z component does not exist. Poisson's equation's for this case is:

$$\frac{1}{r} \cdot \frac{\partial}{\partial r} \left(r \cdot \frac{\partial A}{\partial r} \right) + \frac{1}{r^2} \cdot \frac{\partial^2 A}{\partial \phi^2} = -\mu_0 \cdot (K_Z^S + K_Z^R)$$

The general solution of this equation is:

$$A(r, \phi) = \sum_m (b_m \cdot \sin(m \cdot \phi) + a_m \cdot \cos(m \cdot y)) \cdot (c_m \cdot r^m + d_m \cdot r^{-m})$$

The boundary conditions for tangential magnetic field intensity are:

$$\begin{aligned} r = R_1 &\Rightarrow H_t = 0 \\ r = R_2 &\Rightarrow H_t = -J \end{aligned}$$

The tangential value are calculated as:

$$H_t = -\frac{1}{\mu_0} \cdot \frac{\partial A}{\partial r} = -\frac{1}{\mu_0} \cdot \sum_m (b_m \cdot \sin(m \cdot \phi) + a_m \cdot \cos(m \cdot y)) \cdot m \cdot (c_m \cdot r^{m-1} + d_m \cdot r^{-m-1})$$

For each boundary:

$$\begin{aligned} H_t)_{r=R_1} &= -\frac{1}{\mu_0} \cdot \sum_m (b_m \cdot \sin(m \cdot \phi) + a_m \cdot \cos(m \cdot y)) \cdot m \cdot (c_m \cdot R_1^{m-1} + d_m \cdot R_1^{-m-1}) = 0 \\ H_t)_{r=R_2} &= \frac{1}{\mu_0} \cdot \sum_m (b_m \cdot \sin(m \cdot \phi) + a_m \cdot \cos(m \cdot y)) \cdot m \cdot (c_m \cdot R_2^{m-1} + d_m \cdot R_2^{-m-1}) = J \end{aligned}$$

where J is the current density. If $m \neq p$ we can write:

$$(c_m \cdot R_1^{m-1} + d_m \cdot R_1^{-m-1}) = 0 \Rightarrow c_m = d_m = 0$$

and if $m = p$

$$H_t)_{r=R_2} = \frac{1}{\mu_0} \cdot (b_p \cdot \sin(p \cdot \phi) + a_p \cdot \cos(p \cdot y)) \cdot p \cdot (c_p \cdot R_2^{p-1} + d_p \cdot R_2^{-p-1}) = J$$

The solutions of this system of equations are:

$$x = \frac{R_1}{R_2} \Rightarrow \begin{cases} b_p = 1 \\ a_p = 0 \\ c_p = \frac{\mu_0 \cdot J_{\max}}{p} \cdot \frac{1}{(1-x^{2 \cdot p})} \cdot \frac{1}{R_2^{p-1}} \\ d_p = \frac{\mu_0 \cdot J_{\max}}{p} \cdot \frac{1}{(1-x^{2 \cdot p})} \cdot x^{2 \cdot p} \cdot R_2^{p+1} \end{cases}$$

which J_{\max} is the peak value of current density. The complete solutions resulting from both density currents are obtained by applying the superposition theorem:

$$A(r, \phi, K_Z^S, K_Z^R) = \frac{\mu_0 \cdot K_S}{p} \cdot \frac{1}{(1-x^{2 \cdot p})} \cdot \left(\frac{r^p}{R_2^{p-1}} + \frac{x^{2 \cdot p} \cdot R_2^{p+1}}{r^p} \right) \cdot \cos(p \cdot \phi) +$$

$$\frac{\mu_0 \cdot K_R}{n} \cdot \frac{1}{(1-x^{2 \cdot n})} \cdot \left(x^{2 \cdot n} \cdot \frac{r^n}{R_2^{n-1}} + \frac{R_2^{n+1}}{r^n} \right) \cdot \cos(n \cdot (\phi - \alpha))$$

The magnetic field density is:

$$B_r = \frac{1}{r} \cdot \frac{\partial A}{\partial \phi}$$

$$B_\phi = -\frac{\partial A}{\partial r}$$

$$B_r(r, \phi, K_Z^S, K_Z^R) = -\frac{\mu_0 \cdot K_S}{(1-x^{2 \cdot p})} \cdot \left(\frac{r^{p-1}}{R_2^{p-1}} + \frac{x^{2 \cdot p} \cdot R_2^{p+1}}{r^{p+1}} \right) \cdot \sin(p \cdot \phi) -$$

$$\frac{\mu_0 \cdot K_R}{(1-x^{2 \cdot n})} \cdot \left(x^{2 \cdot n} \cdot \frac{r^{n-1}}{R_2^{n-1}} + \frac{R_2^{n+1}}{r^{n+1}} \right) \cdot \sin(n \cdot (\phi - \alpha))$$

$$B_\phi(r, \phi, K_Z^S, K_Z^R) = -\frac{\mu_0 \cdot K_S}{(1-x^{2 \cdot p})} \cdot \left(\frac{r^{p-1}}{R_2^{p-1}} - \frac{x^{2 \cdot p} \cdot R_2^{p+1}}{r^{p+1}} \right) \cdot \cos(p \cdot \phi) -$$

$$\frac{\mu_0 \cdot K_R}{(1-x^{2 \cdot n})} \cdot \left(x^{2 \cdot n} \cdot \frac{r^{n-1}}{R_2^{n-1}} - \frac{R_2^{n+1}}{r^{n+1}} \right) \cdot \cos(n \cdot (\phi - \alpha))$$

the magnetic field energy is calculated as:

$$W_m = \frac{1}{2} \iiint_{Vol} A \cdot J \cdot dV$$

in this case the differential volume element is:

$$dV = r \cdot dr \cdot d\phi \cdot dz$$

The integration in z direction is simply the longitude L of the machine: only is necessary to integrate in r and in ϕ coordinates:

$$\begin{aligned} W_m &= \frac{1}{2} \iiint_{Vol} A \cdot J \cdot dV = \frac{1}{2} \int_{r_1}^{r_2} \int_0^{2\pi} A \cdot J \cdot r \cdot dr \cdot d\phi \cdot L = \\ &= \frac{L}{2} \int_0^{2\pi} [A(r=R_1) \cdot K_Z^R] \cdot R_1 \cdot d\phi + \frac{L}{2} \int_0^{2\pi} [A(r=R_2) \cdot K_Z^S] \cdot R_2 \cdot d\phi \end{aligned}$$

$$\begin{aligned} A(R_1) &= \frac{\mu_0 \cdot K_s}{p} \cdot \frac{2 \cdot x^p \cdot R_2}{(1-x^{2p})} \cdot \cos(p \cdot \phi) + \frac{\mu_0 \cdot K_R}{n} \cdot \frac{R_1 \cdot (x^{2n} + 1)}{(1-x^{2n})} \cdot \cos(n \cdot (\phi - \alpha)) \\ A(R_2) &= \frac{\mu_0 \cdot K_s}{p} \cdot \frac{R_2 \cdot (x^{2p} + 1)}{(1-x^{2p})} \cdot \cos(p \cdot \phi) + \frac{\mu_0 \cdot K_R}{n} \cdot \frac{2 \cdot xn \cdot R_1}{(1-x^{2n})} \cdot \cos(n \cdot (\phi - \alpha)) \end{aligned}$$

Substituting and integrating yields (all of the integrals are of the type $\cos(p\theta) \cdot \sin(n\theta)$ and these are different to zero only if $p = n$):

$$W_m = \frac{\mu_0 \cdot \pi}{2 \cdot p \cdot (1-x^{2p})} \cdot L \cdot \left\{ (K_R^2 \cdot R_1^2 + K_s^2 \cdot R_2^2) \cdot (1+x^{2p}) + 2 \cdot R_1 \cdot R_2 \cdot K_s \cdot K_R \cdot (2 \cdot x^p) \cdot \cos(p \cdot \phi) \right\}$$

The torque is obtained by derivation of the magnetic energy:

$$M = -\frac{\partial W_m}{\partial \phi} = \frac{\mu_0 \cdot \pi}{(1-x^{2p})} \cdot \{ R_1 \cdot R_2 \cdot L \cdot K_s \cdot K_R \cdot (2 \cdot x^p) \cdot \sin(p \cdot \phi) \}$$

If $x = 1 - \varepsilon \Rightarrow x^{2n} \cong 1 - 2 \cdot n \cdot \varepsilon$ and neglecting ε we can write:

$$M = \frac{\mu_0 \cdot \pi}{p \cdot \varepsilon} \cdot \{ R_1 \cdot R_2 \cdot L \cdot K_s \cdot K_R \cdot \sin(p \cdot \phi) \}$$

The same result can be obtained by use of the Maxwell Tensor:

$$\begin{aligned} \tau_\phi &= \mu_0 \cdot H_r \cdot H_\phi = \frac{1}{\mu_0} \cdot B_r \cdot B_\phi \\ M &= \int_0^{2\pi} \tau_\phi \cdot r \cdot d\phi = \int_0^{2\pi} \frac{1}{\mu_0} \cdot B_r \cdot B_\phi \cdot r \cdot d\phi \end{aligned}$$

Finally we can calculate the torque by using Laplace's law:

$$\begin{aligned} dF &= di \cdot l \cdot B_r \\ dM &= R_2 \cdot dF \end{aligned}$$

the current is:

$$di = J \cdot R_2 \cdot d\phi$$

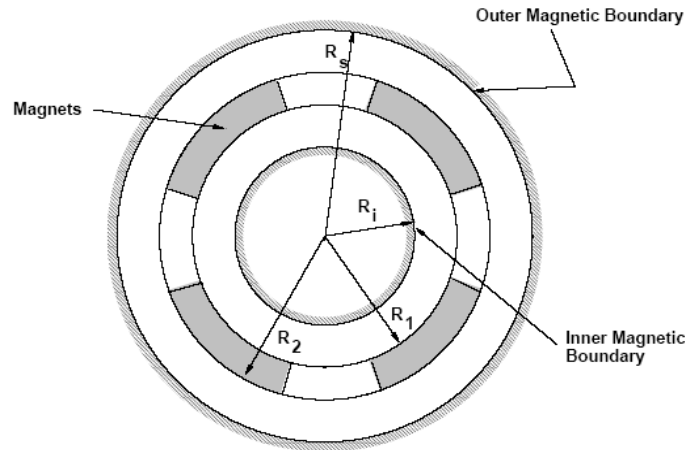
Finally the elemental torque is:

$$dM = R_2^2 \cdot L \cdot B_r(R_2) \cdot J \cdot d\phi$$

Integrating we can obtain the same value calculated by using magnetic energy.

Application. Permanent magnet field analysis

The assumed geometry is shown in the following figure. Assumed iron boundaries are at radii R_i and R_s . The permanent magnets, assumed to be polarized radially and alternately, are located between radii R_1 and R_2 . We assume there are p pole pairs and that each magnet subtends an electrical angle θ_{me} . The electrical angle is just p times the physical angle.



If the magnets are arranged so that the radially polarized magnets are located around the azimuthal origin ($\phi = 0$), the fundamental harmonic of space magnetization is:

$$M_r = M_0 \cdot \cos(p\phi)$$

where the fundamental magnitude is:

$$M_0 = \frac{4}{\pi} \cdot \frac{B_{rem}}{\mu_0} \cdot \sin\left(\frac{\theta_{me}}{2}\right) = \frac{4}{\pi} \cdot \frac{B_{rem}}{\mu_0} \cdot \sin\left(\frac{p \cdot \theta_m}{2}\right)$$

Since there is no current anywhere in this problem, it is convenient to treat the magnetic field as the gradient of a scalar potential:

$$H = -\nabla \psi$$

The divergence of this is:

$$\nabla^2 \psi = -\nabla \cdot H$$

Since magnetic flux density is divergence free ($\nabla \cdot B = 0$), we have:

$$\nabla \cdot H = -\nabla \cdot M$$

or

$$\nabla^2 \psi = -\nabla \cdot H = \nabla \cdot M = \frac{1}{r} \cdot M_0 \cdot \cos(p \cdot \phi)$$

Now, if we let the magnetic scalar potential be the sum of **particular** and **homogeneous** parts:

$$\psi = \psi_p + \psi_h$$

$$\nabla^2 \cdot \psi_h = 0$$

$$\nabla^2 \cdot \psi_p = \frac{1}{r} \cdot M_0 \cdot \cos(p \cdot \phi)$$

We can find a suitable solution to the particular part of this in the region of magnetization by using:

$$\psi_p = C \cdot r^\gamma \cdot \cos(p \phi)$$

Carrying out the Laplacian calculation on this:

$$\nabla^2 \psi_p = C \cdot r^{\gamma-2} \cdot (\gamma^2 - p^2) \cdot \cos(p \phi) = \frac{1}{r} \cdot M_0 \cdot \cos(p \cdot \phi)$$

which works if $\gamma = 1$, in which case:

$$\psi_p = \frac{M_0 \cdot r}{(1 - p^2)} \cdot \cos(p \phi)$$

Of course this solution holds only for the region of the magnets ($R_1 < r < R_2$), and is zero for the regions outside of the magnets. A suitable homogeneous solution satisfies Laplace's equation

$$\nabla^2 \cdot \psi_h = 0$$

and is in general of the form:

$$\psi_h = A \cdot r^p \cdot \cos(p \phi) + B \cdot r^{-p} \cdot \cos(p \phi)$$

then we may write a trial total solution for the flux density as:

$$\begin{aligned}
R_i < r < R_1 & \quad \psi = A_1 \cdot r^p \cdot \cos(p\phi) + B_1 \cdot r^{-p} \cdot \cos(p\phi) \\
R_1 < r < R_2 & \quad \psi = A_2 \cdot r^p \cdot \cos(p\phi) + B_2 \cdot r^{-p} \cdot \cos(p\phi) + \frac{M_0 \cdot r}{(1-p^2)} \cdot \cos(p\phi) \\
R_2 < r < R_s & \quad \psi = A_3 \cdot r^p \cdot \cos(p\phi) + B_3 \cdot r^{-p} \cdot \cos(p\phi)
\end{aligned}$$

The boundary conditions are the following:

- at the inner and outer boundaries at $r = R_i$ and $r = R_s$ require that the azimuthal field vanishes, or $\frac{\partial \psi}{\partial \phi} = 0$.
- At the magnet inner and outer radii, H_ϕ and B_r must be continuous:

$$\begin{aligned}
\blacksquare \quad H_\phi &= -\frac{1}{r} \cdot \frac{\partial \psi}{\partial \phi} \\
\blacksquare \quad B_r &= \mu_0 \cdot \left(-\frac{\partial \psi}{\partial r} + M_r \right)
\end{aligned}$$

After some algebraic transformations, we can obtain:

$$\begin{aligned}
A_1 &= -\frac{M_0}{2 \cdot (R_s^{2p} - R_i^{2p})} \cdot \left(\frac{p+1}{p^2-1} \cdot (R_1^{1-p} - R_2^{1-p}) \cdot R_s^{2p} + \frac{p-1}{p^2-1} \cdot (R_2^{1+p} - R_1^{1+p}) \right) \\
A_3 &= -\frac{M_0}{2 \cdot (R_s^{2p} - R_i^{2p})} \cdot \left(\frac{1}{1-p} \cdot (R_1^{1-p} - R_2^{1-p}) \cdot R_i^{2p} - \frac{1}{1+p} \cdot (R_2^{1+p} - R_1^{1+p}) \right) \\
B_1 &= -R_i^{2p} \cdot A_1 \\
B_3 &= -R_s^{2p} \cdot A_3
\end{aligned}$$

$$\begin{aligned}
\psi &= A_1 \cdot (r^p - R_i^{2p} \cdot r^{-p}) \cdot \cos(p\phi) \quad r < R_1 \\
\psi &= A_3 \cdot (r^p - R_s^{2p} \cdot r^{-p}) \cdot \cos(p\phi) \quad r > R_2
\end{aligned}$$

and:

$$r < R_1$$

$$H_r = \frac{M_0}{2 \cdot (R_s^{2p} - R_i^{2p})} \cdot \left(\frac{p}{p-1} \cdot (R_1^{1-p} - R_2^{1-p}) \cdot R_s^{2p} + \frac{p}{1+p} \cdot (R_2^{1+p} - R_1^{1+p}) \right) \cdot (r^{p-1} + R_i^{2p} \cdot r^{-p-1}) \cdot \cos(p\phi)$$

$$r > R_2$$

$$H_r = \frac{M_0}{2 \cdot (R_s^{2p} - R_i^{2p})} \cdot \left(\frac{p}{p-1} \cdot (R_1^{1-p} - R_2^{1-p}) \cdot R_i^{2p} + \frac{p}{1+p} \cdot (R_2^{1+p} - R_1^{1+p}) \right) \cdot (r^{p-1} + R_s^{2p} \cdot r^{-p-1}) \cdot \cos(p\phi)$$

The case of $p = 1$ appears to be a bit troublesome here, but this is easily handled by noting that:

$$\lim_{p \rightarrow 1} \frac{p}{p-1} \cdot (R_1^{1-p} - R_2^{1-p}) = \ln\left(\frac{R_2}{R_1}\right)$$

Special cases.

- Iron free case, $R_i \rightarrow 0, R_2 \rightarrow \infty$, this becomes:

$$r < R_1$$

$$H_r = \frac{M_0}{2} \cdot \left(\frac{p}{p-1} \cdot (R_1^{1-p} - R_2^{1-p}) \right) \cdot (r^{p-1}) \cdot \cos(p\phi)$$

$$\text{for } p = 1 \quad H_r = \frac{M_0}{2} \cdot \ln\left(\frac{R_2}{R_1}\right) \cdot \cos(p\phi)$$

$$r > R_2$$

$$H_r = \frac{M_0}{2} \cdot \left(\frac{p}{1+p} \cdot (R_2^{1+p} - R_1^{1+p}) \right) \cdot (r^{-p-1}) \cdot \cos(p\phi)$$

- Machines with iron boundaries and windings in slots. We are interested in the fields at the boundaries. In such a case, usually, either: $R_i = R_1$ or $R_s = R_2$. The fields are:

$$r = R_s$$

$$H_r = \frac{M_0 \cdot R_s^{p-1}}{(R_s^{2p} - R_i^{2p})} \cdot \left(\frac{p}{p+1} \cdot (R_2^{p+1} - R_1^{p+1}) + \frac{p}{p-1} \cdot R_i^{2p} (R_1^{1-p} - R_2^{1-p}) \right) \cdot \cos(p\phi)$$

$$r = R_i$$

$$H_r = \frac{M_0 \cdot R_i^{p-1}}{2 \cdot (R_s^{2p} - R_i^{2p})} \cdot \left(\frac{p}{p-1} \cdot (R_1^{1-p} - R_2^{1-p}) \cdot R_s^{2p} + \frac{p}{1+p} \cdot (R_2^{1+p} - R_1^{1+p}) \right) \cdot \cos(p\phi)$$

and the magnetic field density is:

$$r = R_s$$

$$B_r = \mu_0 \cdot H_r = \mu_0 \cdot \frac{M_0 \cdot R_s^{p-1}}{(R_s^{2p} - R_i^{2p})} \cdot \left(\frac{p}{p+1} \cdot (R_2^{p+1} - R_1^{p+1}) + \frac{p}{p-1} \cdot R_i^{2p} (R_1^{1-p} - R_2^{1-p}) \right) \cdot \cos(p\phi)$$

$$B_r = \mu_0 \cdot M_0 \cdot k_g \cdot \cos(p\phi)$$

$$k_g = \frac{R_s^{p-1}}{(R_s^{2p} - R_i^{2p})} \cdot \left(\frac{p}{p+1} \cdot (R_2^{p+1} - R_1^{p+1}) + \frac{p}{p-1} \cdot R_i^{2p} (R_1^{1-p} - R_2^{1-p}) \right)$$

k_g is a geometric factor that describes the geometry of the magnetic gap. The above case is valid for magnets inside and $p \neq 1$. For magnets inside and $p = 1$,

$$k_g = \frac{1}{(R_s^2 - R_i^2)} \cdot \left(\frac{1}{2} \cdot (R_2^2 - R_1^2) + R_i^2 \cdot \ln\left(\frac{R_2}{R_1}\right) \right)$$

For the case of magnets outside and $p \neq 1$:

$$k_g = \frac{R_i^{p-1}}{(R_s^{2p} - R_i^{2p})} \cdot \left(\frac{p}{p+1} \cdot (R_2^{p+1} - R_1^{p+1}) + \frac{p}{p-1} \cdot R_s^{2p} (R_1^{1-p} - R_2^{1-p}) \right)$$

and for magnets outside and $p = 1$:

$$k_g = \frac{1}{(R_s^2 - R_i^2)} \cdot \left(\frac{1}{2} \cdot (R_2^2 - R_1^2) + R_s^2 \cdot \ln \left(\frac{R_2}{R_1} \right) \right)$$

Note that for the case of a small gap, in which both the physical gap g and the magnet thickness h_m are both much less than rotor radius, it is straightforward to show that all of the above expressions approach what one would calculate using a simple, one dimensional model for the permanent magnet:

$$k_g \rightarrow \frac{h_m}{h_m + g}$$

And this is the whole story for the winding in slot, narrow air gap, surface magnet machine.

Flux

The flux linked by a single, full pitched coil which spans an angle from zero to π/p is:

$$\Phi = \oint A \cdot dl = \int_0^{\pi/p} B_r \cdot r \cdot L \cdot d\phi$$

If we consider that B_r is sinusoidal distributed this will have a peak value of:

$$\Phi_p = \frac{2 \cdot R \cdot L \cdot B_r}{p}$$

Now if the actual winding has N_a turns and using the pitch and breadth factors, the total flux linked is simply:

$$\lambda_f = \frac{2 \cdot R \cdot L \cdot B_r}{p} \cdot N_a \cdot k_w$$

$$k_w = k_p \cdot k_b$$

$$k_p = \sin\left(\frac{\alpha}{2}\right) \rightarrow \alpha = 2\pi p \frac{N_p}{K}$$

$$k_b = \frac{\sin \frac{q \cdot \gamma}{2}}{q \cdot \sin \frac{q \cdot \gamma}{2}} \rightarrow \gamma = \frac{2\pi p}{K}$$

Where N_p is the coil span (in slots), K is the total number of slots in the stator and q is the number of slots by phase and pole.

NUMERICAL SOLUTION: BASIC METHODS

PDE	FUNCTIONAL
$\nabla^2 \Phi + k^2 \Phi = g$	$\frac{1}{2} \int_V \left[\nabla \Phi ^2 - k^2 \Phi^2 + 2g\Phi \right] dv$
$\nabla^2 \Phi + k^2 \Phi = 0$	$\frac{1}{2} \int_V \left[\nabla \Phi ^2 - k^2 \Phi^2 \right] dv$
$\nabla^2 \Phi - \frac{1}{k^2} \frac{d^2 \Phi}{dt^2} = 0$	$\frac{1}{2} \int_0^t \left(\int_V \left[\nabla \Phi ^2 - \frac{1}{k^2} \left(\frac{d\Phi}{dt} \right)^2 \right] dv \right) dt$
$\nabla^2 \Phi - k \frac{d\Phi}{dt} = 0$	$\frac{1}{2} \int_0^t \left(\int_V \left[\nabla \Phi ^2 - k\Phi \frac{d\Phi}{dt} \right] dv \right) dt$
$\nabla^2 \Phi = g$	$\frac{1}{2} \int_V \left[\nabla \Phi ^2 + 2g\Phi \right] dv$
$\nabla^2 \Phi = 0$	$\frac{1}{2} \int_V \left[\nabla \Phi ^2 \right] dv$
$ \nabla \Phi ^2 = \left(\frac{d\Phi}{dx} \right)^2 + \left(\frac{d\Phi}{dy} \right)^2 + \left(\frac{d\Phi}{dz} \right)^2$	

NUMERICAL SOLUTION: FUNDAMENTALS AND BASIC METHODS

General concepts

Frequently, a direct analytic solution of PDE is possible only for simple cases or under very restrictive assumptions. For the solution of detailed and realistic models, numerical methods are often the only alternative available. The goal of this chapter is to introduce a number of methods and simple examples, to familiarize the reader with numerical and practical issues in the solution of PDE's.

The main objective of a numerical method is to solve a PDE on a discrete set of points of the solution domain, called discretization. In order to do so, the solution domain is divided into subdomains having the discretization points as vertices. The distance between two adjacent vertices is the mesh size. Time is also subdivided into discrete intervals, and we call timestep the interval between two consecutive times at which the solution is obtained. The PDE is then approximated, or discretized, to obtain a system of algebraic equations, where the unknowns are the solution values at the discretization points. This system of algebraic equations can then be solved on a computer by direct or iterative techniques. It is important to realize that the discretization step replaces the original equation with a new one, and that even an exact solution of the discretized problem will yield an approximate solution of the original PDE, since we introduce a discretization error.

Classification of electromagnetic (EM) problems

EM problems are classified in terms of the equations describing them. The equations could be differential or integral or both. Most EM problems can be stated in terms of an operator equation

$$L\Phi = g$$

where L is an operator (differential, integral, or integro-differential), g is the known source, and Φ is the unknown function to be determined. For example in the electrostatic problem involving Poisson's equation:

$$\nabla^2 V = -\frac{\rho}{\epsilon}$$

So that

$$L = -\nabla^2$$

$$g = \frac{\rho}{\varepsilon}$$

$$\Phi = V$$

As observed before, EM problems involve linear second order partial differential equations. In general, a second order partial differential equations (PDE) is given by (2D formulation):

$$a \frac{\partial^2 \Phi}{\partial x^2} + b \frac{\partial^2 \Phi}{\partial y \partial x} + c \frac{\partial^2 \Phi}{\partial y^2} + d \frac{\partial \Phi}{\partial x} + e \frac{\partial \Phi}{\partial y} + f \Phi = g$$

The coefficients a, b, and c in general are functions of x and y; they may also depend on Φ itself, in which case the PDE is said to be **nonlinear**. A PDE in which g is equals to zero is termed **homogeneous**; it is **inhomogeneous** if $g \neq 0$.

A PDE in general can have both **boundary values and initial values**. PDEs whose boundary conditions are specified are called **steady-state equations**. If only initial values are specified, they are called **transient equations**.

Any linear second order PDE can be classified as **elliptic, hyperbolic, or parabolic** depending on the coefficients a, b, and c. The above equation is said to be:

- elliptic if $b^2 - 4 \cdot a \cdot c < 0$
- hyperbolic if $b^2 - 4 \cdot a \cdot c > 0$
- parabolic if $b^2 - 4 \cdot a \cdot c = 0$

Elliptic equations are associated with steady-state phenomena, i.e., boundary value problems. Typical examples of this type of equation include Laplace's and Poisson's equations:

$$\begin{aligned}\nabla^2 A &= -\mu \cdot J \\ \nabla^2 A &= 0\end{aligned}$$

Hyperbolic PDE arise in propagation problems. A typical example is the wave equation:

$$\nabla^2 V - \mu \cdot \varepsilon \cdot \frac{\partial^2 V}{\partial t^2} = -\frac{\rho}{\varepsilon}$$

Parabolic PDEs are generally associated with problems in which the quantity of interest varies slowly in comparison with the random motions which produce the variations. The most common parabolic PDE is the diffusion or heat equation:

$$\begin{aligned}\nabla^2 A - \mu \cdot \sigma \cdot \frac{\partial A}{\partial t} &= -\mu \cdot J \\ \nabla^2 T - \frac{c}{\lambda} \cdot \frac{\partial T}{\partial t} &= -\frac{Q}{\lambda}\end{aligned}$$

Another type of problem is called **eigenvalue**. The standard eigenproblem is of the form:

$$L\Phi = \lambda\Phi$$

A more general version is the **generalized eigenproblem** having the form:

$$L\Phi = \lambda M\Phi$$

where M , like L , is a linear operator for EM problems. In this equation only some particular values of λ called **eigenvalues** are valid; associated with these values are the corresponding functions Φ called **eigenfunctions**. Eigenproblems are usually encountered in vibration and waveguide problems where the eigenvalues correspond to physical quantities such as resonance and cut-off frequencies, respectively.

Many equations of practical importance may be of a mixed type, or not easily identifiable according to one of the above categories. Nevertheless, the distinction between elliptic, parabolic, and hyperbolic equations provides a very useful guideline for the selection of solution procedures.

There are many approaches which are used for the discretization of the original PDE to obtain a numerical problem. The most important discretization approaches can be classified as

- **Finite Differences**
- **Finite Elements**
- **Boundary elements**
- **Moment's method**
- **Monte Carlo method**
- **Other methods**

In the following pages we explain the formulation of the Finite Differences method and thus we explain the Variational principles, that are common to the Finite elements, Boundary elements and Moment's methods. Before this common introduction we explain about the formulation of each method. Finally we present the Montecarlo method that is an non-deterministic method.

After discretization, it is necessary to check if the approximation is appropriate or if the discretized model can produce a solution at all when programmed into a computer code. For a successful solution, the numerical scheme must be **stable, convergent and consistent**.

- The scheme is **stable** if the solution stays bounded during the solution procedure.
- The scheme is **convergent** if the numerical solution tends to the real solution as the mesh size and the time-step tend to zero.
- The scheme is **consistent** if the truncation error tends to zero as the mesh size and the time-step tend to zero.

If a numerical scheme is consistent, then stability is a necessary and sufficient condition to achieve convergence. A scheme which is stable but not consistent may converge to a solution of a different equation (with which it is consistent). A number of errors are introduced when a PDE is discretized and solved numerically. To summarize, we have:

- **Truncation error** - the error introduced by the finite approximation of the derivatives.
- **Discretization error** - the error in the solution due to the replacement of the continuous equation with a discretized one.
- **Round-off error** - the computational error introduced by digital algorithms, due to the finite number of digits used in the numerical representation.

The round-off error is random, and normally increases when the mesh size is decreased. Conversely, the discretization error decreases with the mesh size, since more mesh points (i.e. more resolution) are introduced.

Finite Differences

The finite difference approach is the most popular discretization technique, owing to its simplicity. Finite difference approximations of derivatives are obtained by using truncated Taylor series. Consider the following Taylor expansions

$$u(x + \Delta x) = u(x) + \Delta x \cdot \frac{\partial u}{\partial x} + O(\Delta x)$$

$$u(x - \Delta x) = u(x) - \Delta x \cdot \frac{\partial u}{\partial x} + O(\Delta x)$$

The first order derivative is given by the following approximations:

- Forward Difference

$$\frac{\partial u}{\partial x} = \frac{u(x + \Delta x) - u(x)}{\Delta x}$$

- Backward Difference

$$\frac{\partial u}{\partial x} = \frac{u(x) - u(x - \Delta x)}{\Delta x}$$

- Central Difference

$$\frac{\partial u}{\partial x} = \frac{u(x + \Delta x) - u(x - \Delta x)}{2 \cdot \Delta x}$$

An approximation for the second order derivative is obtained by use of forward and backward difference:

$$\frac{\partial^2 u}{\partial x^2} = \frac{u(x + \Delta x) - 2 \cdot u(x) + u(x - \Delta x)}{(\Delta x)^2}$$

Finite Differences for Laplace's and Poisson's equations

Let us consider Poisson's equation for homogeneous materials in two-dimensional Cartesian coordinates:

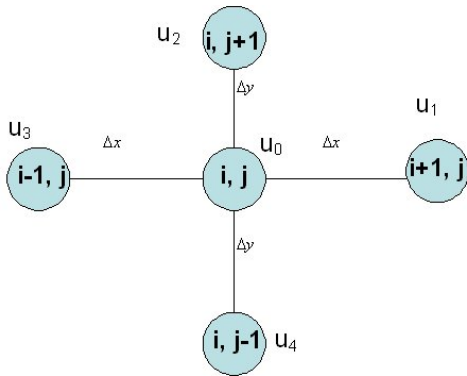
$$k \left(\frac{\partial^2 u}{\partial x^2} + \frac{\partial^2 u}{\partial y^2} \right) = f(x, y)$$

where k is a material property. Using the above approximations we obtain:

$$\frac{\partial^2 u}{\partial x^2} = \frac{u(x + \Delta x) - 2 \cdot u(x) + u(x - \Delta x)}{(\Delta x)^2} = \frac{u_{i+1,j} - 2 \cdot u_{i,j} + u_{i-1,j}}{(\Delta x)^2}$$

$$\frac{\partial^2 u}{\partial y^2} = \frac{u(y + \Delta y) - 2 \cdot u(y) + u(y - \Delta y)}{(\Delta y)^2} = \frac{u_{i,j+1} - 2 \cdot u_{i,j} + u_{i,j-1}}{(\Delta y)^2}$$

Substituting into the Poisson's equation, we obtain:



$$\Delta y \cdot \frac{u_{i+1,j} - 2 \cdot u_{i,j} + u_{i-1,j}}{\Delta x} + \Delta x \cdot \frac{u_{i,j+1} - 2 \cdot u_{i,j} + u_{i,j-1}}{\Delta y} = \frac{f(x, y)}{k} \cdot \Delta x \cdot \Delta y$$

This equation is written for each node in the problem to obtain a set of simultaneous equations. These equations are singular. Only when the potential of at least one of the nodes is specified, the solution of these are possible. We see that for Poisson's equation, the right-hand side is the source function multiplied by the area of the finite difference cell. That is the total source in the cell.

Interfaces between materials

Consider the following figure, in which we have a five-point FD scheme and a boundary between two materials. Here we solve the case of an electrostatic problem. If we assume that the interface has no charge, then the application of Gauss's law will give us an equation for the potential at node 0 that includes the effect of the material interface. Using the dotted line of the difference cell as the Gaussian surface (for simplicity, we use $\Delta x = \Delta y = h$), we obtain:

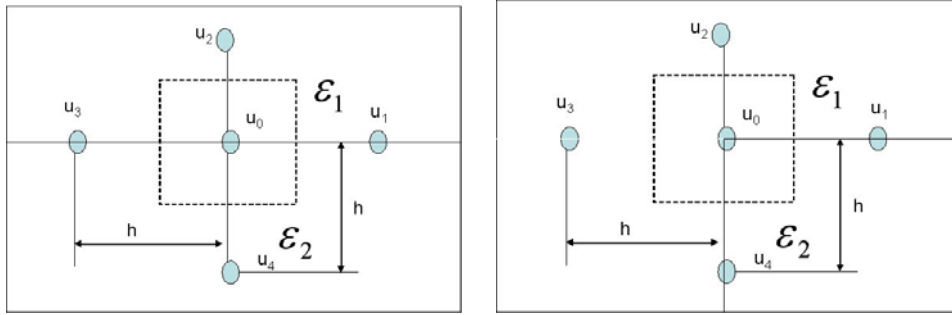
$$\left. \begin{aligned} \iint D \cdot dS &= \iint \epsilon E dS = 0 \\ E &= \frac{dU}{dn} \end{aligned} \right\} \iint \epsilon \frac{dU}{dn} dS \approx \sum \epsilon_i \cdot \frac{\Delta U}{\Delta n} \cdot \frac{h}{2} = 0$$

$$\sum \epsilon_i \cdot \frac{\Delta U}{\Delta n} \cdot \frac{h}{2} =$$

$$\epsilon_1 \cdot \frac{u_0 - u_1}{h} \cdot \frac{h}{2} + \epsilon_1 \cdot \frac{u_0 - u_2}{h} \cdot \frac{h}{2} + \epsilon_1 \cdot \frac{u_0 - u_3}{h} \cdot \frac{h}{2} + \epsilon_2 \cdot \frac{u_0 - u_3}{h} \cdot \frac{h}{2} + \epsilon_2 \cdot \frac{u_0 - u_4}{h} \cdot \frac{h}{2} + \epsilon_2 \cdot \frac{u_0 - u_1}{h} \cdot \frac{h}{2} = 0$$

Rearranging terms, we obtain:

$$2 \cdot u_0 \cdot (\epsilon_1 + \epsilon_2) = \frac{\epsilon_1 + \epsilon_2}{2} \cdot u_1 + \epsilon_1 \cdot u_2 + \frac{\epsilon_1 + \epsilon_2}{2} \cdot u_3 + \epsilon_2 \cdot u_4$$

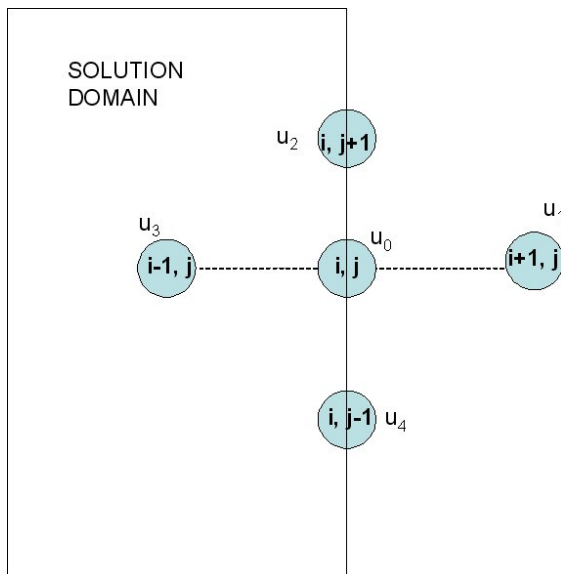


The above figure shows the special case of the corner. Using the same procedure showed above, we obtain the following equation:

$$u_0 \cdot (3 \cdot \varepsilon_1 + \varepsilon_2) = \frac{\varepsilon_1 + \varepsilon_2}{2} \cdot u_1 + \varepsilon_1 \cdot u_2 + \varepsilon_1 \cdot u_3 + \frac{\varepsilon_1 + \varepsilon_2}{2} \cdot u_4$$

Neumann Boundary conditions

For Poisson's equations to have a unique solution, either the potential or the normal derivative of the potential must be specified at every point on the boundary (only 1 point is necessary). If the potential is specified, this is a Dirichlet condition and the unknown nodal potential is eliminated. If the normal derivative is specified, then we can proceed as follows. Consider the following figure.



The potential at point (i,j) is unknown. The point (i+1,j) is outside to the domain of the solution. We express the normal derivative at (i,j) as:

$$\frac{\partial u}{\partial n} = \frac{\partial u}{\partial x} \approx \frac{u_1 - u_3}{2 \cdot \Delta x}$$

Solving this equation for exterior point:

$$u_1 = 2 \cdot \Delta x \cdot \frac{\partial u}{\partial n} + u_3$$

$$u_{i+1,j} = 2 \cdot \Delta x \cdot \frac{\partial u}{\partial n} + u_{i-1,j}$$

Substituting this value in the general finite difference cell

$$\Delta y \cdot \frac{u_{i+1,j} - 2 \cdot u_{i,j} + u_{i-1,j}}{\Delta x} + \Delta x \cdot \frac{u_{i,j+1} - 2 \cdot u_{i,j} + u_{i,j-1}}{\Delta y} = \frac{f(x,y)}{k} \cdot \Delta x \cdot \Delta y$$

we obtain:

$$\Delta y \cdot \frac{2 \cdot \Delta x \cdot \frac{\partial u}{\partial n} - 2 \cdot u_{i,j} + 2 \cdot u_{i-1,j}}{\Delta x} + \Delta x \cdot \frac{u_{i,j+1} - 2 \cdot u_{i,j} + u_{i,j-1}}{\Delta y} = \frac{f(x,y)}{k} \cdot \Delta x \cdot \Delta y$$

A special but very common case is the homogeneous Neumann boundary condition where $\frac{\partial u}{\partial n} = 0$. In this case the equipotential lines are perpendicular to the surface. In this case:

$$u_{i+1,j} = u_{i-1,j}$$

And the equation for the cell becomes:

$$\Delta y \cdot \frac{-2 \cdot u_{i,j} + 2 \cdot u_{i-1,j}}{\Delta x^2} + \Delta x \cdot \frac{u_{i,j+1} - 2 \cdot u_{i,j} + u_{i,j-1}}{\Delta y} = \frac{f(x,y)}{k} \cdot \Delta x \cdot \Delta y$$

Equivalent circuit representation

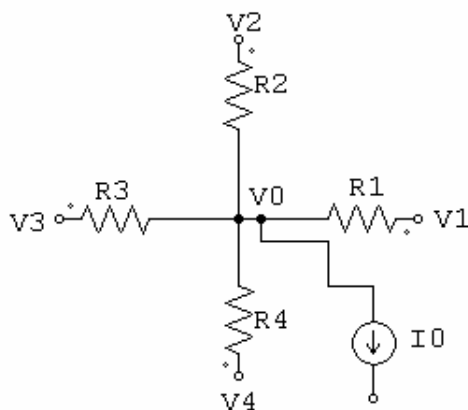
We wish show that the finite difference expression has an equivalent circuit representation. In fact, circuit simulators, such as SPICE, have been used to solve field problems by the use of these equivalent networks. Consider the same finite difference cell showed in the above pages:

$$\Delta y \cdot \frac{u_1 - 2 \cdot u_0 + u_3}{\Delta x^2} + \Delta x \cdot \frac{u_2 - 2 \cdot u_0 + u_4}{\Delta y} = \frac{f(x,y)}{k} \cdot \Delta x \cdot \Delta y$$

This equation can be written as:

$$\frac{u_1 - u_0}{\frac{1}{k} \cdot \frac{\Delta x}{\Delta y}} + \frac{u_3 - u_0}{\frac{1}{k} \cdot \frac{\Delta x}{\Delta y}} + \frac{u_2 - u_0}{\frac{1}{k} \cdot \frac{\Delta y}{\Delta x}} + \frac{u_4 - u_0}{\frac{1}{k} \cdot \frac{\Delta y}{\Delta x}} = f(x,y) \cdot \Delta x \cdot \Delta y$$

The equation for the following circuit, can be written as:



$$\frac{V_1 - V_0}{R_1} + \frac{V_3 - V_0}{R_2} + \frac{V_2 - V_0}{R_3} + \frac{V_4 - V_0}{R_4} = I_0$$

The two above equations have the same form. Identifying terms:

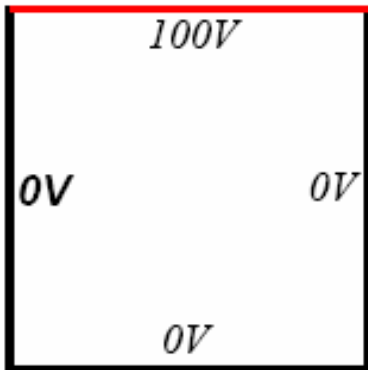
$$V_0 = u_0; V_1 = u_1; V_2 = u_2; V_3 = u_3; V_4 = u_4$$

$$R_1 = R_3 = \frac{1}{k} \cdot \frac{\Delta x}{\Delta y}; \quad R_2 = R_4 = \frac{1}{k} \cdot \frac{\Delta y}{\Delta x}$$

$$I_0 = f(x,y) \cdot \Delta x \cdot \Delta y$$

It is obvious that the nodal voltages have the same **numeric value** as the nodal potential on the finite differences mesh.

Exercise. Consider a square with the upper side connected to a 100 V voltage source and the other side connected to ground (0 V). Determine the potential inside the square.



In this case the governing equation is the Laplace's equation, i.e.: $\nabla^2 u = 0$. Also it is convenient to assign a regular mesh, i.e. $\Delta x = \Delta y$. The equation for a node is reduced to:

$$u_{i+1,j} - 2 \cdot u_{i,j} + u_{i-1,j} + u_{i,j+1} - 2 \cdot u_{i,j} + u_{i,j-1} = 0$$

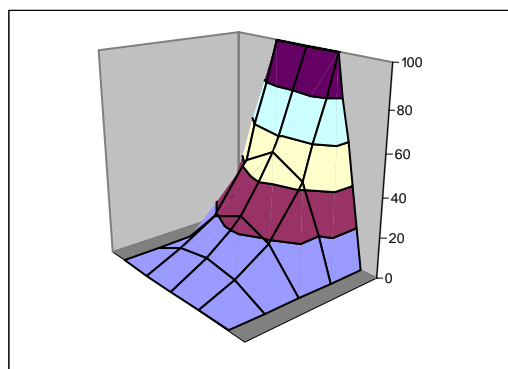
$$u_{i,j} = \frac{u_{i+1,j} + u_{i-1,j} + u_{i,j+1} + u_{i,j-1}}{4}$$

The potential in the centered point is the average of the potential in the surrounding nodes. The solution can be calculated by using of a spreadsheet.

	A	B	C	D	E
1	0	100	100	100	0
2	0	(B1+B3+A2+C2)/4	(C1+C3+B2+D2)/4	(D1+D3+C2+E2)/4	0
3	0	(B2+B4+A3+C3)/4	(C2+C4+B3+D3)/4	(D2+D4+C3+E3)/4	0
4	0	(B3+B5+A4+C4)/4	(C3+C5+B4+D4)/4	(D3+D5+C4+E4)/4	0
5	0	0	0	0	0

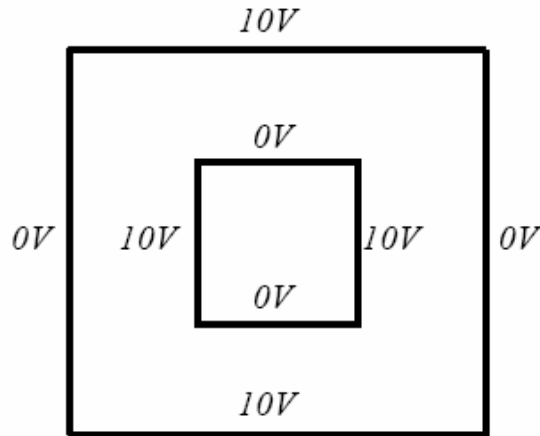
The above figure shows the implementation of this set of equations. On the boundaries, we assign directly the known value and at the interior point we insert the above equation. Using the "iteration mode" in the options menu of the spreadsheet we can solve the problem by iteration (we must select a convergence criterion, for example difference between two consecutive iterations less than 0.01 or the number of iterations must be less than 1000). The solution is shown in the following picture.

	A	B	C	D	E
1	0	100	100	100	0
2	0	42.857572	52.6790006	42.8573574	0
3	0	18.7504292	25.0004292	18.7502146	0
4	0	7.14307172	9.82164315	7.14296443	0
5	0	0	0	0	0



In this case the number of iterations was 26, and the error was less than 0.02. It is obvious that if you use a high density mesh, you can obtain more accurate results.

Exercise to solve. Determine the potential inside this box.



Finite Differences for 1-D Parabolic Equations

We consider here the 1-D diffusion equation

$$a \frac{\partial^2 u}{\partial x^2} = \frac{\partial u}{\partial t}$$

which is discretized in space and time with uniform mesh intervals Δx and time-step Δt . A simple approach is to discretize the time derivative with a forward difference as

$$\frac{\partial u}{\partial t} \cong \frac{u_{i,n+1} - u_{i,n}}{\Delta t}$$

The solution is known at time t_n and a new solution must be found at time $t_{n+1} = t_n + \Delta t$. Starting from the initial condition at $t_1 = 0$, the time evolution is constructed after each time-step either **explicitly**, by direct evaluation of an expression obtained from the discretized equation, or **implicitly**, when solution of a system of equations is necessary.

An explicit approach is readily implemented by substituting the space derivative with the 3-point finite difference evaluated at the current time-step. The algorithm, written for a generic point i of the discretization, is

$$u_{i,n+1} = u_{i,n} + a \cdot \frac{\Delta t}{(\Delta x)^2} \cdot (u_{i-1,n} - 2 \cdot u_{i,n} + u_{i+1,n})$$

Defining $\alpha = a \cdot \frac{\Delta t}{(\Delta x)^2}$, we can write the following matrix equation for the whole system with N point mesh:

$$\begin{bmatrix} u_{1,n+1} \\ u_{2,n+1} \\ \dots \\ u_{N,n+1} \end{bmatrix} = \begin{bmatrix} 1-2\cdot\alpha & \alpha & 0 & \dots & 0 \\ \alpha & 1-2\cdot\alpha & \alpha & \dots & 0 \\ 0 & \dots & \dots & \dots & 0 \\ \dots & \dots & \dots & \dots & \dots \\ 0 & \dots & \dots & \alpha & 1-2\cdot\alpha \end{bmatrix} \cdot \begin{bmatrix} u_{1,n} \\ u_{2,n} \\ \dots \\ u_{N,n} \end{bmatrix}$$

It is easy to show that this system of equations is stable if, and only if:

$$0 < \alpha \leq \frac{1}{2}$$

$$0 < a \cdot \frac{\Delta t}{(\Delta x)^2} \leq \frac{1}{2}$$

In general, the time step must be very small in order to get good results from the explicit approach. Further, if we refine the mesh we must reduce the time step, so in order to achieve high accuracy, the computation time becomes very expensive.

Implicit schemes

A fairly general implicit scheme is obtained by approximation for the space derivative with a weighted average of the finite difference approximation at t_n and t_{n+1} and the time derivative is approximated by a forward difference:

$$a \cdot \frac{\partial^2 u}{\partial x^2} \cong a \cdot \frac{u_{i-1,n} - 2 \cdot u_{i,n} + u_{i+1,n}}{(\Delta x)^2} \cdot (1-\lambda) + a \cdot \frac{u_{i-1,n+1} - 2 \cdot u_{i,n+1} + u_{i+1,n+1}}{(\Delta x)^2} \cdot \lambda$$

$$\frac{\partial u}{\partial t} \cong \frac{u_{i,n+1} - u_{i,n}}{\Delta t}$$

writing the equation in terms of $\alpha = a \cdot \frac{\Delta t}{(\Delta x)^2}$:

$$\alpha \cdot (1-\lambda) \cdot u_{i-1,n} + (1-2\cdot\alpha + 2\cdot\alpha \cdot \lambda) \cdot u_{i,n} + \alpha \cdot (1-\lambda) \cdot u_{i+1,n} + \alpha \cdot \lambda \cdot u_{i-1,n+1} -$$

$$-(2\cdot\alpha \cdot \lambda + 1) \cdot u_{i,n+1} + \alpha \cdot \lambda \cdot u_{i+1,n+1} = 0$$

- When $\lambda = 1$, the scheme is a forward difference equation
- The classic Crank-Nicholson scheme is obtained when $\lambda = 0.5$ and
- when $\lambda = 0$ the explicit scheme is recovered (backward difference equation)

To determine the stability of the method we look at the eigenvalues of the matrix. For the Crank-Nicholson scheme, the matrix equation is:

$$\begin{bmatrix} 2+2\cdot\alpha & -\alpha & 0 & \dots & 0 \\ -\alpha & 2+2\cdot\alpha & -\alpha & \dots & 0 \\ 0 & \dots & \dots & \dots & 0 \\ \dots & \dots & \dots & \dots & \dots \\ 0 & \dots & \dots & -\alpha & 2+2\cdot\alpha \end{bmatrix} \cdot \begin{bmatrix} u_{1,n+1} \\ u_{2,n+1} \\ \dots \\ u_{N,n+1} \end{bmatrix} = \begin{bmatrix} 2-2\cdot\alpha & \alpha & 0 & \dots & 0 \\ \alpha & 2-2\cdot\alpha & \alpha & \dots & 0 \\ 0 & \dots & \dots & \dots & 0 \\ \dots & \dots & \dots & \dots & \dots \\ 0 & \dots & \dots & \alpha & 2-2\cdot\alpha \end{bmatrix} \cdot \begin{bmatrix} u_{1,n} \\ u_{2,n} \\ \dots \\ u_{N,n} \end{bmatrix}$$

$$C \cdot U_{n+1} = S \cdot U_n$$

The matrix C is non-singular and we can solve for the unknowns at the end of the time step as:

$$U_{n+1} = C^{-1} S \cdot U_n = T \cdot U_n$$

We can find the solution at any time step from the initial conditions and a power of the matrix T, so:

$$U_{n+k} = T^{k-1} \cdot U_n$$

In order to ensure stability the eigenvalues of the T matrix must all have magnitude less than 1. These eigenvalues are given by:

$$\lambda_k = \frac{2 - 4 \cdot \alpha \cdot \sin^2\left(\frac{k \cdot \pi}{2N}\right) - 2}{2 + 4 \cdot \alpha \cdot \sin^2\left(\frac{k \cdot \pi}{2N}\right) - 2}$$

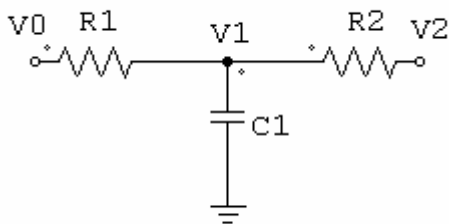
Where N is the order of the matrix. This expression lies between -1 and +1 for any values of α , so the Crank-Nicholson method is stable.

Equivalent circuit representation

Consider the same finite difference cell showed in the above pages:

$$u_{1,n+1} = u_{1,n} + a \cdot \frac{\Delta t}{(\Delta x)^2} \cdot (u_{0,n} - 2 \cdot u_{1,n} + u_{2,n})$$

This equation can be written as:



$$\frac{u_{0,n} - u_{1,n}}{(\Delta x)} + \frac{u_{2,n} - u_{1,n}}{(\Delta x)} + \frac{(\Delta x)}{a} \cdot \frac{u_{1,n+1} - u_{1,n}}{\Delta t} = 0$$

The equation for the circuit showed, can be written as:

$$\frac{V_0 - V_1}{R_1} + \frac{V_2 - V_1}{R_2} + C_1 \frac{dV_1}{dt} = 0$$

And if we discretize the above equation with respect to time, we obtain:

$$\frac{V_{0,n} - V_{1,n}}{R_1} + \frac{V_{2,n} - V_{1,n}}{R_2} + C_1 \frac{V_{1,n+1} - V_{1,n}}{\Delta t} = 0$$

The two above equations have the same form. Identifying terms:

$$V_{0,n} = u_{0,n}; \quad V_{1,n} = u_{1,n}; \quad V_{2,n} = u_{2,n}$$

$$R_1 = R_2 = \Delta x; \quad C_1 = \frac{\Delta x}{a}$$

It is obvious that the nodal voltages have the same **numeric value** as the nodal potential on the finite differences mesh.

Exercise. Solve the following problem:

$$\nabla^2 U = k \cdot \frac{dU}{dt}$$

With: $k=1$ and $0 < t \leq 0.1 \text{ sec}$
 $0 \leq x \leq 1$

$$U(x,0) = 100$$

And the following boundary conditions: $U(0,t) = 0$

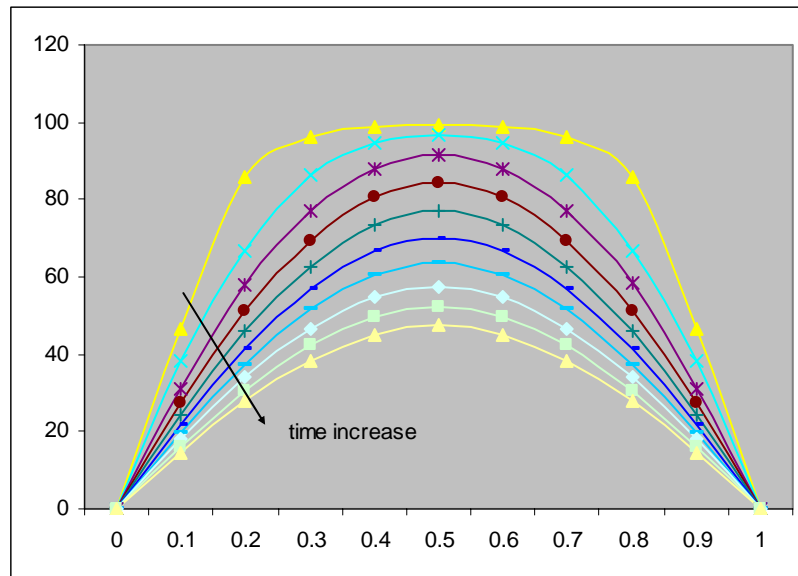
$$U(1,t) = 0$$

To solve this problem we can use a grid with $\Delta x = 0.1$ and the Crank-Nicholson method.
 $\Delta t = 0.01$

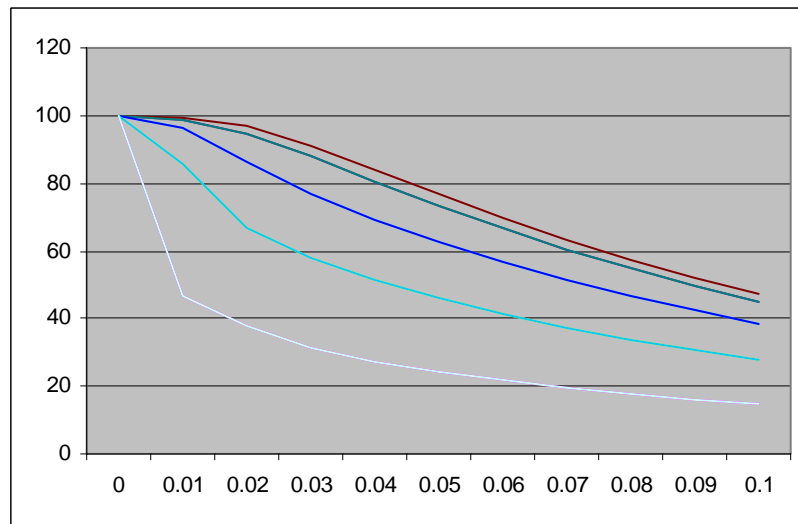
The solution can be calculated by the use of spreadsheet. See the following pictures.

dx	0	0.1	0.2	0.3	0.4	0.5	0.6	0.7	0.8	0.9	1	time
0	100	100	100	100	100	100	100	100	100	100	0	0
0	46	86	96	99	99	99	99	96	86	46	0	0.01
0	38	67	87	95	97	97	95	87	67	38	0	0.02
0	31	58	77	88	91	88	77	58	31		0	0.03
0	27	51	69	80	84	80	69	51	27		0	0.04
0	24	46	63	73	77	73	63	46	24		0	0.05
0	22	41	57	67	70	67	57	41	22		0	0.06
0	20	37	51	60	64	60	51	37	20		0	0.07
0	18	34	47	55	58	55	47	34	18		0	0.08
0	16	31	42	50	52	50	42	31	16		0	0.09
0	15	28	38	45	47	45	38	28	15		0	0.1

The following figure shows the potential at each point (horizontal-axis \rightarrow x coordinate) and each curve represents an interval of time.



The following figure shows the evolution of the potential at each node of the mesh as a function of time (horizontal axis \rightarrow time)



Monte Carlo methods

The Monte Carlo methods are probabilistic numerical methods employed in solving mathematical and physical problems. They are a method of approximately solving problems using sequences of random numbers. Monte Carlo methods are applied in two ways:

- Simulation, for example to simulate a neutron's motion into a reactor wall: its zigzag path being imitated by a random walk.
- Sampling, refers to methods of deducing properties of a large set of elements by studying only a small, random subset. For example, the average value of $f(x)$ over $a < x < b$ can be estimated from its average over a finite number of points selected randomly in the interval. This amounts to a Monte Carlo method of numerical integration.

Here, won't detail the generation of random numbers and variables. You can find this information in any book on statistics.

Numerical Integration

Suppose we wish to evaluate the integral

$$I = \int_R f$$

where R is an n -dimensional space. Let $X = (X^1, X^2, \dots, X^n)$ be a random variable that is uniformly distributed in R . Then $f(X)$ is a random variable whose mean value and variance is given by

$$\overline{f(X)} = \frac{1}{|R|} \int_R f = \frac{1}{|R|}$$

$$\text{Var}(f(X)) = \frac{1}{|R|} \int_R f^2 - \left(\frac{1}{|R|} \int_R f \right)^2$$

where

$$|R| = \int_R dX$$

If we take N independent samples of X , i.e., X_1, X_2, \dots, X_N , all having the same distribution as X and form the average

$$\frac{f(X_1) + f(X_2) + \dots + f(X_N)}{N} = \frac{1}{N} \sum_{i=1}^N f(X_i)$$

we might expect this average to be close to the mean of $f(X)$. Thus we can write:

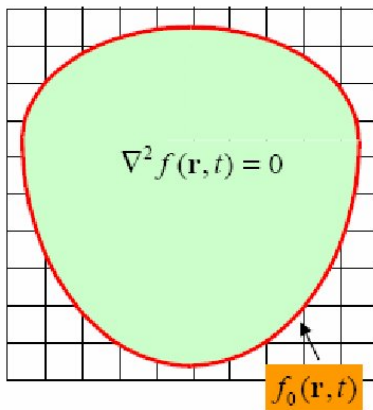
$$I \cong \frac{|R|}{N} \sum_{i=1}^N f(X_i)$$

For one-dimensional and two-dimensional integrals by application of the above equation, we obtain:

$$I = \int_a^b f(x)dx \cong \frac{b-a}{N} \sum_{i=1}^N f(X_i)$$

$$I = \int_a^b \int_c^d f(x)dx dy \cong \frac{(b-a) \cdot (d-c)}{N} \sum_{i=1}^N f(X^1_i, X^2_i)$$

Fixed Random Walk method to solve potential problems



Suppose that the Monte Carlo method is applied to solve Laplace's equation in a region R, subject to Dirichlet boundary conditions:

$$\nabla^2 f = 0$$

$$V = f_0(r, t)$$

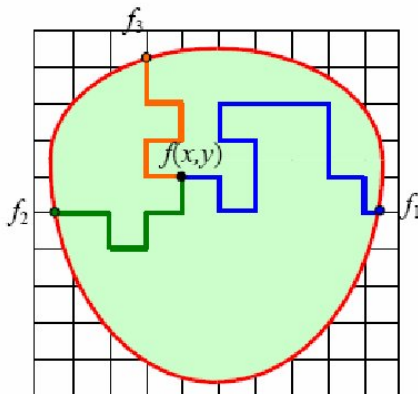
We begin by dividing R into mesh and replacing ∇^2 by its finite difference equivalent equation. The final equation is written as:

$$f(x, y) = p_{x+} \cdot f(x+h, y) + p_{x-} \cdot f(x-h, y) + p_{y+} \cdot f(x, y+h) + p_{y-} \cdot f(x, y-h)$$

where:

$$p_{x+} = p_{x-} = p_{y+} = p_{y-} = 1/4$$

A square grid of mesh size Δ is assumed. The equation may be given a probabilistic interpretation. If a random walking particle is instantaneously at the point (x, y) , it has probabilities $p_{x+}, p_{x-}, p_{y+}, p_{y-}$ of moving from (x, y) to $(x+\Delta, y); (x-\Delta, y); (x, y+\Delta); (x, y-\Delta)$, respectively. A means of determining which way the particle should move is to generate a random number λ , $0 < \lambda < 1$ and instruct the particle to walk as follows:



$$0 < \lambda < 1/4 \Rightarrow (x, y) \rightarrow (x+h, y)$$

$$1/4 < \lambda < 1/2 \Rightarrow (x, y) \rightarrow (x-h, y)$$

$$1/2 < \lambda < 3/4 \Rightarrow (x, y) \rightarrow (x, y+h)$$

$$3/4 < \lambda < 1 \Rightarrow (x, y) \rightarrow (x, y-h)$$

To calculate the potential at (x, y) , a random walking particle is instructed to start at that point. The particle proceeds to wander from node to node in the grid until it reaches the boundary. When it does, the walk is terminated and the prescribed potential V_p at this boundary point is recorded. This value is denoted by f_1 . Then a second particle is released from (x, y) and allowed to wander until it reaches a boundary point, where the walk is terminated

and the corresponding value of the potential is recorded as f_2 . This procedure is repeated for N times. The expected value of this set of potentials is the solution to the problem, i.e.:

$$f(x, y) = \frac{1}{N} \sum_{i=1}^{i=N} f_i$$

where N , the total number of walks, is large. We can repeat this process for the whole set of grid points to obtain the solution at each point. If you need to solve the Poisson's equation

$$\begin{aligned} \nabla^2 V &= -g(x, y) \\ V &= V_p \end{aligned}$$

Then the FD representation is:

$$f(x, y) = p_{x+} \cdot f(x+h, y) + p_{x-} \cdot f(x-h, y) + p_{y+} \cdot f(x, y+h) + p_{y-} \cdot f(x, y-h) + \frac{\Delta^2 g}{4}$$

and the final term must be recorded at each step of the random walk. If m_i steps are required for the i^{th} random walk originating at (x, y) to reach the boundary, then one records

$$f_i + \frac{\Delta^2}{4} \sum_{j=1}^{j=m_i-1} g(x_j, y_j)$$

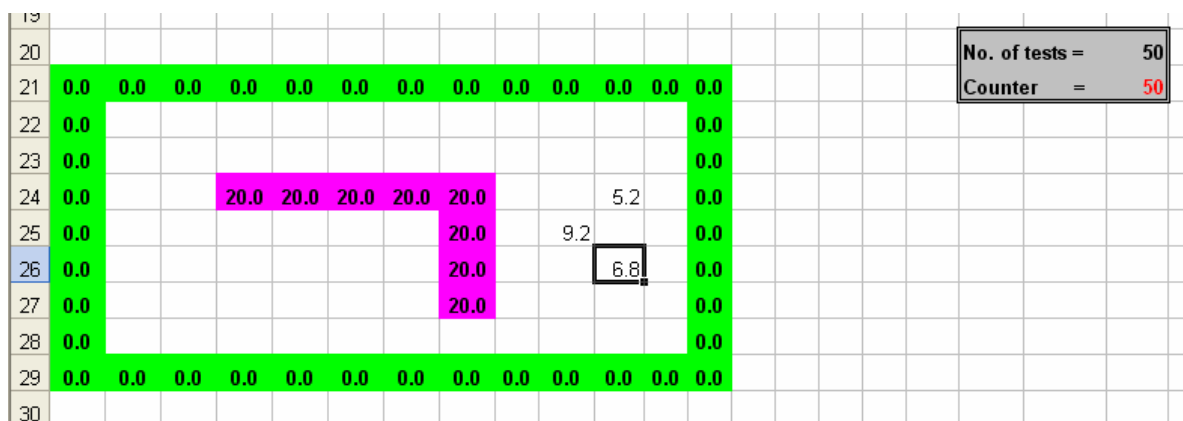
Thus the solution can be expressed as

$$f(x, y) = \frac{1}{N} \sum_{i=1}^{i=N} f_i + \frac{\Delta^2}{4 \cdot N} \sum_{i=1}^{i=N} \left(\sum_{j=1}^{j=m_i-1} g(x_j, y_j) \right)$$

The following figure shows an Excel implementation of this methodology (montec.xls). You must draw the whole system. The boundary values are indicated by colours:

- Dirichlet boundaries: paint the cells and insert the known value.
- Neumann boundaries: paint the cell grey.

Afterwards, select the cell where you wish to calculate the potential and press the start button (not shown in this picture); after the prescribed number of tests (50 in this case) the calculated value is shown.



Note that the area must be closed. If this is open, the solution can't be reached.

Approximation techniques

Consider the following problem: The resolution of a system of differential (or integral) equations established in the general form:

$$\begin{aligned} L(\Phi) - f &= 0 \\ C(\{\Phi\}) &= 0 \end{aligned}$$

where L is a linear operator (for example ∇^2), f is a known function, and Φ is the unknown function to be determined. The operator L is specified in region Ω surrounded by the boundary Γ . Proper boundary conditions (C) are specified on Γ . The function Φ_0 where the subscript represents the exact solution of the problem can be approximated by assuming that it varies according to a set of known functions, each of them multiplied by an unknown coefficient. These approximate function coefficients, whose number can be increased to increase the precision of the results, can then be determined by solving a system of equations. Depending to the approximation method we obtain different equations and methods such as: finite elements, boundary elements, moment's method and others (including finite differences method!) A common feature of all the methods applied is that the approximate solution is assumed to be the finite sum

$$\Phi_n = \varphi_0 + \sum_{j=1}^{j=n} a_j \cdot \varphi_j$$

where φ_j are the known trial (or basis) functions and a_j are the coefficients to be calculated. Differences between the methods appear in the process of determination of coefficients a_j . The trial functions should be linearly independent and form a complete set in region Ω . Function φ_0 is usually specified in order to satisfy Dirichlet boundary conditions on Γ .

We introduce here the so-called residual R_n :

$$L(\Phi_n) - f = R_n$$

The residual function R varies in the domain. Consider now how to distribute the R function. The concept common to all of the methods is that the coefficients a_j are evaluated by orthogonalization of residual R_n to a certain set of n weighting functions w_i , i.e., by zeroing the inner product:

$$\langle R_n, w_i \rangle = \int_{\Omega} R_n \cdot w_i \cdot d\Omega = 0, \quad i = 1, 2, \dots, n$$

Substituting, a set of n simultaneous linear algebraic equations is obtained. The general form is:

$$\langle f - L\varphi_0, w_i \rangle = \sum_{j=1}^{j=n} a_j \cdot \langle w_i, L\varphi_j \rangle$$

If the inner product of two functions defined above

$$\langle u, v \rangle = \int_{\Omega} u \cdot v^* \cdot d\Omega$$

Has the following properties:

$$\begin{aligned}
\langle u, v \rangle &= \langle u, v \rangle^* \\
\langle a_1 u_1 + a_2 u_2, v \rangle &= a_1 \langle u_1, v \rangle + a_2 \langle u_2, v \rangle \\
\langle u, v \rangle &> 0 \text{ if } u \neq 0 \\
\langle u, v \rangle &= 0 \text{ if } u = 0
\end{aligned}$$

We can see that this is symmetric and positively defined. In this case the Variational method (Rayleigh-Ritz method) may be applied. The approximate solution of $L\Phi = g$ is determined as the minimum of the energy functional I_n :

$$I(\Phi) = \langle L\Phi, \Phi \rangle - 2\langle \Phi, g \rangle$$

Substituting the trial functions and minimizing this by partial derivation with respect to each coefficient,

$$\frac{\partial I}{\partial a_1} = \frac{\partial I}{\partial a_2} = \frac{\partial I}{\partial a_n} = 0$$

we obtain the following set of simultaneous equations:

$$\begin{bmatrix} \langle L\phi_1, \phi_1 \rangle & \langle L\phi_1, \phi_2 \rangle & \langle L\phi_1, \phi_N \rangle \\ \cdot & \cdot & \cdot \\ \cdot & \cdot & \cdot \\ \langle L\phi_N, \phi_1 \rangle & \langle L\phi_N, \phi_2 \rangle & \langle L\phi_N, \phi_N \rangle \end{bmatrix} \cdot \begin{bmatrix} a_1 \\ a_2 \\ \cdot \\ a_N \end{bmatrix} = \begin{bmatrix} \langle g, \phi_1 \rangle \\ \langle g, \phi_2 \rangle \\ \dots \\ \langle g, \phi_N \rangle \end{bmatrix}$$

For Laplace's and Poisson's equations and their variations the following table of functionals are applicable.

PDE	FUNCTIONAL
$\nabla^2 \Phi + k^2 \Phi = g$	$\frac{1}{2} \int_V [\nabla \Phi ^2 - k^2 \Phi^2 + 2g\Phi] dv$
$\nabla^2 \Phi + k^2 \Phi = 0$	$\frac{1}{2} \int_V [\nabla \Phi ^2 - k^2 \Phi^2] dv$
$\nabla^2 \Phi - \frac{1}{k^2} \frac{d^2 \Phi}{dt^2} = 0$	$\frac{1}{2} \int_{t_0}^t \left(\int_V [\nabla \Phi ^2 - \frac{1}{k^2} \left(\frac{d\Phi}{dt} \right)^2] dv \right) dt$
$\nabla^2 \Phi - k \frac{d\Phi}{dt} = 0$	$\frac{1}{2} \int_{t_0}^t \left(\int_V [\nabla \Phi ^2 - k\Phi \frac{d\Phi}{dt}] dv \right) dt$
$\nabla^2 \Phi = g$	$\frac{1}{2} \int_V [\nabla \Phi ^2 + 2g\Phi] dv$
$\nabla^2 \Phi = 0$	$\frac{1}{2} \int_V [\nabla \Phi ^2] dv$
$ \nabla \Phi ^2 = \left(\frac{d\Phi}{dx} \right)^2 + \left(\frac{d\Phi}{dy} \right)^2 + \left(\frac{d\Phi}{dz} \right)^2$	

Depending on the weighting function we can obtain different equations to solve.

$$\langle R_n, w_i \rangle = \int_{\Omega} R_n \cdot w_i \cdot d\Omega = 0, \quad i = 1, 2, \dots, n$$

The following table shows the weighting functions and the equations to be solved for each approximation method (for the one-dimensional problem).

- **Moment method.** The weighting functions is the simplest: $1, x, x^2, \dots, x^n$ (for a one dimensional problem). In this way some high order moments of the residual can be set to zero.
- **Point collocation.** In this case N points are chosen in the domain and the residual is set to zero on these points. This operation can be interpreted as defining the weighting functions in terms of Dirac impulse.
- **Sub-domain collocation.** The method is similar to the collocation method described above but now the residual is required to be zero over a certain region, rather than a series of points.
- **Least squares.** In this case we minimize the square of the residual.
- **Galerkin.** In this case the weighting function is the same as the approximating functions.
- **Raleygh- Ritz method (functional minimization).**

Method	Weighting functions	Determination procedure of linear algebraic equations
1. Moments	$w_i = x^i \quad i = 0, 1, 2, \dots$	$\int_{\Omega} R_n \cdot x^i \cdot d\Omega = 0, \quad i = 1, 2, \dots, n$
2. Point collocation	$w_i = \delta(x - x_i)$	$R_n = 0$
3. Sub-domain collocation	$\delta_i = \begin{cases} 1 & a_i \leq x \leq b_i \\ 0 & \text{otherwise} \end{cases}$	$\int_{a_i}^{b_i} R_n \cdot d\Omega = 0$
4. Least squares	$w_i = \frac{\partial R_n}{\partial a_i}$	$\int_a^b R_n \cdot \frac{\partial R_n}{\partial a_i} \cdot d\Omega = 0$
5. Galerkin	$w_i = \varphi_i$	$\int_a^b R_n \cdot \varphi_i \cdot d\Omega = 0$
6. Rayleigh-Ritz	-----	$\frac{\partial I}{\partial a_1} = \frac{\partial I}{\partial a_2} = \frac{\partial I}{\partial a_n} = 0$ (usually the resultant equations are the same as obtained on the Galerkin method)

Example. Solve the following equation by application of each approximation method.

$$\frac{\partial^2 \Phi}{\partial x^2} = -x^2: \quad \Phi(0) = 0 \quad \Phi(1) = 0$$

This equation has the exact solution: $\Phi(x) = \frac{x}{12}(1-x^3)$

We select the following trial functions: $\bar{\Phi}(x) = a_1 \cdot \sin(\pi x) + a_2 \cdot \sin(2\pi x)$ for methods from 2 to 6.

$$\Phi_n = \varphi_0 + \sum_{j=1}^{j=n} a_j \cdot \varphi_j \quad \begin{aligned} \varphi_0 &= 0 \\ \varphi_1 &= \sin(\pi x) \\ \varphi_2 &= \sin(2\pi x) \end{aligned}$$

1. Moment method. We select the following trial function, a simple polynomial in x, which after satisfaction of the boundary conditions results in (for the sake of simplicity only two terms will be considered → only the first two moments are equal to zero):

$$\Phi = x(1-x^2) \cdot (a_1 + a_2 \cdot x)$$

The residual is:

$$R_n = -6 \cdot a_1 \cdot x + a_2 \cdot (2 - 12 \cdot x^2) + x^2$$

and the system of equations to solve is:

$$\begin{aligned} \int_0^1 (-6 \cdot a_1 \cdot x + a_2 \cdot (2 - 12 \cdot x^2) + x^2) \cdot dx &= 0 \\ \int_0^1 (-6 \cdot a_1 \cdot x + a_2 \cdot (2 - 12 \cdot x^2) + x^2) \cdot x \cdot dx &= 0 \end{aligned}$$

The values of the unknown coefficients are:

$$\begin{aligned} a_1 &= \frac{1}{12} \\ a_2 &= \frac{1}{24} \end{aligned}$$

2. Point collocation. We select the following matching points:

$$w_1 = \delta(x - 1/3) \quad w_2 = \delta(x - 2/3)$$

The residual is

$$\begin{aligned} R_n(x) &= \frac{\partial^2 \bar{\Phi}}{\partial x^2} + x^2 = \frac{\partial^2 (a_1 \cdot \sin(\pi x) + a_2 \cdot \sin(2\pi x))}{\partial x^2} + x^2 = \\ &= -a_1 \cdot \pi^2 \cdot \sin(\pi x) - a_2 \cdot \pi^2 \cdot 4 \cdot \sin(2\pi x) + x^2 \end{aligned}$$

and the system of equations to solve is:

$$\begin{aligned} R_n(1/3) &= 0 = -a_1 \cdot \pi^2 \cdot \sin(\pi/3) - a_2 \cdot \pi^2 \cdot 4 \cdot \sin(2\pi/3) + (1/3)^2 \\ R_n(2/3) &= 0 = -a_1 \cdot \pi^2 \cdot \sin(2\pi/3) - a_2 \cdot \pi^2 \cdot 4 \cdot \sin(4\pi/3) + (2/3)^2 \end{aligned}$$

The values of the unknown coefficients are:

$$a_1 = 0.0324987$$

$$a_2 = -0.004847$$

3.Sub-domain collocation. We select the following domains:

$$\delta_1 = 1 \quad 0 \leq x \leq 1/2 \quad \delta_2 = 1 \quad 1/2 \leq x \leq 1$$

The residual is determined as

$$\int_0^{1/2} (-a_1 \cdot \pi^2 \cdot \sin(\pi x) - a_2 \cdot \pi^2 \cdot 4 \cdot \sin(2\pi x) + x^2) \cdot dx = 0$$

$$\int_{1/2}^1 (-a_1 \cdot \pi^2 \cdot \sin(\pi x) - a_2 \cdot \pi^2 \cdot 4 \cdot \sin(2\pi x) + x^2) \cdot dx = 0$$

The values of the unknown coefficients are:

$$a_1 = 0.053052$$

$$a_2 = -0.01989$$

4. Least squares. The residual and the equations to solve are:

$$R_n(x) = -a_1 \cdot \pi^2 \cdot \sin(\pi x) - a_2 \cdot \pi^2 \cdot 4 \cdot \sin(2\pi x) + x^2$$

$$\frac{\partial R_n}{\partial a_1} = -\pi^2 \cdot \sin(\pi x); \quad \frac{\partial R_n}{\partial a_2} = -\pi^2 \cdot 4 \cdot \sin(2\pi x)$$

$$\int_0^1 (-a_1 \cdot \pi^2 \cdot \sin(\pi x) - a_2 \cdot \pi^2 \cdot 4 \cdot \sin(2\pi x) + x^2) \cdot (-\pi^2 \cdot \sin(\pi x)) \cdot dx = 0$$

$$\int_0^1 (-a_1 \cdot \pi^2 \cdot \sin(\pi x) - a_2 \cdot \pi^2 \cdot 4 \cdot \sin(2\pi x) + x^2) \cdot (-\pi^2 \cdot 4 \cdot \sin(2\pi x)) \cdot dx = 0$$

The values of the unknown coefficients are:

$$a_1 = 0.03836$$

$$a_2 = -0.03225$$

5 and 6. Galerkin and Rayleigh-Ritz methods. These two methods have the same equations to solve.

$$w_i = \varphi_i$$

$$\int_a^b R_n \cdot \varphi_i \cdot d\Omega = 0$$

$$\int_0^1 (-a_1 \cdot \pi^2 \cdot \sin(\pi x) - a_2 \cdot \pi^2 \cdot 4 \cdot \sin(2\pi x) + x^2) \cdot (\sin(\pi x)) \cdot dx = 0$$

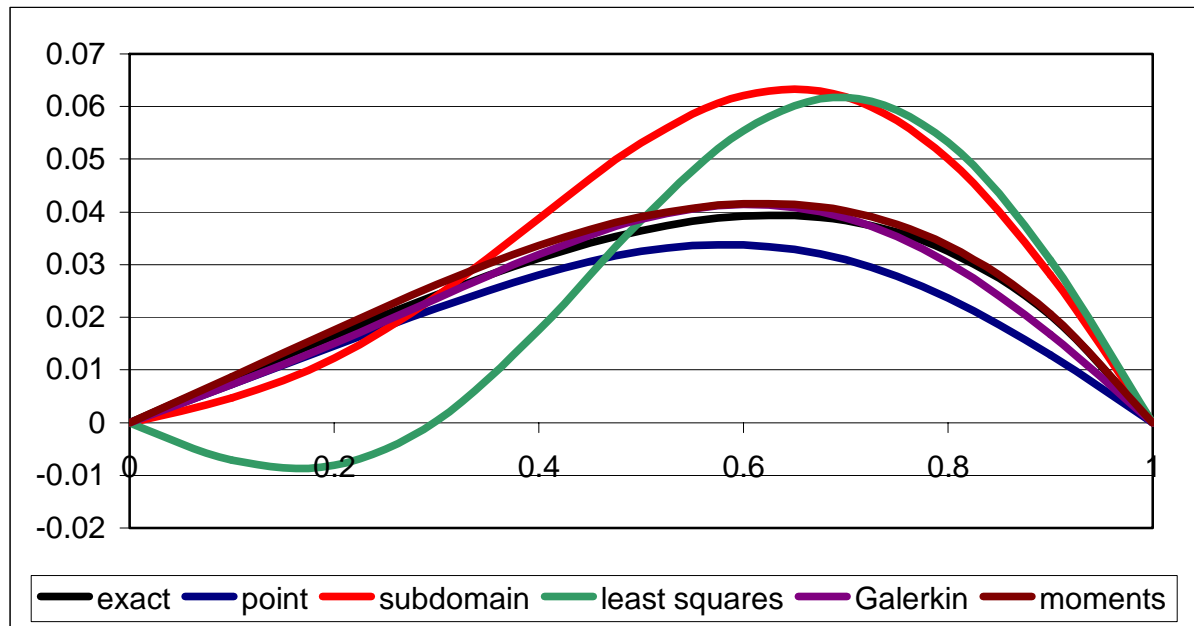
$$\int_0^1 (-a_1 \cdot \pi^2 \cdot \sin(\pi x) - a_2 \cdot \pi^2 \cdot 4 \cdot \sin(2\pi x) + x^2) \cdot (\sin(2\pi x)) \cdot dx = 0$$

The values of the unknown coefficients are:

$$a_1 = 0.03861$$

$$a_2 = -0.00806$$

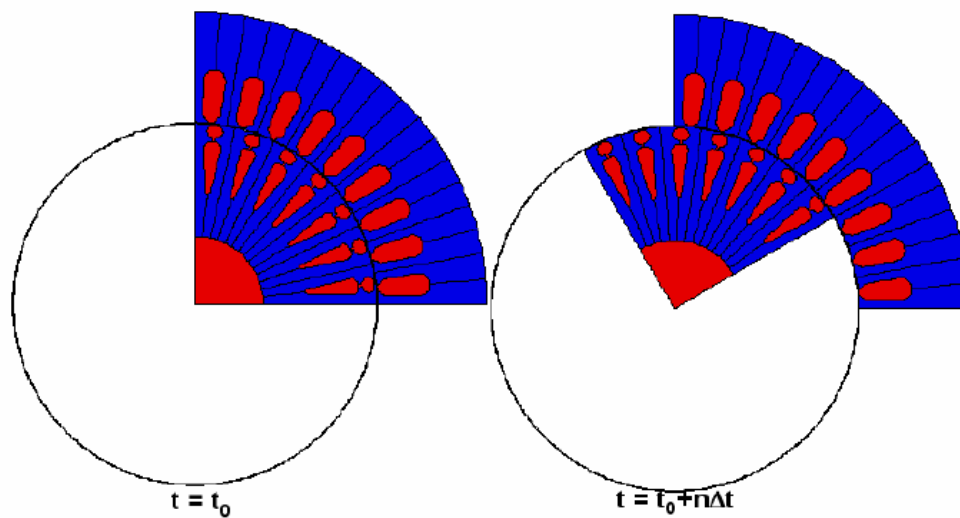
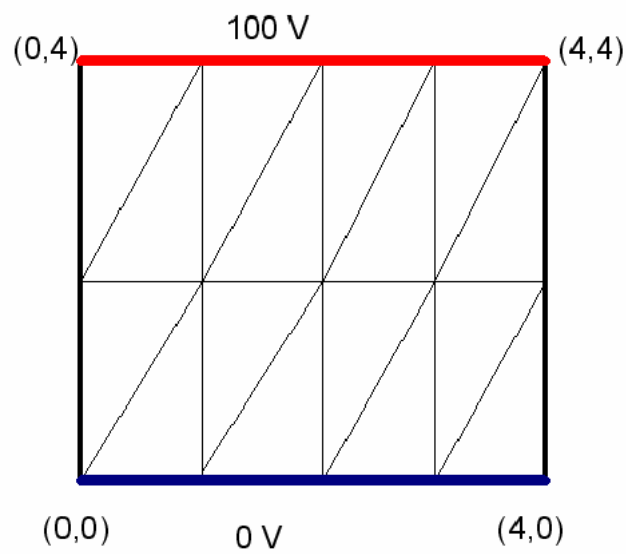
The following figure shows the exact and approximate solutions. The Galerkin and the moment's method have the best accuracy. Note that the moment's method approximation function includes the exact solution in its formulation.



x	exact	moments	point	subdomain	least squares	Galerkin
0.000	0.000	0.000	0.000	0.000	0.000	0.000
0.100	0.008	0.009	0.007	0.005	-0.007	0.007
0.200	0.017	0.018	0.014	0.012	-0.008	0.015
0.300	0.024	0.026	0.022	0.024	0.000	0.024
0.400	0.031	0.034	0.028	0.039	0.018	0.032
0.500	0.036	0.039	0.032	0.053	0.038	0.039
0.600	0.039	0.042	0.034	0.062	0.055	0.041
0.700	0.038	0.040	0.031	0.062	0.062	0.039
0.800	0.033	0.034	0.024	0.050	0.053	0.030
0.900	0.020	0.021	0.013	0.028	0.031	0.017
1.000	0.000	0.000	0.000	0.000	0.000	0.000

The Galerkin and the moment method are the most accurate. Note that the moment method approximation function includes the exact solution in its formulation.

NUMERICAL SOLUTION: FINITE ELEMENT METHOD



FINITE ELEMENT METHOD

ONE DIMENSIONAL FINITE ELEMENT ANALYSIS

The boundary value problem to be considered is defined by the ODE:

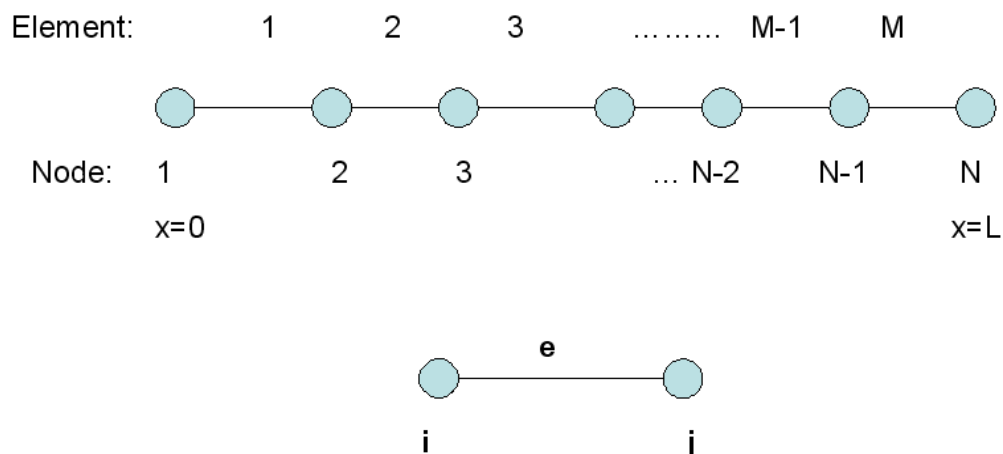
$$-\frac{d}{dx}\left(\alpha \frac{d\Phi}{dx}\right) + \beta\Phi = f \quad x \in (0, L)$$

where Φ is the unknown function, α and β are known parameters and f is a known source. The boundary conditions for Φ are given by:

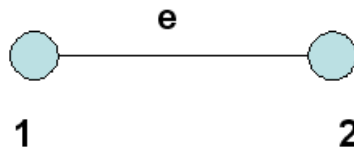
$$\begin{aligned} \Phi|_{x=0} &= p \\ \alpha \frac{d\Phi}{dx} + \gamma\Phi \Big|_{x=L} &= q \end{aligned}$$

Discretization and interpolation

The first step is to divide the solution domain $(0, L)$ into small subdomains, which in this case will be short line segments. Let l^e ($e = 1, 2, 3, \dots, M$) denote the length of the e th segment, with M being the total number of segments. Further, let x_i ($i = 1, 2, 3, \dots, N$) denote the position of the i th node with $x_1 = 0$ and $x_N = L$. Both elements and nodes are numbered in order from left to right as shown in the next figure.



To keep the formulation consistent with two and three dimensional cases, we adopt a local numbering system in the formulation. In the following, the superscript e is used to denote the quantity with a local number as a subscript, while for all other quantities the subscript is a global number.



The local and global systems are related by:

$$x_1^e = x_e$$

$$x_2^e = x_{e+1}$$

$$\text{for } e = 1, 2, \dots, M$$

The second step is to select the interpolation functions. We use linear functions. Within the e th element $\Phi(x)$ may be approximated by:

$$\Phi^e(x) = a^e + b^e x \quad (1)$$

where a^e and b^e are the constant to be determined. For linear elements, there are two nodes associated with each element: one located at x_1^e and the other at x_2^e . Specifying (1) at these two nodes yields:

$$\Phi_1^e = a^e + b^e x_1^e$$

$$\Phi_2^e = a^e + b^e x_2^e$$

where Φ_1^e denotes the value of $\Phi(x)$ at x_1^e . Then solving for a^e and b^e we obtain:

$$b^e = \frac{\Phi_2^e - \Phi_1^e}{l^e}$$

$$a^e = \Phi_1^e - \frac{\Phi_2^e - \Phi_1^e}{l^e} \cdot x_1^e$$

$$l^e = x_2^e - x_1^e$$

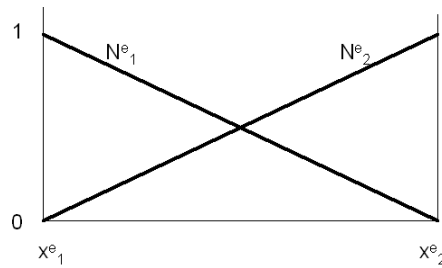
Substituting in (1) we obtain:

$$\Phi^e(x) = \left[\frac{x_2^e - x}{l^e} \right] \cdot \Phi_1^e + \left[\frac{x - x_1^e}{l^e} \right] \cdot \Phi_2^e = \sum_{j=1}^2 N_j^e(x) \cdot \Phi_j^e$$

$$N_1^e(x) = \frac{x_2^e - x}{l^e}$$

$$N_2^e(x) = \frac{x - x_1^e}{l^e}$$

N functions are called the interpolation or basis functions.



Formulation

The third step is the formulation of the system of equations. We can use the Variational approach or the residual weighting formulation (Galerkin method). The residual for the Galerkin method is:

$$r = -\frac{d}{dx}\left(\alpha \frac{d\Phi}{dx}\right) + \beta\Phi - f$$

and for each element the residual can be written as:

$$R_i^e = \int_{x_1^e}^{x_2^e} N_i^e r dx \quad i=1,2$$

We use N_i^e as weighting functions. Substituting we obtain:

$$R_i^e = \int_{x_1^e}^{x_2^e} N_i^e \left(-\frac{d}{dx}\left(\alpha \frac{d\Phi}{dx}\right) + \beta\Phi \right) dx - \int_{x_1^e}^{x_2^e} N_i^e f dx$$

integrating by parts for the first term on the right hand side, we obtain:

$$\left(\begin{array}{l} u = N_i^e \\ dv = -\left(\alpha \frac{d\Phi}{dx}\right) \end{array} \right) \Rightarrow \int u dv = uv - \int v du$$

$$R_i^e = \int_{x_1^e}^{x_2^e} \left(\alpha \frac{dN_i^e}{dx} \frac{d\Phi}{dx} \right) + \beta N_i^e \Phi dx - \int_{x_1^e}^{x_2^e} N_i^e f dx - \alpha N_i^e \frac{d\Phi}{dx} \Big|_{x_1^e}^{x_2^e}$$

The substitution of $\Phi^e(x) = \sum_{j=1}^2 N_j^e(x) \Phi_j^e$ leads to the equation:

$$R_i^e = \sum_{j=1}^2 \Phi_j^e \left(\int_{x_1^e}^{x_2^e} \left(\alpha \frac{dN_i^e}{dx} \frac{dN_j^e}{dx} \right) + \beta N_i^e N_j^e \right) dx - \int_{x_1^e}^{x_2^e} N_i^e f dx - \alpha N_i^e \frac{d\Phi}{dx} \Big|_{x_1^e}^{x_2^e} \right)$$

and in matrix form it becomes:

$$(R^e) = (K^e)(\Phi^e) - (b^e) - (g^e) \quad (3)$$

where:

$$K_{i,j}^e = \int_{x_1^e}^{x_2^e} \left(\alpha \frac{dN_i^e}{dx} \frac{dN_j^e}{dx} \right) + \beta N_i^e N_j^e \right) dx$$

$$b_i^e = \int_{x_1^e}^{x_2^e} N_i^e f dx$$

$$g_i^e = \alpha N_i^e \frac{d\Phi}{dx} \Big|_{x_1^e}^{x_2^e}$$

$$(\Phi^e) = \begin{pmatrix} \Phi_1^e \\ \Phi_2^e \end{pmatrix}$$

We note that (K^e) is symmetric and, if α and β are constants or can be approximated by constants within each element, matrix elements can be evaluated analytically; the result is:

$$K_{11}^e = K_{22}^e = \frac{\alpha^e}{l^e} + \frac{\beta^e}{3l^e}$$

$$K_{12}^e = K_{21}^e = -\frac{\alpha^e}{l^e} + \frac{\beta^e}{6l^e}$$

$$b_1^e = b_2^e = f^e \frac{l^e}{2}$$

With the elemental equation given in (3), we can proceed to form the system of equations by summing it over all elements:

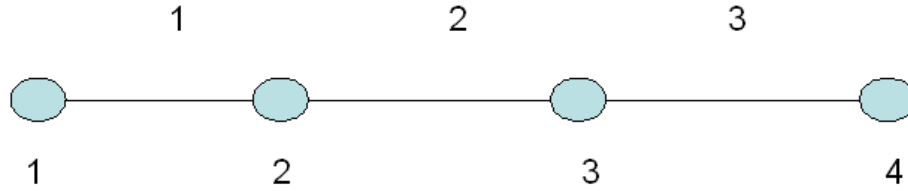
$$(R) = \sum_{e=1}^M (R^e) = \sum_{e=1}^M [(K^e)(\Phi^e) - (b^e) - (g^e)] = 0$$

which can be written as

$$(K)(\Phi) = (b) + (g)$$

Assembly of the equations

To illustrate the assembly of equations, we consider a case within three elements and four nodes.



Using the relationship between the global and local node numbers, we can expand (K^e) into a 4x4 matrix and (Φ^e) into a 4x1 column. These, for the first element can be expanded as:

$$(K^1) = \begin{pmatrix} K_{11}^1 & K_{12}^1 & 0 & 0 \\ K_{21}^1 & K_{22}^1 & 0 & 0 \\ 0 & 0 & 0 & 0 \\ 0 & 0 & 0 & 0 \end{pmatrix}; \quad (\Phi^1) = \begin{pmatrix} \Phi_1^1 \\ \Phi_2^1 \\ 0 \\ 0 \end{pmatrix}$$

and their product becomes:

$$(K^1)(\Phi^1) = \begin{pmatrix} K_{11}^1 & K_{12}^1 & 0 & 0 \\ K_{21}^1 & K_{22}^1 & 0 & 0 \\ 0 & 0 & 0 & 0 \\ 0 & 0 & 0 & 0 \end{pmatrix} \begin{pmatrix} \Phi_1^1 \\ \Phi_2^1 \\ 0 \\ 0 \end{pmatrix} = \begin{pmatrix} K_{11}^1 \Phi_1^1 + K_{12}^1 \Phi_2^1 \\ K_{21}^1 \Phi_1^1 + K_{22}^1 \Phi_2^1 \\ 0 \\ 0 \end{pmatrix}$$

For the second and third element we can write in a similar way:

$$(K^2) = \begin{pmatrix} 0 & 0 & 0 & 0 \\ 0 & K_{11}^2 & K_{12}^2 & 0 \\ 0 & K_{21}^2 & K_{22}^2 & 0 \\ 0 & 0 & 0 & 0 \end{pmatrix}; \quad (\Phi^2) = \begin{pmatrix} 0 \\ \Phi_1^2 \\ \Phi_2^2 \\ 0 \end{pmatrix} \quad (K^2)(\Phi^2) = \begin{pmatrix} 0 \\ K_{11}^2 \Phi_1^2 + K_{12}^2 \Phi_2^2 \\ K_{21}^2 \Phi_1^2 + K_{22}^2 \Phi_2^2 \\ 0 \end{pmatrix}$$

$$(K^3) = \begin{pmatrix} 0 & 0 & 0 & 0 \\ 0 & 0 & 0 & 0 \\ 0 & K_{11}^3 & K_{12}^3 & 0 \\ 0 & 0 & K_{21}^3 & K_{22}^3 \end{pmatrix}; \quad (\Phi^3) = \begin{pmatrix} 0 \\ 0 \\ \Phi_1^3 \\ \Phi_2^3 \end{pmatrix} \quad (K^3)(\Phi^3) = \begin{pmatrix} 0 \\ 0 \\ K_{11}^3 \Phi_1^3 + K_{12}^3 \Phi_2^3 \\ K_{21}^3 \Phi_1^3 + K_{22}^3 \Phi_2^3 \end{pmatrix}$$

When these products are added:

$$\sum_{e=1}^3 (K^e) (\Phi^e) = \begin{pmatrix} K_{11}^1 \Phi_1^1 + K_{12}^1 \Phi_2^1 \\ K_{21}^1 \Phi_1^1 + K_{22}^1 \Phi_2^1 \\ 0 \\ 0 \end{pmatrix} + \begin{pmatrix} 0 \\ K_{11}^2 \Phi_1^2 + K_{12}^2 \Phi_2^2 \\ K_{21}^2 \Phi_1^2 + K_{22}^2 \Phi_2^2 \\ 0 \end{pmatrix} + \begin{pmatrix} 0 \\ 0 \\ K_{11}^3 \Phi_1^3 + K_{12}^3 \Phi_2^3 \\ K_{21}^3 \Phi_1^3 + K_{22}^3 \Phi_2^3 \end{pmatrix} =$$

$$\begin{pmatrix} K_{11}^1 \Phi_1^1 + K_{12}^1 \Phi_2^1 \\ K_{21}^1 \Phi_1^1 + K_{22}^1 \Phi_2^1 + K_{11}^2 \Phi_1^2 + K_{12}^2 \Phi_2^2 \\ K_{21}^2 \Phi_1^2 + K_{22}^2 \Phi_2^2 + K_{11}^3 \Phi_1^3 + K_{12}^3 \Phi_2^3 \\ K_{21}^3 \Phi_1^3 + K_{22}^3 \Phi_2^3 \end{pmatrix}$$

According to the relation between the global and local node numbers:

$$\begin{pmatrix} \Phi_1^1 = \Phi_1 \\ \Phi_2^1 = \Phi_1^2 = \Phi_2 \\ \Phi_2^2 = \Phi_1^3 = \Phi_3 \\ \Phi_2^3 = \Phi_4 \end{pmatrix} \Rightarrow \begin{pmatrix} \Phi_1^1 \\ \Phi_2^1 \\ \Phi_1^2 \\ \Phi_2^2 \\ \Phi_1^3 \\ \Phi_2^3 \end{pmatrix} = \begin{pmatrix} 1 & 0 & 0 & 0 \\ 0 & 1 & 0 & 0 \\ 0 & 1 & 0 & 0 \\ 0 & 0 & 1 & 0 \\ 0 & 0 & 1 & 0 \\ 0 & 0 & 0 & 1 \end{pmatrix} \cdot \begin{pmatrix} \Phi_1 \\ \Phi_2 \\ \Phi_3 \\ \Phi_4 \end{pmatrix}$$

By making these changes, we can write:

$$\sum_{e=1}^3 (K^e) (\Phi^e) = \begin{pmatrix} K_{11}^1 & K_{12}^1 & 0 & 0 \\ K_{21}^1 & K_{22}^1 + K_{11}^2 & K_{12}^2 & 0 \\ 0 & K_{21}^2 & K_{22}^2 + K_{11}^3 & K_{12}^3 \\ 0 & 0 & K_{21}^3 & K_{22}^3 \end{pmatrix} \begin{pmatrix} \Phi_1 \\ \Phi_2 \\ \Phi_3 \\ \Phi_4 \end{pmatrix}$$

Similarly we can expand (b^e) to find that:

$$\sum_{e=1}^3 (b^e) = \begin{pmatrix} b_1^1 \\ b_2^1 + b_1^2 \\ b_2^2 + b_1^3 \\ b_2^3 \end{pmatrix}; \quad \sum_{e=1}^3 (g^e) = \begin{pmatrix} g_1^1 \\ g_2^1 + g_1^2 \\ g_2^2 + g_1^3 \\ g_2^3 \end{pmatrix}$$

Except for g₁ and g₄, the other elements of (g) can be written as:

$$g_i = g_2^{i-1} - g_1^i$$

After substitution of

$$g_i^e = \alpha N_i^e \frac{d\Phi}{dx} \Big|_{x_1^e}^{x_2^e} = \alpha N_i^e \frac{d\Phi}{dx} \Big|_{x=x_2^e} - \alpha N_i^e \frac{d\Phi}{dx} \Big|_{x=x_1^e}$$

this becomes:

$$g_i = \alpha \frac{d\Phi}{dx} \Big|_{x=x_2^{i-1}} - \alpha \frac{d\Phi}{dx} \Big|_{x=x_1^i}$$

from $x_1^e = x_e$ and $x_2^e = x_{e+1}$ we can write:

$$x_2^{i-1} = x_1^i = x_i$$

and since $\alpha \frac{d\Phi}{dx}$ is continuous at x_i , it is obvious that $g_i = 0$ for $i = 2, 3$. Therefore (g) has two only nonzero elements:

$$(g) = \begin{pmatrix} -\alpha \frac{d\Phi}{dx} \Big|_{x=x_1} \\ 0 \\ 0 \\ \alpha \frac{d\Phi}{dx} \Big|_{x=x_4} \end{pmatrix}$$

For a general problem with N nodes we then have:

$$g_1 = -\alpha \frac{d\Phi}{dx} \Big|_{x=x_1} ; \quad g_N = \alpha \frac{d\Phi}{dx} \Big|_{x=x_N}$$

$$g_i = 0 \quad \text{for} \quad i \neq 1, N$$

Boundary conditions

First we consider the Dirichlet condition, that is: $\Phi|_{x=0} = p$. To enforce this condition we need to modify the system of equations: we impose $\Phi_1 = p$ for example by setting:

$$K_{11} = 1; b_1 = p$$

$$\text{And } K_{ij} = 0 \text{ for } j = 2, 3, 4, \dots, N$$

The resultant system becomes:

$$\begin{pmatrix} 1 & 0 & 0 & 0 \\ K_{21} & K_{22} & K_{23} & K_{24} \\ K_{31} & K_{32} & K_{33} & K_{34} \\ K_{41} & K_{42} & K_{43} & K_{44} \end{pmatrix} \begin{pmatrix} \Phi_1 \\ \Phi_2 \\ \Phi_3 \\ \Phi_4 \end{pmatrix} = \begin{pmatrix} p \\ b_2 \\ b_3 \\ b_4 \end{pmatrix}$$

This system is not symmetric. This is not desirable, since symmetry is a very important property which can be exploited to reduce computer memory demanded as well as processing time. To restore the symmetry we may modify the above equation as:

$$\begin{pmatrix} 1 & 0 & 0 & 0 \\ 0 & K_{22} & K_{23} & K_{24} \\ 0 & K_{32} & K_{33} & K_{34} \\ 0 & K_{42} & K_{43} & K_{44} \end{pmatrix} \begin{pmatrix} \Phi_1 \\ \Phi_2 \\ \Phi_3 \\ \Phi_4 \end{pmatrix} = \begin{pmatrix} p \\ b_2 - K_{21}p \\ b_3 - K_{31}p \\ b_4 - K_{41}p \end{pmatrix} \Rightarrow \begin{pmatrix} K_{22} & K_{23} & K_{24} \\ K_{32} & K_{33} & K_{34} \\ K_{42} & K_{43} & K_{44} \end{pmatrix} \begin{pmatrix} \Phi_2 \\ \Phi_3 \\ \Phi_4 \end{pmatrix} = \begin{pmatrix} b_2 - K_{21}p \\ b_3 - K_{31}p \\ b_4 - K_{41}p \end{pmatrix}$$

As a result g_1 should be discarded. Next we consider the boundary condition $\alpha \frac{d\Phi}{dx} + \gamma\Phi \Big|_{x=L} = q$ to be applied at $x = L$. If the boundary condition is the homogeneous Neumann condition ($\gamma = q = 0$), then g_N vanishes. Otherwise, we have:

$$g_N = \alpha \frac{d\Phi}{dx} \Big|_{x=L} = q - \gamma\Phi_N$$

Therefore g_N can be absorbed into (K) and (b):

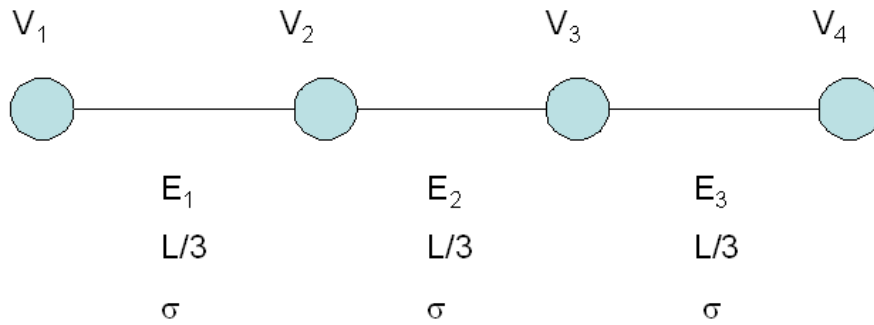
$$\begin{pmatrix} K_{22} & K_{23} & K_{24} \\ K_{32} & K_{33} & K_{34} \\ K_{42} & K_{43} & K_{44} \end{pmatrix} \begin{pmatrix} \Phi_2 \\ \Phi_3 \\ \Phi_4 \end{pmatrix} = \begin{pmatrix} b_2 - K_{21}p \\ b_3 - K_{31}p \\ b_4 - K_{41}p \end{pmatrix} + \begin{pmatrix} 0 \\ 0 \\ q - \gamma\Phi_4 \end{pmatrix}$$

Example. Determine the potential distribution into the wire which is connected to a constant voltage V_0 . Also determine the current that flows for it. The wire has constant section and conductivity. Divide the entire domain in 3 elements.

Solution. The applicable equation is: $\nabla \cdot J = \nabla \cdot \sigma(-\nabla V) = 0$

$$\begin{aligned} \nabla^2 V &= 0 \\ J &= \sigma E \\ x=0 \rightarrow V &= V_0 \\ x=L \rightarrow V &= 0 \end{aligned} \quad -\frac{d}{dx} \left(\alpha \frac{d\Phi}{dx} \right) + \beta\Phi = f \quad \begin{cases} \Phi = V \\ \alpha = 1 \\ \beta = 0 \\ f = 0 \end{cases}$$

We divide the wire into three elements with equal length: $l^e = L/3$.



By direct application of the expressions for K_{ij} and b_i , we can write:

$$K_{11}^e = K_{22}^e = \frac{\alpha^e}{l^e} + \frac{\beta^e}{3l^e} = \frac{3}{L}$$

$$K_{12}^e = K_{21}^e = -\frac{\alpha^e}{l^e} + \frac{\beta^e}{6l^e} = -\frac{3}{L}$$

$$b_1^e = b_2^e = f^e \frac{l^e}{2} = 0$$

$$K\Phi = b + g$$

$$\frac{1}{L} \begin{pmatrix} 3 & -3 & 0 & 0 \\ -3 & 6 & -3 & 0 \\ 0 & -3 & 6 & -3 \\ 0 & 0 & -3 & 3 \end{pmatrix} \begin{pmatrix} \Phi_1 \\ \Phi_2 \\ \Phi_3 \\ \Phi_4 \end{pmatrix} = \begin{pmatrix} 0 \\ 0 \\ 0 \\ 0 \end{pmatrix} + \begin{pmatrix} 0 \\ 0 \\ 0 \\ 0 \end{pmatrix}$$

This is a singular system. By application of BC: $\Phi_1 = V_0$; $\Phi_4 = 0$ we can write:

$$\Phi_1 = p = V_0$$

$$\begin{pmatrix} 1 & 0 & 0 & 0 \\ 0 & 6 & -3 & 0 \\ 0 & -3 & 6 & -3 \\ 0 & 0 & -3 & 3 \end{pmatrix} \begin{pmatrix} \Phi_1 \\ \Phi_2 \\ \Phi_3 \\ \Phi_4 \end{pmatrix} = \begin{pmatrix} V_0 \\ 0 - (-3)V_0 \\ 0 - (0)V_0 \\ 0 - (0)V_0 \end{pmatrix} \Rightarrow \begin{pmatrix} 6 & -3 & 0 \\ -3 & 6 & -3 \\ 0 & -3 & 3 \end{pmatrix} \begin{pmatrix} \Phi_2 \\ \Phi_3 \\ \Phi_4 \end{pmatrix} = \begin{pmatrix} 3 \\ 0 \\ 0 \end{pmatrix} V_0$$

$$\Phi_4 = p = 0$$

$$\begin{pmatrix} 6 & -3 & 0 \\ -3 & 6 & 0 \\ 0 & 0 & 1 \end{pmatrix} \begin{pmatrix} \Phi_2 \\ \Phi_3 \\ \Phi_4 \end{pmatrix} = \begin{pmatrix} 3 \\ 0 \\ 0 \end{pmatrix} V_0 - \begin{pmatrix} (-3)0 \\ (-3)0 \\ (0)0 \end{pmatrix} \Rightarrow \begin{bmatrix} 6 & -3 \\ -3 & 6 \end{bmatrix} \begin{bmatrix} \Phi_2 \\ \Phi_3 \end{bmatrix} = \begin{bmatrix} 3 \\ 0 \end{bmatrix} V_0$$

and finally, we obtain:

$$\begin{bmatrix} \Phi_2 \\ \Phi_3 \end{bmatrix} = \begin{bmatrix} 6 & -3 \\ -3 & 6 \end{bmatrix}^{-1} \begin{bmatrix} 3 \\ 0 \end{bmatrix} V_0 = \begin{bmatrix} \frac{2}{3} \\ \frac{1}{3} \\ 0 \end{bmatrix} V_0$$

$$J = \sigma E = \sigma \frac{dV}{dx} = \sigma \frac{\Delta V}{\Delta x}$$

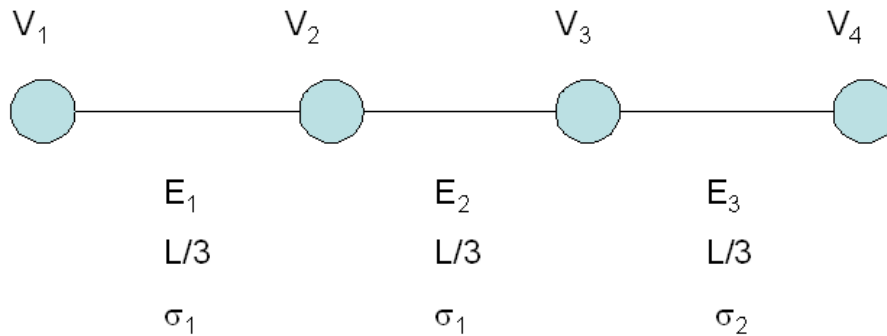
$$\left. \begin{aligned} J_1 &= \sigma \frac{\Phi_2 - \Phi_1}{L/3} = \sigma \frac{V_0}{L} \\ J_2 &= \sigma \frac{\Phi_3 - \Phi_2}{L/3} = \sigma \frac{V_0}{L} \\ J_3 &= \sigma \frac{\Phi_4 - \Phi_3}{L/3} = \sigma \frac{V_0}{L} \end{aligned} \right\} \Rightarrow I = \iint J dS = \iint \sigma \frac{V_0}{L} dS = \sigma \frac{V_0}{L} S = \frac{V_0}{\frac{1}{\sigma} \frac{L}{S}} = \frac{V_0}{\rho \frac{L}{S}} = \frac{V_0}{R}$$

We obtain an analytic solution to compare with numerical results:

$$\frac{d^2 V}{dx^2} = 0 \Rightarrow V = ax + b \rightarrow \begin{cases} x=0 & V = V_0 = b \\ x=L & V = 0 = aL + V_0 \rightarrow a = -\frac{V_0}{L} \end{cases}$$

$$V = V_0 \left(1 - \frac{x}{L}\right) \Rightarrow E = -\frac{dV}{dx} = \frac{V_0}{L} \Rightarrow J = \sigma E = \sigma \frac{V_0}{L}$$

Exercise 2. Solve again if the wire is made of two materials: one from $x = 0$ to $x = 2L/3$ and the other from $x = 2L/3$ to $x = L$.



In this case the relevant equation is: $\nabla \cdot J = \nabla \cdot \sigma (-\nabla V) = 0$

$$-\frac{d}{dx} \left(\sigma \frac{d\Phi}{dx} \right) + \beta \Phi = f \quad \begin{cases} \Phi = V \\ \alpha = \sigma \\ \beta = 0 \\ f = 0 \end{cases}$$

By direct application of the expressions for K_{ij} and b_i , we can write:

$$K_{11}^1 = K_{22}^1 = K_{11}^2 = K_{22}^2 = \frac{\alpha^e}{l^e} + \frac{\beta^e}{3l^e} = \frac{3\sigma_1}{L}$$

$$K_{12}^1 = K_{21}^1 = K_{12}^2 = K_{21}^2 = -\frac{\alpha^e}{l^e} + \frac{\beta^e}{6l^e} = -\frac{3\sigma_1}{L}$$

$$K_{11}^3 = K_{22}^3 = \frac{\alpha^e}{l^e} + \frac{\beta^e}{3l^e} = \frac{3\sigma_2}{L}$$

$$K_{12}^3 = K_{21}^3 = -\frac{\alpha^e}{l^e} + \frac{\beta^e}{6l^e} = -\frac{3\sigma_2}{L}$$

$$b_1^e = b_2^e = f^e \frac{l^e}{2} = 0$$

$$K\Phi = b + g$$

$$\frac{1}{L} \begin{pmatrix} 3\sigma_1 & -3\sigma_1 & 0 & 0 \\ -3\sigma_1 & 6\sigma_1 & -3\sigma_1 & 0 \\ 0 & -3\sigma_1 & 3(\sigma_1 + \sigma_2) & -3\sigma_2 \\ 0 & 0 & -3\sigma_2 & 3\sigma_2 \end{pmatrix} \begin{pmatrix} \Phi_1 \\ \Phi_2 \\ \Phi_3 \\ \Phi_4 \end{pmatrix} = \begin{pmatrix} 0 \\ 0 \\ 0 \\ 0 \end{pmatrix} + \begin{pmatrix} 0 \\ 0 \\ 0 \\ 0 \end{pmatrix}$$

This is a singular system. By application of BC: $\Phi_1 = V_0$; $\Phi_4 = 0$ we can write:

$$\Phi_1 = p = V_0$$

$$\begin{pmatrix} 1 & 0 & 0 & 0 \\ 0 & 6\sigma_1 & -3\sigma_1 & 0 \\ 0 & -3\sigma_1 & 3(\sigma_1 + \sigma_2) & -3\sigma_2 \\ 0 & 0 & -3\sigma_2 & 3\sigma_2 \end{pmatrix} \begin{pmatrix} \Phi_1 \\ \Phi_2 \\ \Phi_3 \\ \Phi_4 \end{pmatrix} = \begin{pmatrix} V_0 \\ 0 - (-3\sigma_1)V_0 \\ 0 - (0)V_0 \\ 0 - (0)V_0 \end{pmatrix} \Rightarrow \begin{pmatrix} 6\sigma_1 & -3\sigma_1 & 0 \\ -3\sigma_1 & 3(\sigma_1 + \sigma_2) & -3\sigma_2 \\ 0 & -3\sigma_2 & 3\sigma_2 \end{pmatrix} \begin{pmatrix} \Phi_2 \\ \Phi_3 \\ \Phi_4 \end{pmatrix} = \begin{pmatrix} 3\sigma_1 \\ 0 \\ 0 \end{pmatrix} V_0$$

$$\Phi_4 = p = 0$$

$$\begin{pmatrix} 6\sigma_1 & -3\sigma_1 & 0 \\ -3\sigma_1 & 3(\sigma_1 + \sigma_2) & 0 \\ 0 & 0 & 1 \end{pmatrix} \begin{pmatrix} \Phi_2 \\ \Phi_3 \\ \Phi_4 \end{pmatrix} = \begin{pmatrix} 3\sigma_1 \\ 0 \\ 0 \end{pmatrix} V_0 - \begin{pmatrix} (-3\sigma_1)0 \\ (-3\sigma_2)0 \\ (0)0 \end{pmatrix} \Rightarrow \begin{bmatrix} 6\sigma_1 & -3\sigma_1 \\ -3\sigma_1 & 3(\sigma_1 + \sigma_2) \end{bmatrix} \begin{bmatrix} \Phi_2 \\ \Phi_3 \end{bmatrix} = \begin{bmatrix} 3\sigma_1 \\ 0 \end{bmatrix} V_0$$

$$\begin{bmatrix} \Phi_2 \\ \Phi_3 \end{bmatrix} = \begin{bmatrix} \frac{\sigma_1 + \sigma_2}{\sigma_1 + 2\sigma_2} \\ \frac{\sigma_1}{\sigma_1 + 2\sigma_2} \end{bmatrix} V_0$$

If, for example $\sigma_1 = 2\sigma_2$, we can obtain:

$$\begin{bmatrix} \Phi_2 \\ \Phi_3 \end{bmatrix} = \begin{bmatrix} \frac{3}{4} \\ \frac{1}{2} \end{bmatrix} V_0$$

$$\begin{aligned}
 J &= \sigma E = \sigma \frac{dV}{dx} = \sigma \frac{\Delta V}{\Delta x} \\
 \left. \begin{aligned}
 J_1 &= \sigma_1 \frac{\Phi_2 - \Phi_1}{L/3} = \sigma_1 \frac{3 V_0}{4 L} \\
 J_2 &= \sigma_1 \frac{\Phi_3 - \Phi_2}{L/3} = \sigma_1 \frac{3 V_0}{4 L} \\
 J_3 &= \sigma_2 \frac{\Phi_4 - \Phi_3}{L/3} = \sigma_2 \frac{3 V_0}{2 L} = \frac{\sigma_1}{2} \frac{3 V_0}{2 L} = \sigma_1 \frac{3 V_0}{4 L}
 \end{aligned} \right\} \Rightarrow
 \end{aligned}$$

$$\left. \begin{aligned}
 I_1 &= \iint J_1 dS = \iint \sigma_1 \frac{3 V_0}{4 L} dS = \sigma_1 \frac{3 V_0}{4 L} S = \frac{\frac{3}{4} V_0}{\frac{1}{\sigma_1} \frac{L}{S}} = \frac{\frac{1}{4} V_0}{\frac{L/3}{\rho_1}} = \frac{\frac{1}{4} V_0}{R_1} \\
 I_2 &= \iint J_2 dS = \iint \sigma_1 \frac{V_0}{L} dS = \sigma_1 \frac{3 V_0}{4 L} S = \frac{\frac{3}{4} V_0}{\frac{1}{\sigma_1} \frac{L}{S}} = \frac{\frac{1}{4} V_0}{\frac{L/3}{\rho_1}} = \frac{\frac{1}{4} V_0}{R_2} \\
 I_3 &= \iint J_3 dS = \iint \sigma_1 \frac{V_0}{L} dS = \sigma_2 \frac{3 V_0}{2 L} S = \frac{\frac{3}{2} V_0}{\frac{1}{\sigma_2} \frac{L}{S}} = \frac{\frac{1}{2} V_0}{\frac{L/3}{\rho_2}} = \frac{\frac{1}{2} V_0}{R_3}
 \end{aligned} \right\} \rightarrow R_1 = R_2 = R_3 / 2$$

Exercise to solve

Solve the following 1D problem:

$$\frac{d^2 u}{dx^2} = f \quad 1 < x < 2$$

Calculate the solution with the use of linear interpolation elements and discretization points: $x_1 = 1$, $x_2 = 1.5$, $x_3 = 1.7$ and $x_4 = 2$.

Solve assuming:

- a) $f = 1$; $u(1) = 5$; $u(2) = 7$.
 b) $f = x$; $u(1) = 5$; $u(2) = 7$.

Solution:

- a) $u = [5 \quad 6.125 \quad 6.505 \quad 7]$
 b) $u = [8755 \quad 6.125 \quad 6.5645 \quad 7]$

TWO DIMENSIONAL FINITE ELEMENT ANALYSIS

The boundary value problem under consideration is defined by the second order PDE:

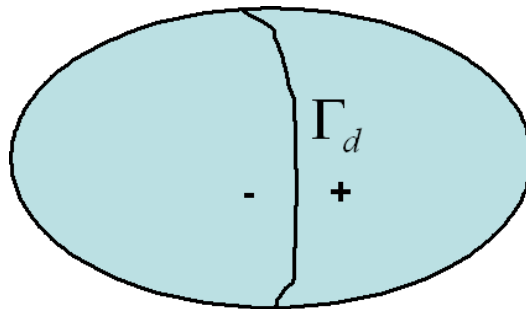
$$-\frac{\partial}{\partial x}\left(\alpha_x \frac{\partial \Phi}{\partial x}\right) - \frac{\partial}{\partial y}\left(\alpha_y \frac{\partial \Phi}{\partial y}\right) + \beta \Phi = f$$

The boundary conditions to be considered are given by:

$$\begin{aligned} \Phi| &= p \quad \text{on} \quad \Gamma_1 \\ \left(\alpha_x \frac{d\Phi}{dx} x + \alpha_y \frac{d\Phi}{dy} y\right)n + \gamma \Phi &= q \quad \text{on} \quad \Gamma_2 \end{aligned}$$

If the properties of the domain characterized by α_x and α_y have discontinuities or abrupt change, and furthermore, if there is no surface source of any kind at the discontinuity interface, Φ then satisfies the continuity conditions:

$$\begin{aligned} \Phi^+ &= \Phi^- \quad \text{on} \quad \Gamma_d \\ \left(\alpha_x^+ \frac{d\Phi^+}{dx} x + \alpha_y^+ \frac{d\Phi^+}{dy} y\right)n &= \left(\alpha_x^- \frac{d\Phi^-}{dx} x + \alpha_y^- \frac{d\Phi^-}{dy} y\right)n \quad \text{on} \quad \Gamma_2 \end{aligned}$$



Domain discretization

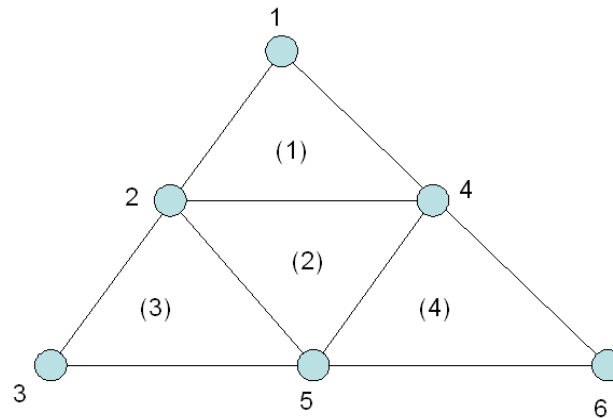
The first step is to divide the domain area into a number of two dimensional elements. We use triangular elements here. To identify each element we can label the elements with a set of integers, and to identify the nodes that are the vertices of the elements, we can label them with another set of integers.

Since each element is related to several nodes (3 for a triangle) a node has its own position in the associated element in addition to its position in the entire system. This position can also be labelled with an integer number referred to as the local number, in contrast to the global number, which indicates its position in the entire system.

To relate these three numbers- the global node number, the local node number, and the element number – we introduce a $3 \times M$ array, denoted by $n(i,e)$, where $i = 1,2,3$ and $e = 1,2,3,\dots, M$ where M denotes the total number of elements.

$n(i,e)$ is called the connectivity array; i is the local number of a node, e is the element number, and the value of $n(i,e)$ is the global number of the node.

To illustrate this we consider the example shown in the following figure. We have 4 elements and 6 nodes. The array $n(i,e)$ can be numbered as:



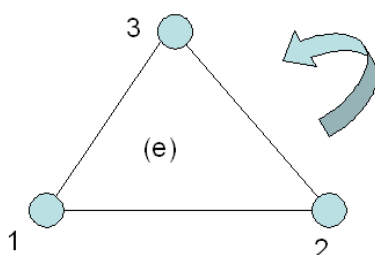
e	$n(1,e)$	$n(2,e)$	$n(3,e)$
1	2	4	1
2	5	4	2
3	3	5	2
4	5	6	4

The numeration is assigned in counter clockwise direction (left \rightarrow right; down \rightarrow up). In addition to the data described above, some other data are also necessary in the FE formulation:

- x_i, y_i , which provide the coordinates of the nodes $i = 1, \dots, N$, where N denotes the total number of nodes.
- The values for $\alpha_x, \alpha_y, \beta$ and f for each element.
- The values of p for the nodes residing in Γ_1 .
- The values of γ and q for each segment coincident with Γ_2 .

Interpolation

If linear triangular elements are used, the unknown function within each element is approximated as:



$$\Phi^e(x,y) = a^e + b^e x + c^e y \quad (1)$$

where a^e, b^e and c^e are constant coefficients to be determined and e is the element number. For linear triangular elements, there are three nodes located at

the vertices of the triangle. The values of Φ at each node are Φ_1^e , Φ_2^e , Φ_3^e respectively. Enforcing (1) at the three nodes, we obtain:

$$\Phi_1^e = a^e + b^e x_1^e + c^e y_1^e$$

$$\Phi_2^e = a^e + b^e x_2^e + c^e y_2^e$$

$$\Phi_3^e = a^e + b^e x_3^e + c^e y_3^e$$

Solving and rearranging terms, we obtain:

$$\Phi^e(x, y) = \sum_{j=1}^3 N_j^e(x, y) \Phi_j^e \quad (2)$$

Where $N_j^e(x, y)$ are the interpolation or expansion functions given by:

$$N_j^e(x, y) = \frac{1}{2\Delta^e} (a_j^e + b_j^e x + c_j^e y) \quad j=1,2,3$$

in which:

$$a_1^e = x_2^e y_3^e - y_2^e x_3^e \quad b_1^e = y_2^e - y_3^e \quad c_1^e = x_3^e - x_2^e$$

$$a_2^e = x_3^e y_1^e - y_3^e x_1^e \quad b_2^e = y_3^e - y_1^e \quad c_2^e = x_1^e - x_3^e$$

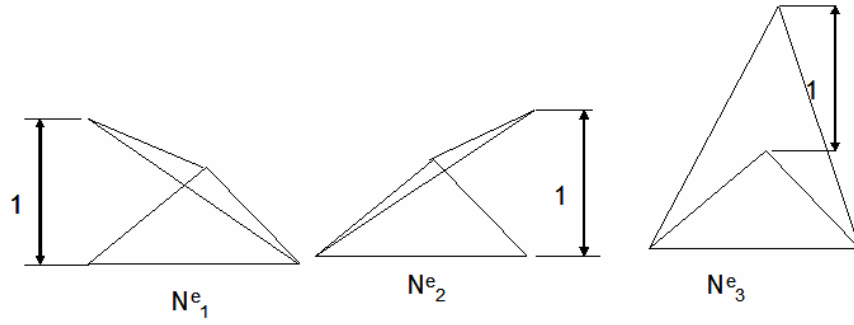
$$a_3^e = x_1^e y_2^e - y_1^e x_2^e \quad b_3^e = y_1^e - y_2^e \quad c_3^e = x_2^e - x_1^e$$

$$\Delta^e = \frac{1}{2} \begin{vmatrix} 1 & x_1^e & y_1^e \\ 1 & x_2^e & y_2^e \\ 1 & x_3^e & y_3^e \end{vmatrix} = \frac{1}{2} (b_1^e c_2^e - b_2^e c_1^e) = \text{AREA of the eth element}$$

In the above equations, x_j^e , y_j^e denote the coordinate values of the j th node in the e th element. It can be easily shown that the interpolation functions have the property:

$$N_i^e(x_j^e, y_j^e) = \begin{cases} 1 & i = j \\ 0 & i \neq j \end{cases}$$

and, as a result, at node i , Φ^e in (2) reduces to its nodal value Φ_i^e . $N_j^e(x, y)$ vanishes when the observation point (x, y) is on the element side opposite to the j th node. Therefore, the value of Φ^e at the element side is not related to the value of Φ at the opposite node, but rather it is determined by the values at the two endpoints of its associated side. This features guarantees the continuity of the solution across the element sides. The following figure shows the interpolation function N_i^e for a triangular element.



Variational formulation

The Variational problem equivalent to boundary value problem is given by:

$$\begin{cases} \delta F(\Phi) = 0 \\ \Phi = p \quad \text{on} \quad \Gamma_1 \end{cases}$$

Where:

$$F(\Phi) = \frac{1}{2} \iint_{\Omega} \left(\alpha_x \left(\frac{\partial \Phi}{\partial x} \right)^2 + \alpha_y \left(\frac{\partial \Phi}{\partial y} \right)^2 + \beta(\Phi)^2 \right) d\Omega + \int_{\Gamma_2} \left(\frac{\gamma}{2} \Phi^2 + q\Phi \right) d\Gamma - \iint_{\Omega} f\Phi d\Omega$$

is the functional equation which must be minimized. For simplicity first consider the Homogeneous Neumann Boundary condition with $\gamma = q = 0$ for which the line integral in the functional vanishes. Thus the functional can be written as:

$$F(\Phi) = \sum_{e=1}^M F^e(\Phi^e)$$

Where M denotes the total number of elements and F^e is the sub-functional given by:

$$F^e(\Phi) = \frac{1}{2} \iint_{\Omega^e} \left(\alpha_x \left(\frac{\partial \Phi^e}{\partial x} \right)^2 + \alpha_y \left(\frac{\partial \Phi^e}{\partial y} \right)^2 + \beta(\Phi^e)^2 \right) d\Omega - \iint_{\Omega} f\Phi^e d\Omega$$

with Ω^e denoting the domain of the eth element. Introducing the expression $\Phi^e(x, y) = \sum_{j=1}^3 N_j^e(x, y) \Phi_j^e$ and differentiating F^e with respect to Φ_i^e yields:

$$\frac{\partial F^e}{\partial \Phi_i^e} = \sum_{j=1}^3 \Phi_j^e \iint_{\Omega^e} \left(\alpha_x \left(\frac{\partial N_i^e}{\partial x} \right) \left(\frac{\partial N_j^e}{\partial x} \right) + \alpha_y \left(\frac{\partial N_i^e}{\partial y} \right) \left(\frac{\partial N_j^e}{\partial y} \right) + \beta N_i^e N_j^e \right) d\Omega - \iint_{\Omega} f N_i^e d\Omega \quad i = 1, 2, 3$$

or:

$$\left[\frac{\partial F^e}{\partial \Phi^e} \right] = [K^e] [\Phi^e] - [t^e]$$

Where:

$$\left[\frac{\partial F^e}{\partial \Phi^e} \right] = \begin{bmatrix} \frac{\partial F^e}{\partial \Phi_1^e} \\ \frac{\partial F^e}{\partial \Phi_2^e} \\ \frac{\partial F^e}{\partial \Phi_3^e} \end{bmatrix}; \quad [\Phi^e] = \begin{bmatrix} \Phi_1^e \\ \Phi_2^e \\ \Phi_3^e \end{bmatrix}$$

The elements of the matrix $[K^e]$ are given by:

$$K_{ij}^e = \iint_{\Omega^e} \left(\alpha_x \left(\frac{\partial N_i^e}{\partial x} \right) \left(\frac{\partial N_j^e}{\partial x} \right) + \alpha_y \left(\frac{\partial N_i^e}{\partial y} \right) \left(\frac{\partial N_j^e}{\partial y} \right) + \beta N_i^e N_j^e \right) d\Omega \quad i=1,2,3$$

and those the vector $[t^e]$ by:

$$t_i^e = \iint_{\Omega} f N_i^e d\Omega \quad i=1,2,3$$

$[K^e]$ is a symmetric matrix. Assuming now that the coefficients $\alpha_x, \alpha_y, \beta, f$ are constant within each element and equal to $\alpha_x^e, \alpha_y^e, \beta^e, f^e$ respectively, the above integrals can be evaluated analytically:

$$\left. \begin{aligned} K_{ij}^e &= \frac{1}{4\Delta^e} (\alpha_x^e b_i^e b_j^e + \alpha_y^e c_i^e c_j^e) + \frac{\Delta^e}{12} \beta^e (1 + \delta_{ij}) \\ t_i^e &= \frac{\Delta^e}{3} f^e \end{aligned} \right\} \delta_{ij} = \begin{cases} 1 & i=j \\ 0 & i \neq j \end{cases}$$

Assembly to form the system of equations

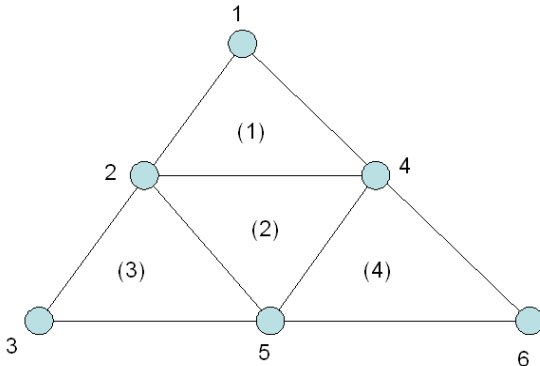
With the elemental equation, we can assemble all M elements, then impose the stationary requirement on F to find the system of equations:

$$\left[\frac{\partial F}{\partial \Phi} \right] = \sum_{e=1}^M \left[\frac{\partial F^e}{\partial \Phi^e} \right] = \sum_{e=1}^M [K^e] [\Phi^e] - [t^e] = 0 \quad (4)$$

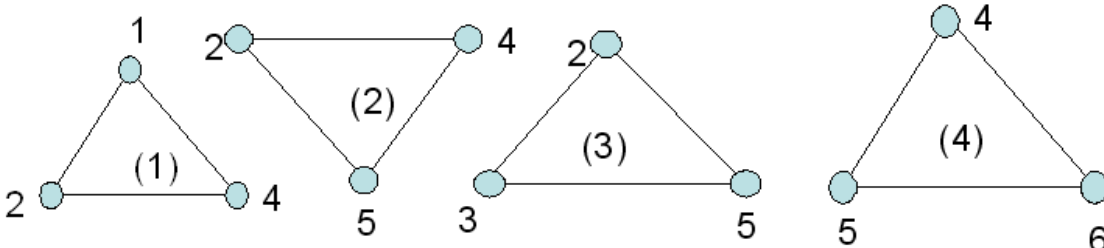
The system of equations can be written compactly as:

$$[K][\Phi] = [t]$$

Where $[K]$ is assembled from $[K^e]$ and $[t]$ is assembled from $[t^e]$. In a similar way on the 1D example, we can show that the $[K]$ and $[t]$ matrix for the four element, 6 node example system is equal to:



e	n(1,e)	n(2,e)	n(3,e)
1	2	4	1
2	5	4	2
3	3	5	2
4	5	6	4



$$[K] = \begin{bmatrix} K_{33}^1 & K_{31}^1 & 0 & K_{32}^1 & 0 & 0 \\ K_{13}^1 & K_{11}^1 + K_{33}^2 + K_{33}^3 & K_{31}^3 & K_{12}^1 + K_{32}^2 & K_{31}^2 + K_{32}^3 & 0 \\ 0 & K_{13}^3 & K_{11}^3 & 0 & K_{12}^3 & 0 \\ K_{23}^1 & K_{21}^1 + K_{23}^2 & 0 & K_{22}^1 + K_{22}^3 + K_{33}^4 & K_{21}^2 + K_{31}^4 & K_{32}^4 \\ 0 & K_{13}^2 + K_{23}^3 & K_{21}^3 & K_{12}^2 + K_{13}^4 & K_{11}^2 + K_{22}^3 + K_{11}^4 & K_{12}^4 \\ 0 & 0 & 0 & K_{23}^4 & K_{21}^4 & K_{22}^4 \end{bmatrix}$$

$$[t] = \begin{bmatrix} t_3^1 \\ t_1^1 + t_3^2 + t_3^3 \\ t_1^3 \\ t_2^1 + t_2^2 + t_3^3 \\ t_1^2 + t_2^3 + t_1^4 \\ t_2^4 \end{bmatrix}$$

Incorporation of the boundary conditions of the third kind

The system above is derived by the assumption that Φ satisfies the homogeneous Neumann boundary condition on Γ_2 . Now let us consider the general case with no vanishing γ and q . We add to the functional an extra term:

$$F_b(\Phi) = \int_{\Gamma_2} \left(\frac{\gamma}{2} \Phi^2 + q\Phi \right) d\Gamma$$

Assuming that Γ_2 is comprised by M_s sides or segments elements, the above equation can then be written as:

$$F_b(\Phi) = \sum_{s=1}^{M_s} \int_S \left(\frac{\gamma^s}{2} \Phi^{s^2} + q^s \Phi^s \right) dS$$

The unknown function Φ within each segment can be approximated as:

$$\Phi^s(x, y) = \sum_{j=1}^2 N_j^s(x, y) \Phi_j^s$$

where: $N_1^s = 1 - \zeta$ in which ζ is the normalized distance measured from node 1 to node 2 in the segment: $\zeta = 0$ at node 1, and $\zeta = 1$ at node 2, and between the two nodes it varies linearly. Substituting and differentiating it with respect to Φ_i^s yields:

$$\frac{\partial F_b(\Phi)}{\partial \Phi_i^s} = \sum_{j=1}^2 \Phi_j^s \int_0^1 \gamma^s N_i^s N_j^s l^s d\zeta - \int_0^1 q N_i^s l^s d\zeta$$

where l^s denotes the length of the segment. In matrix form we can write this as:

$$\left[\frac{\partial F_b^s}{\partial \Phi^s} \right] = [K^s] [\Phi^s] - [t^s]$$

with the elements in $[K^s]$ and $[t^s]$ given by:

$$K_{ij}^s = \int_0^1 \gamma^s N_i^s N_j^s l^s d\zeta \quad i, j = 1, 2$$

$$t_i^s = \int_0^1 q N_i^s l^s d\zeta \quad i = 1, 2$$

if γ and q are constant within each segment and denoted by γ^s and q^s the above integrals can be evaluated analytically and the result is:

$$\left. \begin{aligned} K_{ij}^s &= \gamma^s \frac{l^s}{6} (1 + \delta_{ij}) \\ t_i^s &= \frac{l^s}{2} q^s \end{aligned} \right\} \delta_{ij} = \begin{cases} 1 & i = j \\ 0 & i \neq j \end{cases}$$

To include F_b into the system (4) it should be modified:

$$\left[\frac{\partial F}{\partial \Phi} \right] = \sum_{e=1}^M \left[\frac{\partial F^e}{\partial \Phi^e} \right] + \sum_{s=1}^{M_s} \left[\frac{\partial F_b^s}{\partial \Phi^s} \right] = \sum_{e=1}^M [K^e \Phi^e] - [t^e] + \sum_{s=1}^{M_s} [K^s \Phi^s] - [t^s] = 0$$

Where $\left[\frac{\partial F_b^s}{\partial \Phi^s} \right]$, $[K^s]$, $[\Phi^s]$ and $[t^s]$ have also been augmented. To do this, we need an array that relates the segments and the global number of the associated nodes. This array, $n_s(i,s)$ ($i = 1,2$; $s = 1, \dots, M_s$) plays a similar role as the connectivity array $n(i,e)$. In $n_s(i,s)$ we store the global number of the i th node of the s th segment.

Consider the above example, if Γ_2 comprises the segments in the sides defined by the nodes 6,4,1,2 and 3, the array $n_s(i,s)$ can be numbered as:

s	$n_s(1,s)$	$n_s(2,s)$
1	6	4
2	4	1
3	1	2
4	2	3

$[K^s]$ can be assembled to $[K]$ by adding each K_{ij}^s to $K_{n_s(i,s), n_s(j,s)}$ and similarly $[t^s]$ can be assembled to $[t]$ by adding t_i^s to $t_{n_s(i,s)}$.

Imposition of the Dirichlet boundary condition

We need to impose on the system the Dirichlet boundary condition which applies to the nodes on Γ_1 . To illustrate how that is done, we consider again the example. Assume that the nodes 3, 5 and 6 are on Γ_1 and they have the prescribed values p_3 , p_5 and p_6 respectively. To impose the condition $\Phi_3 = p_3$ we can simply set:

$$K_{33} = 1$$

$$K_{3i} = 0 \quad \text{for } i = 1, 2, 4, 5, 6$$

$$t_3 = p_3$$

This destroys the symmetry of the matrix K , and to restore this property we can make the following modifications:

$$\left. \begin{array}{l} t_i \leftarrow t_i - K_{i3} p_3 \\ K_{i3} = 0 \end{array} \right\} \text{for } i = 1, 2, 4, 5, 6$$

In a similar way, we can impose the other conditions: $\Phi_5 = p_5$, and finally, the matrices K and t become:

$$[K] = \begin{bmatrix} K_{11} & K_{12} & 0 & K_{14} & 0 & 0 \\ K_{21} & K_{22} & 0 & K_{24} & 0 & 0 \\ 0 & 0 & 1 & 0 & 0 & 0 \\ K_{41} & K_{42} & 0 & K_{44} & 0 & 0 \\ 0 & 0 & 0 & 0 & 1 & 0 \\ 0 & 0 & 0 & 0 & 0 & 1 \end{bmatrix}; \quad [t] = \begin{bmatrix} t_1 - K_{13}p_3 - K_{15}p_5 - K_{16}p_6 \\ t_2 - K_{23}p_3 - K_{25}p_5 - K_{26}p_6 \\ p_3 \\ t_4 - K_{43}p_3 - K_{45}p_5 - K_{46}p_6 \\ p_5 \\ p_6 \end{bmatrix}$$

With the deletion of third, fifth and sixth equations, the system becomes:

$$\begin{bmatrix} K_{11} & K_{12} & K_{14} \\ K_{21} & K_{22} & K_{24} \\ K_{41} & K_{42} & K_{44} \end{bmatrix} \begin{bmatrix} \Phi_1 \\ \Phi_2 \\ \Phi_4 \end{bmatrix} = \begin{bmatrix} t_1 - K_{13}p_3 - K_{15}p_5 - K_{16}p_6 \\ t_2 - K_{23}p_3 - K_{25}p_5 - K_{26}p_6 \\ t_4 - K_{43}p_3 - K_{45}p_5 - K_{46}p_6 \end{bmatrix}$$

Another approach commonly used to impose Dirichlet boundary conditions without the modification of the system of equations is to choose a huge number (10^{70}) and set:

$$K_{ii} = 10^{70} \\ t_i = p_i 10^{70}$$

For example to impose $\Phi_3 = p_3$ the equation associated to Φ_3 becomes:

$$K_{13}\Phi_1 + K_{32}\Phi_2 + 10^{70}\Phi_3 + K_{34}\Phi_4 + K_{35}\Phi_5 + K_{36}\Phi_6 = p_3 10^{70}$$

Provided that all matrix elements and unknowns are smaller than 10^{70} , the above equation is effectively equivalent to $\Phi_3 = p_3$. The new system of equations then becomes:

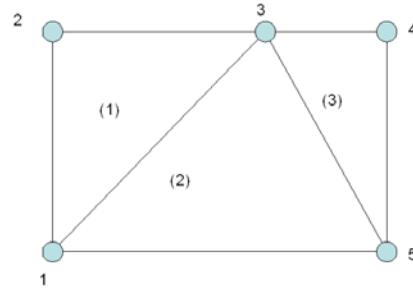
$$\begin{bmatrix} K_{11} & K_{12} & K_{13} & K_{14} & K_{15} & K_{16} \\ K_{21} & K_{22} & K_{23} & K_{24} & K_{25} & K_{26} \\ K_{31} & K_{32} & 10^{70} & K_{34} & K_{35} & K_{36} \\ K_{41} & K_{42} & K_{43} & K_{44} & K_{45} & K_{46} \\ K_{51} & K_{52} & K_{53} & K_{54} & 10^{70} & K_{56} \\ K_{61} & K_{62} & K_{63} & K_{64} & K_{65} & 10^{70} \end{bmatrix} \begin{bmatrix} \Phi_1 \\ \Phi_2 \\ \Phi_3 \\ \Phi_4 \\ \Phi_5 \\ \Phi_6 \end{bmatrix} = \begin{bmatrix} t_1 \\ t_2 \\ p_3 10^{70} \\ t_4 \\ p_5 10^{70} \\ p_6 10^{70} \end{bmatrix}$$

In which here the symmetry is retained. This approach is much simpler than the previous ones as presented. It requires only two operations to impose a boundary condition. More importantly, this technique can easily be applied to

systems whose matrix is stored in a compact form which is necessary for reducing memory demand. However, the technique does not permit elimination of the equations associated with the Γ_1 nodes, which is its major disadvantage.

Example. Solve the magnetostatic problem defined by the following nodes and characteristic elements.

e	n(1,e)	n(2,e)	n(3,e)	μ_r	J (A/m ²)
1	1	3	2	1000	0
2	1	5	3	1	0
3	3	5	4	1	1500



Node	1	2	3	4	5
X	0	0	2	3	3
Y	0	2	2	2	0

$$\frac{1}{\mu} \left(\frac{\partial^2 A}{\partial x^2} + \frac{\partial^2 A}{\partial y^2} \right) = -J$$

$$\alpha_x = \alpha_y = \frac{1}{\mu}$$

$$\beta = 0$$

$$f = J$$

With the boundary conditions: $A_1 = A_2 = 0$.

Intermediate calculations:

$$a_1^e = x_2^e y_3^e - y_2^e x_3^e \quad b_1^e = y_2^e - y_3^e \quad c_1^e = x_3^e - x_2^e$$

$$a_2^e = x_3^e y_1^e - y_3^e x_1^e \quad b_2^e = y_3^e - y_1^e \quad c_2^e = x_1^e - x_3^e$$

$$a_3^e = x_1^e y_2^e - y_1^e x_2^e \quad b_3^e = y_1^e - y_2^e \quad c_3^e = x_2^e - x_1^e$$

$$\Delta^e = \frac{1}{2} \begin{vmatrix} 1 & x_1^e & y_1^e \\ 1 & x_2^e & y_2^e \\ 1 & x_3^e & y_3^e \end{vmatrix} = \frac{1}{2} (b_1^e c_2^e - b_2^e c_1^e) = \text{AREA of the } e\text{th element}$$

e	x ₁	x ₂	x ₃	y ₁	y ₂	y ₃	b ₁	b ₂	b ₃	c ₁	c ₂	c ₃	Δ
(1)	0	2	0	0	2	2	0	2	-2	-2	0	2	2
(2)	0	3	2	0	0	2	-2	2	0	-1	-2	3	3
(3)	2	3	3	2	0	2	-2	0	2	0	-1	1	1

$$K_{ij}^e = \frac{1}{4\Delta_e} \left(\alpha_x^e b_i^e b_j^e + \alpha_y^e c_i^e c_j^e \right) + \frac{\Delta_e}{12} \beta^e (1 + \delta_{ij}) \left. \vphantom{\frac{1}{4\Delta_e}} \right\} \delta_{ij} = \begin{cases} 1 & i = j \\ 0 & i \neq j \end{cases}$$

$$t_i^e = \frac{\Delta_e}{3} f^e$$

1st Element

$$\alpha_x = \alpha_y = \frac{1}{\mu} = \frac{1}{1000\mu_0}; \quad \beta = 0; \quad f = 0 \quad \Delta = 2$$

$$\left. \begin{aligned} K_{11}^1 &= \frac{1}{4 \cdot 1000 \cdot \mu_0 \cdot 2} (0 \cdot 0 + (-2)(-2)) = \frac{0.5}{1000 \cdot \mu_0} \\ K_{12}^1 &= K_{21}^1 = \frac{1}{4 \cdot 1000 \cdot \mu_0 \cdot 2} (0 \cdot 0 + (0)(0)) = 0 \\ K_{13}^1 &= K_{31}^1 = \frac{1}{4 \cdot 1000 \cdot \mu_0 \cdot 2} (0 \cdot 0 + (-2)(2)) = \frac{-0.5}{1000 \cdot \mu_0} \\ K_{22}^1 &= \frac{1}{4 \cdot 1000 \cdot \mu_0 \cdot 2} (2 \cdot 2 + (0)(0)) = \frac{0.5}{1000 \cdot \mu_0} \\ K_{23}^1 &= K_{32}^1 = \frac{1}{4 \cdot 1000 \cdot \mu_0 \cdot 2} (2 \cdot (-2) + (0)(0)) = \frac{-0.5}{1000 \cdot \mu_0} \\ K_{33}^1 &= \frac{1}{4 \cdot 1000 \cdot \mu_0 \cdot 2} ((-2) \cdot (-2) + (2)(2)) = \frac{1}{1000 \cdot \mu_0} \end{aligned} \right\}$$

$$t_1^1 = t_2^1 = t_3^1 = \frac{2}{3} 0 = 0$$

2nd Element

$$\alpha_x = \alpha_y = \frac{1}{\mu} = \frac{1}{\mu_0}; \quad \beta = 0; \quad f = 0 \quad \Delta = 3$$

$$\left. \begin{aligned} K_{11}^2 &= \frac{1}{4 \cdot \mu_0 \cdot 3} ((-2)(-2) + (-1)(-1)) = \frac{0.4166}{\mu_0} \\ K_{12}^2 &= K_{21}^2 = \frac{1}{4 \cdot \mu_0 \cdot 3} ((-2)(2) + (-1)(-2)) = \frac{-0.166}{\mu_0} \\ K_{13}^2 &= K_{31}^2 = \frac{1}{4 \cdot \mu_0 \cdot 3} (0 \cdot 0 + (-1)(3)) = \frac{-0.25}{\mu_0} \\ K_{22}^2 &= \frac{1}{4 \cdot \mu_0 \cdot 3} (2 \cdot 2 + (-2)(-2)) = \frac{0.666}{\mu_0} \\ K_{23}^2 &= K_{32}^2 = \frac{1}{4 \cdot \mu_0 \cdot 3} (0 \cdot 0 + (-2)(3)) = \frac{-0.5}{\mu_0} \\ K_{33}^2 &= \frac{1}{4 \cdot \mu_0 \cdot 3} (0 \cdot 0 + (3)(3)) = \frac{0.75}{\mu_0} \end{aligned} \right\}$$

$$t_1^2 = t_2^2 = t_3^2 = \frac{3}{3} 0 = 0$$

3rd element

$$\alpha_x = \alpha_y = \frac{1}{\mu} = \frac{1}{\mu_0}; \quad \beta = 0; \quad f = 1500; \quad \Delta = 1$$

$$\left. \begin{aligned} K_{11}^2 &= \frac{1}{4 \cdot \mu_0 \cdot 1} ((-2)(2) + (-1)(-1)) = \frac{1}{\mu_0} \\ K_{12}^2 &= K_{21}^2 = \frac{1}{4 \cdot \mu_0 \cdot 1} ((0)(0) + (0)(0)) = 0 \\ K_{13}^2 &= K_{31}^2 = \frac{1}{4 \cdot \mu_0 \cdot 1} ((-2)(2) + (0)(0)) = \frac{-1}{\mu_0} \\ K_{22}^2 &= \frac{1}{4 \cdot \mu_0 \cdot 1} (0 \cdot 0 + (1)(1)) = \frac{0.25}{\mu_0} \\ K_{23}^2 &= K_{32}^2 = \frac{1}{4 \cdot \mu_0 \cdot 1} (0 \cdot 0 + (-1)(1)) = \frac{-0.25}{\mu_0} \\ K_{33}^2 &= \frac{1}{4 \cdot \mu_0 \cdot 1} (2 \cdot 2 + (1)(1)) = \frac{1.25}{\mu_0} \end{aligned} \right\}$$

$$t_1^3 = t_2^3 = t_3^3 = \frac{1}{3} 1500 = 500$$

$$K_1 = \frac{1}{1000\mu_0} \begin{pmatrix} 0.5 & -0.5 & 0 & 0 & 0 \\ -0.5 & 1 & -0.5 & 0 & 0 \\ 0 & -0.5 & 0.5 & 0 & 0 \\ 0 & 0 & 0 & 0 & 0 \\ 0 & 0 & 0 & 0 & 0 \end{pmatrix}; \quad K_2 = \frac{1}{\mu_0} \begin{pmatrix} 0.416 & 0 & -0.25 & 0 & -0.1666 \\ 0 & 0 & 0 & 0 & 0 \\ -0.25 & 0 & 0.75 & 0 & -0.5 \\ 0 & 0 & 0 & 0 & 0 \\ -0.1666 & 0 & -0.5 & 0 & -0.6666 \end{pmatrix}$$

$$K_3 = \frac{1}{\mu_0} \begin{pmatrix} 0 & 0 & 0 & 0 & 0 \\ 0 & 0 & 0 & 0 & 0 \\ 0 & 0 & 1 & -1 & 0 \\ 0 & 0 & -1 & 1.25 & -0.25 \\ 0 & 0 & 0 & -0.25 & 0.25 \end{pmatrix}$$

$$K = K_1 + K_2 + K_3 = \frac{1}{\mu_0} \begin{pmatrix} 0.417 & -5 \cdot 10^{-4} & 0.25 & 0 & -0.1666 \\ -5 \cdot 10^{-4} & 10^{-3} & -5 \cdot 10^{-4} & 0 & 0 \\ -0.25 & -5 \cdot 10^{-4} & 1.7505 & -1 & -0.25 \\ 0 & 0 & -1 & 1.25 & -0.25 \\ -0.1666 & 0 & -0.5 & -0.25 & 0.916 \end{pmatrix}$$

$$t = \begin{pmatrix} 0 \\ 0 \\ 500 \\ 500 \\ 500 \end{pmatrix}; \quad A = \begin{pmatrix} 0 \\ 0 \\ A_3 \\ A_4 \\ A_5 \end{pmatrix}$$

By application of Boundary conditions, we can obtain the following equation:

$$\begin{pmatrix} 1.7505 & -1 & -0.5 \\ -1 & 1.25 & -0.25 \\ -0.5 & -0.25 & 0.916 \end{pmatrix} \begin{pmatrix} A_3 \\ A_4 \\ A_5 \end{pmatrix} = \begin{pmatrix} 500 \\ 500 \\ 500 \end{pmatrix} \mu_0$$

$$\begin{pmatrix} A_3 \\ A_4 \\ A_5 \end{pmatrix} = \begin{pmatrix} 3600.3 \\ 4000.9 \\ 3603.0 \end{pmatrix} \mu_0 = \begin{pmatrix} 4.526 \\ 5.027 \\ 4.527 \end{pmatrix} \cdot 10^{-3} \text{ Wb/m}$$

Example. Determine the elements for K and T matrix in the case of diffusion equation:

$$\frac{1}{\mu} \left(\frac{\partial^2 A}{\partial x^2} + \frac{\partial^2 A}{\partial y^2} \right) = -J + j\omega\sigma A$$

$$\alpha_x = \alpha_y = \frac{1}{\mu}$$

$$\beta = j\omega\sigma$$

$$f = J$$

By use of the general equation for K and t

$$\left. \begin{aligned} K_{ij}^e &= \frac{1}{4\Delta_e} (\alpha_x^e b_i^e b_j^e + \alpha_y^e c_i^e c_j^e) + \frac{\Delta_e}{12} \beta^e (1 + \delta_{ij}) \\ t_i^e &= \frac{\Delta_e}{3} f^e \end{aligned} \right\} \delta_{ij} = \begin{cases} 1 & i = j \\ 0 & i \neq j \end{cases}$$

we can write for each element:

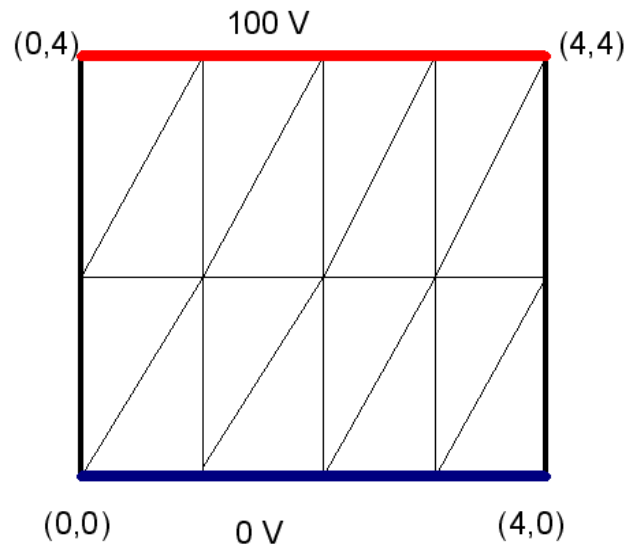
$$K = \frac{1}{4\mu\Delta_e} \begin{pmatrix} b_1^2 + c_1^2 & b_1 b_2 + c_1 c_2 & b_1 b_3 + c_1 c_3 \\ b_1 b_2 + c_1 c_2 & b_2^2 + c_2^2 & b_2 b_3 + c_2 c_3 \\ b_1 b_3 + c_1 c_3 & b_2 b_3 + c_2 c_3 & b_3^2 + c_3^2 \end{pmatrix} + j \frac{\Delta_e}{12} \omega\sigma \begin{pmatrix} 2 & 1 & 1 \\ 1 & 2 & 1 \\ 1 & 1 & 2 \end{pmatrix}$$

$$T = \frac{\Delta_e J}{3} \begin{pmatrix} 1 \\ 1 \\ 1 \end{pmatrix}$$

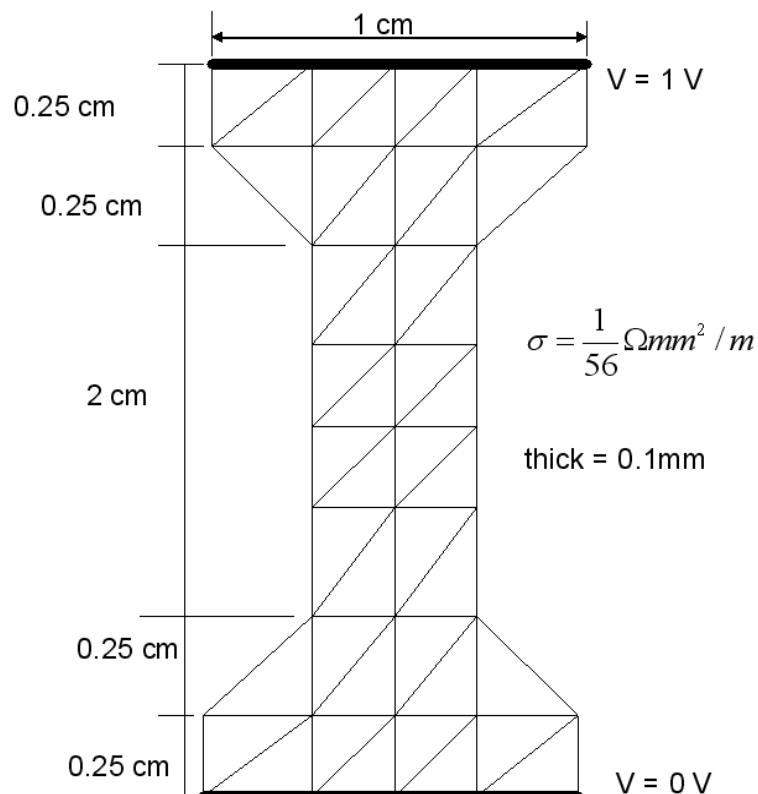
K becomes a complex matrix!

Exercises to solve.

a) Determine the potential in the intermediate nodes.



b) Determine the current density, and the total current in the fuse showed in the following figure.



Nonlinear problems

In the analysis of electrical machines and other magnetic apparatus, the problems becomes nonlinear due to the presence of ferromagnetic materials. Good designs operate at, or near, the saturation point. The permeability $\mu = B/H$ is a function of the local magnetic field, which is an unknown at the start of the problem. The permeability appears in all of the elements of matrix K, and we must use an iterative process and keep correcting the permeability until it is consistent with the field solution.

The most popular method of dealing with nonlinear problems in magnetics is the Newton-Raphson method. We explain this method in the following pages.

For the Newton-Raphson method, the magnetic reluctivity, $\nu = 1/\mu$ as a function of B^2 must be continuous and differentiable. A number of approximations are possible from polynomials to exponentials.

Newton-Raphson method

Consider first the single non-linear equation:

$$g(x) = 0$$

We would like to find the roots of g. We can expand the above equation around x^0 in a Taylor series:

$$g(x) = g(x^0) + \left. \frac{dg}{dx} \right|_{x=x^0} (x - x^0) + \dots = 0$$

Keeping only the first order terms and rearranging, we can write:

$$x \approx x^0 - \frac{g(x^0)}{\left. \frac{dg}{dx} \right|_{x=x^0}}$$

From the initial estimation of x, x^0 , we can find other approximate value:

$$x^1 = x^0 - \frac{g(x^0)}{\left. \frac{dg}{dx} \right|_{x=x^0}}$$

and so forth:

$$x^2 = x^1 - \frac{g(x^1)}{\left. \frac{dg}{dx} \right|_{x=x^1}}$$

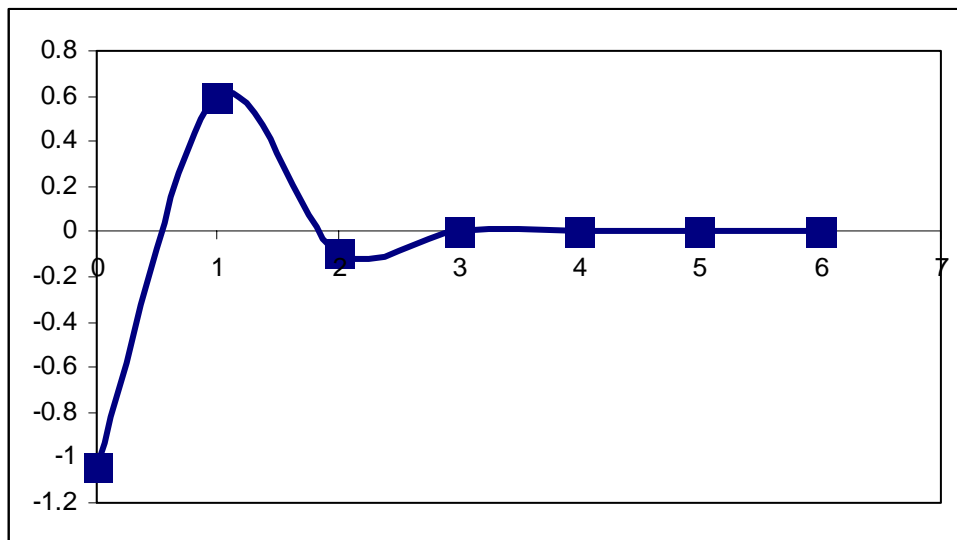
$$x^3 = x^2 - \frac{g(x^2)}{\left. \frac{dg}{dx} \right|_{x=x^2}}$$

Example. Solve the following equation:

$$f(x) = \cos(2x) - \frac{x}{2} = 0$$

$$x^1 = x^0 - \frac{f(x^0)}{\left. \frac{df}{dx} \right|_{x=x^0}} = x^0 - \frac{\cos(2x) - \frac{x}{2}}{-2\sin(2x) - \frac{1}{2}}$$

n	x	f	df	deltax
0	0.1	0.93006658	-0.89733866	-1.0364722
1	1.1364722	-1.21409524	-2.02691319	0.59898729
2	0.53748491	0.20701633	-2.25915159	-0.09163455
3	0.62911946	-0.00706658	-2.40310059	0.00294061
4	0.62617885	-5.3502E-06	-2.39945083	2.2297E-06
5	0.62617662	-3.1132E-12	-2.39944804	1.2975E-12



error versus iteration's number

Consider the following multidimensional system of non-linear equations with independent variables x_1, x_2, \dots, x_n :

$$F(x) = \begin{pmatrix} f_1(x_1, x_2, \dots, x_n) \\ f_2(x_1, x_2, \dots, x_n) \\ \vdots \\ f_n(x_1, x_2, \dots, x_n) \end{pmatrix} = 0$$

Expanding in a Taylor series and truncating it after the first order terms gives:

$$J(x)\{x^{k+1} - x^k\} = -F(x^k)$$

Where J is the Jacobian matrix given by:

$$J(x) = \begin{pmatrix} \frac{\partial f_1}{\partial x_1} & \frac{\partial f_1}{\partial x_2} & \dots & \frac{\partial f_1}{\partial x_n} \\ \frac{\partial f_2}{\partial x_1} & \frac{\partial f_2}{\partial x_2} & \dots & \frac{\partial f_2}{\partial x_n} \\ \vdots & \vdots & \ddots & \vdots \\ \frac{\partial f_n}{\partial x_1} & \frac{\partial f_n}{\partial x_2} & \dots & \frac{\partial f_n}{\partial x_n} \end{pmatrix}$$

The k+1 approximation can be calculated by:

$$\begin{aligned} x^{k+1} &= x^k - J^{-1}(x) \cdot F(x^k) \\ x^{k+1} - x^k &= -J^{-1}(x) \cdot F(x^k) \\ \Delta x^{k+1} &= -J^{-1}(x) \cdot F(x^k) \end{aligned}$$

Application of the N-R method to an element

We consider here the two dimensional nonlinear Poisson equation for the magnetic vector potential. We have found that the equations for a two dimensional first order triangle are:

$$\frac{\nu}{4\Delta} \begin{pmatrix} k_{ii} & k_{ij} & k_{ik} \\ k_{ji} & k_{jj} & k_{jk} \\ k_{ki} & k_{kj} & k_{kk} \end{pmatrix} \begin{pmatrix} A_i \\ A_j \\ A_k \end{pmatrix} = \frac{\Delta}{3} \begin{pmatrix} J_e \\ J_e \\ J_e \end{pmatrix}$$

This equation could be written as:

$$F = \begin{pmatrix} f_1 \\ f_2 \\ f_3 \end{pmatrix} = \frac{\nu}{4\Delta} \begin{pmatrix} k_{ii} & k_{ij} & k_{ik} \\ k_{ji} & k_{jj} & k_{jk} \\ k_{ki} & k_{kj} & k_{kk} \end{pmatrix} \begin{pmatrix} A_i \\ A_j \\ A_k \end{pmatrix} - \frac{\Delta}{3} \begin{pmatrix} J_e \\ J_e \\ J_e \end{pmatrix} = 0$$

To calculate the Jacobian, we differentiate these equations with respect to the nodal vector potentials. For f_1 this gives:

$$\begin{aligned}\frac{\partial f_1}{\partial A_i} &= \frac{\nu}{4\Delta} k_{ii} + \frac{1}{4\Delta} (k_{ii} A_i + k_{ij} A_j + k_{ik} A_k) \frac{\partial \nu}{\partial B^2} \frac{\partial B^2}{\partial A_i} \\ \frac{\partial f_1}{\partial A_j} &= \frac{\nu}{4\Delta} k_{ij} + \frac{1}{4\Delta} (k_{ii} A_i + k_{ij} A_j + k_{ik} A_k) \frac{\partial \nu}{\partial B^2} \frac{\partial B^2}{\partial A_j} \\ \frac{\partial f_1}{\partial A_k} &= \frac{\nu}{4\Delta} k_{ik} + \frac{1}{4\Delta} (k_{ii} A_i + k_{ij} A_j + k_{ik} A_k) \frac{\partial \nu}{\partial B^2} \frac{\partial B^2}{\partial A_k}\end{aligned}$$

The first equation for the N-R iteration is:

$$\begin{aligned}\frac{\partial f_1}{\partial A_i} \Delta A_i + \frac{\partial f_1}{\partial A_j} \Delta A_j + \frac{\partial f_1}{\partial A_k} \Delta A_k &= -f_1 \\ \frac{\nu}{4\Delta} [k_{ii} \Delta A_i + k_{ij} \Delta A_j + k_{ik} \Delta A_k] + \frac{1}{4\Delta} (k_{ii} A_i + k_{ij} A_j + k_{ik} A_k) \frac{\partial \nu}{\partial B^2} \left[\frac{\partial B^2}{\partial A_i} \Delta A_i + \frac{\partial B^2}{\partial A_j} \Delta A_j + \frac{\partial B^2}{\partial A_k} \Delta A_k \right] &= \\ = -\frac{\nu}{4\Delta} [k_{ii} A_i + k_{ij} A_j + k_{ik} A_k] + \frac{\Delta}{3} J_e &\end{aligned}$$

In matrix notation this becomes:

$$\begin{aligned}\frac{\nu}{4\Delta} \begin{pmatrix} k_{ii} & k_{ij} & k_{ik} \end{pmatrix} \begin{pmatrix} \Delta A_i \\ \Delta A_j \\ \Delta A_k \end{pmatrix} + \frac{1}{4\Delta} \frac{\partial \nu}{\partial B^2} \left(\left(\sum_{n=i}^k k_{in} A_n \right) \frac{\partial B^2}{\partial A_i} \quad \left(\sum_{n=i}^k k_{in} A_n \right) \frac{\partial B^2}{\partial A_j} \quad \left(\sum_{n=i}^k k_{in} A_n \right) \frac{\partial B^2}{\partial A_k} \right) \begin{pmatrix} \Delta A_i \\ \Delta A_j \\ \Delta A_k \end{pmatrix} &= \\ = -\frac{\nu}{4\Delta} \begin{pmatrix} k_{ii} & k_{ij} & k_{ik} \end{pmatrix} \begin{pmatrix} A_i \\ A_j \\ A_k \end{pmatrix} + \frac{\Delta}{3} J_e &\end{aligned}$$

we now do the same for the second and third equations to get the whole element equation:

$$\begin{aligned}\frac{\nu}{4\Delta} \begin{pmatrix} k_{ii} & k_{ij} & k_{ik} \\ k_{ji} & k_{jj} & k_{jk} \\ k_{ki} & k_{kj} & k_{kk} \end{pmatrix} \begin{pmatrix} \Delta A_i \\ \Delta A_j \\ \Delta A_k \end{pmatrix} + \frac{1}{4\Delta} \frac{\partial \nu}{\partial B^2} \begin{pmatrix} \sum_{n=i}^k k_{in} A_n & \sum_{n=i}^k k_{in} A_n & \sum_{n=i}^k k_{in} A_n \\ \sum_{n=i}^k k_{jn} A_n & \sum_{n=i}^k k_{jn} A_n & \sum_{n=i}^k k_{jn} A_n \\ \sum_{n=i}^k k_{kn} A_n & \sum_{n=i}^k k_{kn} A_n & \sum_{n=i}^k k_{kn} A_n \end{pmatrix} \begin{pmatrix} \frac{\partial B^2}{\partial A_i} & 0 & 0 \\ 0 & \frac{\partial B^2}{\partial A_j} & 0 \\ 0 & 0 & \frac{\partial B^2}{\partial A_k} \end{pmatrix} \begin{pmatrix} \Delta A_i \\ \Delta A_j \\ \Delta A_k \end{pmatrix} &= \\ = -\frac{\nu}{4\Delta} \begin{pmatrix} k_{ii} & k_{ij} & k_{ik} \\ k_{ji} & k_{jj} & k_{jk} \\ k_{ki} & k_{kj} & k_{kk} \end{pmatrix} \begin{pmatrix} A_i \\ A_j \\ A_k \end{pmatrix} + \frac{\Delta}{3} \begin{pmatrix} 1 \\ 1 \\ 1 \end{pmatrix} J_e &\end{aligned}$$

The vector potentials here are taken for the previous iteration. We find $\frac{\partial \nu}{\partial B^2}$ from the saturation curve representation. To evaluate $\frac{\partial B^2}{\partial A_i}$ we proceed as follows:

$$B^2 = \left(\frac{\partial A}{\partial x} \right)^2 + \left(\frac{\partial A}{\partial y} \right)^2$$

For triangular first order elements:

$$A = \frac{1}{2\Delta} (a_i + b_i x + c_i y) A_i + \frac{1}{2\Delta} (a_j + b_j x + c_j y) A_j + \frac{1}{2\Delta} (a_k + b_k x + c_k y) A_k$$

$$\frac{\partial A}{\partial x} = \frac{A_i b_i + A_j b_j + A_k b_k}{2\Delta}$$

$$\frac{\partial A}{\partial y} = \frac{A_i c_i + A_j c_j + A_k c_k}{2\Delta}$$

$$B^2 = \left(\frac{A_i b_i + A_j b_j + A_k b_k}{2\Delta} \right)^2 + \left(\frac{A_i c_i + A_j c_j + A_k c_k}{2\Delta} \right)^2 = \frac{(A_i b_i + A_j b_j + A_k b_k)^2 + (A_i c_i + A_j c_j + A_k c_k)^2}{4\Delta^2}$$

$$\frac{\partial B^2}{\partial A_i} = \frac{2b_i (A_i b_i + A_j b_j + A_k b_k) + 2c_i (A_i c_i + A_j c_j + A_k c_k)}{4\Delta^2}$$

We can summarize the process as follows:

STEP	PROCESS
1	Assume a value for ν and A for each element and node
2	Evaluate the matrices K_e using these values and the material coefficients
3	Assemble the matrix in the normal way
4	Apply boundary conditions and solve for the ΔA vector
5	Find the new A by adding ΔA to the previous value of A
6	Apply a stopping or convergence test, such as the relative change in ΔA is smaller than ε
7	If the test fails, recomputed the matrix and repeat the process from step 2

Permanent magnets (PM) modelling

The development of high energy permanent magnet materials such as SmCo and NdFeB has led to increased interest in the use of permanent magnet material in electrical machines and actuators. As mentioned in the last section, ferromagnetic materials are characterised by a narrow hysteresis loop. In contrast, hard magnetic materials such as PM exhibit wide loops. It is often

acceptable to consider the magnetic characteristic of a PM by a straight line in the second quadrant of the hysteresis loop. The intersection of the hysteresis loop with the ordinate is called the residual or remanence flux density B_r . The intersection of the abscissa and the loop is called the coercitive force H_c . There are two possibilities for the modelling of a PM material:

- Magnetisation model
- Current sheet approach

Although these two methods have a different starting point, they both result in the same set of equations. Assuming a straight line as the characteristic of the PM material, there are only two parameters required to define the characteristic:

- The slope of the line μ_m
- The y-axis intercept B_r

Magnetic vector model

The demagnetisation characteristic is defined by

$$B = \mu_0 \cdot ((1 + \chi_m) \cdot H + M)$$

where χ_m is the magnetic susceptibility, M the magnetisation vector and H the field strength at the operating point. In terms of the remanent flux density

$$B_r = \mu_0 \cdot M$$

The incremental permeability, the slope of the demagnetisation characteristic is

$$\frac{\partial |B|}{\partial |H|} = \mu_0 \cdot (1 + \chi_m)$$

χ_m is a very small positive number so that the apparent permeability of the magnet is only slightly larger than that of the free space. The reluctivity is defined as

$$\nu = \frac{1}{\mu_0 \cdot (1 + \chi_m)}$$

and applying this to the demagnetisation characteristic, yields

$$H = \nu \cdot (B - \mu_0 \cdot M)$$

using the Maxwell equation for a magnetostatic problem:

$$\nabla \times H = J$$

yields

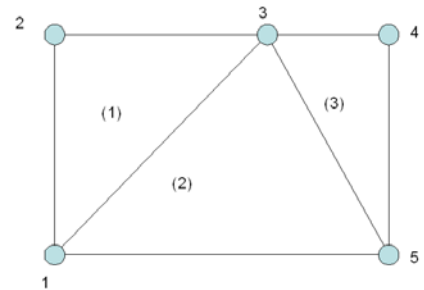
$$\nabla \times (\nu \cdot B) = J + \nabla \times (\nu \cdot \mu_0 \cdot M)$$

The second term, the magnetic vector, on the right-hand side represents a source term and can be identified as an equivalent magnetic current. The matrix T must be recomputed to include this term. This term can be computed with:

$$\iint_{\Omega} \nu \mu_0 \left(M_x \frac{\partial N}{\partial y} - M_y \frac{\partial N}{\partial x} \right) dx dy = \frac{\nu \mu_0}{2} \left(M_x \begin{pmatrix} c_i \\ c_j \\ c_k \end{pmatrix} - M_y \begin{pmatrix} b_i \\ b_j \\ b_k \end{pmatrix} \right)$$

Example. Solve the magnetostatic problem defined by the following nodes and characteristic elements.

e	n(1,e)	n(2,e)	n(3,e)	μ_r	J (A/m ²)	M
1	1	3	2	1000	0	0
2	1	5	3	1	0	0
3	3	5	4	1	0	$\mu_r = 1.05$ $B_r = 0.8T$



Direction of magnetization along y axis.

Node	1	2	3	4	5
X	0	0	2	3	3
Y	0	2	2	2	0

$$\frac{1}{\mu} \left(\frac{\partial^2 A}{\partial x^2} + \frac{\partial^2 A}{\partial y^2} \right) = -J + \nabla \times (\nu \cdot \mu_0 \cdot M)$$

With the boundary conditions: $A_1 = A_2 = 0$.

The K and T matrix are the same for the 1st and 2nd elements, the third element values are divided by the relative permeability $\mu_r = 1.05$:

$$\begin{aligned}
K_1 &= \frac{1}{1000\mu_0} \begin{pmatrix} 0.5 & -0.5 & 0 & 0 & 0 \\ -0.5 & 1 & -0.5 & 0 & 0 \\ 0 & -0.5 & 0.5 & 0 & 0 \\ 0 & 0 & 0 & 0 & 0 \\ 0 & 0 & 0 & 0 & 0 \end{pmatrix}; \quad K_2 = \frac{1}{\mu_0} \begin{pmatrix} 0.416 & 0 & -0.25 & 0 & -0.1666 \\ 0 & 0 & 0 & 0 & 0 \\ -0.25 & 0 & 0.75 & 0 & -0.5 \\ 0 & 0 & 0 & 0 & 0 \\ -0.166 & 0 & -0.5 & 0 & -0.666 \end{pmatrix} \\
K_3 &= \frac{1}{\mu_0} \begin{pmatrix} 0 & 0 & 0 & 0 & 0 \\ 0 & 0 & 0 & 0 & 0 \\ 0 & 0 & 0.952 & -0.952 & 0 \\ 0 & 0 & -0.952 & 1.19 & -0.238 \\ 0 & 0 & 0 & -0.238 & 0.238 \end{pmatrix} \\
K &= K_1 + K_2 + K_3 = \frac{1}{\mu_0} \begin{pmatrix} 0.417 & -5 \cdot 10^{-4} & 0.25 & 0 & -0.1666 \\ -5 \cdot 10^{-4} & 10^{-3} & -5 \cdot 10^{-4} & 0 & 0 \\ -0.25 & -5 \cdot 10^{-4} & 1.7029 & -0.952 & -0.5 \\ 0 & 0 & -0.952 & 1.19 & -0.238 \\ -0.1666 & 0 & -0.5 & -0.238 & 0.9047 \end{pmatrix}
\end{aligned}$$

The major difference is in the right hand side where the current vector is replaced by the magnetization vector using the above equation. In this case $M_x = 0$ and the new vector T becomes:

$$t = \begin{pmatrix} 0 \\ 0 \\ -\frac{M_y b_3}{\mu_{r3}} \\ -\frac{M_y b_5}{\mu_{r3}} \\ -\frac{M_y b_4}{\mu_{r3}} \end{pmatrix} = \begin{pmatrix} 0 \\ 0 \\ -\frac{0.8 \cdot 2}{1.05} \\ -\frac{0.8 \cdot (-2)}{1.05} \\ \frac{0.8 \cdot 0}{1.05} \end{pmatrix} = \begin{pmatrix} 0 \\ 0 \\ -1.5238 \\ 1.5238 \\ 0 \end{pmatrix}$$

We can apply the appropriate boundary equations to solve the problem. The vector potential solution is:

$$A = \begin{pmatrix} 0 \\ 0 \\ 0.07701 \\ -0.60154 \\ -0.11574 \end{pmatrix} \text{ Wb/m}$$

Transient solution.

We explain the case of the two dimensional transient magnetic problem. The PDE in this case is:

$$\nabla \cdot (\nu \nabla A) - \sigma \frac{\partial A}{\partial t} = -J$$

The functional for this equation is:

$$F = \frac{1}{2} \iint_{\Omega^e} \left(\nu^e |\nabla A|^2 - 2J_0^e A + 2\sigma^e A \frac{\partial A}{\partial t} \right) d\Omega_e$$

The first and second terms are the same as those that are encountered in the static case. The third term yields:

$$\begin{aligned} \iint_{\Omega^e} \left(\sigma^e A \frac{\partial A}{\partial t} \right) d\Omega_e &= \sum_{i=1}^3 \sum_{j=1}^3 A_i \sigma^e \iint_{\Delta^e} N_i N_j d\Omega \frac{\partial A_j}{\partial t} = \sum_{i=1}^3 \sum_{j=1}^3 A_i R_{ij}^e \frac{\partial A_j}{\partial t} \\ R_{ij}^e &= \sigma^e \iint_{\Delta^e} N_i N_j d\Omega \\ R_{ij}^e &= \begin{cases} \sigma^e \frac{\Delta^e}{6} & i = j \\ \sigma^e \frac{\Delta^e}{12} & i \neq j \end{cases} \end{aligned}$$

The system of equations in matrix vector notation can be written as:

$$KA + R \frac{\partial A}{\partial t} = T$$

The solution is only computed at discrete points in time, spaced in finite intervals Δt , the time steps. The Galerkin approach can be applied in the time domain. First, we select the shape functions (of time, of course) as:

$$\begin{aligned} A(t) &= \alpha \tau A_k + \alpha(1 - \tau) A_{k-1} \\ T(t) &= \alpha \tau T_k + \alpha(1 - \tau) T_{k-1} \end{aligned}$$

with:

$$\begin{aligned} \tau &= \frac{t - t_{k-1}}{t_k - t_{k-1}} = \frac{t - t_{k-1}}{\Delta t} \\ \frac{\partial A}{\partial t} &= \frac{\partial A}{\partial \tau} \frac{\partial \tau}{\partial t} = \frac{A_k - A_{k-1}}{\Delta t} \end{aligned}$$

Then we apply the Residue minimization with $\alpha\tau$ as a weighting function:

$$\int_0^1 \alpha\tau \left\{ K(\alpha\tau A_k + \alpha(1-\tau)A_{k-1}) + R \frac{A_k - A_{k-1}}{\Delta t} - (\alpha\tau T_k + \alpha(1-\tau)T_{k-1}) \right\} d\tau = 0$$

After some algebraic manipulation, we obtain:

$$\left(\alpha K + \frac{R}{\Delta t} \right) A_k + \left((1-\alpha)K - \frac{R}{\Delta t} \right) A_{k-1} - (\alpha T_k + (1-\alpha)T_{k-1}) = 0$$

Comments:

- This expression is unconditionally stable for $\alpha \geq 1/2$.
- For $\alpha = 1$ this is also free of oscillations.
- For $\alpha = 0$ we obtain the forward difference Euler method. This is an explicit method because the term KA is evaluated at the beginning of the time interval:

$$\left(\frac{R}{\Delta t} \right) A_k = \left(K - \frac{R}{\Delta t} \right) A_{k-1} + (T_{k-1})$$

- For $\alpha = 1$ it gives the backward difference fully implicit method since the term KA is evaluated at the end of the time interval:

$$\left(K + \frac{R}{\Delta t} \right) A_k = \left(\frac{R}{\Delta t} \right) A_{k-1} + (T_k)$$

- For $\alpha = 1/2$ it gives the Crank-Nicholson scheme:

$$\left(\frac{1}{2} K + \frac{R}{\Delta t} \right) A_k = - \left(\left(\frac{1}{2} \right) K - \frac{R}{\Delta t} \right) A_{k-1} + (\alpha T_k + (1-\alpha)T_{k-1})$$

Voltage fed electromagnetic devices

Up to this point, we have assumed that the source of the magnetic field is a current density J . In many cases, the system is voltage fed and the current in the coil is an unknown. To solve this problem, both the field equations and the coil voltage equation must be solved simultaneously. The voltage equation for the coil can be written as:

$$U = ri + n \frac{d\Phi}{dt}$$

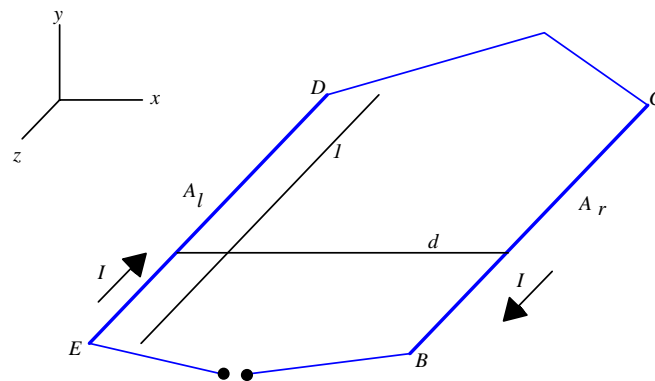
Where U is the voltage on the coil, r and n are the coil resistance and the number of turns; Φ is the magnetic flux (in Wb/m, we can justify this unit later) generated in the solution domain and linked by the coil.

The current contribution of an element of the mesh is given by:

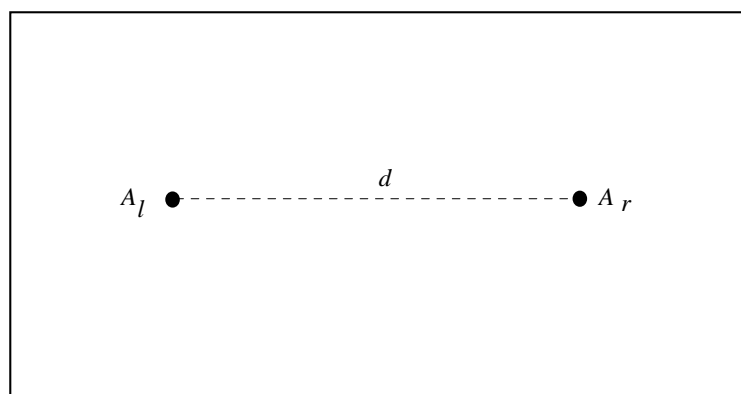
$$\frac{J\Delta^e}{3} \begin{bmatrix} 1 \\ 1 \\ 1 \end{bmatrix}$$

Where J is the current density and Δ^e is the area of the element. Now define a new parameter κ as the coil turn density (turns/m²). If I is the current of one turn, we have:

$$J = \kappa I \Rightarrow \frac{\kappa\Delta^e}{3} \begin{bmatrix} 1 \\ 1 \\ 1 \end{bmatrix} I = PI$$



A turn carrying a DC current I , infinitely long in z -direction: only one unit in z -direction is represented. Distance between conductors is d .



The x-y representation of the turn.

Let us now consider the flux (per unit length in z -direction) of B across a surface that has the turn as contour. It reads, obviously:

$$\varphi_s(B) = \int_S B \cdot n dS$$

where S is the surface of the turn for one unit in z -direction, and n is the outward normal to S . By substituting in the above equation the expression for B as a function of A :

$$\varphi_s(B) = \int_S \nabla \times A \cdot n dS$$

Application of Stokes theorem results in the following:

$$\varphi_s(B) = \int_{+\partial S} A \cdot d(+\partial S)$$

where the line integral in the rhs is defined along the turn. On the basis of the assumptions previously made, the flux of B can be rewritten as:

$$\varphi_s(B) = \int_B^C A dz + \int_{+\partial S} A d(+\partial S) + \int_D^E A dz$$

The first and third integral have, respectively, the following values: A_r and $-A_l$ (the vector potential has the same value when the x - and y -coordinate of the point do not change and the z -coordinate of the point changes). On the other hand, the study was performed with reference of one unit in z -direction, and moreover it should be noted that the integration path moves in opposite directions along the conductors. The second integral is obviously negligible with respect to the first and third since the wires are infinitely long: we studied just one unit of their length in z -direction, but the extension of their active length is infinitely greater than the length of the connections. We arrive at the following formula:

$$\varphi_s(B) = A_r - A_l$$

for the flux by unity of depth. If the length is finite, the total flux is:

$$\Phi_s(B) = (A_r - A_l)l$$

As the zero magnetic vector potential value is usually present in the field evaluation as a result of the calculation or by means of the Dirichlet boundary condition, one can calculate the magnetic flux with respect to the null value and then rewrite the above equation as

$$\Phi = Al$$

Where A is the potential at any point in the solution domain. Further, assuming that A is the average potential in a triangular element, we get:

$$A = \frac{1}{3}(A_i + A_j + A_k)$$

If n is the number of turns within the element, we get:

$$n = \kappa \cdot \Delta^e \Rightarrow n\Phi = \frac{\kappa \cdot \Delta^e l}{3}(A_i + A_j + A_k)$$

$$n\Phi = \frac{\kappa \cdot \Delta^e l}{3} \begin{bmatrix} 1 & 1 & 1 \end{bmatrix} \begin{bmatrix} A_i \\ A_j \\ A_k \end{bmatrix} = QA$$

$$Q = \frac{\kappa \cdot \Delta^e l}{3} \begin{bmatrix} 1 & 1 & 1 \end{bmatrix}$$

Using Euler's scheme to discretize the time derivative, we obtain:

$$n = \kappa \cdot \Delta^e \Rightarrow n\Phi = \frac{\kappa \cdot \Delta^e l}{3}(A_i + A_j + A_k)$$

$$n \frac{d\Phi}{dt} = Q \frac{dA}{dt} = \frac{Q}{\Delta t} \begin{bmatrix} A_i(k+1) - A_i(k) \\ A_j(k+1) - A_j(k) \\ A_k(k+1) - A_k(k) \end{bmatrix} = \frac{Q}{\Delta t}(A_k - A_{k-1})$$

$$U = ri + n \frac{d\Phi}{dt} \Rightarrow U_k = [r]I_k + \frac{Q}{\Delta t}(A_k - A_{k-1})$$

$$\left(K + \frac{R}{\Delta t}\right)A_k = \left(\frac{R}{\Delta t}\right)A_{k-1} + (T_k) = \left(\frac{R}{\Delta t}\right)A_{k-1} + PI_k + D_k$$

D_k is a term related to the permanent magnet or other currents.

$$\begin{pmatrix} \left(K + \frac{R}{\Delta t}\right) & -P \\ \frac{Q}{\Delta t} & [r] \end{pmatrix} \begin{pmatrix} A_k \\ I_k \end{pmatrix} = \begin{pmatrix} \left(\frac{R}{\Delta t}\right) & 0 \\ \frac{Q}{\Delta t} & 0 \end{pmatrix} \begin{pmatrix} A_{k-1} \\ I_{k-1} \end{pmatrix} + \begin{pmatrix} D_k \\ U_k \end{pmatrix}$$

We can also include an additional term to taken into account the external resistance and inductance

$$U = ri + n \frac{d\Phi}{dt} + r_a i + L_a \frac{di}{dt}$$

the final equation is:

$$\begin{pmatrix} \left(K + \frac{R}{\Delta t}\right) & -P \\ \frac{Q}{\Delta t} & [r] + [r_a] + \frac{1}{\Delta t}[L_a] \end{pmatrix} \begin{pmatrix} A_k \\ I_k \end{pmatrix} = \begin{pmatrix} \left(\frac{R}{\Delta t}\right) & 0 \\ \frac{Q}{\Delta t} & \frac{1}{\Delta t}[L_a] \end{pmatrix} \begin{pmatrix} A_{k-1} \\ I_{k-1} \end{pmatrix} + \begin{pmatrix} D_k \\ U_k \end{pmatrix}$$

Coupling of field and electrical circuit equations.

Two types of conductors are often present in electrical machines. There can be “thin” or “thick” conductors. In the first case the eddy currents must be neglected.

Thick conductors

The following figure shows a thick conductor with section S_t and length l . We can write that:

$$\frac{\partial}{\partial z} \left(\sigma \frac{\partial V}{\partial z} \right) = 0$$

Thus, we can define a scalar electric potential as:

$$V = V_1 z + V_0$$

The voltage U_t on the conductor is given by:

$$U_t = - \int_0^l \frac{dV}{dz} dz = -V_1 l$$

The current density in the conductor is determined by:

$$J = \sigma E = \sigma \left(-\frac{\partial A}{\partial t} - \nabla V \right) \Rightarrow J = \sigma \left(-\frac{\partial A}{\partial t} - \frac{dV}{dz} \right) = \sigma \left(-\frac{\partial A}{\partial t} - V_1 \right) = \sigma \left(-\frac{\partial A}{\partial t} + \frac{U_t}{l} \right)$$

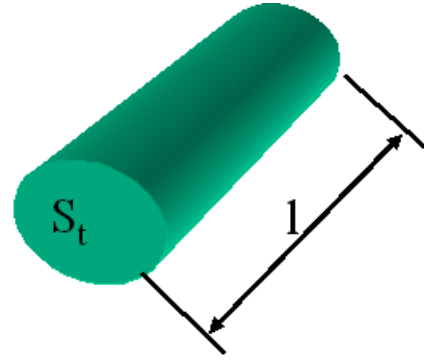
and the total current in the conductor is determined by:

$$\begin{aligned} I_t &= \iint_{S_t} J dS_t = - \iint_{S_t} \sigma \frac{\partial A}{\partial t} dS_t + \iint_{S_t} \sigma \frac{U_t}{l} dS_t \\ I_t &= \iint_{S_t} J dS_t = - \iint_{S_t} \sigma \frac{\partial A}{\partial t} dS_t + \frac{U_t}{\frac{1}{\sigma} \frac{l}{S_t}} = - \iint_{S_t} \sigma \frac{\partial A}{\partial t} dS_t + \frac{U_t}{R_t} \end{aligned}$$

Rearranging this equation, we can write:

$$U_t = R_t I_t + R_t \iint_{S_t} \sigma \frac{\partial A}{\partial t} dS_t$$

This equation shows that the voltage in a thick conductor is equal to the sum of the voltage drop over the DC resistance and a voltage drop due to eddy currents. This equation, with the addition of the field equation:

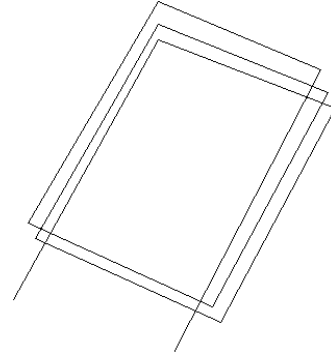


$$\nabla \cdot (\nu \nabla A) = -J = -\sigma E = -\sigma \left(-\frac{\partial A}{\partial t} - \nabla V \right) \Rightarrow \nabla \cdot (\nu \nabla A) - \sigma \frac{\partial A}{\partial t} + \sigma \frac{U_t}{l} = 0$$

solves the problem.

Thin conductors

The figure shows a coil made of N_{co} turns of thin conductors with cross section s , serial connected. In this conductor the current density is considered uniform over the cross-section. We call I_f the current in a conductor.



$$\left. \begin{aligned} \nabla \cdot (\nu \nabla A) - \sigma \frac{\partial A}{\partial t} + \sigma \frac{U_t}{l} &= 0 \\ U_t &= R_t I_t + R_t \iint_{s_t} \sigma \frac{\partial A}{\partial t} dS_t \end{aligned} \right\} \nabla \cdot (\nu \nabla A) - \sigma \frac{\partial A}{\partial t} + \sigma \frac{R_t I_t + R_t \iint_{s_t} \sigma \frac{\partial A}{\partial t} dS_t}{l} \Downarrow$$

$$\nabla \cdot (\nu \nabla A) - \sigma \frac{\partial A}{\partial t} + \frac{I_f}{s} + \frac{1}{s} \iint_{s_t} \sigma \frac{\partial A}{\partial t} dS_t = 0$$

As the induced current density $\sigma \frac{\partial A}{\partial t}$ is uniform over the cross section S , we can write:

$$\frac{1}{s} \iint_{s_t} \sigma \frac{\partial A}{\partial t} dS_t = \sigma \frac{\partial A}{\partial t}$$

and substituting in the above equation, this is reduced to:

$$\nabla \cdot (\nu \nabla A) + \frac{I_f}{s} = 0$$

If the total surface of the coil is $S_f = N_{co} s$, we get:

$$\nabla \cdot (\nu \nabla A) + \frac{N_{co}}{S_f} I_f = 0$$

The voltage U_f at the terminal of the winding can be written as:

$$\begin{aligned}
U_f &= N_{co} U_t = N_{co} R_t I_t + N_{co} R_t \iint_s \sigma \frac{\partial A}{\partial t} ds = \\
N_{co} \frac{l}{\sigma s} I_f + N_{co} \frac{l}{\sigma s} \iint_s \sigma \frac{\partial A}{\partial t} ds &= N_{co} \frac{l}{\sigma s} I_f + N_{co} \frac{l}{\sigma s} \sigma \frac{\partial A}{\partial t} s = \\
N_{co} \frac{l}{\sigma s} I_f + \frac{l}{s} S_f \frac{\partial A}{\partial t} & \\
\text{or} & \\
U_f &= N_{co} \frac{l}{\sigma s} I_f + N_{co} \frac{l}{S_f} \iint_{S_f} \frac{\partial A}{\partial t} ds \\
U_f &= R_f I_f + N_{co} \frac{l}{S_f} \iint_{S_f} \frac{\partial A}{\partial t} ds
\end{aligned}$$

The first term is the voltage drop over the coil resistance. The second term is the voltage induced in the coil. In the thin conductors domain, the equations become:

$$\begin{aligned}
U_f &= R_f I_f + N_{co} \frac{l}{S_f} \iint_{S_f} \frac{\partial A}{\partial t} ds \\
\nabla \cdot (\nu \nabla A) + \frac{N_{co}}{S_f} I_f &= 0
\end{aligned}$$

Equations for the whole domain.

According to the above explained, the set of equations for an electromagnetic device presenting magnetic materials, permanent magnets, thick and thin conductors is:

$$\begin{aligned}
\nabla \cdot (\nu \nabla A) + \frac{N_{co}}{S_f} I_f - \sigma \frac{\partial A}{\partial t} + \sigma \frac{U_t}{l} &= \nabla \times (\nu \cdot \mu_0 \cdot M) \\
U_f &= R_f I_f + N_{co} \frac{l}{S_f} \iint_{S_f} \frac{\partial A}{\partial t} ds \\
U_t &= R_t I_t + R_t \iint_{S_t} \sigma \frac{\partial A}{\partial t} dS_t
\end{aligned}$$

After applying the Variational or Galerkin method to the above equations, a set of matrix equations is obtained as follows:

$$KA + R \frac{\partial A}{\partial t} - PI_f - P'U_t = D$$

$$Q' \frac{d}{dt} A + R' I_t = U_t$$

$$Q \frac{d}{dt} A + R'' I_f + L \frac{d}{dt} I_f = U_f$$

Matrix R'' is the d.c. resistance of the thin conductors windings and L is the matrix of additional inductances. R' is a matrix containing the DC resistance of thick conductors. Matrices K , R , P , P' , D , Q , and Q' are obtained by assembling the element matrices:

$$K_{kj} = \iint_{S_i} \nabla N_j^t \nu \nabla N_k ds$$

$$R_{kj} = \iint_{S_i} \sigma N_k^t N_j ds$$

$$P_{kj} = \iint_{S_i} \frac{N_{coj}}{S_{\bar{j}}} N_k ds$$

if the node k belongs to the region of winding j , or $P_{kj} = 0$ if node k is elsewhere.

$$P'_{kj} = \iint_{S_i} \frac{\sigma_j}{l} N_k ds$$

if node k is in the region of winding j , or equal to 0 elsewhere.

$$D(k) = \iint_{\Omega} \nu \mu_0 \left(M_x \frac{\partial N_k}{\partial y} - M_y \frac{\partial N_k}{\partial x} \right) dx dy$$

$$Q_{kj} = \iint_{S_i} \frac{N_{cok} l}{S_{kj}} N_j ds$$

if node k belongs the region of winding j , or equal to zero elsewhere.

$$Q'_{kj} = \iint_{S_i} R_{tk} \sigma_k N_j ds$$

if node k belongs to the thick conductor k , or equal to zero elsewhere. Different combinations of thin and thick conductors windings can be found in electrical devices. We will not consider these here in detail: a complete formulation must consider the connexion between the different coils and the restrictions in voltage and current must be considered. In general form, we can write:

$$[I_f] = [C_1][I_1]; \quad [I_t] = [C_2][I_2]$$

$$[U_f] = [C_3][U_1]; \quad [U_t] = [C_4][U_2]$$

U_1 , U_2 , I_1 and I_2 are the external voltage and currents (for example a three phase symmetrical system) and C_1 , C_2 , C_3 and C_4 are the connexion matrices that relate the external values to the internal values.

Movement modelling for electrical machines

The basic equations of motion are as follows:

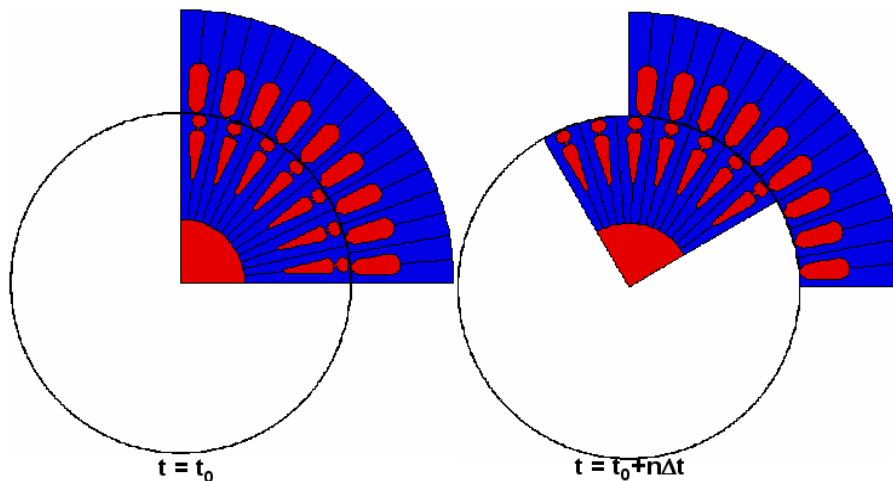
$$J \frac{d\omega}{dt} + \rho \omega = M_i - M_c$$

$$\omega = \frac{d\theta}{dt}$$

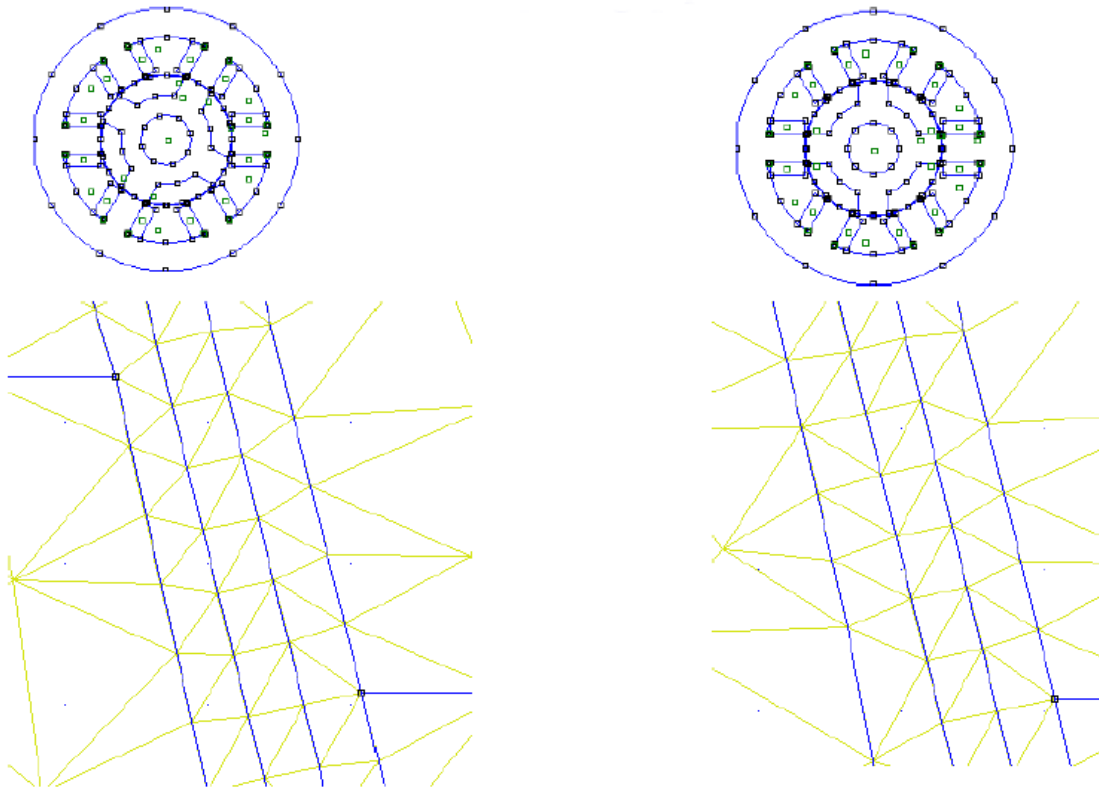
Where:

- J is the moment of inertia
- ρ is the damping coefficient
- ω is the rotational speed
- θ is the rotation angle
- M_i is the electromagnetic torque
- M_c is the externally applied mechanical torque.

All of the above pertain to the moving part. The following figure shows an electric motor where the rotor is rotating. There is an important question:

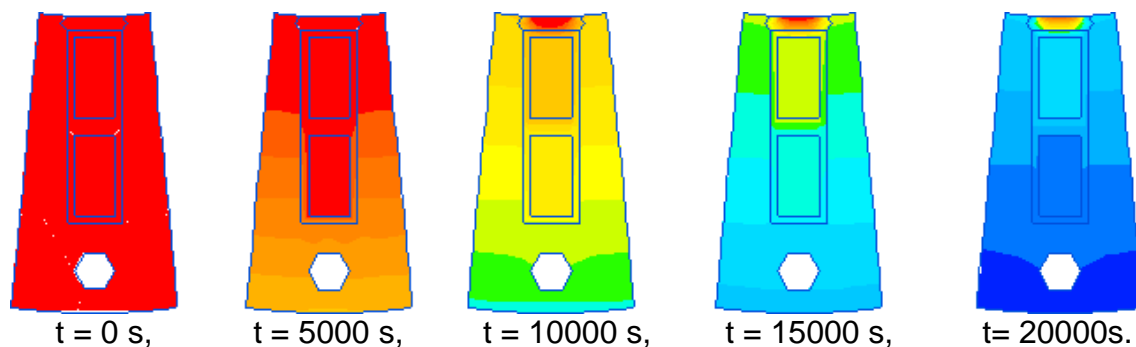


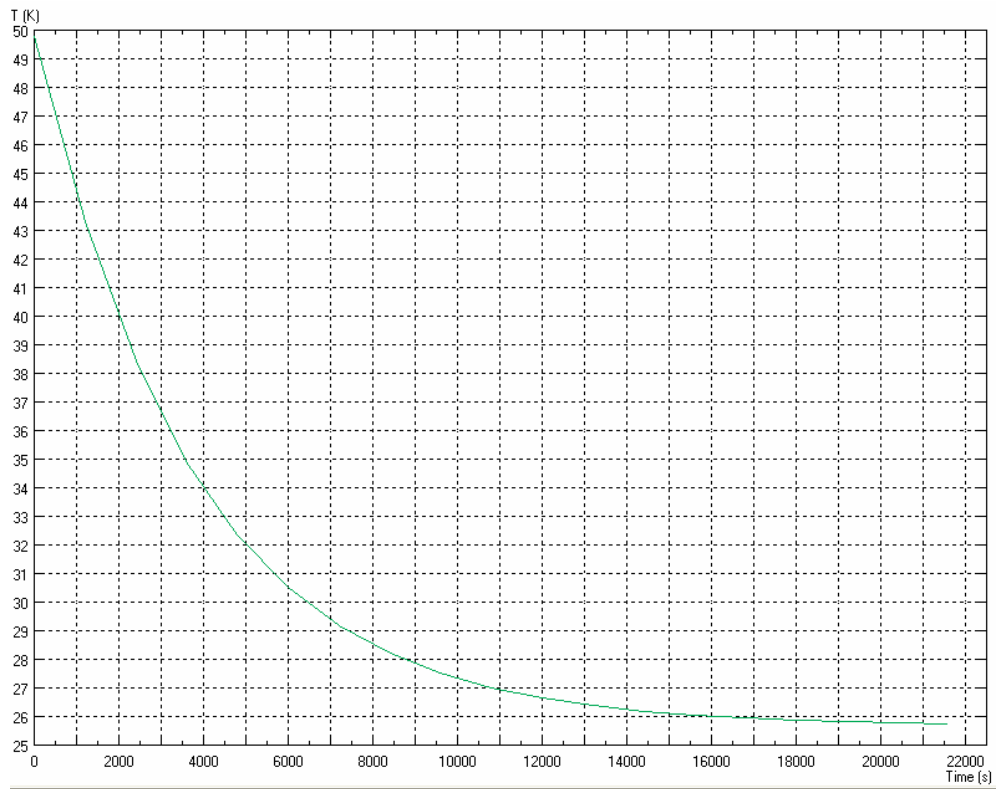
If the system is in movement, the matrix of the whole system are time-dependent? The response is Yes! Apparently we need to recompute ALL of the elements on the system matrices. If you construct a grid with a moving band in the air-gap and only the elements in the air gap (or free space) are permitted to deform, the conductivity σ in such elements is zero, which nullifies the contribution of the R , P' and Q' matrices (additionally the elements of P and Q matrices are also nulls because there are no conductors and current in the air). Therefore, only the time dependence of the K matrix requires consideration: we only need to recompute the values of the elements in the moving band.



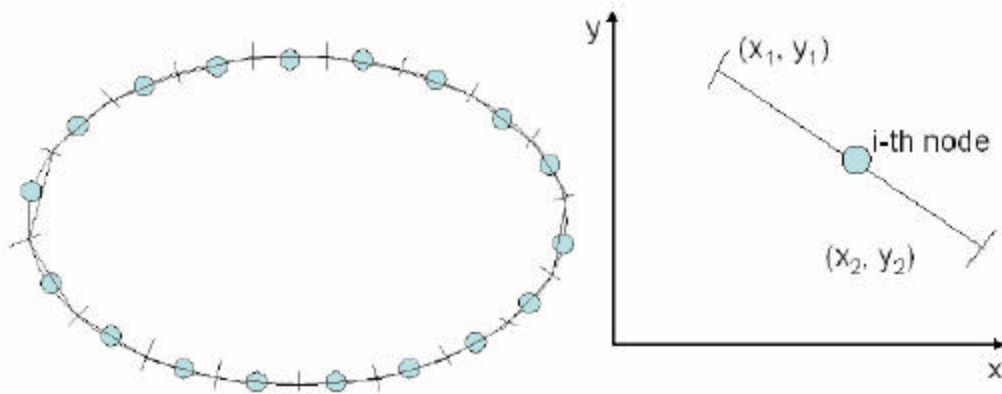
It is adequate to create three or four layers in the air gap and apply the moving band to the intermediate layers. These layers are in free space.

Example. The following sequence of pictures shows the evolution of the temperature in a slot of an electrical machine. Initially the machine is hot. At $t = 0$ s the machine is disconnected from the network and remains motionless. The temperature falls to ambient values.





NUMERICAL SOLUTION: INTEGRAL EQUATION METHOD



INTEGRAL EQUATION METHOD

An integral equation (IE) is any equation involving an unknown function Φ under the integral sign.

The Linear integral equations that are most frequently studied fall into two categories named Fredholm and Volterra. The following table shows the first, second and third kinds of these (for the one-dimensional case)

Kind	Fredholm	Volterra
1	$f(x) = \int_a^b K(x,t) \cdot \Phi(t) \cdot dt$	$f(x) = \int_a^x K(x,t) \cdot \Phi(t) \cdot dt$
2	$f(x) = \Phi(x) - \lambda \cdot \int_a^b K(x,t) \cdot \Phi(t) \cdot dt$	$f(x) = \Phi(x) - \lambda \cdot \int_a^x K(x,t) \cdot \Phi(t) \cdot dt$
3	$f(x) = a(x) \cdot \Phi(x) - \lambda \cdot \int_a^b K(x,t) \cdot \Phi(t) \cdot dt$	$f(x) = a(x) \cdot \Phi(x) - \lambda \cdot \int_a^x K(x,t) \cdot \Phi(t) \cdot dt$

Where λ is a scalar (real or complex) parameter. Functions $K(x,t)$ and $f(x)$ and the limits a and b are known, while $\Phi(x)$ is unknown. The parameter λ is sometimes equal to unity. The function K is known as the kernel of the integral equation. Notice that in the case of Volterra Integral equations the upper limit of integration is a variable.

If $f(x)=0$, the integral equations become homogeneous.

Connection between differential and integral equations

Most ordinary differential equations can be expressed as integral equations, but the reverse is not true. While boundary conditions are imposed externally in differential equations, they are incorporated within integral equations.

For example, consider the following differential equation:

$$\begin{aligned} \frac{d\Phi}{dx} &= F(x, \Phi), \quad a \leq x \leq b \\ \Phi(a) &= c_1 \end{aligned}$$

Integrating we obtain a Volterra equation of the second kind:

$$\Phi(x) = \int_a^x F(t, \Phi(t)) \cdot dt + c_1$$

Another example:

$$\frac{d^2\Phi}{dx^2} = F(x, \Phi), \quad a \leq x \leq b$$

Integrating once yields:

$$\frac{d\Phi(x)}{dx} = \int_a^x F(x, \Phi(t)) \cdot dt + \Phi'(a)$$

Integrating again (by parts) we obtain:

$$\Phi(x) = \Phi(a) + (x-a) \cdot \Phi'(a) + \int_a^x (x-t) \cdot F(x, \Phi) \cdot dt$$

Green's functions

A more systematic means to obtain an IE from a PDE is by constructing an auxiliary function known as the **Green's function** for that problem. The Green's function, also known as the **source function or influence function**, is the **kernel** function obtained from a linear boundary value problem and forms the essential link between the differential and integral formulations.

To obtain the field caused by a distributed source by the Green's function technique, we find the effects of **each elementary portion of source and sum them up**. If $G(\mathbf{r}, \mathbf{r}')$ is the field at the observation point (or field point) \mathbf{r} caused by a unit point source at the source point \mathbf{r}' , then the field at \mathbf{r} by a source distribution $g(\mathbf{r}')$ is the integral of $g(\mathbf{r}')G(\mathbf{r}, \mathbf{r}')$ over the range of \mathbf{r}' occupied by the source. The function G is the Green's function. Thus, physically, the Green's function represents the potential at \mathbf{r} due to a unit point charge at \mathbf{r}' . For example the solution to the problem:

$$\nabla^2 \Phi = g \quad \text{in} \quad R$$

$$\Phi = f \quad \text{on} \quad B$$

Is given by:

$$\Phi = \int_R g(\mathbf{r}') \cdot G(\mathbf{r}, \mathbf{r}') \cdot dv' + \oint_B f \cdot \frac{\partial G}{\partial n} \cdot dS$$

Where n denotes the outward normal to the boundary B of the solution region R . It is obvious that the solution Φ can be determined if the Green's function G is known. So the real problem is not that of finding the solution but that of constructing the Green's function for the problem. We now illustrate how to construct the Green's function G corresponding to a PDE. It is usually convenient to let G be the sum of a particular integral of the inhomogeneous equation $LG = g$ and the solution of the associated homogeneous equation $LG = 0$. We let

$$G(\mathbf{r}, \mathbf{r}') = F(\mathbf{r}, \mathbf{r}') + U(\mathbf{r}, \mathbf{r}')$$

Where F , known as the free-space Green's function or fundamental solution, satisfies:

$$LF = \delta(r, r') \quad \text{in } R$$

And U satisfies

$$LU = 0 \quad \text{in } R$$

So that by superposition $G = F + U$ satisfies $LG = \delta(r, r')$. Also $G = f$ on the boundary B requires that:

$$U = -F + f \quad \text{on } B$$

Notice that F need not satisfy the boundary condition. For $L = \nabla^2$ the fundamental solution F is equal to

- $F = \frac{1}{2\pi} \ln r$ for the two-dimensional case and
 $r = \sqrt{(x-x')^2 + (y-y')^2}$
- $F = -\frac{1}{4 \cdot \pi} \cdot \frac{1}{r}$ for the three-dimensional case
 $r = \sqrt{(x-x')^2 + (y-y')^2 + (z-z')^2}$

The Green's function of each case is equal to:

$$G = F + U = F = \frac{1}{2\pi} \ln r + U$$

$$G = F + U = F = -\frac{1}{4 \cdot \pi} \cdot \frac{1}{r} + U$$

U is chosen so that G satisfies prescribed boundary conditions.

The following table shows some Green's functions that are commonly used in the solution of electromagnetic related problems.

Operator Equation	Laplace's Equation	Steady-State Helmholtz's equation $\nabla^2 G + k^2 \cdot G = \delta(r, r')$	Modified steady-state Helmholtz's equation $\nabla^2 G - k^2 \cdot G = \delta(r, r')$
Solution's region	$\nabla^2 G = \delta(r, r')$		
1-dimensional	No solution	$-\frac{j}{2k} e^{jk(x-x')}$	$-\frac{j}{2k} e^{-jk(x-x')}$
2-dimensional	$\frac{1}{2\pi} \ln r$	$-\frac{j}{4} H_0(k \cdot r)$	$-\frac{j}{4} K_0(k \cdot r)$
3-dimensional	$-\frac{1}{4 \cdot \pi} \cdot \frac{1}{r}$	$-\frac{1}{4\pi \cdot r} e^{jk(x-x')}$	$-\frac{1}{4\pi \cdot r} e^{-jk(x-x')}$

With the aid of the Green's function, we can construct the integral equation corresponding to the Poisson's equation:

$$\nabla^2 V = -\frac{\rho}{\varepsilon}$$

As

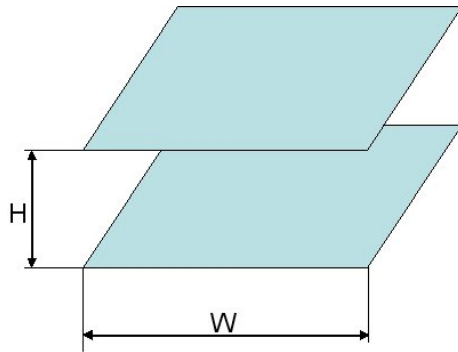
$$V = \int \frac{\rho}{\varepsilon} \cdot G(r, r') \cdot dV$$

In three dimensions this equation results in:

$$V = \int \frac{\rho}{\varepsilon} \cdot \frac{1}{4 \cdot \pi} \cdot \frac{1}{r} \cdot dV$$

THE MOMENT METHOD

The moment method has been applied to so many EM problems. We will consider a typical problem: the determination of the capacity of a strip transmission line (or a grounded system). Consider the strip transmission line of the following figure.

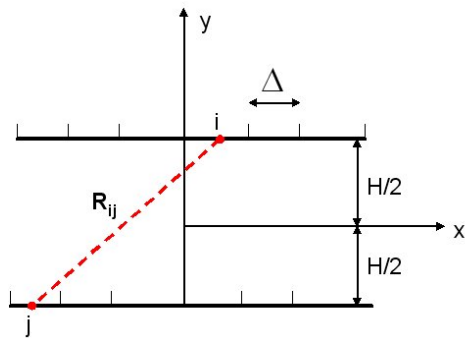


If the line is assumed to be infinitely long, the problem is reduced to a two-dimensional problem in a plane. Let the potential difference of the strips be $V = 2U$ V so that strip 1 is maintained at $+U$ V while strip 2 is at $-U$ V. Our objective is to find the surface charge density $\rho(x, y)$ on the strips so that the total charge per unit length on one strip can be found as

$$Q_l = \int \rho dl$$

Q_l is the charge per unit length as distinct from the total charge on the strip because we are treating a three-dimensional problem as a two-dimensional one. Once Q is known, the capacitance per unit length C_l can be found from

$$C_l = \frac{Q_l}{V}$$



To find $\rho(x, y)$ using the moment method, we divide each strip into n sub-areas of equal width Δ so that sub-areas in strip 1 are numbered $1, 2, \dots, n$, while those in strip 2 are numbered $n+1, n+2, \dots, 2n$. The potential at an arbitrary field point is:

$$V(x, y) = \frac{1}{2 \cdot \pi \cdot \varepsilon} \int \rho(x', y') \cdot \ln\left(\frac{R}{r_0}\right) \cdot dx' \cdot dy'$$

$$R = \sqrt{(x - x')^2 + (y - y')^2}$$

Since the integral may be regarded as rectangular sub-areas, the potential at the centre of a typical sub-area S_i is

$$V_i = \frac{1}{2 \cdot \pi \cdot \varepsilon} \sum_{j=1}^{j=2n} \rho_j \int_{S_i} \ln \left(\frac{R_{ij}}{r_0} \right) \cdot dx'$$

Or

$$V_i = \sum_{j=1}^{j=2n} A_{ij} \cdot \rho_j$$

Where

$$A_{ij} = \frac{1}{2 \cdot \pi \cdot \varepsilon} \int_{S_i} \ln \left(\frac{R_{ij}}{r_0} \right) \cdot dx'$$

R_{ij} is the distance between the i th and j th sub-areas, and $A_{ij} \cdot \rho_j$ represents the potential at point i due to the sub-area j . In the above equations we assume that the charge density is constant within each sub-area (this is true if the areas are small compared with the total dimensions of the strip). For all the sub-areas we have:

$$\begin{aligned} V_1 &= \sum_{j=1}^{j=2n} A_{1j} \cdot \rho_j = U & V_{n+1} &= \sum_{j=1}^{j=2n} A_{(n+1)j} \cdot \rho_j = -U \\ V_2 &= \sum_{j=1}^{j=2n} A_{2j} \cdot \rho_j = U & \dots\dots\dots & \\ \dots & & V_{2n} &= \sum_{j=1}^{j=2n} A_{(2n)j} \cdot \rho_j = -U \\ V_n &= \sum_{j=1}^{j=2n} A_{nj} \cdot \rho_j = U \end{aligned}$$

Then we obtain a set of $2n$ simultaneous equations with $2n$ unknown charge densities. In matrix form

$$\begin{pmatrix} A_{11} & A_{12} & \dots\dots\dots & A_{1,2n} \\ A_{21} & A_{22} & \dots\dots\dots & A_{2,2n} \\ \dots & \dots & \dots\dots\dots & \dots \\ A_{2n,1} & A_{2n,2} & \dots\dots\dots & A_{2n,2n} \end{pmatrix} \cdot \begin{pmatrix} \rho_1 \\ \rho_2 \\ \dots \\ \rho_{2n} \end{pmatrix} = \begin{pmatrix} U \\ U \\ \dots \\ -U \end{pmatrix}$$

$$A \cdot \rho = U$$

$$\rho = A^{-1} \cdot U$$

Once ρ is known, we determine C_i :

$$C_i = \frac{Q_i}{V} = \frac{\int \rho dl}{2 \cdot U} \cong \frac{\sum_{j=1}^n \rho_j \cdot \Delta}{2 \cdot U}$$

It is easy to show that the elements of matrix A can be reduced to:

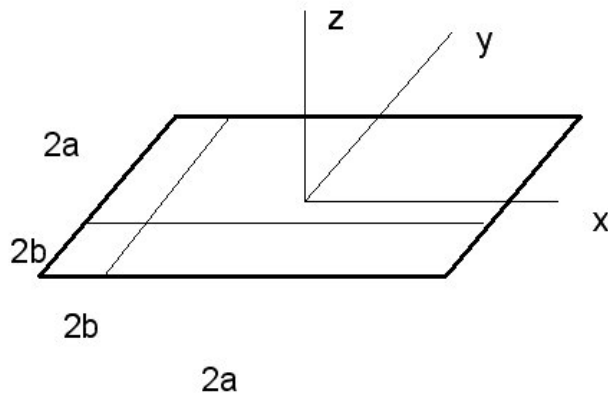
$$A_{ij} = \begin{cases} \frac{\Delta}{2 \cdot \pi \cdot \varepsilon} \cdot \ln \left(\frac{R_{ij}}{r_0} \right) & i \neq j \\ \frac{\Delta}{2 \cdot \pi \cdot \varepsilon} \cdot \left[\ln \left(\frac{\Delta}{r_0} \right) - 1.5 \right] & i = j \end{cases}$$

r_0 is a constant scale factor commonly taken as unity.

The following table presents the computed value of the capacitance per length unit for a different number of segments per strip, n . $H = 2\text{m}$; $W = 5\text{m}$; $\varepsilon = \varepsilon_0$.

n	3	7	11	18	39	59
C (pF)	62.8	65.29	66.05	66.18	67.08	67.22

Example. Consider a square conducting plate $2a$ meters on a side and lying on the $z = 0$ plane, with centre at the origin, as shown in the following figure.



Let ρ be the surface charge density on the plate, assumed to have zero thickness. The potential at any point in space is:

$$V(x, y) = \iint \frac{\rho(x', y')}{4\pi\epsilon R} dx' dy'$$

$$R = \sqrt{(x - x')^2 + (y - y')^2 + (z)^2}$$

The boundary condition is $V = U$ (constant on the plate). The unknown to be determined is the charge density and the capacitance of the plate. Consider the plate divided into N square subsections, as shown in the above figure. Using the results from earlier, we can write:

$$V_m = \sum_{n=1}^{n=N} A_{mn} \cdot \rho_n$$

Where:

$$A_{mn} = \int_{\Delta x_n} dx' \int_{\Delta y_n} \frac{1}{4\pi\epsilon \sqrt{(x_m - x')^2 + (y_m - y')^2}} dy'$$

To simplify the solution we define the following function: $f_n = \begin{cases} 1 & \text{on } S_n \\ 0 & \text{out} \end{cases}$ in this case

we can write: $\rho(x, y) \approx \sum_{n=1}^N a_n \cdot f_n$ and finally we obtain the following expression:

$$V \approx \sum_{n=1}^N A_{mn} \cdot a_n \quad \text{for } m = 1, 2, \dots, N$$

In this case the capacitance can be calculated as

$$C = \frac{Q}{V} = \frac{\int \rho dS}{U} \cong \frac{\sum_{j=1}^n \rho_j \cdot S_n}{U} \approx \frac{1}{U} \sum_{n=1}^N a_n \cdot S_n = \sum_{n=1}^N A^{-1}_{mn} \cdot S_n$$

For numerical results the A_{mn} elements must be evaluated. Let $2b = \frac{2a}{\sqrt{N}}$ denote the side length of each S_n :

$$A_{mn} = \int_{\Delta x_n} dx' \int_{\Delta y_n} \frac{1}{4\pi\epsilon\sqrt{(x_m - x')^2 + (y_m - y')^2}} dy' = \begin{cases} m = n & \frac{2b}{\pi\epsilon} \ln(1 + \sqrt{2}) \\ m \neq n & \approx \frac{S_n}{4\pi\epsilon R_{mn}} = \frac{b^2}{\pi\epsilon\sqrt{(x_m - x_n)^2 + (y_m - y_n)^2}} \end{cases}$$

Consider the following case (this corresponds to a grounding system of an electric central unit):

$$2a \cdot 2a = 20 \cdot 20 = 400m^2; \quad 2b \cdot 2b = 10 \cdot 10 = 100m^2; \quad N = 4$$

These values yield:

$$A_{11} = A_{22} = A_{33} = A_{44} = \frac{8.82}{\pi\epsilon}$$

$$A_{12} = A_{21} = A_{23} = A_{32} = \dots = A_{41} = A_{14} = \frac{2.50}{\pi\epsilon}$$

$$A_{13} = A_{31} = A_{24} = A_{42} = \frac{1.76}{\pi\epsilon}$$

$$A_{mn} = \frac{1}{\pi\epsilon} \begin{bmatrix} 8.82 & 2.5 & 1.76 & 2.5 \\ 2.5 & 8.82 & 2.5 & 1.76 \\ 1.76 & 2.5 & 8.82 & 2.5 \\ 2.5 & 1.76 & 2.5 & 8.82 \end{bmatrix}$$

$$A^{-1}_{mn} = \pi\epsilon \begin{bmatrix} 0.132 & -0.0287 & -9.97e-3 & -0.0287 \\ -0.0287 & 0.132 & -0.0287 & -9.97e-3 \\ -9.97e-3 & -0.0287 & 0.132 & -0.0287 \\ -0.0287 & -9.97e-3 & -0.0287 & 0.132 \end{bmatrix}$$

And the capacitance is:

$$C \approx \frac{1}{V} \sum_{n=1}^N a_n \cdot \Delta S_n = \sum_{n=1}^N A^{-1}_{nn} \cdot S_n = 718.1\epsilon_r \text{ pF}$$

$$\frac{C}{2a \cdot \epsilon_r} = \frac{718.1}{20} = 35.90 \text{ pF/m}$$

The following table shows capacitance per unit length calculated by using the above equation for various sub areas:

Number of sub areas (N)	1	4	9	16	25	64	100	225
$\frac{C}{2a \cdot \epsilon_r}$ (pF/m)	31.51	35.90	37.32	38.18	38.71	39.51	39.78	40.12

A good estimate of the true capacitance is 40 pF/m.

BOUNDARY ELEMENT METHOD (BEM)

The basic idea of the BEM is to discretize the integral equation using boundary elements. The well-known moment method is equivalent to BEM when using sub-sectional bases and the delta function as weighting functions. Thus, BEM can be regarded as a combination of the classical boundary integral equation method and the discretization concepts originated from FEM.

Consider the case of the Laplace's equation, i.e.

$$\begin{aligned}\nabla^2 u &= 0 \text{ in } \Omega \\ u &= \bar{u} \text{ in } \Gamma_1 \\ q = \frac{\partial u}{\partial n} &= \bar{q} \text{ in } \Gamma_2 \\ \Gamma &= \Gamma_1 + \Gamma_2\end{aligned}$$

By application of the weighted residual method we obtain:

$$\int_{\Omega} \nabla^2 u \cdot W \cdot d\Omega = 0$$

Using the following identities:

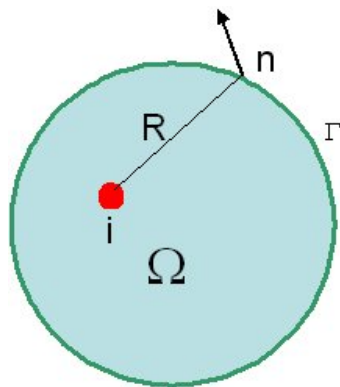
$$\begin{aligned}\nabla(\nabla u W) &= \nabla^2 u W + \nabla u \nabla W \\ \nabla(u \nabla W) &= u \nabla^2 W + \nabla u \nabla W\end{aligned}$$

And applying the Gauss theorem, we can write:

$$\int_{\Omega} W \cdot \nabla^2 u \cdot d\Omega = \int_{\Gamma} W \cdot \frac{\partial u}{\partial n} \cdot d\Gamma - \int_{\Gamma} u \cdot \frac{\partial W}{\partial n} \cdot d\Gamma + \int_{\Omega} u \cdot \nabla^2 W \cdot d\Omega = 0$$

The weighting function W is chosen to be the fundamental solution, determined earlier:

$$\nabla^2 W = \delta(r - r')$$



Thus the domain integral in the above equation can be written as:

$$\int_{\Omega} u \cdot \nabla^2 W \cdot d\Omega = - \int_{\Omega} u \cdot \delta(r - r') \cdot d\Omega = -u_i$$

For any point inside the domain. Combining the above equations, the following integral relation is obtained:

$$u_i = \int_{\Gamma} W \cdot \frac{\partial u}{\partial n} \cdot d\Gamma - \int_{\Gamma} u \cdot \frac{\partial W}{\partial n} \cdot d\Gamma$$

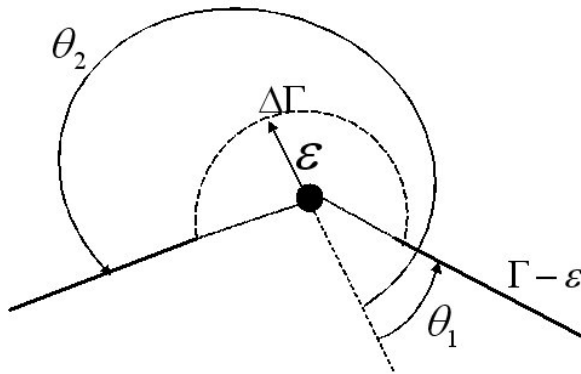
Performing similar mathematical manipulations we can obtain the following integral relation for the Poisson equation ($\nabla^2 u = -f$):

$$u_i = \int_{\Gamma} W \cdot \frac{\partial u}{\partial n} \cdot d\Gamma - \int_{\Gamma} u \cdot \frac{\partial W}{\partial n} \cdot d\Gamma - \int_{\Omega} f \cdot W \cdot d\Omega$$

Notes:

- Neumann boundary conditions ($\frac{\partial u}{\partial n}$) are taken into account by the first integral
- Dirichlet boundary conditions (u) are taken into account by the second integral.
- Any source point (f) inside the domain Ω is taken into account by the domain integral in the above equation.
- From the Poisson's equation, the residual to be minimized can be written as:

$$\int_{\Omega} (\nabla^2 u + f) \cdot W \cdot d\Omega = 0$$



When the observation point “i” is located on the boundary Γ , the boundary integral becomes singular as R approaches zero.

To extract the singularity on the boundary, we rewrite the equation

$$u_i = \int_{\Gamma} W \cdot \frac{\partial u}{\partial n} \cdot d\Gamma - \int_{\Gamma} u \cdot \frac{\partial W}{\partial n} \cdot d\Gamma$$

In the following form:

$$u_i = \int_{\Gamma - \Delta\Gamma} W \cdot \frac{\partial u}{\partial n} \cdot d\Gamma + \int_{\Delta\Gamma} W \cdot \frac{\partial u}{\partial n} \cdot d\Gamma - \int_{\Gamma - \Delta\Gamma} u \cdot \frac{\partial W}{\partial n} \cdot d\Gamma - \int_{\Delta\Gamma} u \cdot \frac{\partial W}{\partial n} \cdot d\Gamma$$

We present in detail the two-dimensional case. In this case:

$$W = -\frac{1}{2\pi} \ln r$$

And:

$$\begin{aligned} \int_{\Delta\Gamma} W \cdot \frac{\partial u}{\partial n} \cdot d\Gamma &= -\frac{1}{2\pi} \int_{\Delta\Gamma} \ln r \cdot \frac{\partial u}{\partial n} \cdot d\Gamma = -\frac{1}{2\pi} \lim_{\varepsilon \rightarrow 0} \left[\int_{\theta_1}^{\theta_2} \ln \varepsilon \cdot \frac{\partial u}{\partial n} \cdot \varepsilon \cdot d\theta \right] = 0 \\ - \int_{\Delta\Gamma} u \cdot \frac{\partial W}{\partial n} \cdot d\Gamma &= -\frac{1}{2\pi} \int_{\Delta\Gamma} \frac{1}{r} \cdot u \cdot d\Gamma = -\frac{1}{2\pi} \lim_{\varepsilon \rightarrow 0} \left[\int_{\theta_1}^{\theta_2} \frac{1}{\varepsilon} \cdot u \cdot \varepsilon \cdot d\theta \right] = -\frac{\theta_2 - \theta_1}{2\pi} \cdot u_i \end{aligned}$$

Substituting in the earlier equation we obtain:

$$c_i \cdot u_i = \int_{\Delta\Gamma} W \cdot \frac{\partial u}{\partial n} \cdot d\Gamma - \int_{\Delta\Gamma} u \cdot \frac{\partial W}{\partial n} \cdot d\Gamma$$

Where:

$$c_i = \begin{cases} 1 & i \in \Omega \\ 1 - \frac{\theta_2 - \theta_1}{2\pi} & i \in \Gamma \\ 0 & i \notin \Omega \end{cases}$$

If we consider Poisson's equation:

$$\begin{aligned} \int_{\Omega} f \cdot W \cdot d\Omega &= \int_{\Omega - \Delta\Omega} f \cdot W \cdot d\Omega + \int_{\Delta\Omega} f \cdot W \cdot d\Omega \\ \int_{\Delta\Omega} f \cdot W \cdot d\Omega &= -\frac{1}{2\pi} \int_{\Delta\Omega} f \cdot \ln r \cdot d\Omega = -\frac{1}{2\pi} \lim_{\varepsilon \rightarrow 0} \left[\int_{\theta_1}^{\theta_2} \ln \varepsilon \cdot f \cdot \varepsilon \cdot d\theta \cdot d\varepsilon \right] = 0 \end{aligned}$$

The final equation is:

$$c_i \cdot u_i = \int_{\Delta\Gamma} W \cdot \frac{\partial u}{\partial n} \cdot d\Gamma - \int_{\Delta\Gamma} u \cdot \frac{\partial W}{\partial n} \cdot d\Gamma - \int_{\Omega} f \cdot W \cdot d\Omega$$

In general either u or $\frac{\partial u}{\partial n}$ on the boundary must be known. Determining all values of solution u and its normal derivatives on the boundary the solution at an arbitrary point of the domain can be calculated. The electrostatic and magnetostatic problems are then defined by the following equations:

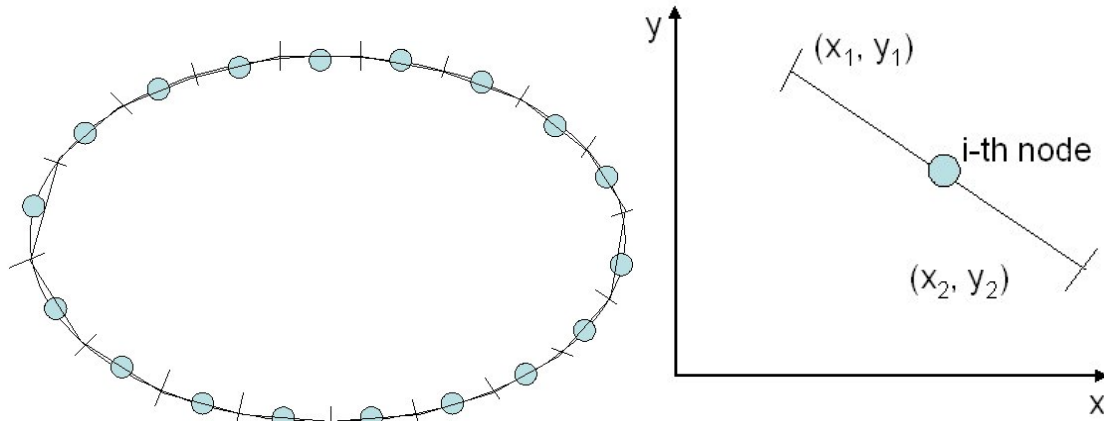
$$\begin{aligned} c_i \cdot \Phi_i &= \int_{\Delta\Gamma} W \cdot \frac{\partial \Phi}{\partial n} \cdot d\Gamma - \int_{\Delta\Gamma} \Phi \cdot \frac{\partial W}{\partial n} \cdot d\Gamma + \int_{\Omega} \frac{\rho}{\varepsilon} \cdot W \cdot d\Omega \\ c_i \cdot A_i &= \int_{\Delta\Gamma} W \cdot \frac{\partial A}{\partial n} \cdot d\Gamma - \int_{\Delta\Gamma} A \cdot \frac{\partial W}{\partial n} \cdot d\Gamma + \int_{\Omega} \mu \cdot J \cdot W \cdot d\Omega \end{aligned}$$

Where Φ denotes the electrostatic potential and A is the magnetic potential vector.

Boundary element discretization

The basic idea of the BEM is to discretize the boundary of the domain under consideration into a set of elements. The unknown solution over each element is approximated by an interpolation function, which is associated with the values of the functions at the element nodes, so that the integral equation can be converted into a system of algebraic equations. The boundary geometry can be discretized in a series of elements.

The simplest solution is to use a set of constant boundary elements (other solutions are available, such as linear or quadratic elements). The geometry of the constant boundary element for the two-dimensional case is shown in the following figure.



Using the constant boundary element approximation the integral equation formulation of the problem defined by the Poisson's equation becomes:

$$c_i \cdot u_i = \sum_{j=1}^{j=M} \left[\left. \frac{\partial u}{\partial n} \right|_j \cdot \int_{\Gamma_j} W \cdot d\Gamma - u_j \cdot \int_{\Gamma_j} \frac{\partial W}{\partial n} \cdot d\Gamma \right] - \int_{\Omega_s} f \cdot W \cdot d\Omega$$

Where f is the constant value of the source on segment domain containing sources. Introducing the following notation

$$\left. \frac{\partial u}{\partial n} \right|_j = Q_j$$

$$u_j = U_j$$

$$G_{ij} = \int_{\Gamma_j} W \cdot d\Gamma$$

$$H_{ij} = \int_{\Gamma_j} \frac{\partial W}{\partial n} \cdot d\Gamma$$

$$P_i = - \int_{\Omega_s} f \cdot W \cdot d\Omega$$

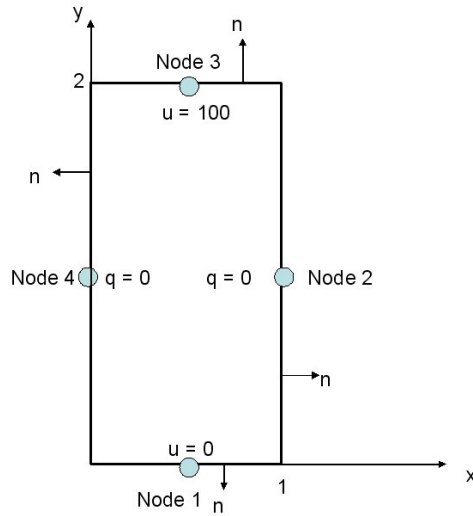
The above equation can be written for each i as

$$c_i \cdot u_i = \sum_{j=1}^{j=M} [G_{ij} \cdot Q - H_{ij} \cdot U_j] + P_i$$

This algebraic equation system can also be written in matrix form as follows:

$$H \cdot U = G \cdot Q + P$$

Example. Solve Laplace's equation in a rectangular box. At the horizontal boundary lines the potential $u = U$ are prescribed. At the vertical boundary lines the normal derivative q is given.



We use constant elements for the solution. For simplicity we use a coarse discretization with 4 elements. In this case only the boundary values u_2, u_4, q_1 and q_3 are unknown. For each element we need to calculate the following expression:

$$c_i \cdot u_i = \sum_{j=1}^{j=M} \left[\frac{\partial u}{\partial n} \Big|_j \cdot \int_{\Gamma_j} W \cdot d\Gamma - u_j \cdot \int_{\Gamma_j} \frac{\partial W}{\partial n} \cdot d\Gamma \right] - \int_{\Omega_s} f \cdot W \cdot d\Omega$$

In our case:

- $f = 0.$
- $$c_i = \begin{cases} 1 & i \in \Omega \\ 1 - \frac{\theta_2 - \theta_1}{2\pi} = 1 - \frac{\pi}{2\pi} = \frac{1}{2} & i \in \Gamma \\ 0 & i \notin \Omega \end{cases}$$

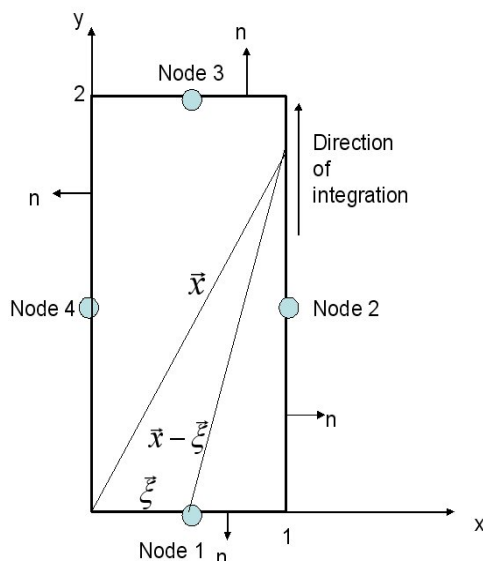
We can write:

$$\frac{1}{2} \cdot u_i = \sum_{j=1}^{j=M} \left[\frac{\partial u}{\partial n} \Big|_j \cdot \int_{\Gamma_j} W \cdot d\Gamma - u_j \cdot \int_{\Gamma_j} \frac{\partial W}{\partial n} \cdot d\Gamma \right]$$

in this case four equations for the four unknown boundary values are obtained if “i” takes the values 1 to 4. In matrix notation these equations are:

$$\frac{1}{2} \cdot \begin{bmatrix} u_1 \\ u_2 \\ u_3 \\ u_4 \end{bmatrix} = H \cdot \begin{bmatrix} u_1 \\ u_2 \\ u_3 \\ u_4 \end{bmatrix} + G \cdot \begin{bmatrix} q_1 \\ q_2 \\ q_3 \\ q_4 \end{bmatrix}; \quad \begin{aligned} G_{ij} &= \int_{\Gamma_j} W \cdot d\Gamma \\ H_{ij} &= \int_{\Gamma_j} \frac{\partial W}{\partial n} \cdot d\Gamma \end{aligned}; \quad \begin{aligned} W &= -\frac{1}{2\pi} \ln \bar{r} \\ \frac{dW}{dn} &= -\frac{1}{2\pi} \frac{\bar{r}}{r^2} \end{aligned}$$

Calculation of matrix elements



- H_{12} and G_{12}

$$H_{12} = \frac{1}{2\pi} \int_0^2 \frac{1/2}{\left(y^2 + \left(\frac{1}{2}\right)^2\right)} \cdot dy = \frac{1}{2\pi} \cdot a \tan(2y) \Big|_0^2 = 0.2110$$

$$G_{12} = \frac{1}{2\pi} \int_0^2 \ln \left(\sqrt{y^2 + \left(\frac{1}{2}\right)^2} \right) \cdot dy =$$

$$G_{12} = \frac{1}{4\pi} \cdot \left[y \cdot \ln \left(\sqrt{y^2 + \left(\frac{1}{2}\right)^2} \right) - 2y + a \tan(2y) \right] \Big|_0^2 = -0.0175$$

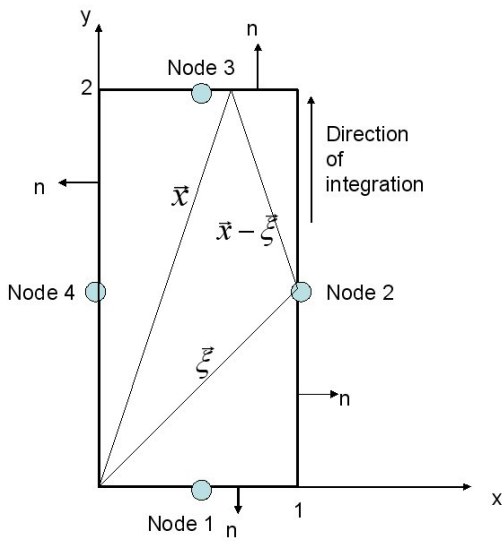
Due to the spatial isotropy of the problem, we can write:

$$H_{14} = H_{34} = H_{32} = H_{12}$$

$$G_{14} = G_{34} = G_{32} = G_{12}$$

These symmetries do NOT hold in general for BEM.

- H_{23} and G_{23}



$$H_{23} = \frac{1}{2\pi} \int_1^0 \frac{1}{((x-1)^2 + (1)^2)} \cdot dx = \frac{1}{2\pi} \cdot a \tan(x-1) \Big|_1^0 = 0.125$$

$$G_{23} = \frac{1}{2\pi} \int_1^0 \ln\left(\sqrt{((x-1)^2 + (1)^2)}\right) \cdot dx =$$

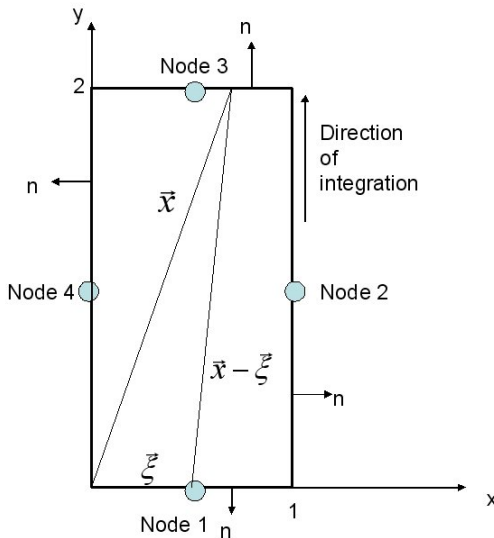
$$\frac{1}{2\pi} \cdot \left[\frac{1}{2} (x-1) \ln(((x-1)^2 + (1)^2)) - 2(x-1) + 2a \tan(x-1) \right] \Big|_1^0 = -0.0210$$

Due to the spatial isotropy of the problem, we can write:

$$H_{21} = H_{41} = H_{43} = H_{23}$$

$$G_{21} = G_{41} = G_{43} = G_{23}$$

- H_{13} and G_{13}



$$H_{13} = \frac{1}{2\pi} \int_1^0 \frac{2}{\left(\left(x - \frac{1}{2}\right)^2 + (2)^2\right)} \cdot dx = \frac{1}{2\pi} \cdot a \tan\left(\frac{x}{2} - \frac{1}{4}\right) \Big|_1^0 = 0.0780$$

$$G_{13} = \frac{1}{2\pi} \int_1^0 \ln\left(\sqrt{\left(\left(x - \frac{1}{2}\right)^2 + (2)^2\right)}\right) \cdot dx =$$

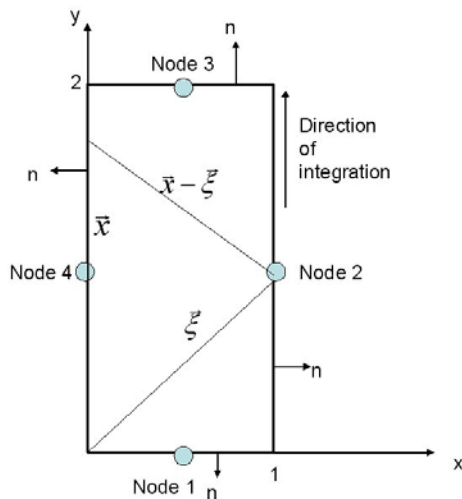
$$\frac{1}{2\pi} \cdot \left[\frac{1}{2} \left(x - \frac{1}{2}\right) \ln\left(\left(\left(x - \frac{1}{2}\right)^2 + 4\right)\right) - 2x + 4a \tan\left(\frac{x}{2} - \frac{1}{4}\right) \right] \Big|_1^0 = -0.1119$$

And by symmetry:

$$H_{31} = H_{13}$$

$$G_{31} = G_{13}$$

- H_{24} and G_{24}



$$H_{24} = \frac{1}{2\pi} \int_2^0 \frac{1}{((1)^2 + (y-1)^2)} \cdot dy = \frac{1}{2\pi} \cdot a \tan(y-1) \Big|_2^0 = 0.250$$

$$G_{24} = \frac{1}{2\pi} \int_2^0 \ln\left(\sqrt{((y-1)^2 + (1)^2)}\right) \cdot dy =$$

$$\frac{1}{2\pi} \cdot \left[\frac{1}{2} (y-1) \ln(((y-1)^2 + (1)^2)) - 2y + 2a \tan(y-1) \right] \Big|_2^0 = -0.0420$$

- Diagonal terms $H_{11} = H_{22} = H_{33} = H_{44} = 0$. Because the vector \vec{r} is perpendicular to \vec{n} when the load point and field point are located at the same element.
- Diagonal terms G_{11} to G_{44} . Making a change of coordinates such that

$$r = \left| \xi \cdot \frac{L}{2} \right|$$

Where L is the element length. After some algebraic manipulations we can write:

$$G_{ii} = \frac{1}{2\pi} \int_{P_{o\text{int}1}}^{P_{o\text{int}2}} \ln\left(\frac{1}{r}\right) \cdot dr = \frac{1}{\pi} \cdot \frac{L}{2} \cdot \left(\ln\left(\frac{2}{L}\right) + 1 \right)$$

The numerical values are:

$$G_{11} = G_{33} = 0.2695 \quad (L=1)$$

$$G_{22} = G_{44} = 0.3183 \quad (L=2)$$

Assembling the above equations yields:

$$\begin{aligned} \frac{1}{2} \cdot \begin{bmatrix} u_1 \\ u_2 \\ u_3 \\ u_4 \end{bmatrix} &= H \cdot \begin{bmatrix} u_1 \\ u_2 \\ u_3 \\ u_4 \end{bmatrix} + G \cdot \begin{bmatrix} q_1 \\ q_2 \\ q_3 \\ q_4 \end{bmatrix} \\ \frac{1}{2} \cdot \begin{bmatrix} u_1 \\ u_2 \\ u_3 \\ u_4 \end{bmatrix} &= \begin{bmatrix} 0 & 0.2110 & 0.0780 & 0.2110 \\ 0.125 & 0 & 0.125 & 0.250 \\ 0.0780 & 0.2110 & 0 & 0.2110 \\ 0.125 & 0.250 & 0.125 & 0 \end{bmatrix} \cdot \begin{bmatrix} u_1 \\ u_2 \\ u_3 \\ u_4 \end{bmatrix} + \\ &+ \begin{bmatrix} 0.2695 & -0.0175 & -0.1119 & -0.0175 \\ -0.0210 & 0.3183 & -0.0210 & -0.0420 \\ -0.1119 & -0.0175 & 0.2695 & -0.0175 \\ -0.0210 & -0.0420 & -0.0210 & 0.3183 \end{bmatrix} \cdot \begin{bmatrix} q_1 \\ q_2 \\ q_3 \\ q_4 \end{bmatrix} \end{aligned}$$

Substituting the known values:

$$\begin{bmatrix} u_1 \\ u_2 \\ u_3 \\ u_4 \end{bmatrix} = \begin{bmatrix} 0 \\ u_2 \\ 100 \\ u_4 \end{bmatrix}; \quad \begin{bmatrix} q_1 \\ q_2 \\ q_3 \\ q_4 \end{bmatrix} = \begin{bmatrix} q_1 \\ 0 \\ q_3 \\ 0 \end{bmatrix}$$

We can solve the resultant system of equations and obtain the following result:

$$\begin{bmatrix} u_1 \\ u_2 \\ u_3 \\ u_4 \end{bmatrix} = \begin{bmatrix} 0 \\ 50 \\ 100 \\ 50 \end{bmatrix}; \quad \begin{bmatrix} q_1 \\ q_2 \\ q_3 \\ q_4 \end{bmatrix} = \begin{bmatrix} -75.77 \\ 0 \\ 75.77 \\ 0 \end{bmatrix}$$

Numerical Integration

The above example shows the difficulties of making an analytical solution for the integrals involved in this method. It is convenient to use a numerical method to compute those integrals. The most used method is the Gauss integration method. In the following pages we show the practical application of this method.

The integral can be approximated as:

$$I = \int_a^b f(x)dx \approx \frac{b-a}{2} \sum_{i=1}^N w_i \cdot f\left(\frac{z_i \cdot (b-a) + (a+b)}{2}\right) + E$$

Where N is the number of integration points, z_i is the coordinate of the i th integration point, w_i is the associated weighting factor and E is the error. Values of z_i and w_i are listed in the following table. Values for more points can be obtained in numerical methods references.

N	$\pm z_i$	w_i
2	0.57735	1
3	0	0.88888
	0.77459	0.55555
4	0.33998	0.65214
	0.86113	0.34785
5	0	0.56888
	0.53846	0.47862
	0.90618	0.23693
6	0.23862	0.46791
	0.66121	0.36076
	0.93247	0.17132
7	0	0.41796
	0.40584	0.38183
	0.74153	0.27970
	0.94911	0.12948
8	0.18343	0.36268
	0.52553	0.31370
	0.79666	0.22238
	0.96029	0.10123

In our case, the integrals for G and H can be calculated by application to the following equations:

$$\begin{aligned}
L &= \sqrt{(x_2 - x_1)^2 + (y_2 - y_1)^2} \\
A_x &= \frac{(x_2 - x_1)}{2}; \quad B_x = \frac{(x_2 + x_1)}{2}; \quad A_y = \frac{(y_2 - y_1)}{2}; \quad B_y = \frac{(y_2 + y_1)}{2} \\
N_x &= -2 \cdot \frac{A_y}{L}; \quad N_y = 2 \cdot \frac{A_x}{L} \\
Z_{xk} &= A_x \cdot z_k + B_x; \quad Z_{yk} = A_y \cdot z_k + B_y \\
R_k &= \sqrt{(x_p - Z_{xk})^2 + (y_p - Z_{yk})^2} \\
R_{xk} &= -\frac{(x_p - Z_{xk})}{R_k}; \quad R_{yk} = -\frac{(y_p - Z_{yk})}{R_k} \\
G_{ij} &\cong \frac{1}{2 \cdot \pi} \cdot \frac{L}{2} \cdot \sum_{k=1}^N \ln\left(\frac{1}{R_k}\right) \cdot w_k \\
H_{ij} &\cong -\frac{1}{2 \cdot \pi} \cdot \frac{L}{2} \cdot \sum_{k=1}^N \frac{R_{xk} \cdot N_y + R_{yk} \cdot N_x}{R_k} \cdot w_k
\end{aligned}$$

Where:

- x_p, y_p are the coordinates of the collocation point.
- L is the element length
- N_x, N_y are the components of the unit normal.
- R_k is the distance from the collocation point to the Gauss integration points on the boundary element.
- R_{xk}, R_{yk} are the radius derivatives.

In our case and as a result to the application of the above algorithm we obtain the same values for the matrix coefficients.

Computation of solution into the domain

Using the general expression we can write:

$$c_i \cdot u_i = \sum_{j=1}^{j=M} \left[\frac{\partial u}{\partial n} \Big|_j \cdot \int_{\Gamma_j} W \cdot d\Gamma - u_j \cdot \int_{\Gamma_j} \frac{\partial W}{\partial n} \cdot d\Gamma \right]$$

In our case: $c_i = \begin{cases} 1 & i \in \Omega \\ 1 - \frac{\theta_2 - \theta_1}{2\pi} = 1 - \frac{\pi}{2\pi} = \frac{1}{2} & i \in \Gamma \\ 0 & i \notin \Omega \end{cases}$ we obtain the following equation, valid

for each interior point:

$$u_i = \sum_{j=1}^{j=M} \left[\frac{\partial u}{\partial n} \Big|_j \cdot \int_{\Gamma_j} W \cdot d\Gamma - u_j \cdot \int_{\Gamma_j} \frac{\partial W}{\partial n} \cdot d\Gamma \right]$$

For example, determine the potential at point (0.5;1). By application of the above algorithm we obtain the following values:

$$\begin{aligned}
u_i &= G_{i1}q_1 + G_{i2}q_2 + G_{i3}q_3 + G_{i4}q_4 + H_{i1}u_1 + H_{i2}u_2 + H_{i3}u_3 + H_{i4}u_4 = \\
&= 0.00618 \cdot q_1 - 0.1049 \cdot q_2 + 0.00618 \cdot q_3 - 0.1049 \cdot q_4 + \\
&\quad - 0.1476 \cdot u_1 - 0.3397 \cdot u_2 - 0.1476 \cdot u_3 - 0.3397 \cdot u_4 = \\
&= 0.00618 \cdot (-75.77) - 0.1049 \cdot (0) + 0.00618 \cdot (75.77) - 0.1049 \cdot (0) + \\
&\quad - (-0.1476 \cdot (0) - 0.3397 \cdot (50) - 0.1476 \cdot (100) - 0.3397 \cdot (50)) = \\
&= 48.73
\end{aligned}$$

Comparison with the analytical solution

The analytical solution is the following:

$$u = 50 \cdot y$$

It is easy to verify that this solution is compatible with all of boundary conditions. The fluxes in x and y direction are:

$$\begin{aligned}
q_y &= \frac{du}{dy} = 50 \cdot \vec{e}_y \cdot \vec{n} \\
q_x &= 0
\end{aligned}$$

The following table summarizes the analytical and numerical results for every point

Point	Coordinates	U (analytical)	U(numerical)	Q(analytical)	Q(numerical)
1	(0.5;0)	0	0	-50	-75.77
2	(1;1)	50	50	0	0
3	(0.5;2)	100	100	50	75.77
4	(0;1)	50	50	0	0
Interior	(0.5;1)	50	48.73	50	---

The comparison between analytical and numerical solution shows the following:

- For the potential (Dirichlet variable) u even a coarse discretization leads to good accuracy.
- The larger error for the flux (Neumann variable) q can be explained by the fact that the differentiated quantity requires finer discretization because integration smoothes while differentiation creates roughness.

If you use a finer boundary mesh with, for example, six constant elements of length 1, you could obtain the following matrix equation:

$$\begin{bmatrix}
 0.5 & -0.1762 & -0.0348 & -0.0780 & -0.0348 & -0.1762 \\
 -0.1762 & 0.5 & 0 & -0.0936 & -0.0826 & -0.1476 \\
 -0.0936 & 0 & 0.5 & -0.1762 & -0.1476 & -0.0826 \\
 -0.0780 & -0.0348 & -0.1762 & 0.5 & -0.1762 & -0.0348 \\
 -0.0936 & -0.0826 & -0.1476 & -0.1762 & 0.5 & 0 \\
 -0.1762 & -0.1476 & -0.0826 & -0.0936 & 0 & 0.5
 \end{bmatrix}
 \begin{bmatrix}
 u_1 \\
 u_2 \\
 u_3 \\
 u_4 \\
 u_5 \\
 u_6
 \end{bmatrix}
 =
 \begin{bmatrix}
 0.2695 & 0.0533 & -0.0708 & -0.1120 & -0.0708 & 0.0533 \\
 0.0533 & 0.2695 & 0.0072 & -0.0750 & -0.0553 & -0.0062 \\
 -0.0750 & 0.0072 & 0.2695 & 0.0533 & -0.0062 & -0.0553 \\
 -0.1120 & -0.0708 & 0.0533 & 0.2695 & 0.0533 & 0.0708 \\
 -0.0750 & -0.0553 & -0.0062 & 0.0533 & 0.2695 & 0.0072 \\
 0.0533 & -0.0062 & -0.0553 & -0.0750 & 0.0072 & 0.2695
 \end{bmatrix}
 \begin{bmatrix}
 q_1 \\
 q_2 \\
 q_3 \\
 q_4 \\
 q_5 \\
 q_6
 \end{bmatrix}$$

$$\begin{bmatrix} u_1 \\ u_2 \\ u_3 \\ u_4 \\ u_5 \\ u_6 \end{bmatrix} = \begin{bmatrix} 0 \\ u_2 \\ u_3 \\ 100 \\ u_5 \\ u_6 \end{bmatrix}; \quad \begin{bmatrix} q_1 \\ q_2 \\ q_3 \\ q_4 \\ q_5 \\ q_6 \end{bmatrix} = \begin{bmatrix} q_1 \\ 0 \\ 0 \\ q_4 \\ 0 \\ 0 \end{bmatrix}$$

The solution of the above system of equations is:

$$\begin{bmatrix} q_1 \\ u_2 \\ u_3 \\ q_4 \\ u_5 \\ u_6 \end{bmatrix} = \begin{bmatrix} -56.39 \\ 23.87 \\ 76.13 \\ 56.39 \\ 76.13 \\ 23.87 \end{bmatrix}$$

The following table summarizes the analytical and numerical results for every point

Point	Coordinates	U (analytical)	U(numerical)	Q(analytical)	Q(numerical)
1	(0.5;0)	0	0	-50	-56.39
2	(1;0.5)	25	23.87	0	0
3	(1;1.5)	75	76.13	0	0
4	(0.5;2)	100	100	50	56.39
5	(0;1.5)	75	76.13	0	0
6	(0;0.5)	25	23.87	0	0

In this case the solution is more accurate as the earlier and coarse solution.

Comparison of the FE and BE Methods

We comment here on some of the major differences between the two methods. Depending on the application some of these differences can either be considered as advantageous or disadvantageous to a particular scheme.

FEM	BEM	OBS.
An entire domain mesh is required.	A mesh of the boundary only is required.	(1)
Entire domain solution is calculated as a part of the solution.	Solution on the boundary is calculated first, and then the solution at domain points (if required) are found as a separate step.	(2)
Reactions on the boundary typically less accurate than the dependent variables.	Both u and q are of the same accuracy.	---
Differential Equation is being approximated.	Only boundary conditions are being approximated.	(3)
Sparse symmetric matrix is generated.	Fully populated non symmetric matrices are generated.	(4)
Element integrals are easy to evaluate.	Integrals are more difficult to evaluate, and some contain integrands that become singular.	(5)
Widely applicable. Handles nonlinear problems well.	Cannot even handle all linear problems.	(6)
Relatively easy to implement.	Much more difficult to implement.	(7)

(1) Because of the reduction in size of the mesh, one often hears of people saying that the problem size has been reduced by one dimension. This is one of the major pluses of the BEM - construction of meshes for complicated objects, particularly in 3D, is a very time consuming exercise.

(2) There are many problems where the details of interest occur on the boundary, or are localised to a particular part of the domain, and hence an entire domain solution is not required.

(3) The use of the Green-Gauss theorem and a fundamental solution in the formulation means that the BEM involves no approximations of the differential Equation in the domain - only in its approximations of the boundary conditions.

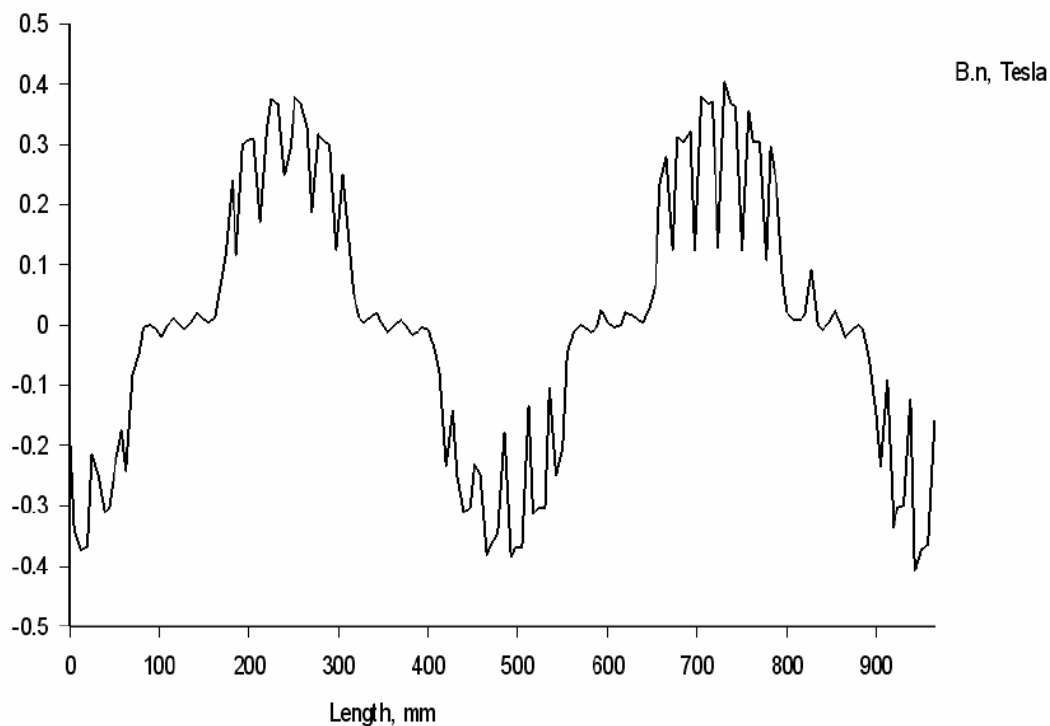
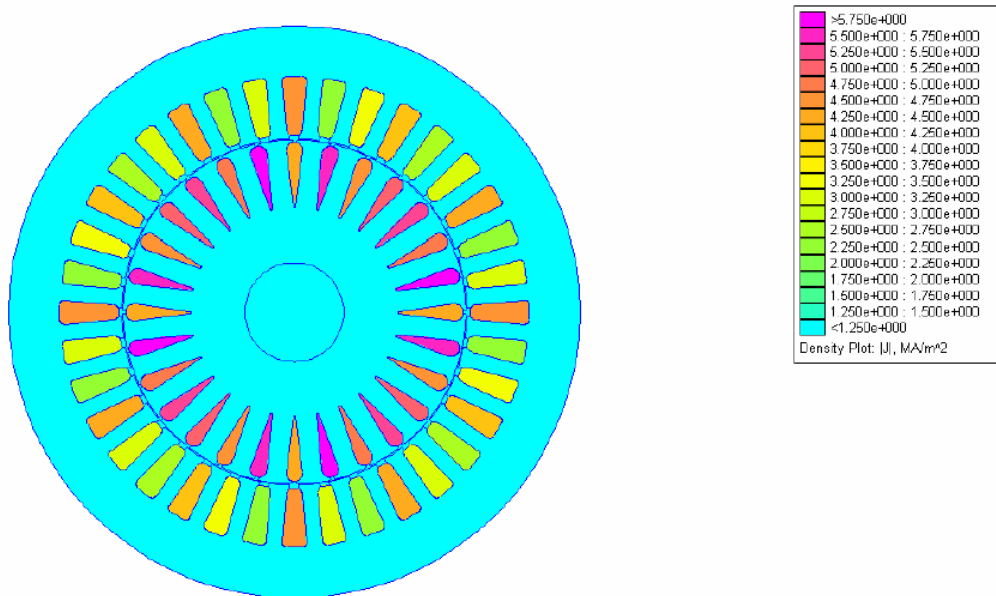
(4) The matrices are generally of different sizes due to the differences in size of the domain mesh compared to the surface mesh. There are problems where either method can give rise to the smaller system and quickest solution - it depends partly on the volume to surface ratio. For problems involving infinite or semi-infinite domains, BEM is to be favoured.

(5) BEM integrals are far harder to evaluate. Also the integrals that are the most difficult (those containing singular integrands) have a significant effect on the accuracy of the solution, so these integrals need to be evaluated accurately.

(6) A fundamental solution must be found (or at least an approximate one) before the BEM can be applied. There are many linear problems (e.g., virtually any non homogeneous equation) for which fundamental solutions are not known. There are certain areas in which the BEM is clearly superior, but it can be rather restrictive in its applicability.

(7) The need to evaluate integrals involving singular integrands makes the BEM at least an order of magnitude more difficult to implement than a corresponding finite element procedure.

COMPUTATION OF OTHER QUANTITIES. Post-processing

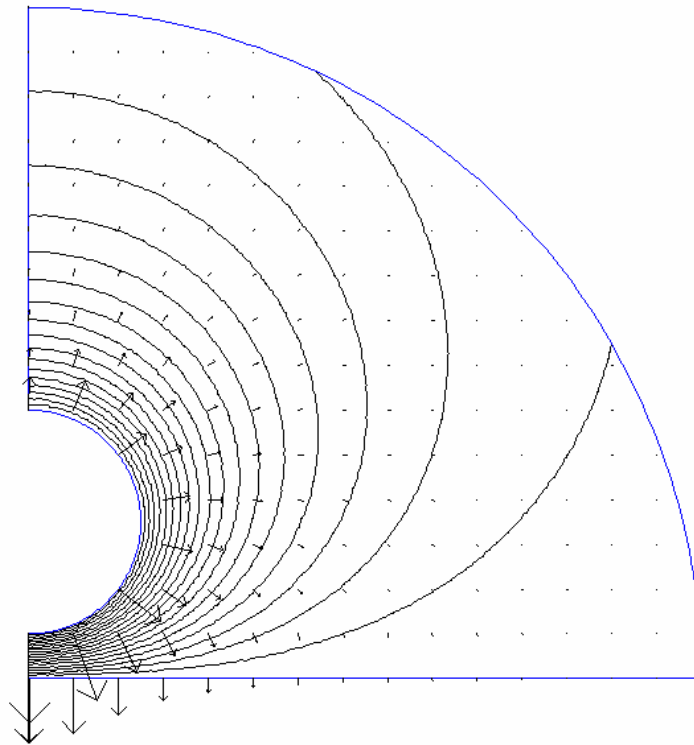


COMPUTATION OF OTHER QUANTITIES. Post-processing

The purpose of post-processing is to derive extra information by the use of direct solution (usually potential in nodes)

The first result is, usually, graphical information. This information is useful to control, in first approximation, the validity of solution: in a symmetrical device, such as an electrical machine, the result must be symmetric.

- Contour plot of constant-value lines of potential, i.e. $A = K$ or $V = K$.



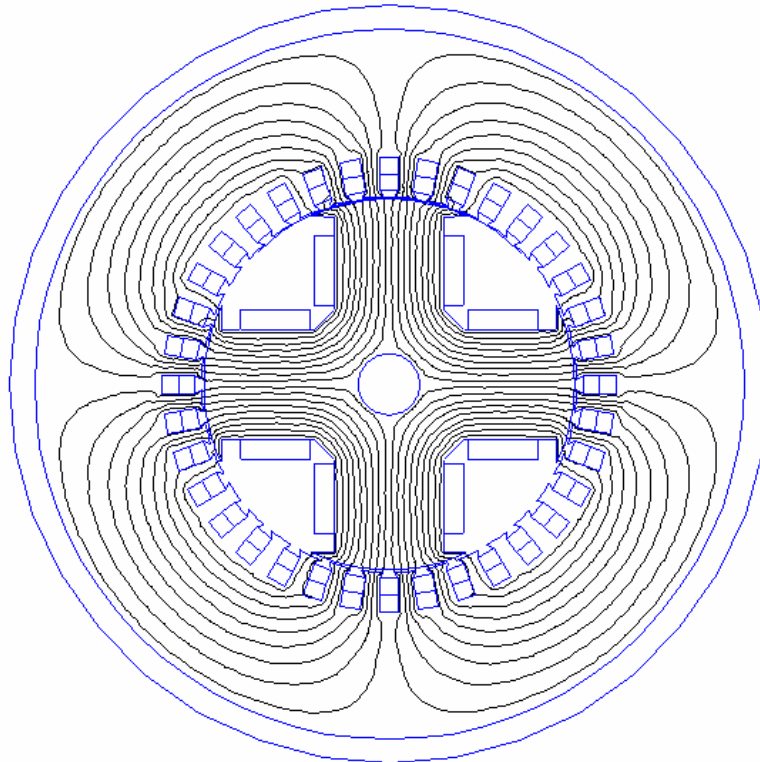
The above figure shows an electrostatic case. The lines show the constant potential lines in the system. The arrow lines indicate the electric field intensity E . This drawing is useful to show the approximate direction of the field. Remember that

$$E = -\frac{dV}{dn}$$

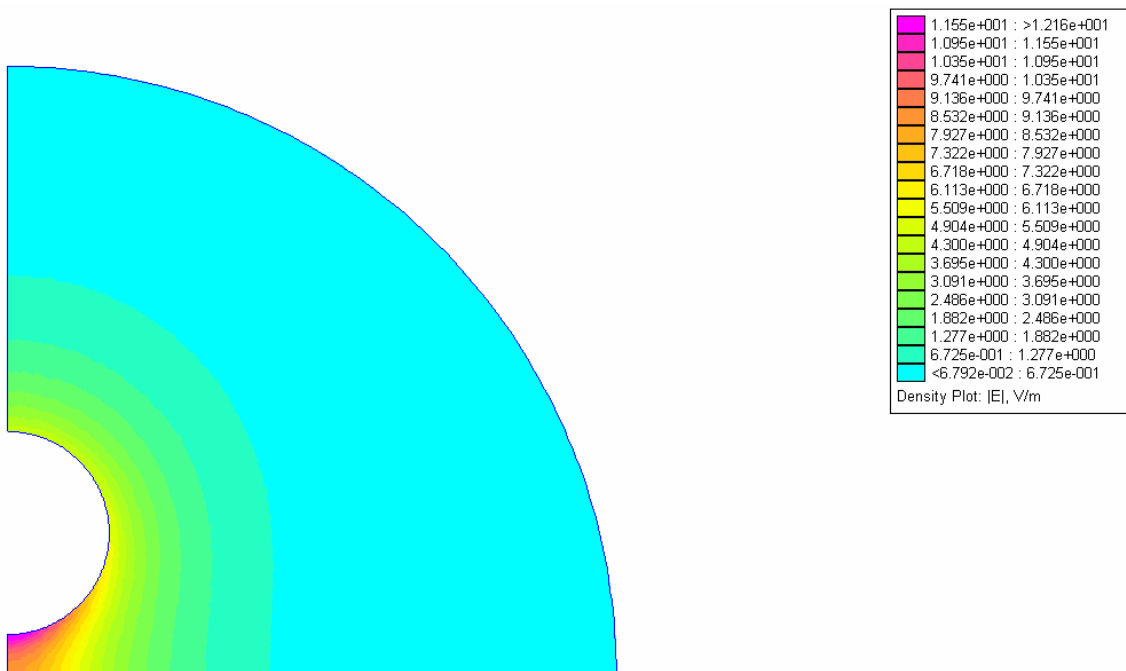
Also E is perpendicular to V .

The following figure shows the lines of constant vector potential A in a synchronous machine. These lines are lines of constant induction:

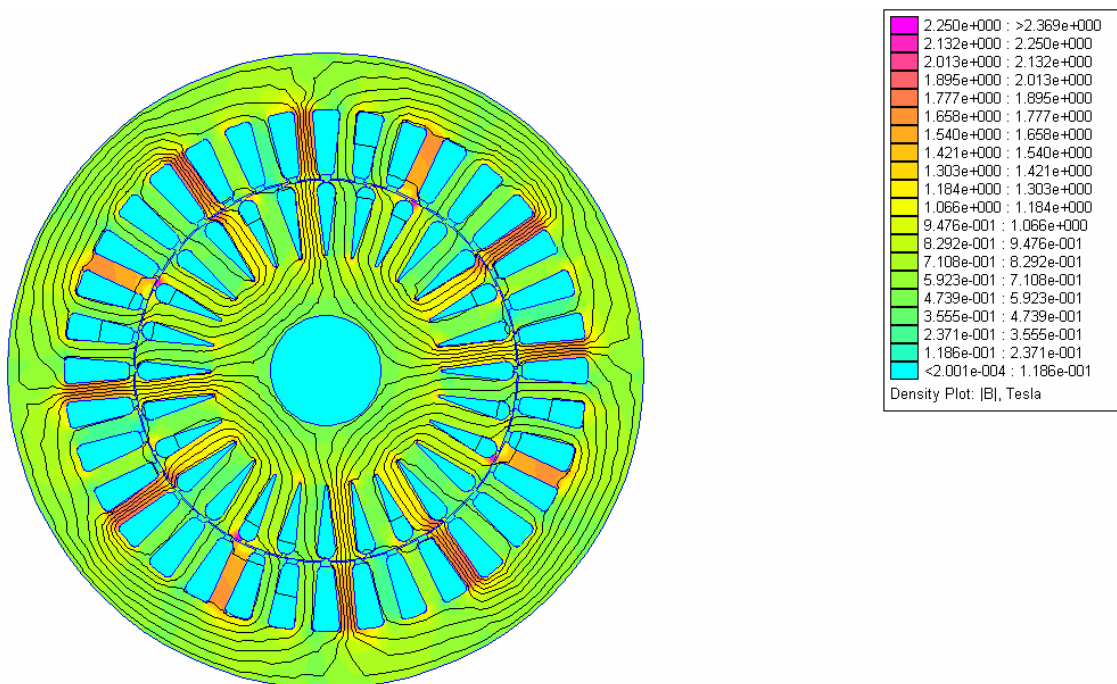
$$A = K \rightarrow \frac{dA}{dn} = 0 \Rightarrow B = k$$



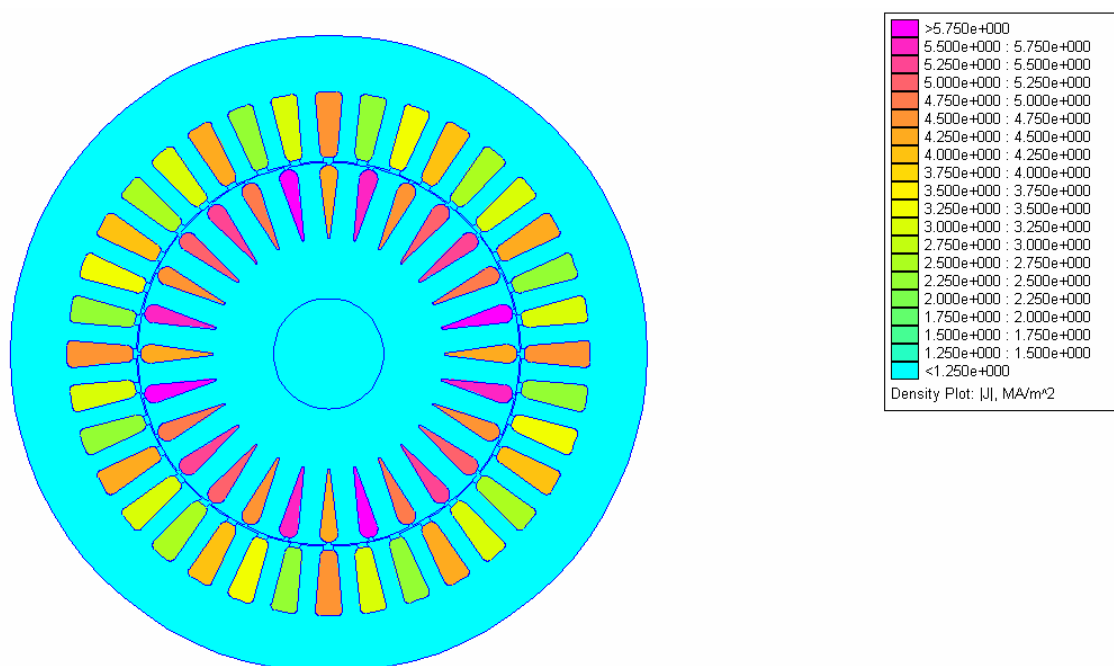
- Field maps. The use of coloured bands or shading to display elements subject to stresses in specific ranges, e.g. 0.1 to 2.2 T in 0.1 T bands, is of considerable help when evaluating a design. It is also usually possible to pick a point to obtain the actual stress at this point. The following figure shows the map of Electric field intensity E in a device.



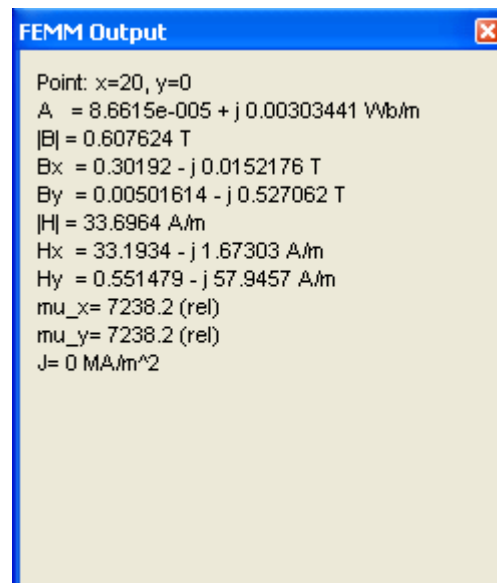
The following figure is a map of induction machine. The stator teeth are highly saturated as indicated by the coloured field map.



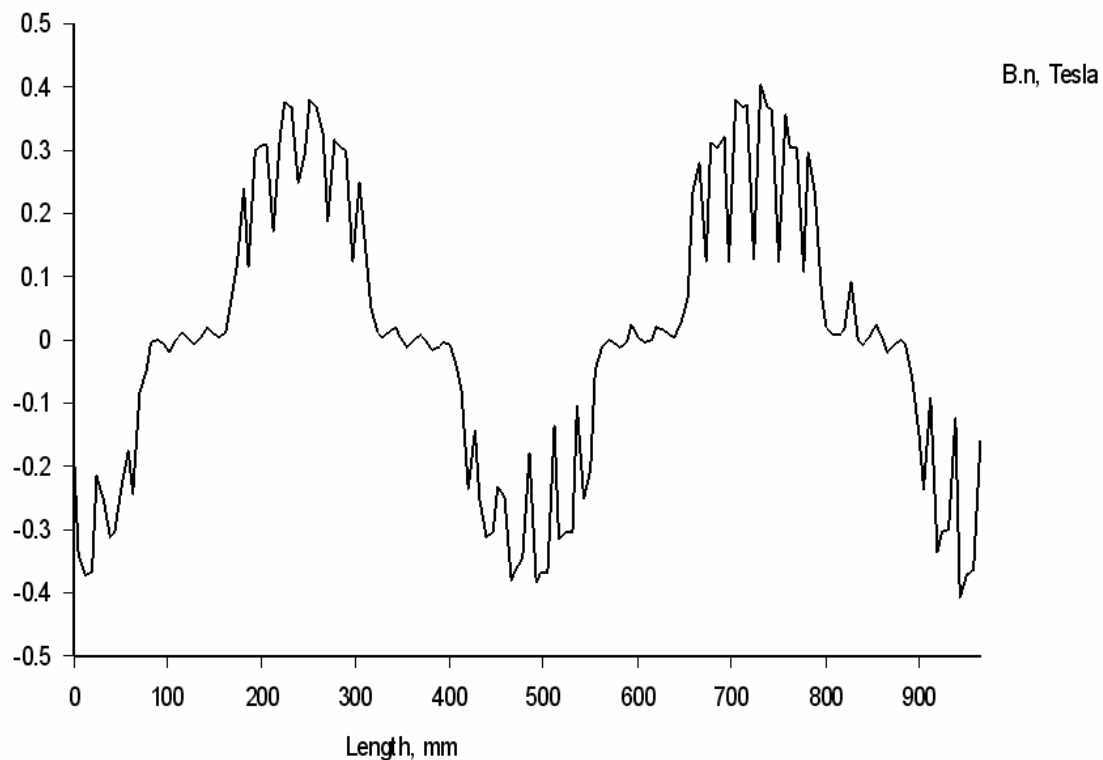
The following figure shows the density current distribution.



The following figure shows a typical point value table.



- Distribution along a line. This is useful to show a spatial distribution of some interesting variables, such as induction, voltage, Electric field or Magnetic field intensity. The following figure shows the distribution of B along the airgap for the above synchronous machine

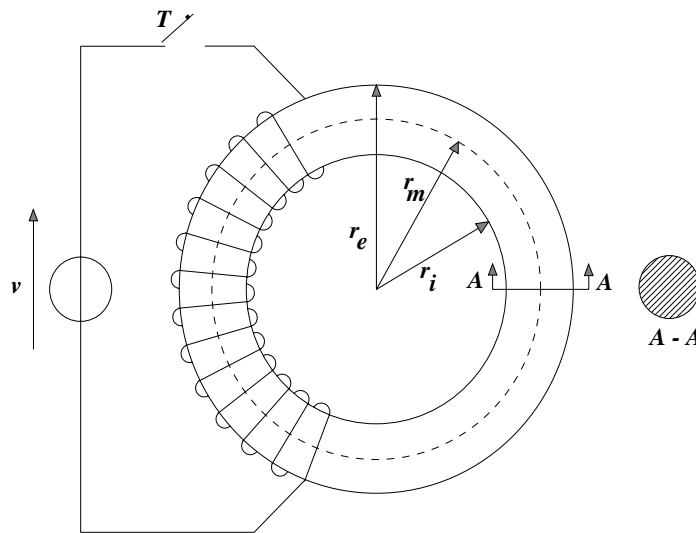


These data can usually be exported to other programs, such as Excel in a tabular form.

Energy Stored in the Magnetic Field

The energy stored into the magnetic field is a quantity of primary importance for a good understanding of what follows. The simplest way to evaluate the magnetic energy stored into a given material consists of the measurement of the energy flow between an electrical source and the material itself: this is because we are very good at evaluating electric energy.

Let us consider a torus of magnetic material on which there is a winding of N turns is wound. The geometry of the torus is such that the difference between the external radius r_e and the internal radius r_i is negligible ($r_e / r_i \cong 1$). In the following, the significant dimensions of the torus will be the mean radius r_m and the area of the cross section S .



An experimental device for the evaluation of the energy stored in a magnetic material.

The magnetisation characteristic of the material will be considered to be completely general. At any point on the magnetisation curve it is possible to define a permeability μ such that:

$$B = \mu(B)H$$

In linear materials the permeability μ is constant, no matter the value of B or H ; in non linear materials, the permeability is a rather complicated function of B and H . Let the winding be fed by a dc voltage source v . If the breaker T is closed, a current flows into the winding. By introducing an equivalent resistance R that takes into account the Joule losses in the windings, the Ohm law for this circuit reads:

$$v(t) = Ri(t) + N \frac{d\phi(t)}{dt}$$

Since the flux of the magnetic flux density B is constant across each cross section:

$$v(t) = Ri(t) + NS \frac{dB(t)}{dt}$$

Multiplying by $i dt$ both lhs and rhs:

$$vidt = Ri^2 dt + NSidB$$

and by applying the Ampère law to the mean circumference of the torus:

$$vidt = Ri^2 dt + S r_m H dB$$

The lhs in the above equation represents the energy supplied by the voltage generator in a time interval dt . In the rhs of the same equation, the first term represents the energy losses (in a time interval dt) in the equivalent resistance, and the second term is the variation of the energy stored in the magnetic field between time instants t and $t + dt$. The term $S r_m$ is the volume V of the torus.

By integrating between the time instants $t = 0$ and $t = +\infty$:

$$\int_0^{+\infty} vidt - \int_0^{+\infty} Ri^2 dt = V \int_0^B H(b) db$$

In the lhs there is the difference between the energy supplied by the voltage generator and the energy dissipated by the Joule effect in the equivalent resistance. Their difference, i.e. the rhs, is the remaining energy present in the system under consideration: the energy stored into the magnetic material. If the status of a non-linear material is such that it works in a point (H^*, B^*) the specific energy is the area between the curve and the B -axis from $B = 0$ to $B = B^*$. For linear materials, the integral in the rhs of the above equation becomes:

$$\int_0^B H(b) db = \frac{B^2}{2\mu} = \frac{BH}{2} = \frac{\mu H^2}{2}$$

This quantity has the physical dimensions of a energy per unit volume [J/m^3] and is commonly called *specific magnetic energy*. Once the vector potential in the interpolatory nodes has been found, the numerical evaluation of the magnetic energy is rather simple. Proceeding element by element one has:

$$W_{el} = \frac{1}{2\mu_{el}} \int_{\Omega_{el}} B^2 dV_{el} = \frac{1}{2\mu_{el}} \int_{\Omega_{el}} (\nabla \times A)^2 dV_{el}$$

The integral can be expressed in terms of the numerical values of the interpolatory nodes and in terms of the surface integrals of the shape functions:

$$W_{el} = \frac{L}{2\mu_{el}} \sum_{i=1}^3 \sum_{j=1}^3 A_i A_j \int_{\Omega_{el}} \nabla \alpha_i \nabla \alpha_j d\Omega_{el}$$

Another form for this equation is:

$$\begin{aligned} W_{el} &= \frac{1}{2\mu_{el}} \int_{\Omega_{el}} B^2 dV_{el} = \frac{1}{2} \int_{\Omega_{el}} B H dV_{el} = \frac{1}{2} \int_{\Omega_{el}} (\nabla \times A) H dV_{el} \\ \nabla \cdot (A \times H) &= (\nabla \times A) \cdot H - (\nabla \times H) \cdot A = (\nabla \times A) \cdot H - J \cdot A \\ W_{el} &= \frac{1}{2} \int_{\Omega_{el}} J A dV_{el} + \frac{1}{2} \int_{\Omega_{el}} \nabla \cdot (A \times H) dV_{el} \\ W_{el} &= \frac{1}{2} \int_{\Omega_{el}} J A dV_{el} + \frac{1}{2} \oint A \times H dS \end{aligned}$$

If we let the surface over which we take the second integral go to infinity, then

$A \propto \frac{1}{r}$, $H \propto \frac{1}{r^2}$, $S \propto r^2$ the surface integral goes to zero and

$$W_{el} = \frac{1}{2} \int_{\Omega_{el}} J A dV_{el}$$

Linked Flux

A magnetic field is said to be two-dimensional (2D) when there exists a symmetry that makes possible to find a repetitiousness of the physical phenomena plane by plane, from here to infinity. This is the situation when the currents always have a direction parallel to a z-axis, and the transverse sections to this axis always present the same geometry and the same materials, point by point. This is equivalent to saying that $B(x, y, z_1) = B(x, y, z_2)$, whatever z_1 and z_2 .

In this case, a significant simplification can be achieved. In fact, any partial derivative respect to z vanishes, and it is found that the vector potential is always parallel to z-axis, and therefore

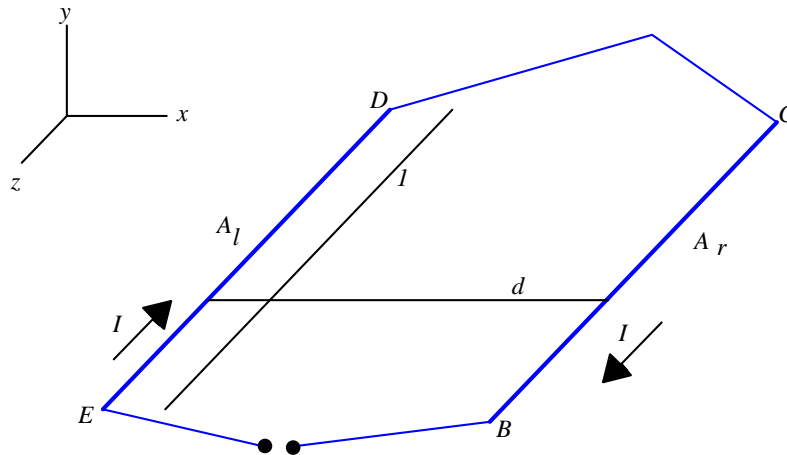
$$A = i_z A_z$$

In the following, for the sake of simplicity, A_z will be referred to simply as A . This will not generate any ambiguity, since, for the said property, in 2-D static fields the vector potential is in fact a scalar potential; more precisely, it is a vector which exhibits only one component.

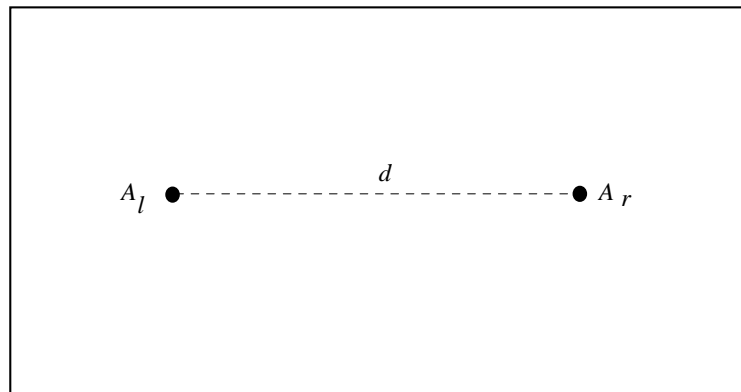
By developing the vector product in $B = \nabla \times A$ it is easily found for the components of B:

$$B_x = \frac{\partial A}{\partial y} \quad B_y = -\frac{\partial A}{\partial x}$$

What about the physical meaning of the vector potential? (we will continue to use this name). Let us consider a 2D field, in which there are two infinitely long conductors parallel to z-axis, of negligible cross section, carrying a dc current $+I$ and $-I$, respectively. The magnetic field B is the same in any point having the same x and y coordinates, no matter the z coordinate of the point: the same is true for the vector potential, which is assumed to have the value A_r in the right conductor of the turn and the value A_l in the left conductor. The following figure shows this physical situation, and the next figure shows the 2D geometry.



A turn carrying a dc current I , infinitely long in z -direction: only one unit in z -direction is represented. Distance between conductors is d .



The x-y representation of the turn in Fig. 6.6.1.

Let us now consider the flux (per unit length in z -direction) of B across a surface that has the turn as contour:

$$\varphi_S(B) = \int_S B \cdot n dS$$

where S is the surface of the turn for one unit in z -direction, and n is the outward normal to S . By substituting the expression for B as a function of A :

$$\varphi_S(B) = \int_S \nabla \times A \cdot n dS$$

Application of Stokes' theorem transforms the above equation into the following:

$$\varphi_S(B) = \int_{+\partial S} A \cdot d(+\partial S)$$

where the line integral in the rhs is defined along the turn. On the basis of the assumptions previously made, the flux of B can be rewritten as:

$$\varphi_S(B) = \int_B^C Adz + \int_{+\partial S} Ad(+\partial S) + \int_D^E Adz$$

The first and third integral have, respectively, the following values: A_r and $-A_l$ (the vector potential has the same value when the x - and y -coordinate of the point do not change and the z -coordinate of the point changes). On the other hand, the calculation was performed with a reference of one unit in z -direction, and moreover it should be noted that the integration path moves in opposite directions along the conductors.

The second integral is obviously negligible with respect to first and third since the wires are infinitely long: we studied just one unit of their length in z -direction, but the extension of their active length is infinitely greater than the length of the connections. We arrive at the following formula:

$$\varphi_S(B) = A_r - A_l$$

that presents a very interesting property of the vector potential: ***in 2D magnetostatic problems, the difference between vector potential in two points (x_1, y_1) and (x_2, y_2) represents the flux of B through a surface having unitary length in z -direction and having the traces of the sides parallel to the z -axis at the points (x_1, y_1) and (x_2, y_2) .***

This physical aspect of the vector potential in 2D magnetostatic problems is very interesting for the analysis of magnetic fields, since in these problems the flux of B is in general of greater interest than B itself. The property in the above equation reveals also that we are not in general interested in the value of the vector potential: rather, we are interested in the differences between vector potential in two points. Moreover, lines where A is constant are also flux lines: since the flux of B is related only to the difference between vector potentials, no matter the points where the difference is calculated, if this difference is calculated along two flux lines.

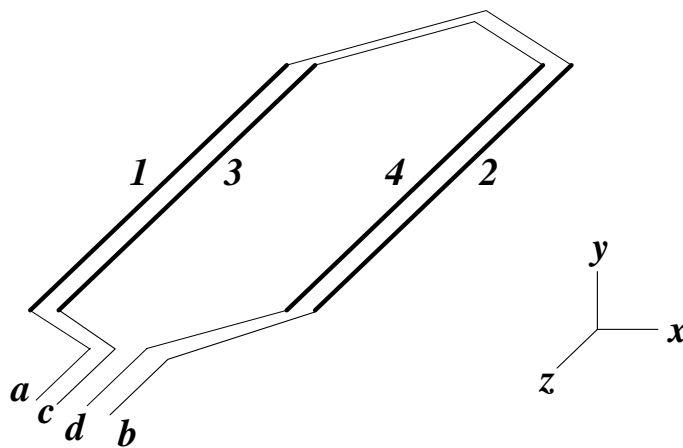
We already deduced a useful relationship between the magnetic potential and the flux of B . Now we want to give a definition for a very important quantity: the flux linked with a coil.

Let us consider two turns lying in the same plane x, y where there is a known distribution of vector potential $A(x, y)$. We shown that the flux of B through the surfaces of the turns (per unit length) is:

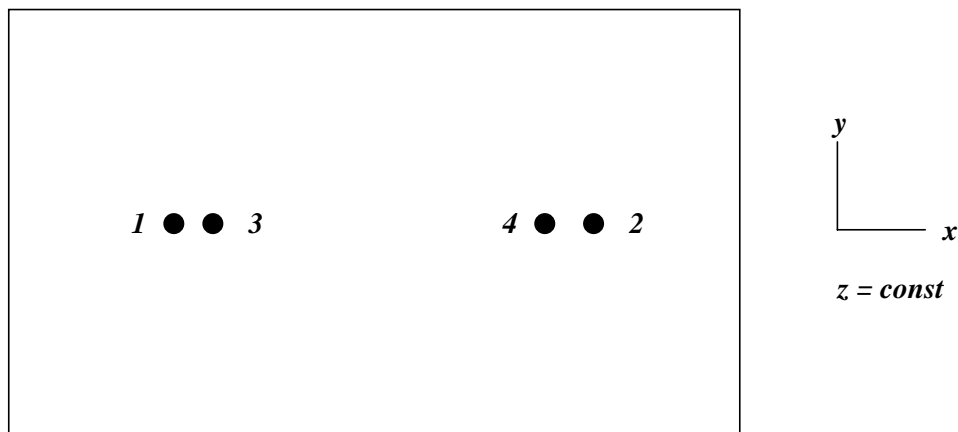
$$\varphi(a, b) = A_1 - A_2 \qquad \varphi(c, d) = A_3 - A_4$$

If the turns are series-connected (for instance by connecting with a short-circuit points b and c), the situation remains practically unchanged: in fact there is a new surface (singly-bordered, two-faces) were the flux of B can be evaluated:

$$\varphi(a, d) = \varphi(a, b) + \varphi(c, d) = (A_1 - A_2) + (A_3 - A_4) = (A_1 + A_3) - (A_2 + A_4)$$



Two turns that can be series- or parallel-connected. This is an experimental test simulation for the numerical evaluation of the flux linked with a coil.



2D x-y representation of the structure

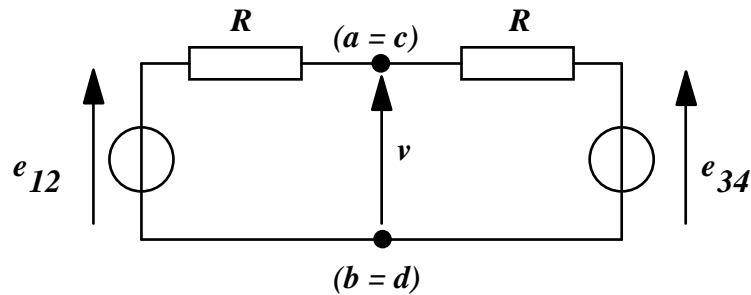
The situation changes completely if the turns are parallel-connected, if points a , c and b , d are short-circuited. In this case it is in fact impossible to define a

two-faced, singly-bordered surface. In other words, it is impossible to define the flux of B through a surface, since this surface does not exist. But we are not interested only in knowledge of the flux; we are also interested in some related quantities, such as the back emf induced in a system of turns. For instance, what is the numerical value of the voltage between points $(a = c)$ and $(b = d)$? The answer can be found by considering the following figure, where each turn is represented in a physical schematisation as a voltage generator in series with a resistance.

$$e_{12} = s\phi_{12} = s(A_1 - A_2)$$

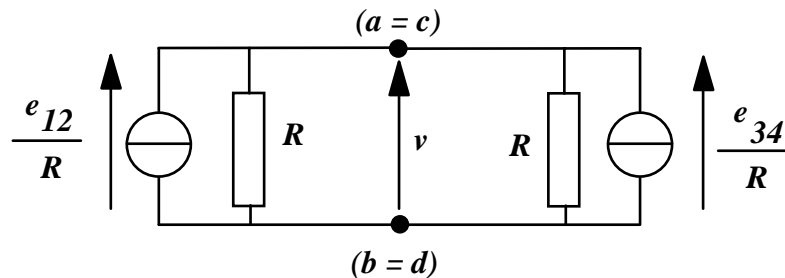
$$e_{34} = s\phi_{34} = s(A_3 - A_4)$$

where s is the Laplace operator.



The circuit equivalent of the structure.

Norton's theorem can be applied to both sides of the circuit obtaining the circuit in the following figure



Norton transformation of the circuit.

Voltage v is readily found to be:

$$v = \left(\frac{e_{12}}{R} + \frac{e_{34}}{R} \right) \left(\frac{R^2}{2R} \right) = \frac{e_{12} + e_{34}}{2}$$

It should be noted that in the above equation resistances are not explicitly present: the only constraint on them is in the fact that they are equal. In presence of N turns parallel connected:

$$v = \frac{1}{N} \sum_{k=1}^N e_k = s \frac{1}{N} \sum_{k=1}^N \varphi_k$$

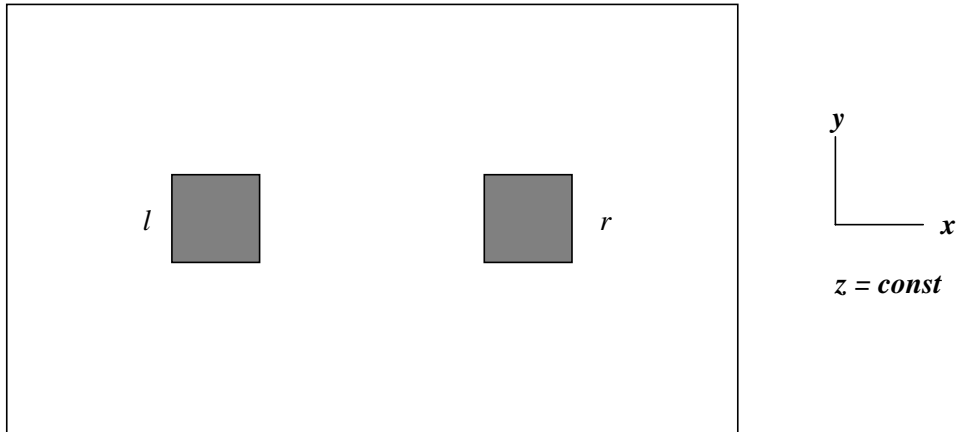
Formally, this equation is the expression of the Faraday's law, since a voltage appears as the derivative of a quantity that has the dimensions of a magnetic flux. It is reasonable to define this quantity as a flux: the flux linked with the coil ψ

$$\psi = \frac{1}{N} \sum_{k=1}^N \varphi_k$$

Let us now consider a massive turn, made up by a conductor of finite dimensions in x - and y -directions. This turn can be seen as the parallel connection of infinite sub-conductors, each one having the same resistance but a different flux to B . The flux linked with the massive turn is:

$$\psi = \lim_{N \rightarrow \infty} \frac{1}{N} \sum_{k=1}^N \varphi_k = \lim_{N \rightarrow \infty} \frac{1}{N} \sum_{k=1}^N (A_{kl} - A_{kr})$$

where suffixes l and r denote the left and the right part of the turn respectively (with reference to the above case of two elementary turns, l represents the part of the winding where sub-turns have odd numbers, r the part where sub-turns have even numbers). The following figure represents a 2D view of the turn.



x-y representation of a massive turn: the current is z-directed.

By multiplying both numerator and denominator of above equation by S , the cross-section of the turn:

$$\psi = \lim_{N \rightarrow \infty} \frac{S}{S} \frac{1}{N} \sum_{k=1}^N (A_{kl} - A_{kr}) = \frac{1}{S} \lim_{N \rightarrow \infty} \sum_{k=1}^N (A_{kl} - A_{kr}) \Delta S$$

where $\Delta S = S / N$ is the surface of the cross-section of the elementary turn. The limit of the sum in this equation is just the definition of integral. Therefore we have for the linked flux:

$$\psi = \frac{1}{S} \left(\int_S A dS \Big|_l - \int_S A dS \Big|_r \right)$$

where the integrals have to be evaluated on the left and on the right part of the cross-section of the turn.

Numerical evaluation of the integrals is rather simple; since regular integrals are summable functions, it is possible to proceed element-by-element. Say N_{el} is the number of triangular elements that cover without holes and/or super positions the region S where the integrals have to be evaluated. One has:

$$\int_S A dS = \sum_{i=1}^{N_{el}} \int_{\Omega_i} A d\Omega_i = \sum_{i=1}^{N_{el}} \sum_{k=1}^3 A_{ik} \int_{\Omega_i} \alpha_{ik} d\Omega_i$$

where A_{ik} and α_{ik} denote the k -th node potential and shape function in i -th triangular element.

Inductance

The definition itself of inductance is directly linked with the definitions of magnetic energy and of linked flux. In general, the inductance of a winding is given by the ratio between the flux linked with the winding and the current into the winding:

$$L = \frac{\psi}{i}$$

If the system under consideration is linear, it is easily seen that equation is equivalent to:

$$L = \frac{\psi}{i} = \frac{NBS}{i} = \frac{NiBS}{i^2} = \frac{HlBS}{i^2} = 2 \frac{HB}{2} \frac{V}{i^2} = \frac{2W}{i^2}$$

In the above pages, the numerical evaluation of the linked flux and of the energy stored in the magnetic field have already been discussed; the numerical evaluation of the inductance is therefore immediate when the linked flux or the energy are known as:

- the ratio between the linked flux and the current;
- the ratio between twice the magnetic energy and the current squared.

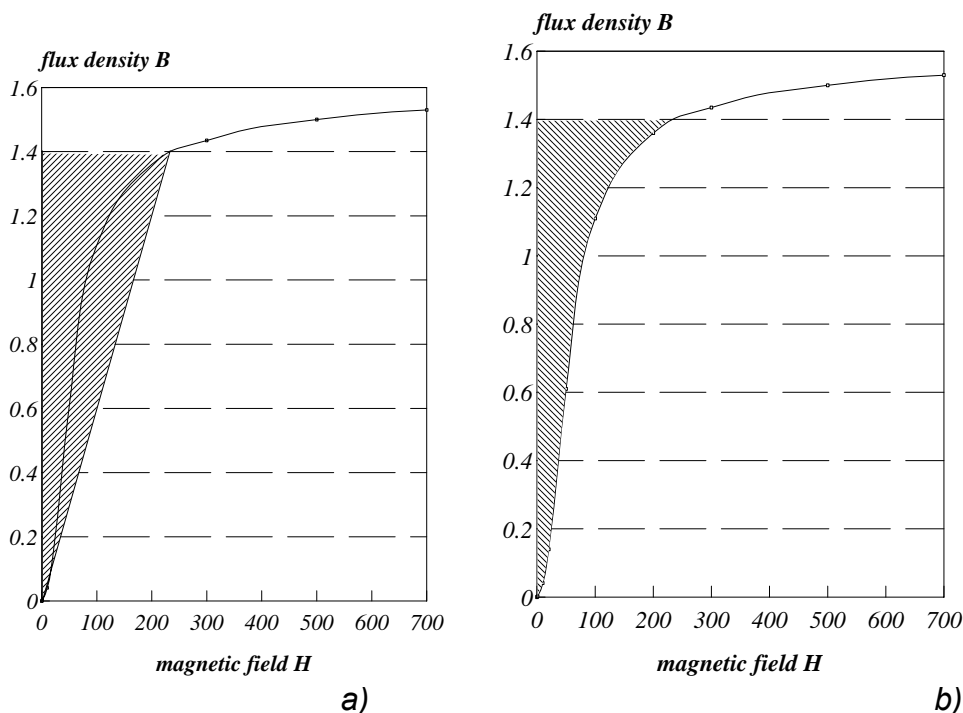
For non-linear problems, the situation is completely different. Evaluation of inductance from the above equations leads in general to completely different results, those coming from $L = \frac{\psi}{i}$ having greater values than those from

$L = \frac{2W}{i^2}$. Let us suppose that the toroidal device shown earlier is made by a non-linear material, and that the current in the winding is such that the flux density in each point of the material is 1.4 T . If no leakage flux is present, there is proportionality between the flux linked with the coil and the flux density, as well as between the current and the magnetic field:

$$\psi = NBS$$

$$Hl = Ni$$

therefore, if the definition $L = \frac{\psi}{i}$ is adopted, the inductance is proportional to the product (BH) , while, following definition $L = \frac{2W}{i^2}$, the inductance is proportional to the integral of the magnetic field. This situation is shown in the following figure: in a) the quantity $BH/2$ is shown; in b) is graphed the integral of H vs. B .



The definition of inductance for a non-linear material: a) from linked flux, b) from energy stored in magnetic field.

From this figure it is evident that:

$$\int_0^B H(b)db \leq \frac{BH}{2}$$

the equality being valid only for linear materials. By introducing inequality we can obtain:

$$\frac{2W}{i^2} = \frac{2V}{i^2} \int_0^B H(b)db \leq \frac{2V}{i^2} \frac{BH}{2} = \frac{2(Sl)}{(Hl)^2 / N^2} \frac{BH}{2} = \frac{N^2 SB}{Hl} = \frac{\psi}{i}$$

It has been shown that the inductance calculation from stored energy leads to numerical values smaller than that from linked flux, but the question is the following: what definition of inductance should I use in non-linear problems? The answer is simple: it depends on what I am looking for, and on how I defined the inductance itself.

Let us consider again the device. The winding is now fed by means of a time-varying voltage current. If we define the inductance as the ratio between the linked flux and the current, we have:

$$v(t) = Ri(t) + \frac{d}{dt}(L_{\psi}i) = Ri(t) + L_{\psi}(i) \frac{di(t)}{dt} + i(t) \frac{dL_{\psi}}{dt}$$

since now the inductance (note: the ratio between linked flux and current) is not more constant, but it varies with the current. Integration of the above equation is not very simple, since there is a term that implies the knowledge of the variation of the inductance (always the ratio between linked flux and current) with time. A simplification of this equation can be achieved by rewriting it as:

$$v(t) = Ri(t) + L_{\psi}(i) \frac{di(t)}{dt} + i(t) \frac{dL_{\psi}(i)}{di} \frac{di(t)}{dt}$$

It will be seen in the following that this equation is the key to solving transient problems involving non-linear material. It should be evident by now that the calculation of $(dL(i) / di)$ is not so difficult (at least in principle), since it will suffice to determine the behaviour of the inductance (again, the ratio between the linked flux and the current) vs. the current, and to derive it with respect to the current itself.

Let us suppose that the current has the value i^* . Is the energy stored in the magnetic field equal to $L_{\psi} i^{*2} / 2$? Certainly not. If we want to determine the specific energy by means of the inductance, we have to calculate the quantity L_{ψ} (that, obviously, depends on the current) and successively we have to evaluate $L_{\psi} i^{*2} / 2$. So, also for non-linear problems, both definitions of the inductance hold: the only difference with linear problems is in that they do not coincide. Therefore, each definition of inductance can be used, depending on which kind of result we want to obtain.

Self and Mutual Inductance

In this paragraph the attention will be focused on linear problems. Numerical evaluation of inductance from the flux linkage as defined above is rather simple. Simply to solve the FEM problem, to determine the linked flux and to divide it by the current: the inductance has been found, or, alternatively, to evaluate the total magnetic energy and to divide it by one half of the current squared.

Particular attention should be paid to the fact that, if we utilise symmetry properties, we determine linked fluxes and energies that are smaller than the complete geometry case.

To determine the mutual inductance between two windings, there are again two possibilities:

- from magnetic energy;
- from linked flux.

In the first case, two FEM analyses are needed. In the first one, the current in both inductances are the same; in the second one, the current in one of the inductances has to be reversed. The magnetic energy in the first FEM analysis is:

$$W_{m1} = \frac{1}{2} L_1 i^2 + \frac{1}{2} L_2 i^2 + M_{12} i^2$$

In the second FEM analysis the magnetic energy is:

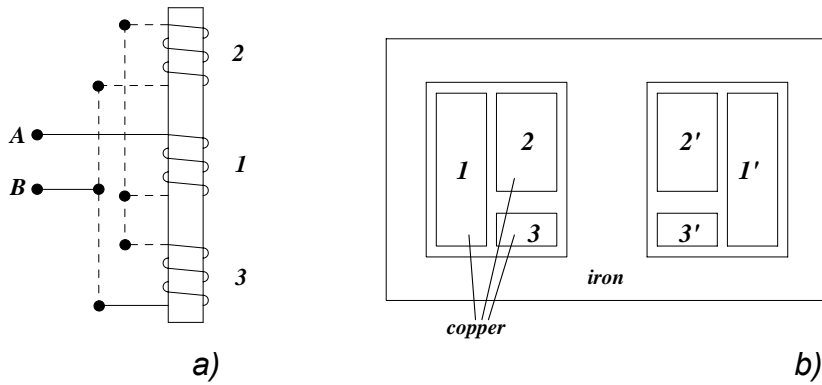
$$W_{m2} = \frac{1}{2} L_1 i^2 + \frac{1}{2} L_2 i^2 - M_{12} i^2$$

From the difference between W_{m1} and W_{m2} , the numerical value of the mutual inductance from magnetic energy is easily evaluated. The evaluation of the same parameter from the linked flux is even simpler: suffice to feed winding 1 with a given current, to perform FEM analysis, to evaluate the flux linked with winding 2, and to divide this quantity by the current in winding 1.

Self and Mutual Inductance in Complex Winding Systems

The problem of the numerical evaluation of the inductance, however, is not so simple as at a first sight. It may be said that the last steps to evaluate this quantity are simple if the approach to the problem was approached correctly since the first steps of the FEM analysis.

As an example of this statement, let us consider the core inductor in the following figure, that is made up by three sub-windings. In *a*) the connections of the three windings are shown: windings 2 and 3 are connected in parallel, and their complex is connected in series with winding 1; in *b*) the cross-section of this core is shown. From the external network, this arrangement of windings is seen as a single winding, no matter the internal connections. The question is the following: what is the numerical value of the inductance from terminals A and B? (to be honest, this arrangement is very strange, and it would be rather difficult to find this inductor in practice).

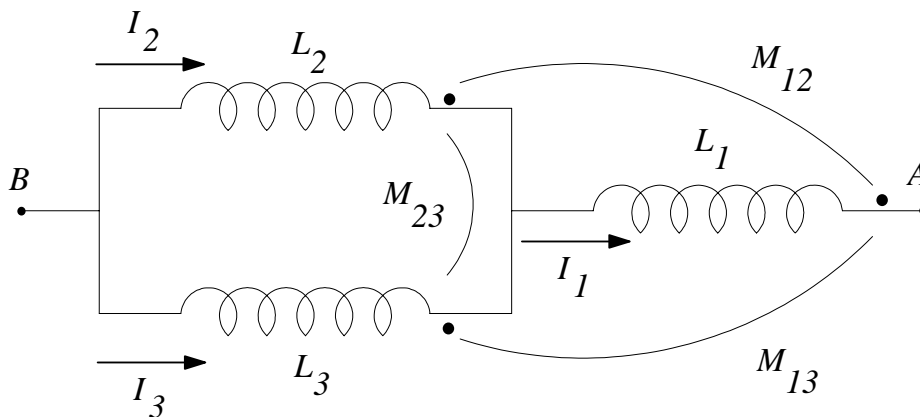


A three-windings core. a) the internal connections: dotted lines represent internal connections, and slim lines represent external connections; b) the cross section of the core (primed numbers denote the return conductors: currents in regions 1 and 1' are the same with opposite directions).

For this kind of analysis, resistive phenomena are neglected as well as eddy current effects. To evaluate the external inductance, the complex of the three windings may be feed with a unit current; once a field solution is known, both linked flux and energy can be calculated, and from these quantities the inductance.

One of the most common errors consists in feeding the three windings with the same current. Apart the differences between the current densities, this is a major error, because the total current in the three windings is different. Often, the currents in windings of the type 1 and 2 are supposed to be equal: therefore, in this case, another error could be to set $I_2 = 0.5$ and $I_3 = 0.5$.

From the circuit schematisation in the above figure it is evident that, if in A there is a unit current, winding 1 carries the same unit current. But what about windings 2 and 3? The sum of the currents in the said windings is surely one, but there is no information that allows to evaluate *a-priori* the numerical values of currents I_2 and I_3 . The fact is that no circuit information is included in FEM schematisation. Therefore we need to make this schematisation separately. For our case, the equivalent circuit is shown in the following figure



The equivalent circuit of the inductor.

We are looking for the inductance seen from the external circuit, i.e. from points $A - B$. Since we do not know the values of I_2 and I_3 , or equivalently their ratio, the only solution is to evaluate separately the six inductive parameters, that can be done in three FEM analyses. In each one of these, only one winding is fed, the remaining two windings carrying a zero current. At the end of each FEM analysis, the self inductance of the fed winding is known, as well as the mutual inductances between this winding and the two non-fed windings. In this way, three self inductances can be determined, and six mutual inductances. Suppose that we fed winding i , and that we found the numerical value of M_{ij} . In principle, when feeding winding j we should not determine the value of M_{ji} , saving thus the computer time to determine this inductance value.

Obviously, $M_{ij} = M_{ji}$, but numerical elaborations are affected by rounding and truncation errors. This means that, with a practically zero computational effort, we can compare the numerical values of M_{ij} and M_{ji} . This is a good estimation of the accuracy of the calculations. For practical purposes, two mutual inductances can be considered equal if their difference is less than 0.1 %, the basis being the smaller. Once this task has been accomplished, the external inductance can be found by means of a simple circuit analysis.

Back emf

Between the machine parameters, back emf is in general the first step for the determination of the overall performances of a design, and in the following it will be shown how it is possible to deduce accurately back emf at the machine terminals starting from FEM analysis.

The logical sequence of this technique starts from the knowledge of the vector potential: back emf is computed by means of a small number of integral data closely related to the flux through a surface. It will be evident that numerical derivation of such integral data is necessary throughout the work, and therefore a great accuracy is required in FEM computations. This means not only to refine successive FEM solutions, but also to control the evolution of such numerical parameters from one FEM analysis to another. This is not only in a single FEM analysis, but also comparatively from one solution to another, if several FEM solutions are required for various geometrical configurations of the same design (with reference to a rotating machine, for different stator-rotor relative positions).

Let now us consider a 2D section of a rotating machine. The following hypotheses are adopted:

- electromagnetic fields can be considered 2D;
- magnetic materials are linear, and hysteresis is not present in ferromagnetic materials (iron and PMs);
- losses in active materials are not taken into account;
- the rotor speed ω_r is constant.

A FEM solution in terms of vector potential is considered below. By definition, the flux linked with a surface that has in the (x, y) plane its traces in the points 1 and 2, is $\phi = A_1 - A_2$. The flux linked with a coil (ψ) is:

$$\psi = \frac{1}{S} \int A(x, y) dS$$

where S is the area of the transverse section of the coil and $A(x, y)$ is the vector potential (here and in the following the number of conductors in series per slot will be taken as one; the same holds for the number of pole pairs).

This is the value of the flux linked with a test coil at time t_0 ; values for different times can be obtained with new relative positions between stator and rotor. However, the flux linked with the test coil at time t_1 is the same flux linked at t_0 with the coil which is at an angle $(t_1 - t_0)\omega_r$ from the current coil, where ω_r is the rotating speed of the rotor. This allows to limit the number of FEM calculations to one, if the magnetic structure is isotropic. When the geometry under consideration presents a small number of coils per pole and per phase, the relevant magnetic structures present characteristics not constant in space. Therefore, the number of FEM calculations to perform is at least two: the first one when the axis of the magnets are superimposed to the axis of a slot, the second one when the axis of the magnets are superimposed to the axis of a tooth.

When the flux linked with a coil (or with a phase) is known, the computation of the relevant back emf is in principle a simple task, by applying the Faraday law:

$$e(t) = -\frac{d\phi(t)}{dt} = -\frac{d\phi(\theta)}{d\theta} \frac{d\theta}{dt} = -\frac{d\phi(\theta)}{d\theta} \omega_r$$

where θ is the angular position, in a reference frame rigidly connected to the rotating field, of the axis of the coil, and ω_r is the angular velocity of the rotating field. From the above equation it is evident that numerical derivation of the linked flux is the basis for the determination of the back emf.

One possibility is to calculate the back emf in a turn by means of direct numerical derivation of the flux. Accuracy reachable in this way is poor, since the linked flux is known in a small number of points of the interval; no matter what kind of numerical derivation algorithm, derivatives of degree greater than one are not taken into account. If the linked flux varies suddenly near the point under consideration, the numerical values of higher derivatives are not negligible, and this results in great numerical errors.

Linked flux can be approximated by means of analytical functions, such as: Fourier expansions, Lagrange polynomials, Tchebishev polynomials, cubic polynomial splines. If an analytical approximation for the linked flux is determined, the back emf can be found by means of analytical derivation, that can be obtained without numerical errors and with no significant computational

efforts. This is a general interpolation problem, where a number N of pairs of (θ, ψ) values are known in a closed interval of the θ -axis. However, adequate choice of the interval along θ -axis allows the *a-priori* knowledge of more constraints on the derivative of the linked flux: for instance, the back emf in the interpole axis (the back emf is maximum) or in the pole axis (the back emf is zero).

A Fourier approach to the interpolation does not seem to be useful, since the precision in the numerical evaluation of the Fourier coefficients decreases as the order of the harmonic increases. In principle this is not a great problem, since the numerical value of the said parameter decreases when the order of the harmonics increases, and the error in the numerical value of the flux is often not appreciable. On the other hand, back emf is calculated by means of analytical derivation as in the following Eq:

$$e(\theta) = -\frac{d\phi(\theta)}{d\theta} = -\sum_{k=1}^N k \phi_k \sin(k \theta)$$

It can be seen from the above equation that the higher the order of the harmonic, the greater the weight. Numerical tests show that N should be kept small: addition of two or three harmonics to a qualitatively good $e(\theta)$ curve often results in wild jumps of the new curve that, at least in principle, should be more precise.

Resistance. Joule losses power.

In a fixed instant the current density vector J is known in any point of the volume of the analyzed system. The instantaneous Joule losses are

$$p_J = \iiint_V \rho J^2 dV$$

With alternative currents, varying sinusoidally with the time, the average Joule losses are:

$$p_J = \iiint_V \frac{1}{2} \rho |J|^2 dV$$

The equivalent electrical resistance can be computed as:

$$R = \frac{P_J}{I^2}$$

Capacitance and Resistance.

By application of the basic concepts for the electrostatic field and conduction media, we can determine the capacitance and resistance for the complex geometric configurations:

$$C = \frac{\oint_S \epsilon \cdot E \cdot dS}{\int_L E \cdot dl}$$

$$R = \frac{\int_L E \cdot dl}{\oint_S \sigma \cdot E \cdot dS}$$

Note the symmetry in the two formulations. For linear materials we can use the electrostatic energy approach to calculate the capacity of a conductor:

$$C = \frac{2 \cdot U}{V^2};$$

$$U = \frac{1}{2} \int_{Vol} D \cdot E \cdot dVol = \frac{1}{2} \int_{Vol} \epsilon \cdot E^2 \cdot dVol$$

U is the electrostatic energy and V the potential difference.

Eddy current losses

The eddy current density is:

$$J = j\sigma\omega A$$

If A corresponds to the peak value of the vector potential, then the loss in a element will be

$$p_J = REAL\left(\frac{1}{2\sigma} \iint_S JJ^* dx dy\right)$$

Since A varies linearly over the element, then by the above equation so does J:

$$J = \frac{1}{2\Delta} \left\{ (a_i + b_i x + c_i y) J_i + (a_j + b_j x + c_j y) J_j + (a_k + b_k x + c_k y) J_k \right\}$$

Substituting and integrating over an element, we obtain:

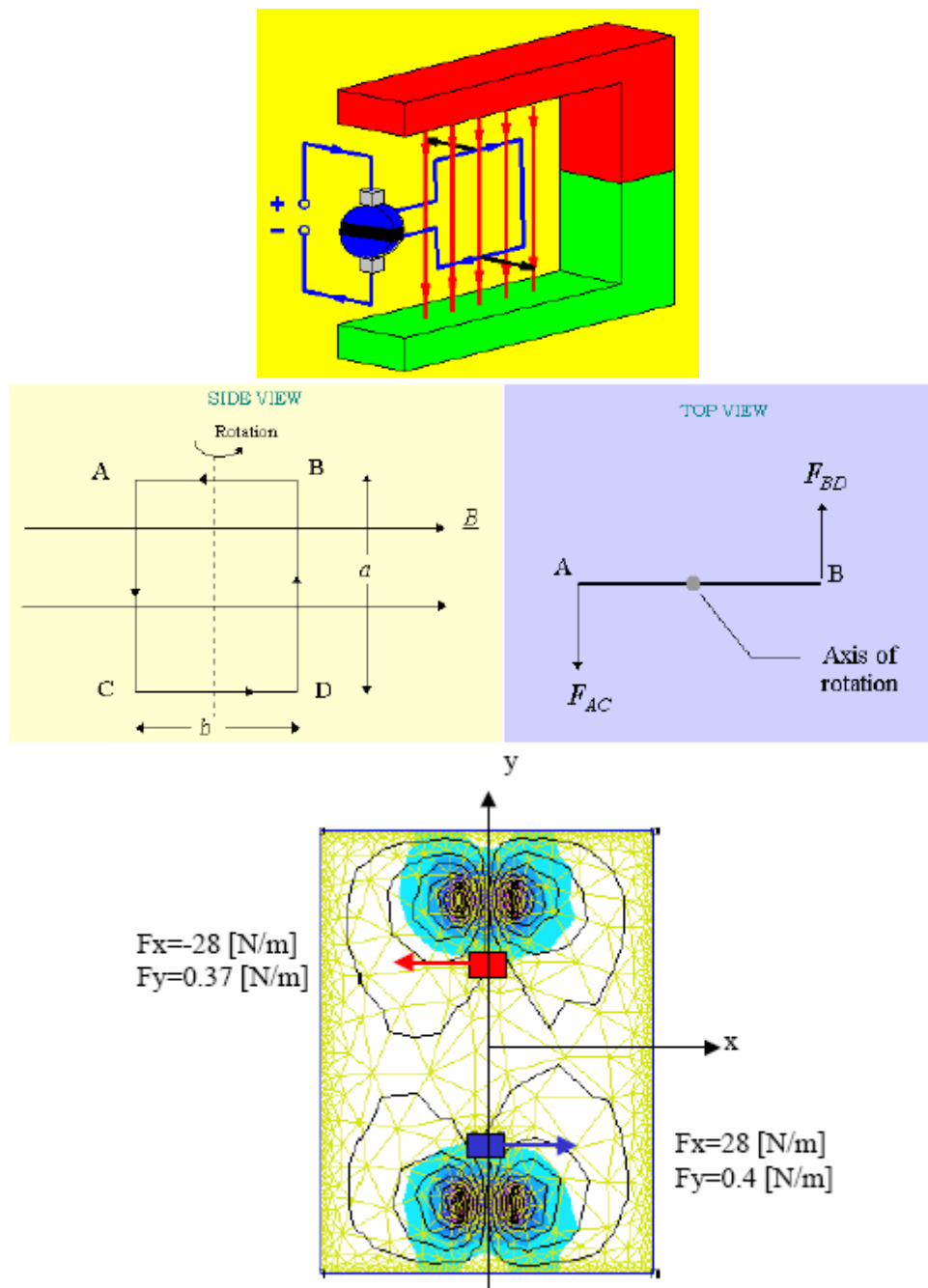
$$P = \frac{\Delta}{12\sigma} \left\{ |J_i|^2 + |J_j|^2 + |J_k|^2 \right\} + REAL(J_i J_j^* + J_i J_k^* + J_j J_k^*)$$

Force and Torque

Lorenz's Force law is straightforward and simple to apply to obtain the force applied to a conductor. Given the local value of flux density, B and current density we find the local force vector as

$$dF = f = J \times B$$

This equation is useful for finding the force on conductors. For example considers a DC motor showed in the following figures.



By application of Lorenz Force expression we obtain the force acts over the conductor. The torque is given by:

$$M = 2 \cdot F_x \cdot r$$

Maxwell Stresses

Substituting the Maxwell's equations in the Lorenz force expression:

$$\nabla \times H = J \Rightarrow \frac{1}{\mu} \nabla \times B = \nu \nabla \times B = J$$

we obtain:

$$f = (\nu \nabla \times B) \times B$$

Developing this equation, we obtain the following equation (we only show the equation for X – component):

$$f_x = \nu \left(B_z \frac{\partial B_x}{\partial z} - B_z \frac{\partial B_z}{\partial x} - B_y \frac{\partial B_y}{\partial x} + B_y \frac{\partial B_x}{\partial y} \right)$$

If a term $\nu B_x \frac{\partial B_x}{\partial x}$ is added and subtracted from the above equation, and the identity

$$\frac{\partial}{\partial x} (B_x^2) = 2 B_x \frac{\partial B_x}{\partial x}$$

is used, then the force component becomes:

$$f_x = \nu \left(\frac{1}{2} \frac{\partial}{\partial x} (B_x^2) + B_z \frac{\partial B_x}{\partial z} + B_y \frac{\partial B_x}{\partial y} - \frac{1}{2} \frac{\partial}{\partial x} (B_x^2 + B_y^2 + B_z^2) \right)$$

Some further manipulations gives:

$$f_x = \nu \left(\frac{\partial}{\partial x} \left(B_x^2 - \frac{1}{2} |B|^2 \right) + \frac{\partial (B_x B_z)}{\partial z} + \frac{\partial (B_x B_y)}{\partial y} - B_x \nabla \cdot B \right) \Rightarrow (\nabla \cdot B = 0)$$

$$f_x = \nu \left(\frac{\partial}{\partial x} \left(B_x^2 - \frac{1}{2} |B|^2 \right) + \frac{\partial (B_x B_z)}{\partial z} + \frac{\partial (B_x B_y)}{\partial y} \right)$$

The remaining expression may be recognized as the divergence of a vector f_x , whose components are:

$$\nabla \cdot T_x = \begin{cases} \frac{\partial T_x}{\partial x} = f_{xx} = \nu \left(B_x^2 - \frac{1}{2} |B|^2 \right) \\ \frac{\partial T_x}{\partial y} = f_{xy} = \nu (B_x B_z) \\ \frac{\partial T_x}{\partial z} = f_{xz} = \nu (B_x B_y) \end{cases}$$

A similar development holds for each of the other force components (f_y and f_z). Thus these vectors can be combined into a Tensor T:

$$T = \nu \begin{pmatrix} \left(B_x^2 - \frac{1}{2} |B|^2 \right) & (B_x B_y) & (B_x B_z) \\ (B_y B_x) & \left(B_y^2 - \frac{1}{2} |B|^2 \right) & (B_y B_z) \\ (B_z B_x) & (B_z B_y) & \left(B_z^2 - \frac{1}{2} |B|^2 \right) \end{pmatrix}$$

The force density can now be written as the divergence of this tensor:

$$f = \nabla \cdot T$$

The total force can be found by integration over the volume:

$$F = \iiint_V f dV = \iiint_V \nabla \cdot T dV$$

Using the divergence theorem, this volume integral may be reduced to a surface integral:

$$F = \iiint_V \nabla \cdot T dV = \oint_S T dS$$

We limit the following development to two dimensional geometry, so that the surface of integration is a line (we consider a unit depth). The unit normal and tangential vectors to the surface are:

$$\begin{aligned} \vec{a}_t &= s_x \vec{a}_x + s_y \vec{a}_y \\ \vec{a}_n &= s_x \vec{a}_y - s_y \vec{a}_x \end{aligned}$$

The incremental integration path is then: $ds = \vec{a}_n dl$ where dl is a differential length along the integration path. The incremental force is now:

$$f = T \cdot ds$$

$$f = \nu \begin{pmatrix} \left(B_x^2 - \frac{1}{2} |B|^2 \right) & (B_x B_y) \\ (B_y B_x) & \left(B_y^2 - \frac{1}{2} |B|^2 \right) \end{pmatrix} \begin{pmatrix} -s_y \\ s_x \end{pmatrix} dl$$

The tangential and normal component are:

$$f_t = f \cdot \vec{a}_t = \nu \cdot dl \left((B_x B_y) (s_x^2 - s_y^2) + s_x s_y (B_y^2 - B_x^2) \right)$$

$$f_n = f \cdot \vec{a}_n = \nu \cdot dl \left(B_x^2 s_y^2 + B_y^2 s_x^2 - \frac{1}{2} |B|^2 - 2 B_x B_y s_x s_y \right)$$

The tangential and normal components of the flux density are:

$$\vec{B}_t = B_x s_x + B_y s_y$$

$$\vec{B}_n = -B_x s_y + B_y s_x$$

Substituting and some after algebraic manipulations, we can write:

$$f_t = \nu (B_n B_t) dl$$

$$f_n = \frac{1}{2} \nu (B_n^2 - B_t^2) dl$$

The torque on an arc of radius r is given by:

$$M = \nu \int B_n B_t r \cdot dl$$

Virtual Work method

The principle of the virtual work technique to estimate the force is used in conservative energy systems. It is based on the comparison of the energy balance between two different positions, supposing a virtual movement along the direction where the force is computed.

In electromagnetic problems, the force is expressed as the partial derivative of magnetic coenergy with respect to the coordinates, along which the force component must be computed:

$$F_x = \frac{\partial W'}{\partial x} \approx \frac{W'(x) - W'(x + \Delta x)}{\Delta x}$$

We can also use the energy:

$$F_x = -\frac{\partial W}{\partial x} \approx \frac{W(x) - W(x + \Delta x)}{\Delta x}$$

Some commentaries:

- If the variation Δx is small, the numerical solution is not appreciable.
- If it is too big an excessive change of the magnetic energy is achieved
- The result may be affected by the variation of the mesh in the two positions.
- This technique requires at least two field solutions.

Core Losses

In general, the magnetic iron losses can be calculated by the composition of three losses:

- *Hysteresis losses.*
- *Eddy current losses.*
- *Excess losses* also called anomalous losses

Below we treat each of these three losses separately.

Hysteresis Losses

Hysteresis losses are owing to the discontinuous character at the microscopic scale of the magnetization process, that is, are due to the energy lost by each Barkhausen jump.

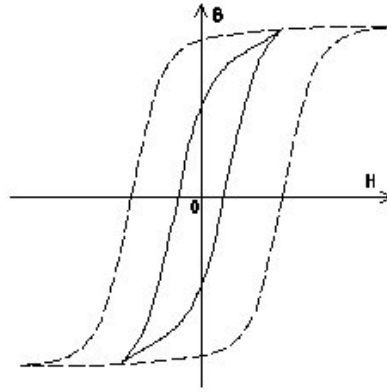
The classic procedure to determine hysteresis losses is the Steinmetz equation:

$$P_h = \eta V f B_{\max}^\alpha$$

One better choice is to apply the fact that the volumetric density of the energy lost owing to the Barkhausen jumps is the area of the quasistatic hysteresis cycle, and hence the energy lost is the area of the quasistatic cycle A_h multiplied by the volume of the sample V . Then hysteresis losses can be calculated with the following expression:

$$P_h = f V A_h$$

where f is the frequency of the external applied field.



Eddy current or classical Losses

We saw in earlier sections that in a conducting material submitted to time-varying field, loops of induced currents (Eddy currents) are created. In a slab with thickness d and electric conductivity σ , under a periodic field with period T , these losses can be determined by:

$$P_{cl}(t) = \frac{\sigma d^2}{12} \frac{1}{T} V \int_0^T \left(\frac{\partial B(t)}{\partial t} \right)^2 dt$$

For non-sinusoidal fluxes these losses can be calculated by using a Fourier expansion of the induction and summing the effects of all of the harmonics:

$$P_{cl} = \frac{\sigma \pi^2 f^2 d^2}{6} \sum_n n^2 B_n^2$$

where B_n is the amplitude of the n^{th} harmonic.

EXCESS LOSSES

The excess losses are due to the existence of magnetic domains, which enhance eddy currents in the proximities of domain walls. The classical model based on Maxwell's equations used in the classical losses deduction does not consider the presence of domains and supposes a magnetization process perfectly homogeneous on space, that is, neglecting the magnetic skin effect. But owing to the effect of domains, in reality dynamic losses are greater than classical losses; this difference of losses is called excess losses.

$$P_{ex}(t) = P_{din}(t) - P_{cl}(t)$$

The Bertotti [7] theory establishes that the behaviour of domains on a large scale can be described by the dynamics of magnetic objects. These magnetic objects are groups of domain walls correlated. In materials with large domains, as in the case of oriented grain, one magnetic object corresponds to one domain wall. The change of magnetizations is recorded, on a given moment, by means of the simultaneous intervention of n magnetic objects. The

magnetization process is represented as a distribution of coercive fields locally associated with magnetic objects. There is a dynamic balance among the field necessary to maintain a certain variation of B and the counter fields due to eddy currents. Time variation of B implies a variation in the balance and hence a modification of eddy currents.

If we define excess field $H_{ex}(t)$ as the part of the external field applied to compensate the field created by the movement of the magnetic objects, excess losses can be calculated by means of the following expression [7]:

$$P_e = \sqrt{\sigma G V_o} \frac{1}{T} \int_0^T \left| \frac{dB(t)}{dt} \right|^{1.5} dt$$

where G is the friction coefficient, which represents the constant of proportionality between the excess field and the rate of change of flux:

$$H_{ex} = G\sigma \frac{d\phi(t)}{dt}$$

The parameter V_o is related to the number of magnetic objects and the excess field. Experimentally it has been determined that the relationship between them is linear [8]:

$$n(t) = \frac{1}{V_o} H_{ex}(t)$$

Practical implementation of core loss calculation

In general, the suppliers of magnetic materials supply two characteristics of its materials:

- Saturation characteristic: $B = f(H)$
- Total losses $P_{FE} = f(B_{max}, f)$. Usually this relationship is approximated by the following equation:

$$p_m = K_m \cdot f^\beta \cdot B^\gamma \quad \beta > 1; \gamma \approx 1.6 \dots 2.2$$

To calculate the magnetic losses we can proceed as shown:

- First, we determine the potential vector and the induction at any point of the modelled domain.
- Thus we can determine the average value of induction in each element:

$$B_{avelement} = \frac{B_i + B_j + B_k}{3}$$

In the above expression we consider that the elements are small. If the elements are big, the better approximation is to consider the average value as the induction at the centroid of the element.

- Using these values we determine the magnetic losses in each element:

$$P_{FEelement} = f(B_{avelement}, f)$$

- Finally by summation of these values we obtain the total magnetic losses.

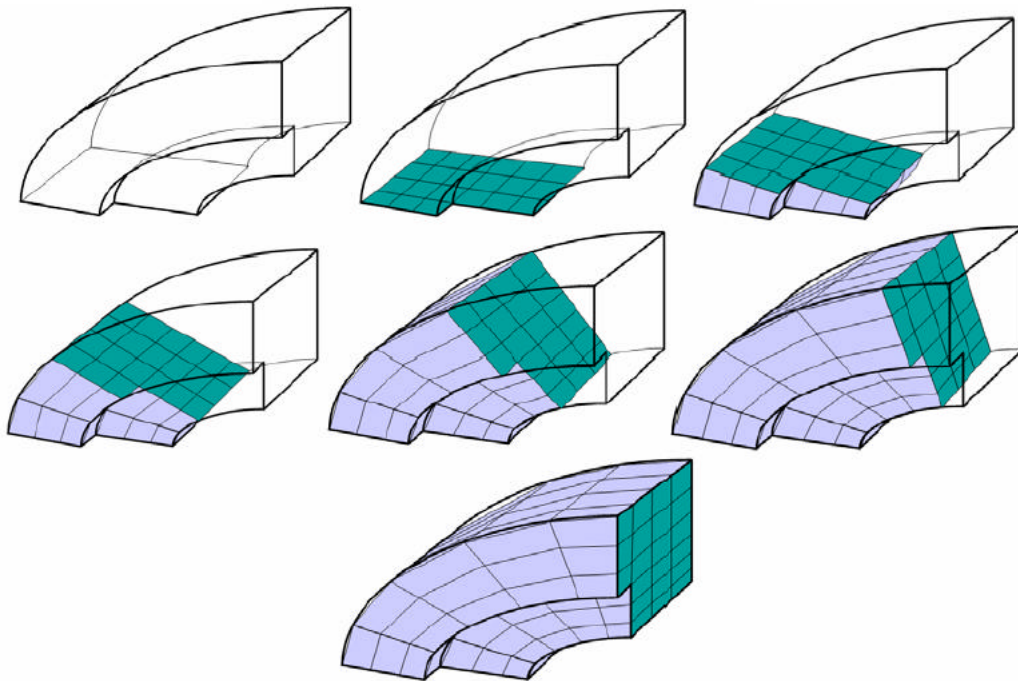
$$P_{FE} = \sum P_{FEelement}$$

The above process is valid only in the case of sinusoidal field distribution. For other cases (usually encountered in the practical applications) these values will be adapted. An effective solution to this problem still hasn't been found.

References

- [1] de Blas A., Bargalló R., de la Hoz J., Pereirinha, P., Lemos Antunes C., "Desarrollo de un modelo de hysteresis dinámico tipo-Preisach y su aplicación al cálculo de máquinas eléctricas" (in spanish), *Congresso de Métodos Computacionais em Engenharia, (CMCE'2004)*, 31 May – 2 June, Lisbon, Portugal
- [2] Mayergoyz, I.D., "Mathematical Models of Hysteresis and their applications", Elsevier, 2003
- [3] de Blas, A., Bargalló R., de la Hoz J., "Modelizado del ciclo de histéresis mediante el modelo de Preisach" (in spanish) *Revista Internacional Investigación Tecnológica*, Vol. nº3, May-June 2004
- [4] Bertotti, G., "Dynamic generalization of the Scalar Preisach model of Hysteresis", *IEEE Transactions on Magnetics*, Vol.28, nº5, pp. 2599-2601, September 1992
- [5] Fiorillo F., Novikov A., "An improved approach to power losses in magnetic laminations under non-sinusoidal induction waveform", *IEEE Transactions on magnetics*, Vol.26, nº5, pp. 2904-2910, September 1990
- [6] Bertotti G., "General properties of power losses in soft ferromagnetic materials, *IEEE Transactions on magnetics*, Vol.24, nº1, pp. 621-629, January 1988
- [7] Bertotti G., "Hysteresis in magnetism", Academic Press, 1998.
- [8] Bertotti G., Pasquale M., "Physical interpretation of induction and frequency dependence of power losses in soft magnetic materials", *IEEE Transactions on magnetics*. Vol.28, nº5, pp. 2787-2789, September 1992.

GENERAL ARCHITECTURE OF CAD SYSTEM



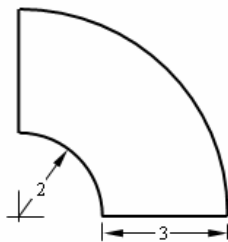
GENERAL ARCHITECTURE OF CAD SYSTEM BASED ON THE FINITE ELEMENT METHOD

In practice the analysis of any device involves three steps:

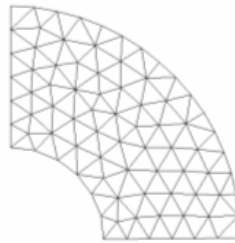
- The description of the geometry, the physical characteristics and the mesh
- The application of the FEM
- The visualization and interpretation of the results of the simulation

These three steps are different and correspond to the three different modules:

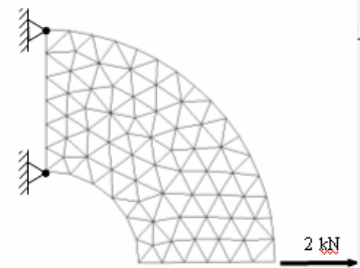
- The data entry module: Pre-processor.



1. Build CAD Model



2. Mesh



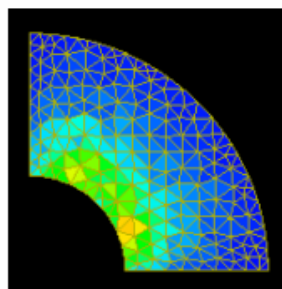
3. Apply Loads and Boundary Conditions

- The module to perform the analysis: Solver.



4. Computational Analysis

- The module to analyse the results: Postprocessor.



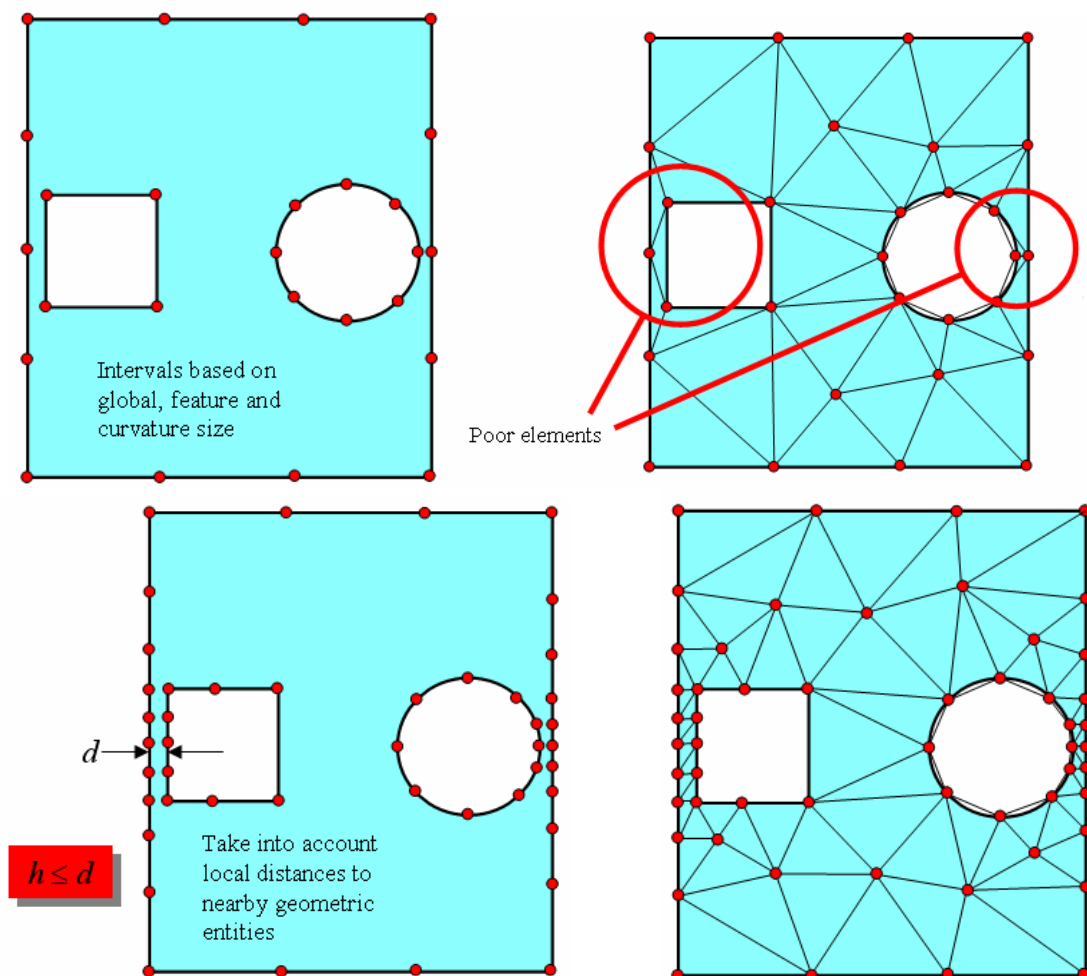
5. Visualization

The data entry module

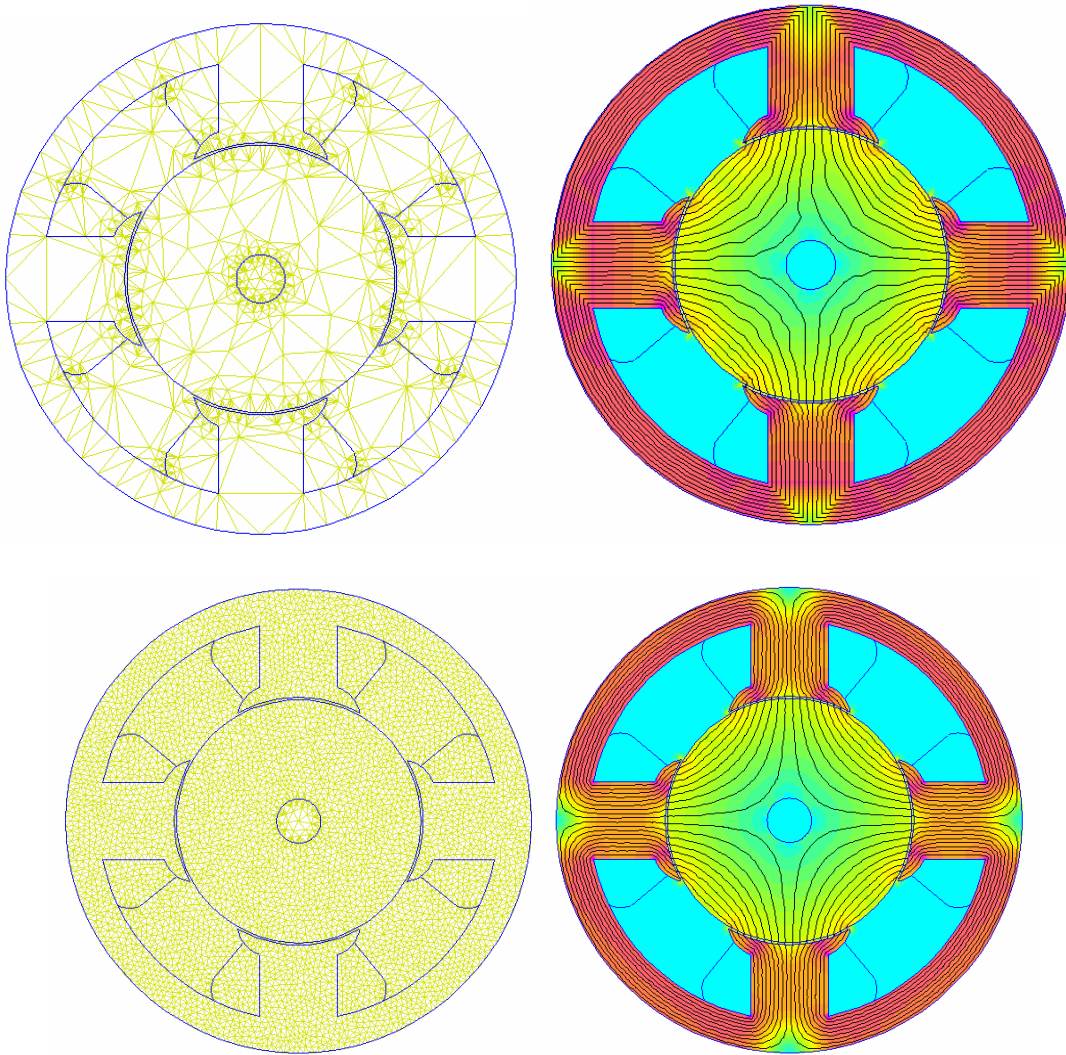
The data entry module is used for entering all the information necessary for the analysis of the problem. This module accomplishes the following three functions:

- Description of the geometry of the object
- Mesh generation
- Definition of the regions and the boundaries

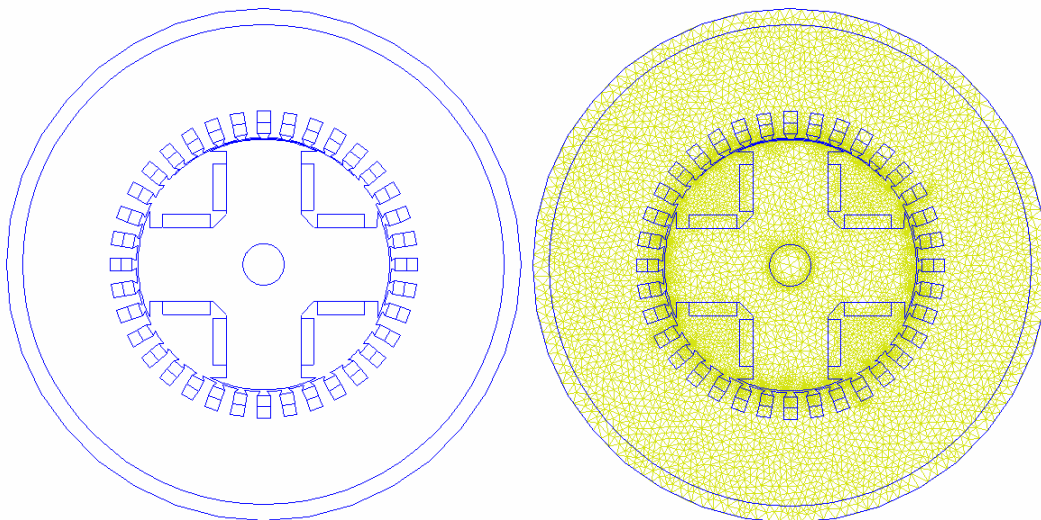
The mesh generation consists of finding a collection of nodes and a collection of finite elements which form an acceptable discretization of the domain. Such a discretization must respect the boundaries of the domain and the interfaces between different regions. Also, the shape of the FE mustn't be too irregular. The following figures show an incorrect and improved mesh for a particular problem.

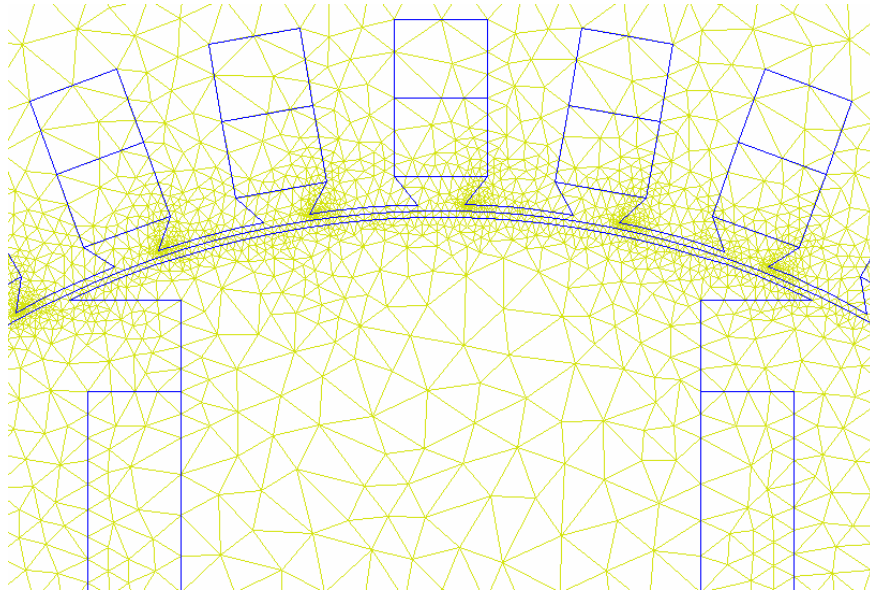


The following figures show the solution of the magnetic field in a direct current machine with the use of two meshes. The first is coarse and the results are poor. The second is a refined mesh; the solution is fine.

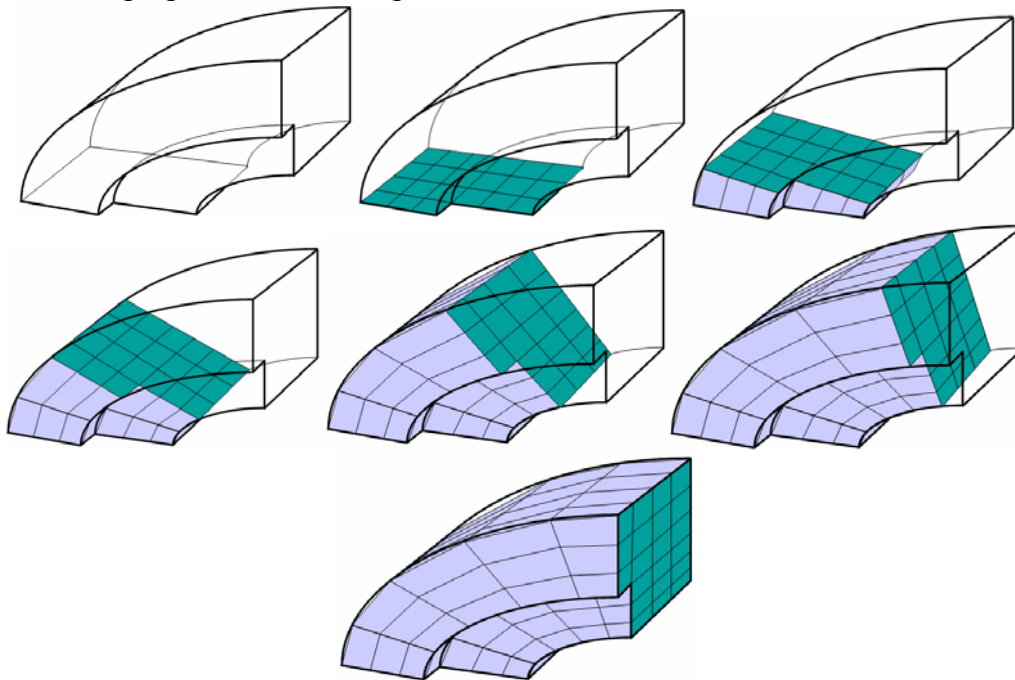


The following figures show a case of an synchronous machine and the detail of mesh in the air gap area. To obtain a high resolution we need to mesh the air gap with a very fine mesh.





The following figures show the generation of three-dimensional mesh.



The nodes are defined by their coordinates while the elements are characterized by their type and a list of their nodes. In some cases we include the information about the characteristics of materials and sources in this file.

The solver

The solver computes the unknowns in the FE problem, i.e it solves the linear (or non-linear) systems of equations. Its input is the domain discretization, in some cases the physical characteristics of the materials, the sources and the boundary conditions. Additional information such as type of problem, interval of time calculation and maximum error is in some cases compulsory.

Before the solution of algebraic equations, we must :

- Create the submatrix and subvectors corresponding to each element.
- Assemble these elementary matrices and vectors to build the system matrix.
- Apply Boundary conditions and symmetries if these exist.

The solution of linear algebraic systems can be done in several ways:

- Direct methods: Gauss, Choleski
- Semi direct methods: ICCG
- Block iterative methods: Gauss-Seidel

When the system of equations is not linear, these operations are repeated in an iterative scheme: Gauss-Seidel, Newton-Raphson, etc.

The postprocessor

The postprocessor perform two tasks:

- Extraction of significant information.
- Synthetic presentation of the numerical data via graphic facilities.

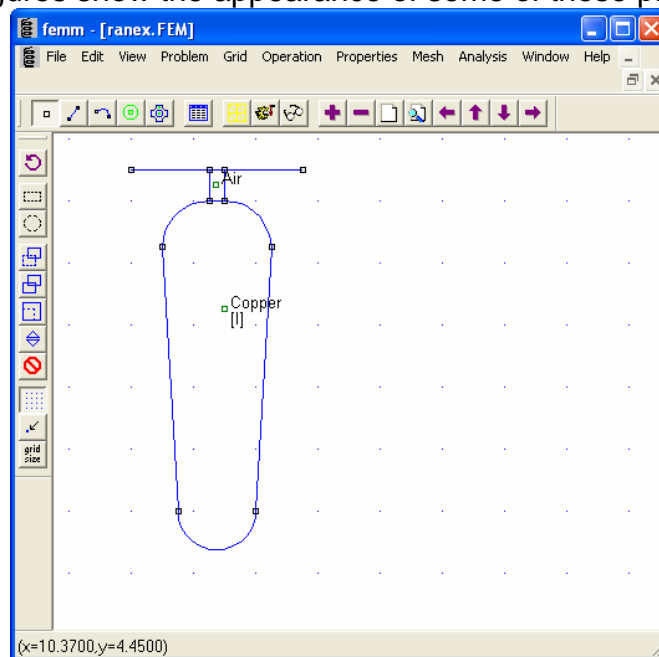
In most cases the pre-processor and the postprocessor have the same interface. The difference is in the information available at each time. For the post processes we need to know the value of potential at every node and the physical characteristics of every element. In the pre-processor it is only necessary to know the coordinate points.

Examples(2D): FEMM, MAXWELL_SV.

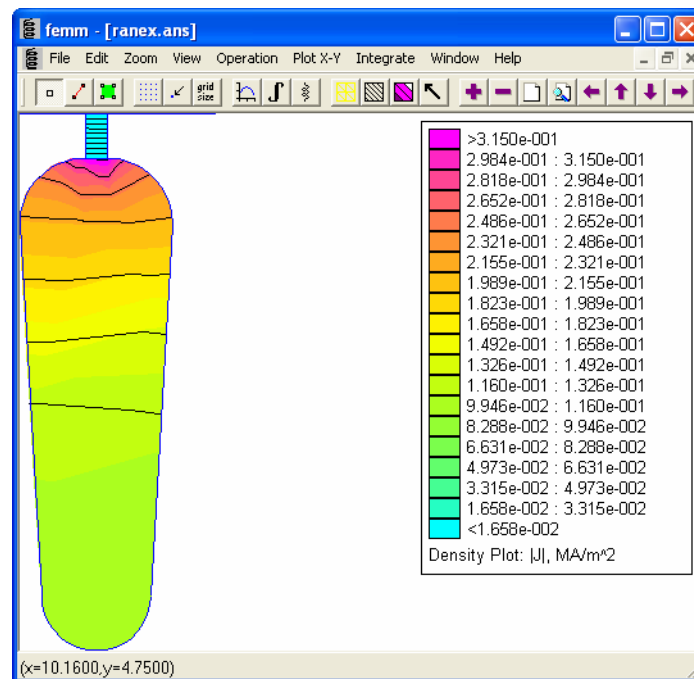
We present here some characteristics of two programs: FEMM, MAXWELL_SV.

	FEMM	MAXWELL_SV
Electrostatic	Yes	Yes
DC conduction	No	Yes
AC conduction	Yes	Yes
Magnetostatic	Yes	Yes
Transient	No	No
Transient + Voltage source	No	No
Thermal	No	No
Movement	No	No
Number of nodes	No limited	No limited
Non-linearity	Yes	Yes
Equiline map	Yes	Yes
Colour maps	Yes	Yes
Vector maps	Yes	Yes
Numerical results. Point values	Yes	Yes
Graphical representation of derived quantities	Yes	Yes
Mesh	Automatic	Automatic
Complementary calculation	Yes. Some integrals of line and area	Yes. True "calculator" with a hundred of options.
Operating system	Windows	Windows

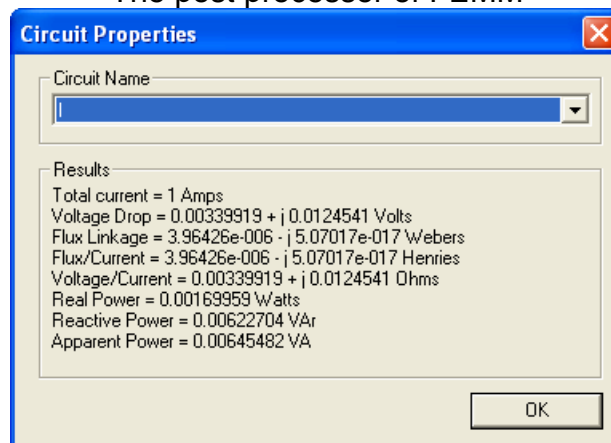
The following figures show the appearance of some of these programs.



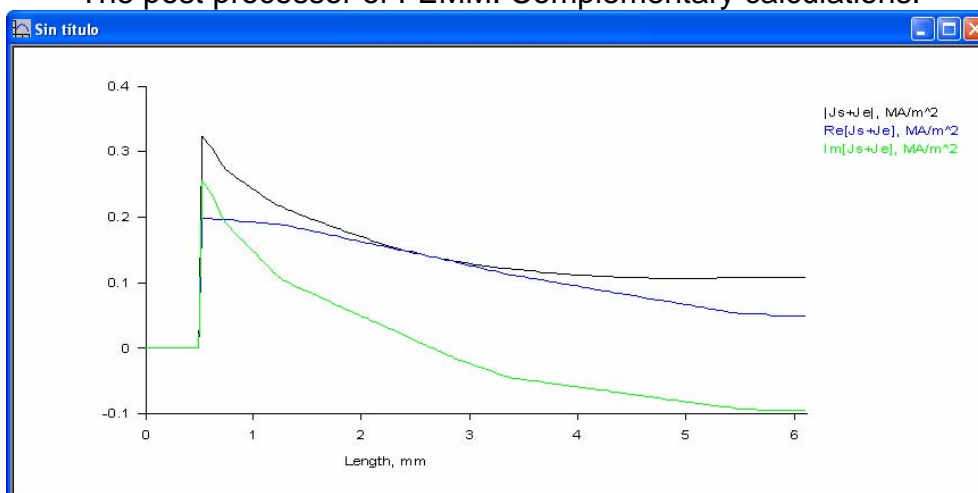
The pre-processor of FEMM



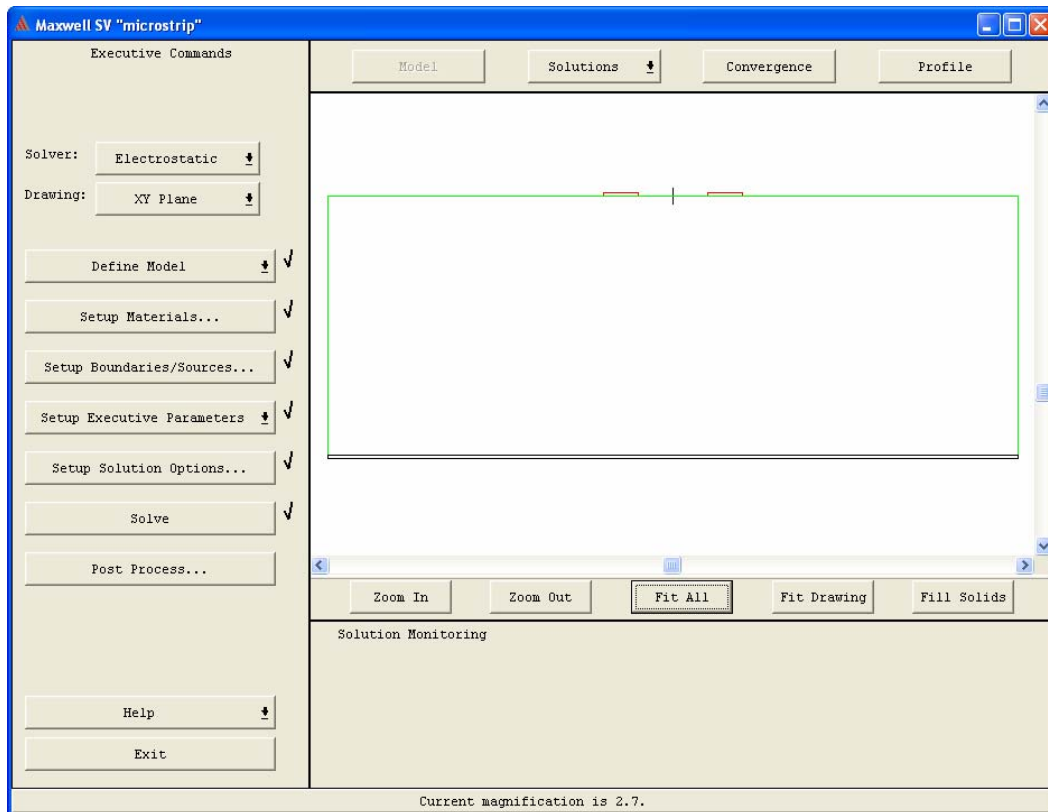
The post processor of FEMM



The post processor of FEMM. Complementary calculations.



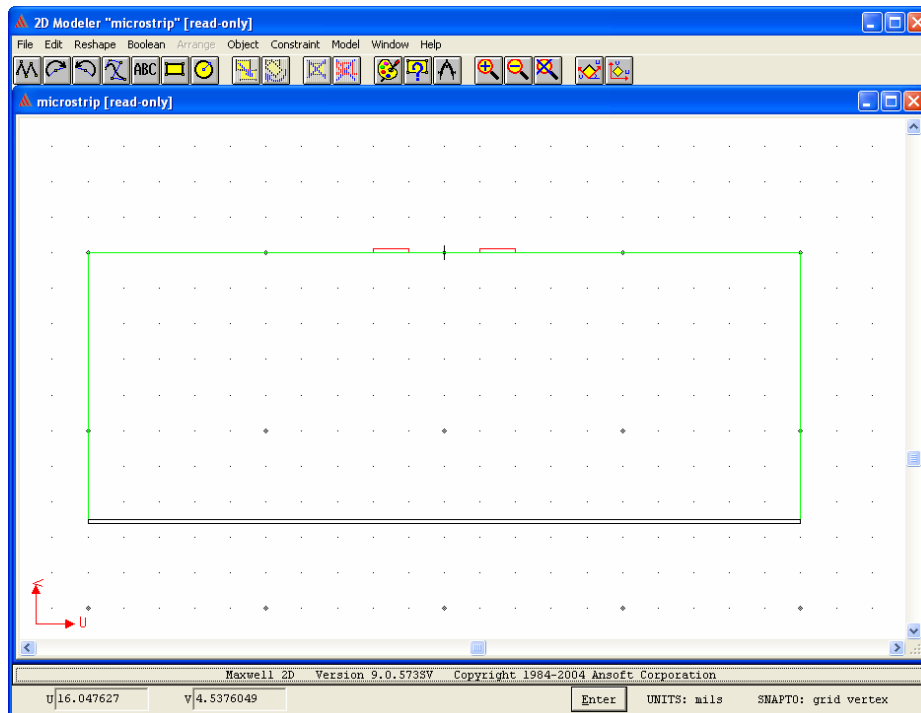
The post processor of FEMM. Graphical representation of derived quantities



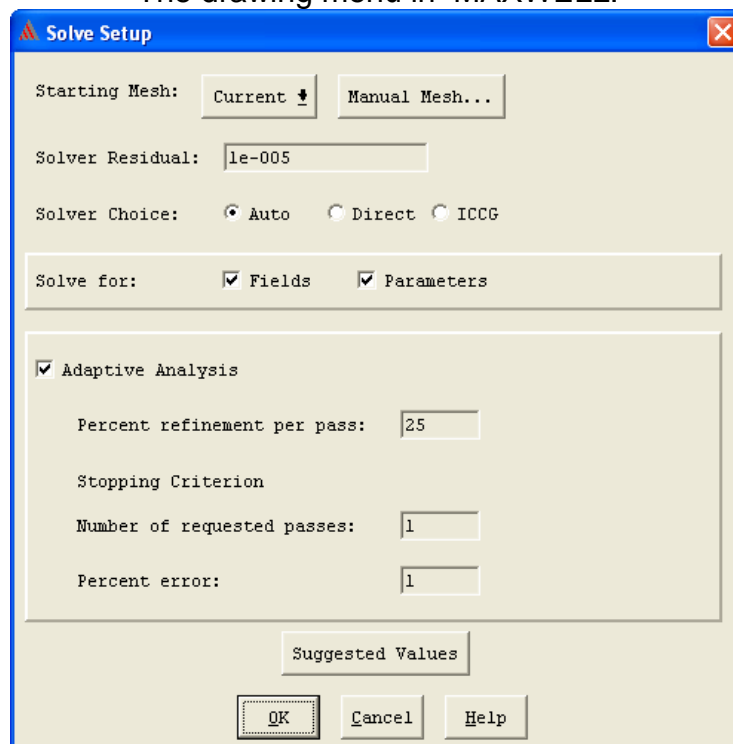
The pre-processor of MAXWELL.

MAXWELL has an extensive management program. The above figure shows the management window. In it we can see different options to create a project:

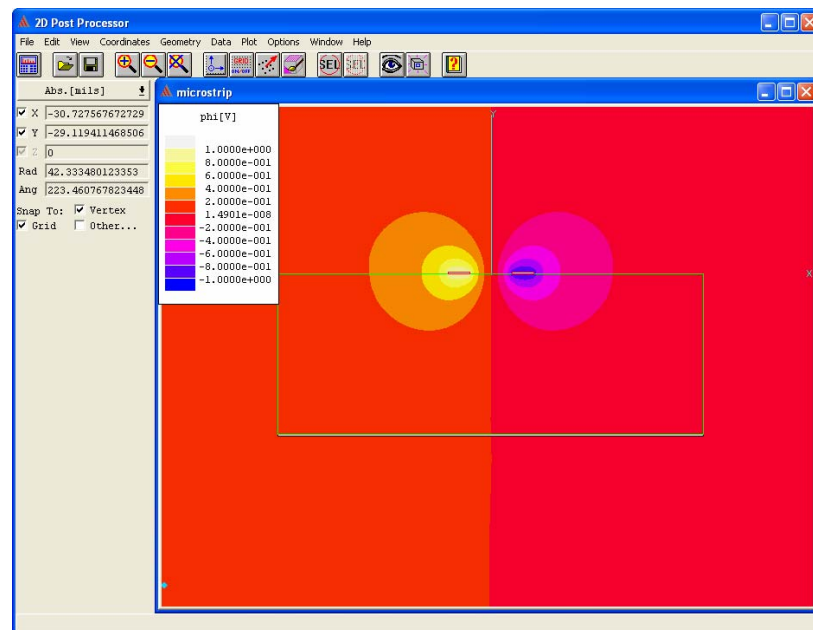
- Define model. To draw the problem model
- Setup materials. To assign materials to every area.
- Setup boundary and sources. To assign both: boundary conditions and sources of excitation (voltage and current)
- Setup executive parameters. To describe what quantities must be calculated automatically (usually force, torque, inductance and others)
- Setup solution options. To select the options of calculation: manual/automatic mesh, etc.
- Solve. To solve the system
- Post process. To enter the post-process program.



The drawing menu in MAXWELL.



The Setup options in MAXWELL

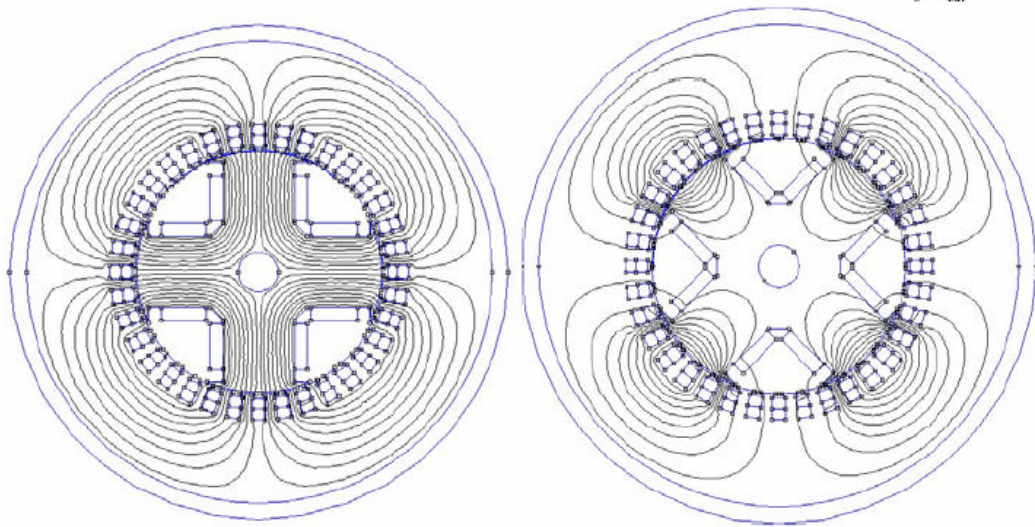


The post-processing menu in MAXWELL



The “calculator” in the post process menu in MAXWELL

EXAMPLES



These examples are solved by Quickfield software. You can find the indicated files in the course CD-ROM.

Exercise N 1. Slot embedded conductor.

Models [lab1.zip](#) and [lab1_2.zip](#)

Task

Draw a plot of current distribution within the conductor placed in the slot of electric motor.

Experiment

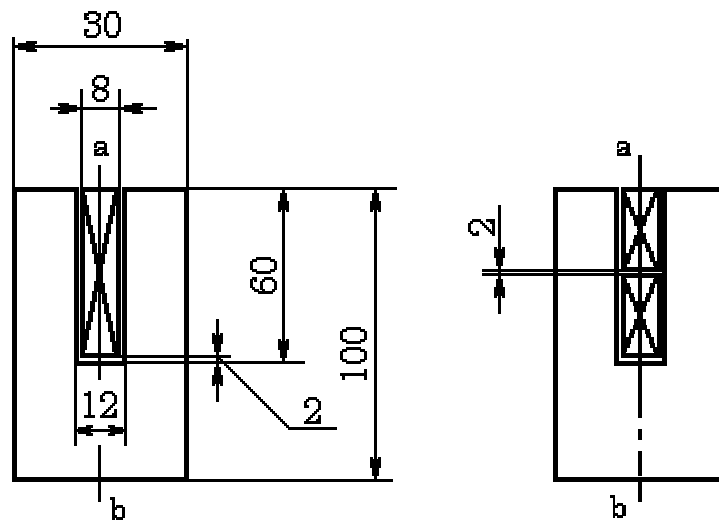
Current density is obtained by potential measuring along the part of conductor done by voltmeter. Phase is determined by digital phasemeter.

Problem type

Plane-parallel time-harmonic linear magnetic problem.

Geometry

Problem area is to the right of symmetry axis (line *ab*), corresponding boundary conditions are set.



Given data

Relative permeability of steel $\mu = 100$.

Relative permeability of air & copper $\mu = 1$.

Conductivity of copper $\sigma = 57000000 \text{ S/m}$.

The steel is laminated, so its conductivity along the bar is $\sigma = 0 \text{ S/m}$.

Frequency $f = 50 \text{ Hz}$.

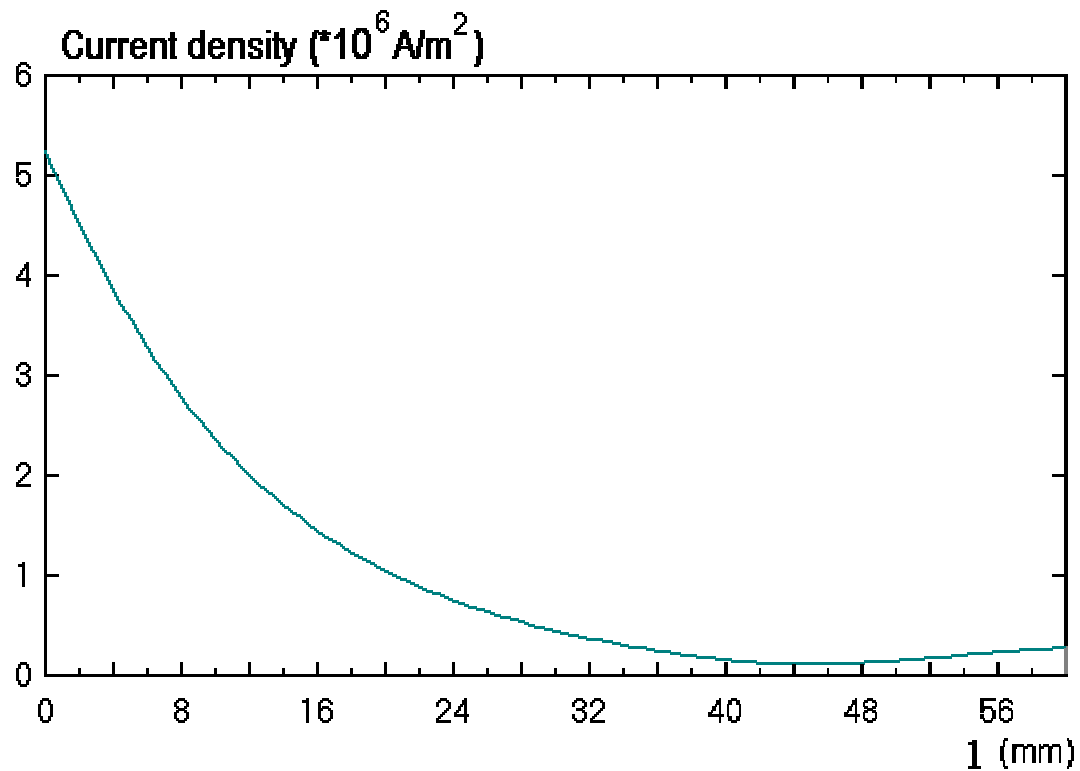
The total current per the bar is 600 A, or 300 A if there are two bars in the slot.

Boundary conditions

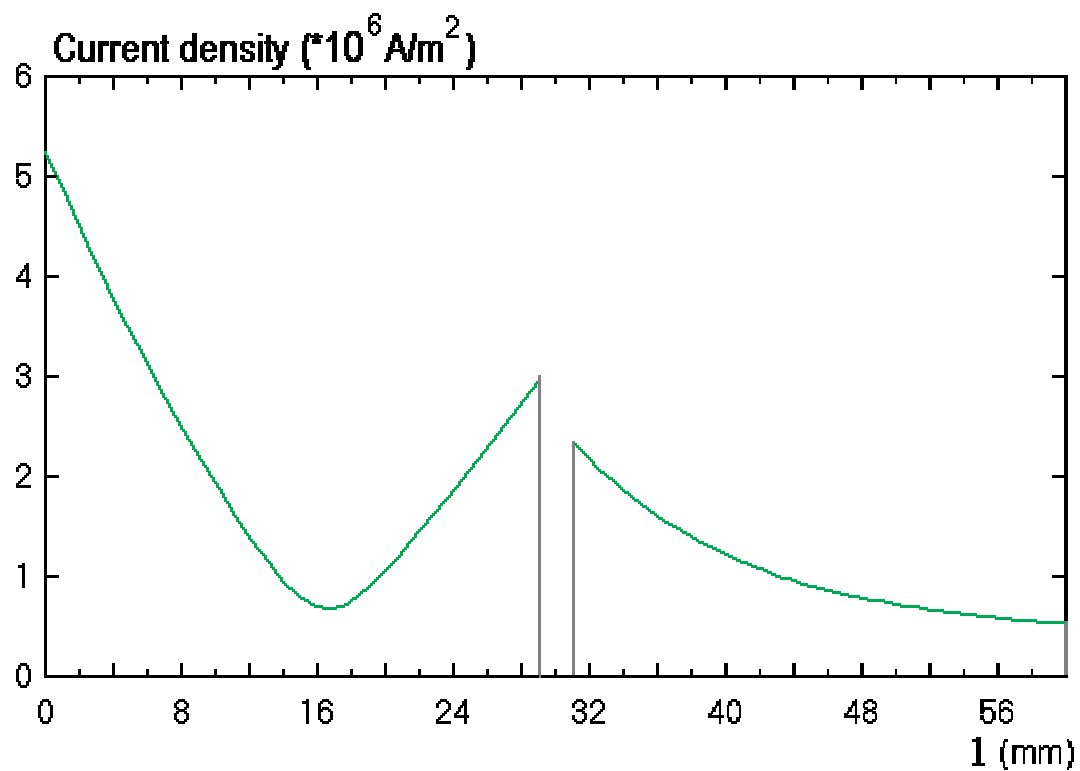
At the vertical axis of symmetry (line *ab*) $H_t = 0$.

The field fades within ferromagnetics, thus at other boundaries the field is zero $A = 0$.

Vertical distribution of current density along the single copper bar ($I = 0$ at the upper boundary of upper bar). Problem file [lab1.zip](#).



Vertical distribution of current density along two copper bars ($l = 0$ at the upper boundary of upper bar).
Problem file [lab1_2.zip](#).



Exercise N 2. Force of interaction of two cylindrical coaxial coils.

See following models

Task

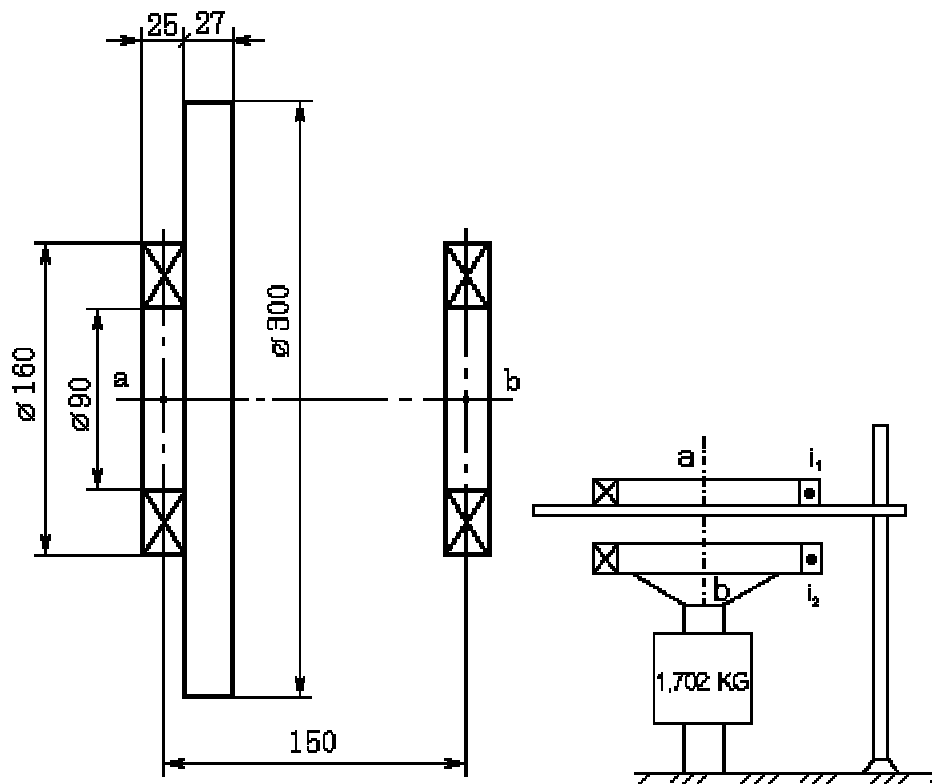
Find the force applied to the coils with current with and without the shield between them.

Experiment

Forces are measured by use of digital balance on which one of coils is installed (see the right picture below). Test are performed with currents varying, and different conductors and ferromagnetics are placed between coils.

Geometry

Due to symmetry of the formulation only upper half of the problem (above ab line) is defined, and at the axis of symmetry (line ab) the boundary conditions are set.



Given data

Current density in the coil $j = 100000 \text{ A/m}^2$.

Relative magnetic permeability of air, aluminum and copper coils $\mu = 1$.

Relative magnetic permeability of the steel shield $\mu = 1000$.

Electrical conductivity of steel $\sigma = 10000000 \text{ Sm/m}$.

Electrical conductivity of aluminum $\sigma = 37000000 \text{ Sm/m}$.

Coils are wound by insulated wire, so cross-section conductivity in coils $\sigma = 0 \text{ Sm/m}$.

Boundary conditions

Along the horizontal symmetry axis (line ab) $B_n = 0$.

Equation $B = \text{rot } A$ in cylindrical coordinate system leads to $A = \text{const}$ at the axis ab . The field fades at the infinity, so due to the condition of continuity of the potential $A = 0$ at the line ab .

Time-harmonic electromagnetic field, $f = 50$ Hz.

Shield type	Mean force of interaction, mN	Model
No shield	0.65989	lab2.pbm
Steel	0.196	lab2_Fe.pbm
Aluminum	0.207	lab2_Al.pbm

DC magnetic field.

Shield type	Mean force of interaction, mN	Model
No shield	0.65989	lab2c.pbm
Steel	0.232	lab2c_Fe.pbm

Exercise N 3. Proximity effect.

Models [lab3_Cu.zip](#) and [lab3_Fe.zip](#)

Task

Find the current density distribution along the cross section of long parallel conductors. Two types of conductors are analyzed: two copper rods and two steel tubes.

Experiment

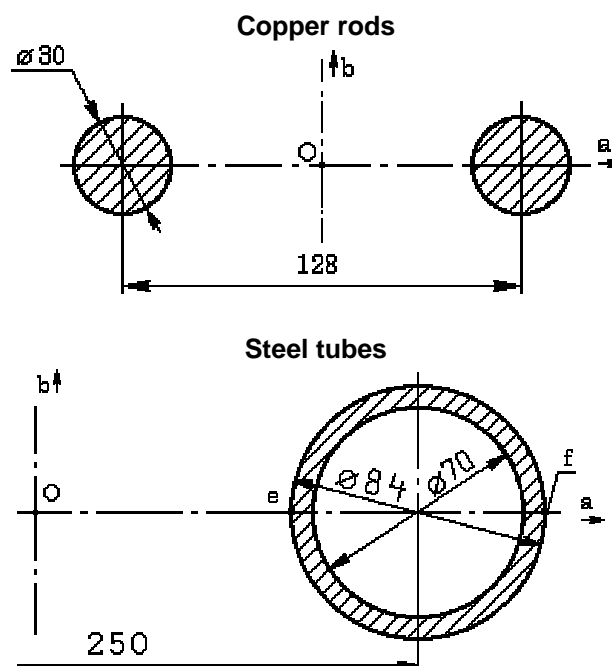
Current density is defined by measuring the voltages on the conductor segments, the phase of current is measured separately by the digital phasemeter.

Problem type

Linear plane-parallel problem of time-harmonic electromagnetic field.

Geometry

Due to problem symmetry only upper-right quarter aOb is defined, and at the axes of symmetry the boundary conditions are set.



Given data

Relative magnetic permeability of copper and air $\mu = 1$.

Relative magnetic permeability of steel $\mu = 100$.

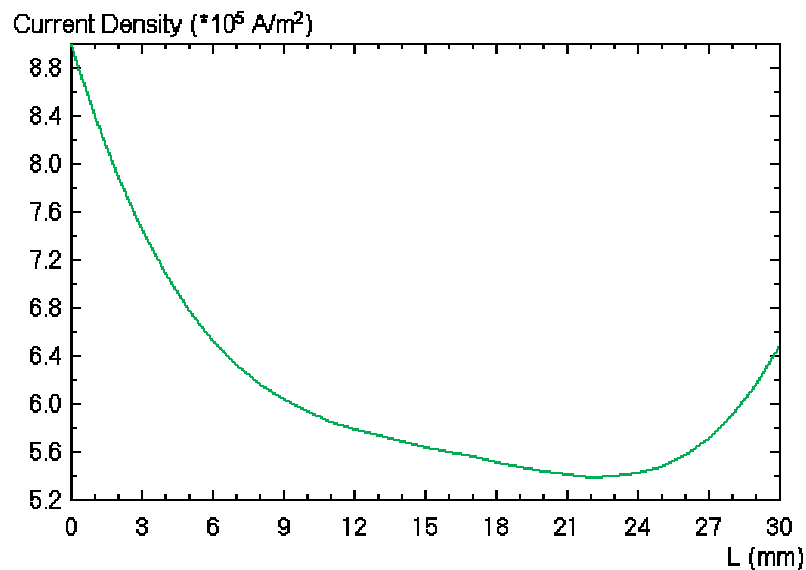
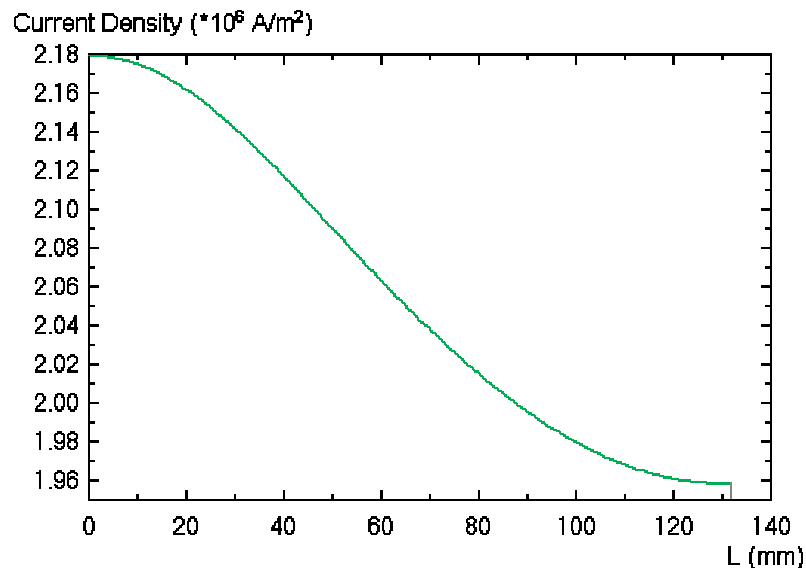
Total current $J = 300$ A. Frequency $f = 50$ Hz.

Electric conductivity of copper $\sigma = 57000000$ Sm/m.

Electric conductivity of steel $\sigma = 10000000$ Sm/m.

Boundary conditions

At the horizontal axis of symmetry (line Oa) $H_t = 0$. At the vertical axis of symmetry Ob $B_n = 0$. Equation $B = \text{rot } A$ in the cylindrical coordinate system leads to $A = \text{const}$ at the axis Ob . Field fades at the infinity so at the other boundaries $A = 0$.

Current density distribution along the line Oa for copper rods. [Model lab3_Cu.zip](#)**Current density distribution along the steel tube perimeter (from the point e to point f clockwise). [Model lab3_Fe.zip](#)**

Exercise N 4. Electromagnetic shielding.

See the following models.

Task

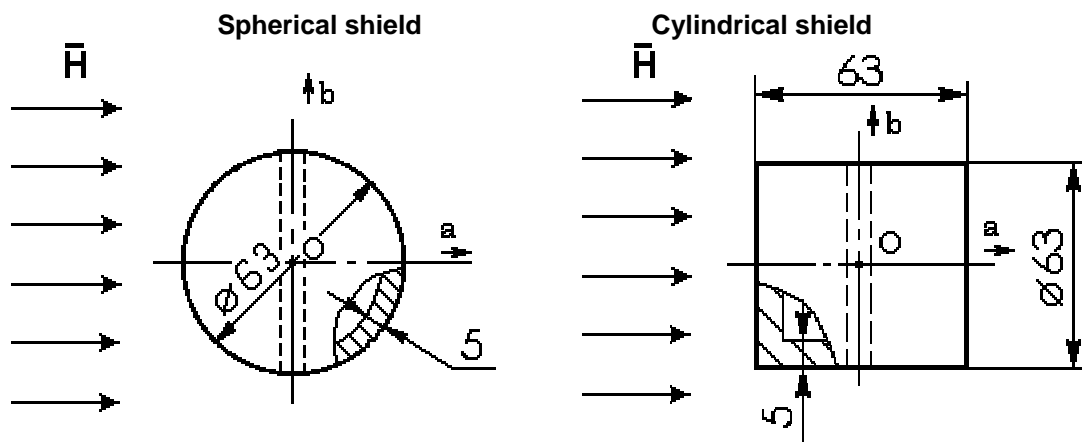
Find the level of magnetic field reduction inside the shield. Shields made of steel and copper of the same geometry are analyzed.

Experiment

Uniform external magnetic field is produced by the electric magnet. The shield with the measuring coil inside is placed between its poles. EMF in the coil is measured: in case of DC current in the coil - by ballistic galvanometer (in the moment of switching on), in case of AC current - by use of millivoltmeter.

Geometry

The shield consists of two halves. Possible positions of the slot in the shield is shown by dotted line. The slot could be enlarged up to 2 mm by sheets of non-magnetic materials. Due to symmetry only right-upper quarter aOb is analyzed, and at the axes of symmetry the boundary conditions are set.



Given data

Relative magnetic permeability of air and copper $\mu = 1$.

Relative magnetic permeability of steel $\mu = 1000$.

Magnetic field is uniform, $B = 0.139 \text{ T}$.

Boundary conditions

Due to symmetry at the line Ob $H_t = 0$. At the line Oa $B_n = 0$. Equation $B = \text{rot } A$ in the cylindrical coordinate system leads to $A = \text{const}$ (0.0695) at the axis Oa . Field fades at the infinity, so due to continuity at the line Oa $A = 0$ also. The field is uniform, and the right boundary has the same condition as the left one $H_t = 0$.

Shielding coefficient - relation of magnetic flux densities outside and inside the shield.

Time-harmonic electromagnetic field , $f = 50$ Hz.

Shield type	Magnetic flux density inside the shield (in mT), while external uniform field is 139 mT	Shielding coefficient	Model
Steel sphere without slot	0.082	1691	lab4_Fe.pbm
Steel sphere with slot	35.9	3.87	lab4Fe+.pbm
Steel cylinder without slot	0.336	413.69	lab4c_Fe.pbm
Steel cylinder with slot	40.3	3.45	lab4c_Fe+.pbm
Copper sphere without slot	97.97	1.42	lab4_Cu.pbm
Copper sphere with slot	100	1.39	lab4_Cu+.pbm
Copper cylinder without slot	69.16	2.00	lab4c_Cu.pbm
Copper cylinder with slot	70.99	1.96	lab4c_Cu+.pbm

DC magnetic field.

Shield type	Magnetic flux density inside the shield (in mT), while external uniform field is 139 mT	Shielding coefficient	Model
Steel sphere without slot	1.52	91.45	lab4_f.pbm
Steel sphere with slot	41.2	3.37	lab4_f+.pbm
Steel cylinder without slot	2.08	66.83	lab4c_f.pbm
Steel cylinder with slot	48.8	2.84	lab4c_f+.pbm

Exercise N 5. Magnetic field of the cylindrical coil.

See models [lab5.zip](#) and [lab5_Fe.zip](#)

Task

Make a plot of magnetic flux density at the axis of the coil with and without steel core.

Experiment

Magnetic flux density is measured in laboratory by microwebermeter.

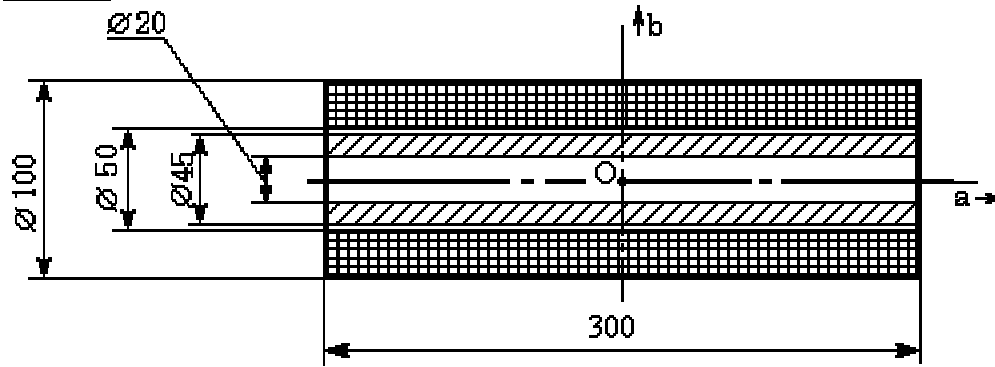
Problem type

Linear axisymmetrical problem of magnetostatics.

Geometry

Due to problem symmetry only upper-right quarter aOb is defined, and at the axes of symmetry [boundary](#)

conditions are set.



Given data

Current density in the coil $j = 100000 \text{ A/m}^2$.

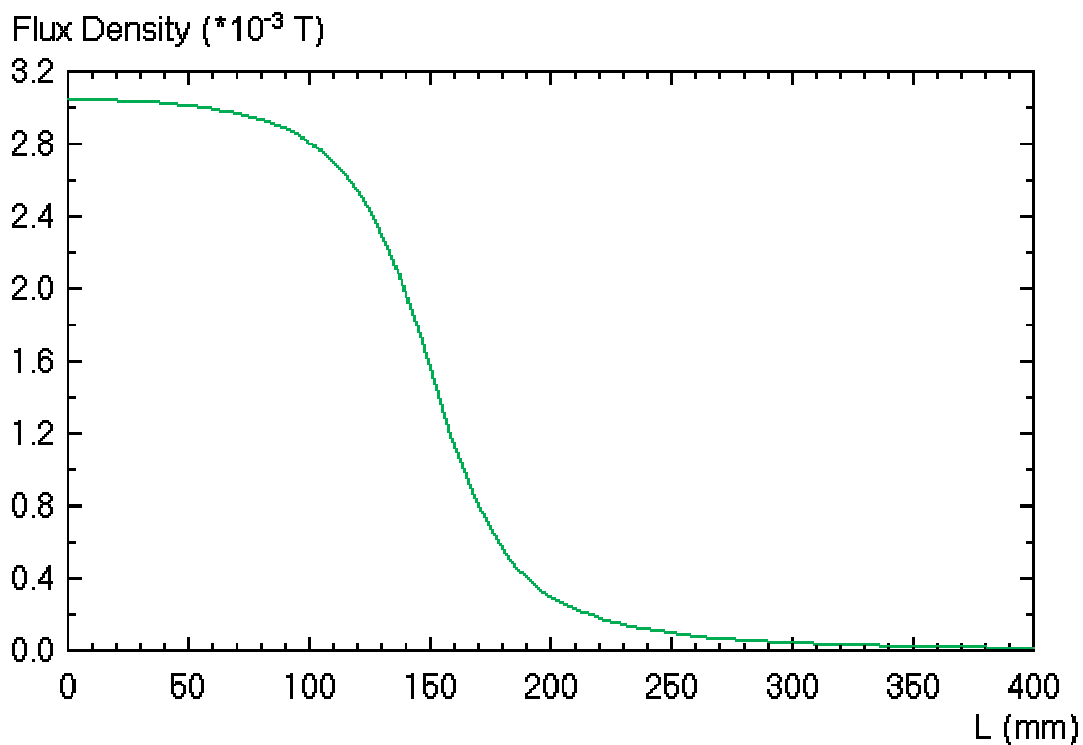
Relative magnetic permeability of air and copper $\mu = 1$.

Relative magnetic permeability of steel of the core $\mu = 500$.

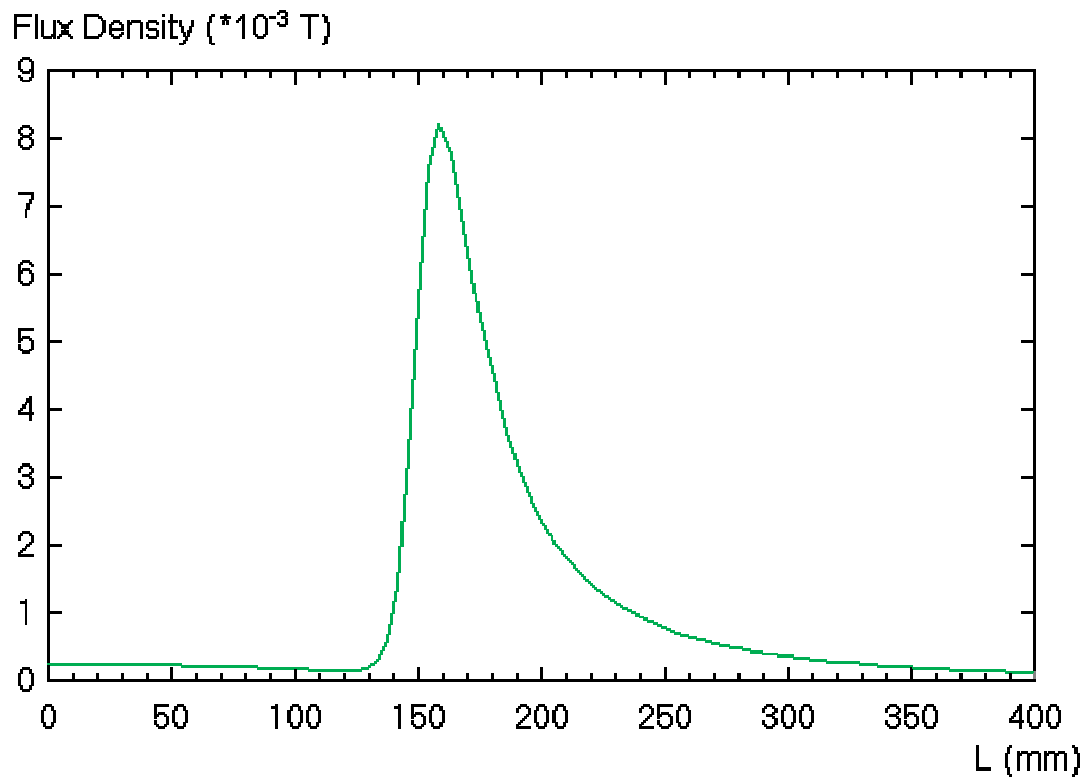
Boundary conditions

At the vertical axis of symmetry (line Ob) $H_t = 0$. At the horizontal axis of symmetry Oa $B_n = 0$. From $B = \text{rot } A$ in the cylindrical coordinate system we have at the axis Oa $A = \text{const}$. Field fades at the infinity, so at the line Oa $A = 0$ due to continuity of A.

Dependence of the magnetic flux density upon the distance to the coil center. No core. [Model lab5.zip](#)



Dependence of the magnetic flux density upon the distance to the coil center. Steel core. [Model lab5_Fe.zip](#)



Exercise N 6. Mutual inductance of coils.

See model [lab6.zip](#)

Task

Find the dependence of mutual inductance of coaxial cylindrical coils upon the distance between them.

Experiment

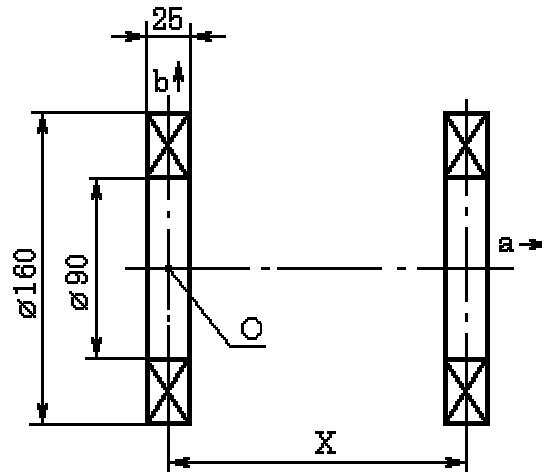
EMF in the right coil is measured by ballistic galvanometer (at the switching on).

Problem type

Linear axisymmetrical problem of magnetostatics.

Geometry

The field source is the left coil. Due to the field symmetry only upper-right quarter aOb is defined. At the axes of symmetry the boundary conditions are set.

**Given data**

Relative magnetic permeability of air and copper coils $\mu = 1$.

Current density in the left coil $j = 100000 \text{ A/m}^2$.

There is no current in the right coil, thus it has no affection to the field shape.

Boundary conditions

At the vertical axis of symmetry (line Ob) $H_t = 0$. At the horizontal axis of symmetry Oa $B_n = 0$. From $B = \text{rot } A$ in the cylindrical coordinate system we have at the axis Oa $A = \text{const}$. Field fades at the infinity, so at the line Oa $A = 0$ due to continuity of A.

Mutual inductance M - relation of the flux connected with all turns of the right coil Ψ to the current in the left coil J (which is the origin of the flux).

$$L = \Psi / J$$

$$\Psi = \Phi \cdot w$$

Here w is number of turns of the right coil, Φ - flux across the right coil.

Total current $J = j \cdot S_{\text{section}} = 100000 \cdot 0.000875 = 87.5 \text{ A}$. See model [lab6.zip](#)

X, mm	Flux across the right coil, μWb .	Mutual inductance M, μH .
70	2.656	$0.0306 \cdot w$
150	0.637	$0.0073 \cdot w$
210	0.285	$0.0033 \cdot w$

Exercise N 7. Magnetic field simulation in the air gap of DC electric motor.

See models [lab7.zip](#) and [lab7exp.zip](#)

Task

Draw the lines of magnetic field in DC electric motor in the non-ferromagnetic region. Calculate pole dissipation coefficients for two formulations. First - the coil is defined by current distribution, the magnetic permeability of steel is finite. Second - simplified formulation: steel assumed to be with infinite permeability and the coil is modeled by current layer.

Problem type

Liner plane-parallel magnetostatic problem.

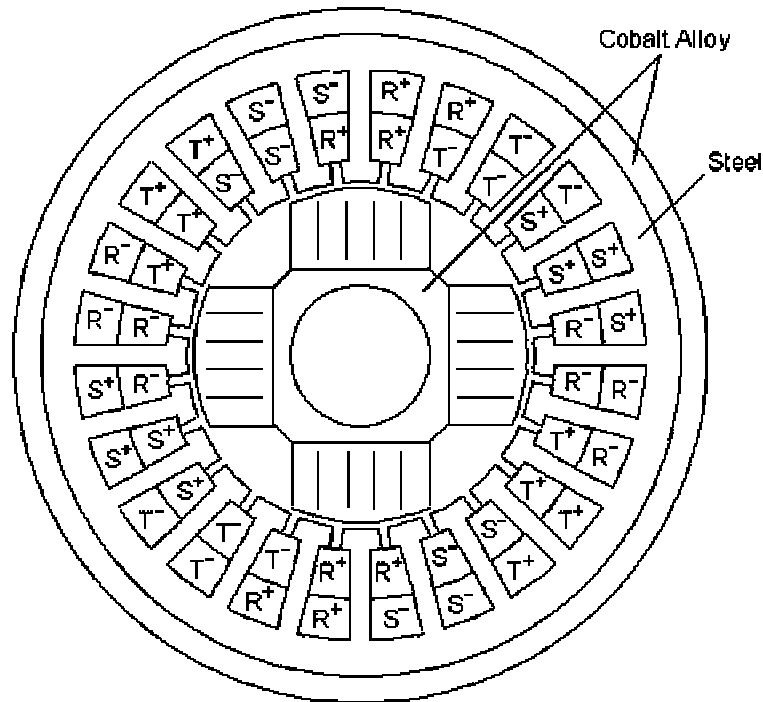
Electric motor

A brushless DC motor with permanent magnets and three phase coil excitation.

Problem Type:

A nonlinear plane-parallel problem of magnetostatics.

Geometry:



Axial length of the motor is 40 mm.

The four magnets are made of Samarium-Cobalt with relative permeability of 1.154 and coercive force of 550000 A/m. The current densities for the coil slots are as follows:

1,300,000 A/m² on R⁺, -1,300,000 A/m² on R⁻,
1,300,000 A/m² on S⁺, -1,300,000 A/m² on S⁻,
and zero on T⁺ and T⁻.

The inner and outer frames are made of Cobalt-Nickel-Copper-Iron alloy.

The B-H curve for the Cobalt-Nickel-Copper-Iron alloy:

H (A/m)	20	60	80	95	105	120	140	160	180	200	240	2500
B (T)	0.19	0.65	0.87	1.04	1.18	1.24	1.272	1.3	1.32	1.34	1.36	1.45

The B-H curve for the steel:

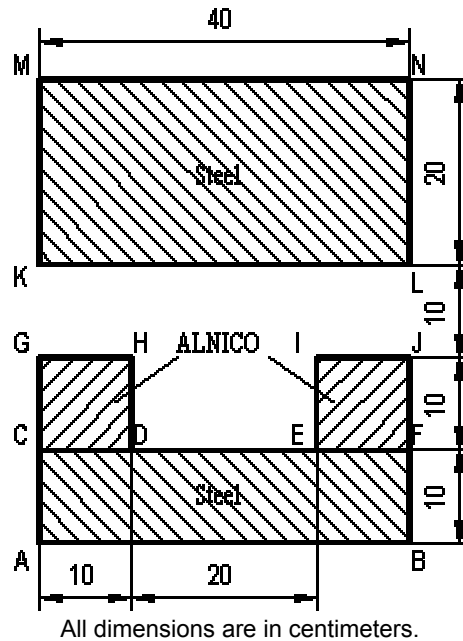
H (A/m)	400	600	800	1000	1400	2000	3000	4000	6000
B (T)	0.73	0.92	1.05	1.15	1.28	1.42	1.52	1.58	1.60

Magn1: Nonlinear permanent magnet

A permanent magnet and a steel keeper in the air

Problem Type:

A nonlinear plane-parallel problem of magnetostatics.

Geometry:**Given:**

The permanent magnets are made of ALNICO, coercive force is 147218 A/m. The polarizations of the magnets are along vertical axis opposite to each other. The demagnetization curve for ALNICO:

H, A/m	-14728	-119400	-99470	-79580	-53710	-19890	0
B, T	0	0.24	0.4	0.5	0.6	0.71	0.77

The B-H curve for the steel:

H, A/m	400	600	800	1000	1400	2000	3000	4000	6000
B, T	0.73	0.92	1.05	1.15	1.28	1.42	1.52	1.58	1.60

Problem:

Find maximum flux density in Y-direction

Solution:

To avoid the influence of the boundaries while modelling the unbounded problem, we'll enclose the magnet in a rectangular region of air and specify zero Dirichlet boundary condition on its sides.

H (A/m)	460	640	720	890	1280	1900	3400	6000
B (T)	0.80	0.95	1.00	1.10	1.25	1.40	1.55	1.65

Problem:

Obtain the magnetic field in the solenoid and a force applied to the plunger.

Solution:

This magnetic system is almost closed, therefore outward boundary of the model can be put relatively close to the solenoid core. A thicker layer of the outside air is included into the model region at the plunger side, since the magnetic field in this area cannot be neglected.

Mesh density is chosen by default, but to improve the mesh distribution, three additional vertices are added to the model. We put one of these vertices at the coil inner surface next to the plunger corner, and two others next to the corner of the core at the both sides of the plunger.

A contour for the force calculation encloses the plunger. It is put in the middle of the air gap between the plunger and the core. While defining the contour of integration, use a strong zoom-in mode to avoid sticking the contour to existing edges.

The calculated force applied to the plunger $F = 374.1$ N.

Comparison of results

Maximum flux density in Z-direction in the plunger:

	B_z(T)
Reference	0.933
QuickField	1.0183

Reference

D. F. Ostergaard, *"Magnetics for static fields"*, ANSYS revision 4.3, Tutorials, 1987.

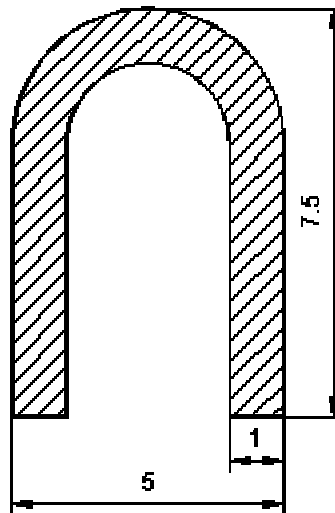
Magn3: Ferromagnetic C-magnet

A permanent C-magnet in the air. The example demonstrates how to model curved permanent magnet using the equivalent surface currents.

Problem Type:

Plane problem of magnetics.

Geometry of the magnet:

**Given:**

Relative permeability of the air $\mu = 1$;
 Relative permeability of the magnet $\mu = 1000$;
 Coercive force of the magnet $H_c = 10000 \text{ A/m}$.

The polarization of the magnet is along its curvature.

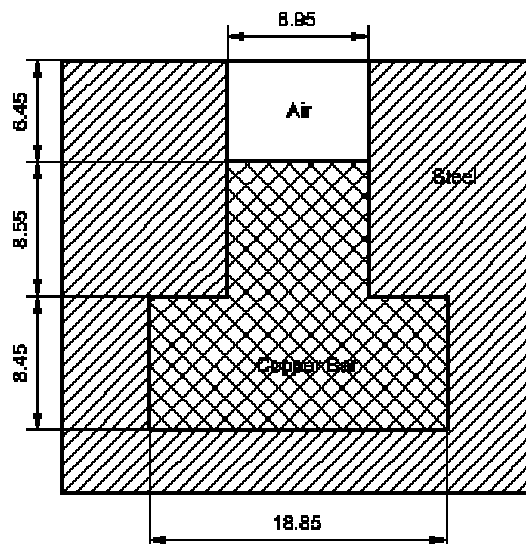
Solution:

To avoid the influence of the boundaries while modelling the unbounded problem, we'll enclose the magnet in a rectangular region of air and specify zero Dirichlet boundary condition on its sides.

Magnetization of straight parts of the magnet is specified in terms of coercive force vector. Effective surface currents simulate magnetization in the middle curved part of the magnet.

HMagn1: Slot embedded conductor**Problem Type:**

A plane problem of time-harmonic magnetic field.

Geometry:

A solid copper conductor embedded in the slot of an electric machine carries a current I at a frequency f .

Given:

Magnetic permeability of air $\mu = 1$;
 Magnetic permeability of copper $\mu = 1$;
 Conductivity of copper $\sigma = 58,005,000$ S/m;
 Current in the conductor $I = 1$ A;
 Frequency $f = 45$ Hz.

Problem:

Determine current distribution within the conductor and complex impedance of the conductor.

Solution:

We assume that the steel slot is infinitely permeable and may be replaced with a Neumann boundary condition. We also assume that the flux is contained within the slot, so we can put a Dirichlet boundary condition along the top of the slot. See HMagn1.pbm problem in the Examples folder for the complete model.

The complex impedance per unit length of the conductor can be obtained from the equation

$$Z = V / I$$

where V is a voltage drop per unit length. This voltage drop on the conductor can be obtained in **Local Values** mode of the postprocessing window, clicking an arbitrary point within the conductor.

Comparison of Results

	Re Z (Ohm/m)	Im Z (Ohm/m)
Reference	0.00017555	0.00047113
QuickField	0.00017550	0.00047111

Reference

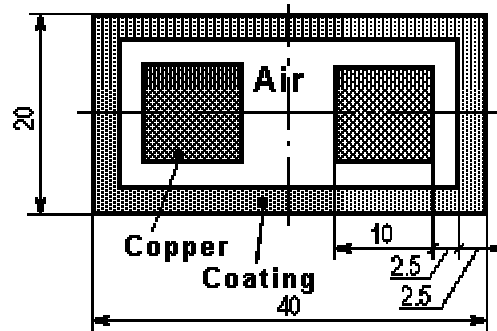
A. Konrad, "Integrodifferential Finite Element Formulation of Two-Dimensional Steady-State Skin Effect Problems", IEEE Trans. Magnetics, Vol MAG-18, No. 1, January 1982.

HMagn2: Symmetric double line of conductors

Problem Type:

A plane problem of time-harmonic magnetic field.

Geometry:



Two copper square cross-section conductors with equal but opposite currents are contained inside rectangular ferromagnetic coating. All dimensions are in millimeters.

Given:

Magnetic permeability of air $\mu = 1$;
 Magnetic permeability of copper $\mu = 1$;
 Conductivity of copper $\sigma = 56,000,000$ S/m;
 Magnetic permeability of coating $\mu = 100$;
 Conductivity of coating $\sigma = 1,000,000$ S/m;
 Current in the conductors $I = 1$ A;
 Frequency $f = 100$ Hz.

Problem:

Determine current distribution within the conductors and the coating, complex impedance of the line, and power losses in the coating.

Solution:

We assume that the flux is contained within the coating, so we can put a Dirichlet boundary condition on the outer surface of the coating. The complex impedance per unit length of the line can be obtained from the equation

$$Z = (V_1 - V_2) / I$$

where V_1 and V_2 are voltage drops per unit length in each conductor. These voltage drops are equal with opposite signs due to the symmetry of the model. To obtain a voltage drop, switch to Local Values mode in postprocessing window, and then pick an arbitrary point within a conductor.

The impedance of the line $Z = 0.000493 + i 0.000732$ Ohm/m.

To obtain power losses in the coating:

1. In the postprocessing mode, choose **Pick Elements** and pick the coating block to create the contour.
2. Choose **Integral Values** and select *Joule heat* from the list of integral quantities and choose **Calculate**.

The power losses in the coating $P = 0.0000437$ W/m.

Elec1: Microstrip transmission line

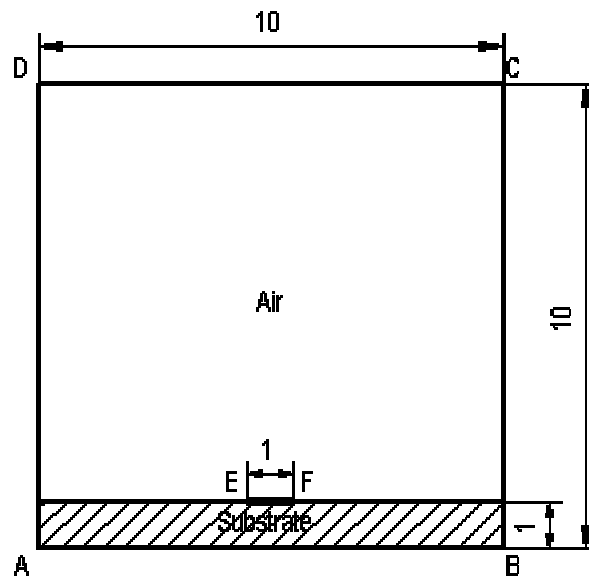
A shielded microstrip transmission line consists of a substrate, a microstrip, and a shield.

Problem Type:

Plane-parallel problem of electrostatics.

Geometry:

The transmission line is directed along z-axis, its cross section is shown on the sketch. The rectangle $ABCD$ is a section of the shield, the line EF represents a conductor strip.



Given:

Relative permittivity of air $\epsilon = 1$;
Relative permittivity of substrate $\epsilon = 10$.

Problem:

Determine the capacitance of a transmission line.

Solution:

There are several different approaches to calculate the capacitance of the line:

- To apply some distinct potentials to the shield and the strip and to calculate the charge that arises on the strip;
- To apply zero potential to the shield and to describe the strip as having constant but unknown potential and carrying the charge, and then to measure the potential that arises on the strip.

Both these approaches make use of the equation for capacitance:

$$C = q / U.$$

Other possible approaches are based on calculation of stored energy of electric field. When the voltage is known:

$$C = 2 \cdot W / U^2,$$

and when the charge is known:

$$C = q^2 / 2 \cdot W$$

Experiment with this example shows that energy-based approaches give little bit less accuracy than approaches based on charge and voltage only. The first approach needs to get the charge as a value of integral along some contour, and the second one uses only a local value of potential, this approach is the simplest and in many cases the most reliable.

See the Elec1_1.pbm and Elec1_2.pbm problems in [Elec1](#) for the corresponding the 1,3 approaches and the 2,4 approaches respectively.

Results:

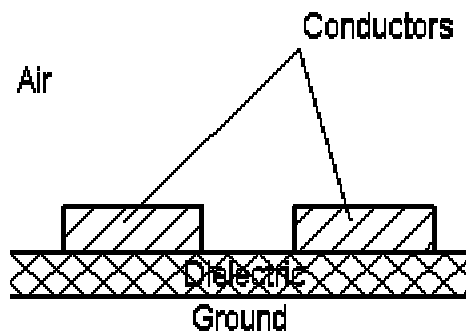
Theoretical result	$C = 178.1 \text{ pF/m.}$
Approach 1	$C = 177.83 \text{ pF/m (99.8\%)}$
Approach 2	$C = 178.47 \text{ pF/m (100.2\%)}$
Approach 3	$C = 177.33 \text{ pF/m (99.6\%)}$
Approach 4	$C = 179.61 \text{ pF/m (100.8\%)}$

Elec2: Two conductor transmission line

Problem Type:

A plane problem of electrostatics.

Geometry:



The problem's region is bounded by ground from the bottom side and extended to infinity on other three sides.

Given:

Relative permittivity of air $\epsilon = 1$;

Relative permittivity of dielectric $\epsilon = 2$.

Problem:

Determine self and mutual capacitance of conductors.

Solution:

To avoid the influence of outer boundaries, we'll define the region as a rectangle large enough to neglect side effects. To calculate the capacitance matrix we set the voltage $U = 1$ V on one conductor and $U = 0$ on the another one.

Self capacitance: $C_{11} = C_{22} = Q_1 / U_1$,

Mutual capacitance: $C_{12} = C_{21} = Q_2 / U_1$,

where charge Q_1 and Q_2 are evaluated on rectangular contours around conductor 1 and 2 away from their edges. We chose the contours for the C_{11} and C_{12} calculation to be rectangles $-6 \leq x \leq 0$, $0 \leq y \leq 4$ and $0 \leq x \leq 6$, $0 \leq y \leq 4$ respectively.

Comparison of Results

	C_{11} (F/m)	C_{12} (F/m)
Reference	$9.23 \cdot 10^{-11}$	$-8.50 \cdot 10^{-12}$
QuickField	$9.43 \cdot 10^{-11}$	$-8.57 \cdot 10^{-12}$

Reference

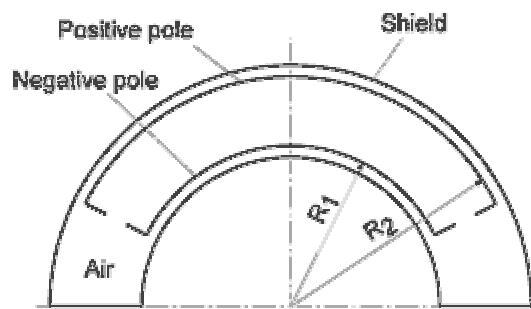
A. Khebir, A. B. Kouki, and R. Mittra, "An Absorbing Boundary Condition for Quasi-TEM Analysis of Microwave Transmission Lines via the Finite Element Method", Journal of Electromagnetic Waves and Applications, 1990.

Elec3: Cylindrical Deflector Analyzer**Problem Type:**

Plane-parallel electrostatic problem

Geometry:

Cylindrical deflector analyzer (CDA) is a part of a cylindrical capacitor with angular sector of $127^\circ 17'$. CDA has two slits made for the particles to enter and exit the CDA field.



In this example the beam of electrons enters the CDA perpendicular to the cylinder's radius with initial kinetic energy $E_0 = 1500$ eV and angle dispersion of 6°

Given:

Radius of external cylinder $R_2 = 0.1$ m
 Radius of internal cylinder $R_1 = 0.07$ m

CDA voltage $U = 1000$ V
Initial kinetic energy of electrons $E_0 = 1500$ eV
Relative permittivity of air $\varepsilon = 1$;

Problem:

Define the beam focus point.

Solution:

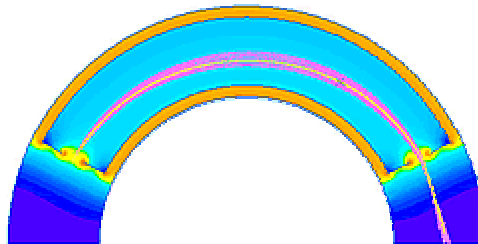
At the beginning we solve the electrostatic problem calculating the CDA field. After that we open the **Point Source Emitter** dialog using the **Particle Trajectory** command (**View** menu). Using the **Emitter** dialog page we position the point particle emitter at the center of the CDA's entrance slit ($x = -0.076$ m, $y = 0.037$ m) and specify the range for the starting angles between 62 and 68 degrees. Using the **Particle** dialog page we choose the desired particle type - electron - from the list, and define the value of initial kinetic energy $E_0 = 1500$ eV. To obtain the result, we click **Apply** and view the particle trajectories on screen.

Results

The beam focus point: (0.081, 0.027).
The focusing angle (approx.): $127^\circ + 8.5^\circ = 135.5^\circ$.

Theory says that with some value of CDA voltage depending on the energy of electrons, the beam will be focused at the exit slit. In ideal case the voltage for our example would be $U = 1070$ V. The focusing angle and the CDA voltage in our example are slightly different because of the CDA fringing effects.

G



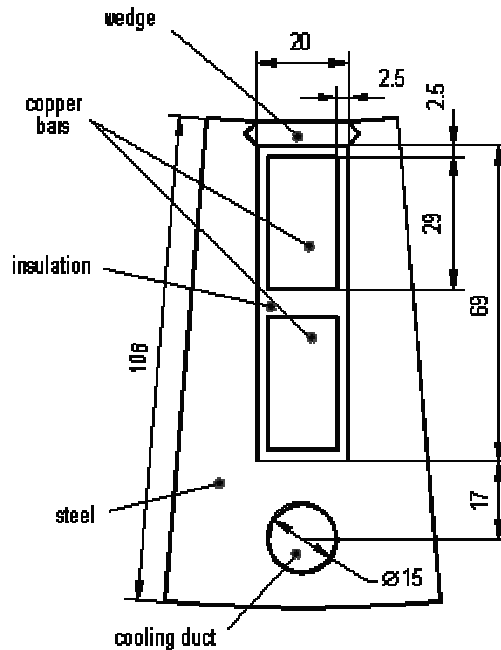
Heat1: Slot of an electric machine

Temperature field in the stator tooth zone of power synchronous electric machine.

Problem Type:

The plane-parallel problem of heat transfer with convection.

Geometry:



All dimensions are in millimeters. Stator outer diameter is 690 mm. Domain is a 10-degree segment of stator transverse section. Two armature bars laying in the slot release ohmic loss. Cooling is provided by convection to the axial cooling duct and both surfaces of the core.

Given:

Specific copper loss: 360000 W/m^3 ;
 Heat conductivity of steel: $25 \text{ J/K}\cdot\text{m}$;
 Heat conductivity of copper: $380 \text{ J/K}\cdot\text{m}$;
 Heat conductivity of insulation: $0.15 \text{ J/K}\cdot\text{m}$;
 Heat conductivity of wedge: $0.25 \text{ J/K}\cdot\text{m}$;

Inner stator surface:

Convection coefficient: $250 \text{ W/K}\cdot\text{m}^2$;
 Temperature of contacting air: 40°C .

Outer stator surface:

Convection coefficient: $70 \text{ W/K}\cdot\text{m}^2$;
 Temperature of contacting air: 20°C .

Cooling duct:

Convection coefficient: $150 \text{ W/K}\cdot\text{m}^2$;
 Temperature of contacting air: 40°C .

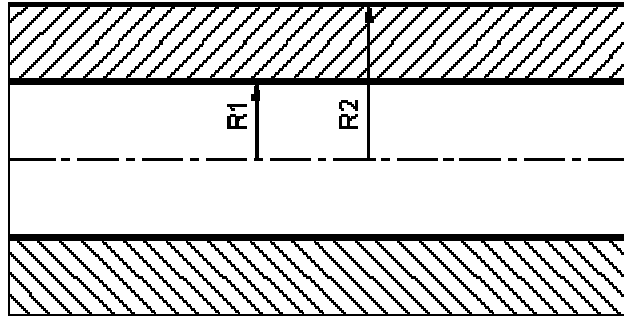
Heat2: Cylinder with temperature dependent conductivity

A very long cylinder (infinite length) is maintained at temperature T_i along its internal surface and T_o along its external surface. The thermal conductivity of the cylinder is known to vary with temperature according to the linear function $\lambda(T) = C_0 + C_1 \cdot T$.

Problem Type:

An axisymmetric problem of nonlinear heat transfer.

Geometry:



Given:

$R1 = 5 \text{ mm}$, $R2 = 10 \text{ mm}$;
 $T_i = 100 \text{ }^\circ\text{C}$, $T_o = 0 \text{ }^\circ\text{C}$;
 $C_0 = 50 \text{ W/K}\cdot\text{m}$, $C_1 = 0.5 \text{ W/K}\cdot\text{m}$.

Problem:

Determine the temperature distribution in the cylinder.

Solution:

The axial length of the model is arbitrarily chosen to be 5 mm.

Comparison of Results

Radius (cm)	Temperature (°C)	
	QuickField	Theory
0.6	79.2	79.2
0.7	59.5	59.6
0.8	40.2	40.2
0.9	20.7	20.8

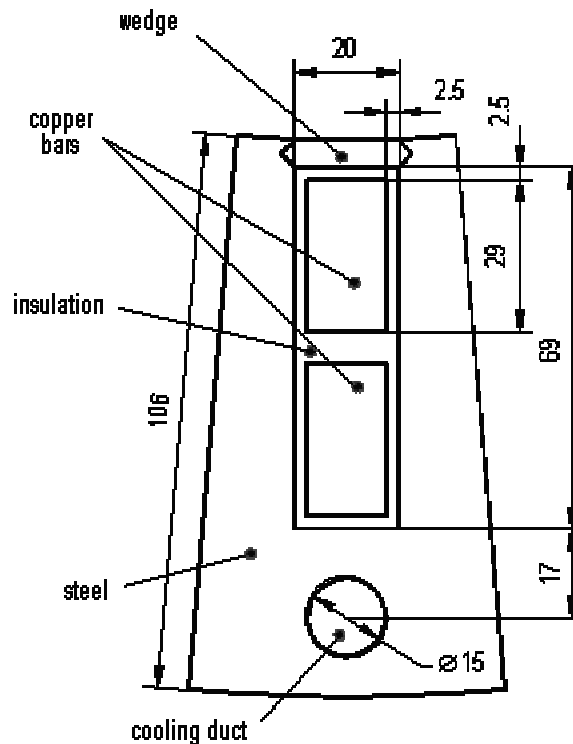
Heat1: Heating and Cooling of a Slot of an Electric Machine

Changing temperature field in the stator tooth zone of power synchronous electric motor during a loading-unloading cycle.

Problem Type:

The plane-parallel problem of heat transfer with convection.

Geometry:



All dimensions are in millimeters. Stator outer diameter is 690 mm. Domain is a 10-degree segment of stator transverse section. Two armature bars laying in the slot release ohmic loss. Cooling is provided by convection to the axial cooling duct and both surfaces of the core.

Given:

1. Working cycle

We assume the uniformly distributed temperature before the motor was suddenly loaded. The cooling conditions supposed to be constant during the heating process. We keep track of the temperature distribution until it gets almost steady state. Then we start to solve the second problem - getting cold of the suddenly stopped motor. The initial temperature field is imported from the previous solution. The cooling condition supposed constant, but different from those while the motor was being loaded.

2. Material Properties

The thermal conductivity values are the same as in the Heat1 example. For transient analysis the values of specific heat C and volume density are also required:

	Heat Conductivity (J/K·m)	Specific Heat (J/K·m)	Mass Density (kg/m ³)
Steel Core	25	465	7833
Copper Bar	380	380	8950
Bar Insulation	0.15	1800	1300
Wedge	0.25	1500	1400

3. Heat sources and cooling conditions

During the loading phase the slot is heated by the power losses in copper bars. The specific power loss is 360000 W/m^3 . When unloaded, the power loss are zero. We suppose the temperature of contacting air to be the same for both phases of working cycle. In turn, the convection coefficients are different, because the cooling fan is supposed to be stopped when the motor is unloaded.

	Loading		Stopped	
	Convection coefficient ($\text{W/K}\cdot\text{m}^2$)	Temperature of contacting air ($^{\circ}\text{C}$)	Convection coefficient ($\text{W/K}\cdot\text{m}^2$)	Temperature of contacting air ($^{\circ}\text{C}$)
Inner stator surface	250	40	20	40
Outer stator surface	70	20	70	20
Cooling duct	150	40	20	40

Solution

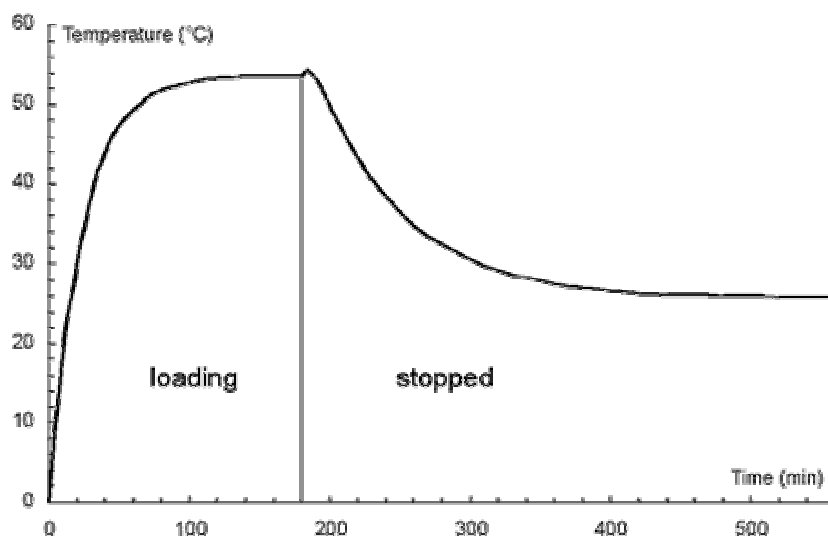
Each phase of the loading cycle is modeled by a separate QuickField problem. For the loading phase the initial temperature is set to zero, and for the cooling phase the initial thermal distribution is imported from the final time moment of the previous solution.

Moreover, we decide to break the cooling phase into two separate phases. For the first phase we choose time step as small as 100 s, because the rate of temperature change is relatively high. This allows us to see that the temperature at the slot bottom first increases by approximately 1 grad for 300 seconds, and then begins decreasing. The second stage of cooling, after 1200 s, is characterized by relatively low rate of temperature changing. So, we choose for this phase the time step to be 600 s.

For heating process the time step of 300 s is chosen. Please see following problems in the *Examples* folder:

- THeat1Ld.pbm for loading phase, and
- THeat1S1.pbm for the beginning of stopped phase, and
- THeat1S2.pbm for the end of stopped phase

Results



Temperature vs. time dependence at the bottom of the slot (where a temperature sensor usually is placed).

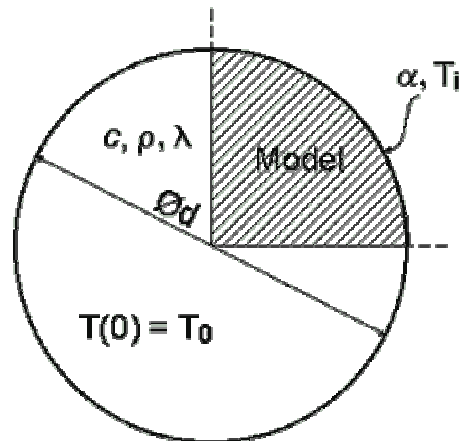
THeat2: Temperature Response of a Suddenly Cooled Wire

Determine the temperature response of a copper wire of diameter d , originally at temperature T_0 , when suddenly immersed in air at temperature T_i . The convection coefficient between the wire and the air is α .

Problem Type:

An axisymmetric problem of nonlinear heat transfer.

Geometry:



Given:

$d = 0.015625$ in;
 $T_i = 37.77^\circ\text{C}$, $T_0 = 148.88^\circ\text{C}$;
 $C = 380.16$ J/kg·K, $\rho = 8966.04$ kg/m³;
 $\alpha = 11.37$ W/K·m².

Problem:

Determine the temperature in the wire.

Solution:

The final time of 180 s is sufficient for the theoretical response comparison. A time step of 4.5 s is used.

Comparison of Results

	Temperature, °C		
Time	QuickField	ANSYS	Reference
45 s	91.37	91.38	89.6
117 s	54.46	54.47	53.33
180 s	43.79	43.79	43.17

See the THeat2.pbm (main) and THeat2_i.pbm (auxiliary) problems in the *Examples* folder.

Reference

Kreif F., "Principles of Heat Transfer", International Textbook Co., Scranton, Pennsylvania, 2nd Printing, 1959, Page 120, Example 4-1.

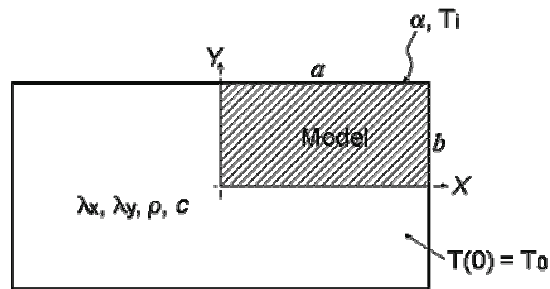
THeat3: Transient Temperature Distribution in an Orthotropic Metal Bar

A long metal bar of rectangular cross-section is initially at a temperature T_0 and is then suddenly quenched in a large volume of fluid at temperature T_i . The material conductivity is orthotropic, having different X and Y directional properties. The surface convection coefficient between the wire and the air is α .

Problem Type:

An axisymmetric problem of nonlinear heat transfer.

Geometry:



Given:

$a = 2$ in, $b = 1$ in
 $\lambda_x = 34.6147$ W/K·m, $\lambda_y = 6.2369$ W/K·m;
 $T_i = 37.78^\circ\text{C}$, $T_0 = 260^\circ\text{C}$;
 $\alpha = 1361.7$ W/K·m²;
 $C = 37.688$ J/kg·K, $\rho = 6407.04$ kg/m³.

Problem:

Determine the temperature distribution in the slab after 3 seconds at the center, corner edge and face centers of the bar.

Solution:

To set the non-zero initial temperature we have to solve an auxiliary steady state problem, whose solution is uniform distribution of the temperature T_0 . A time step of 0.1 sec is used.

Comparison of Results

	Temperature, °C		
Point	QuickField	ANSYS	Reference
(0,0) in	238.7	239.4	237.2
(2,1) in	66.43	67.78	66.1
(2,0) in	141.2	140.6	137.2
(0,1) in	93.8	93.3	94.4

See the THeat3.pbm (main) and THeat3_i.pbm (auxiliary) problems in the *Examples* folder.

Reference

Schneider P.J., "Conduction Heat Transfer", Addison-Wesley Publishing Co., Inc, Reading, Mass., 2nd Printing, 1957, Page 261, Example 10-7.

Stres1: Perforated plate

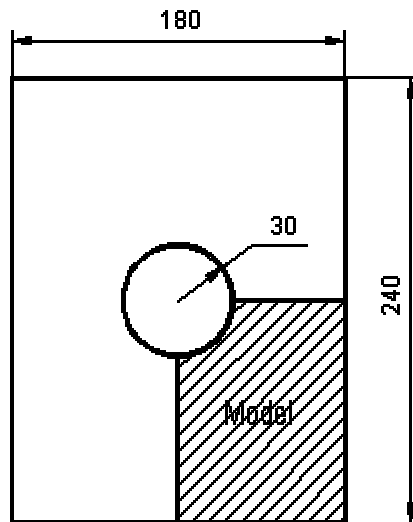
A thin rectangular sheet with a central hole subject to tensile loading.

Problem Type:

Plane problem of stress analysis (plane stress formulation).

Geometry of the plate:

Length: 240 mm;
Width: 180 mm;
Radius of central opening: 30 mm;
Thickness: 5 mm.

**Given:**

Young's modulus $E = 207000 \text{ N/mm}^2$

Poisson's ratio $\nu = 0.3$.

The uniform tensile loading (40 N/mm^2) is applied to the bottom edge of the structure.

Problem:

Determine the concentration factor due to presence of the central opening.

Solution:

Due to mirror symmetry one quarter of the structure is presented, and internal boundaries are restrained in X and Y directions respectively.

The concentration factor may be obtained from the loading stress (40 N/mm^2) and the maximum computed stress (146 N/mm^2) as

$$k = 146 / 40 = 3.65.$$

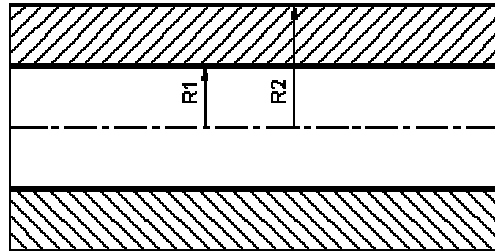
Coupl1: Stress distribution in a long solenoid

A very long, thick solenoid has a uniform distribution of circumferential current. The magnetic flux density and stress distribution in the solenoid has to be calculated.

Problem Type:

An axisymmetric problem of magneto-structural coupling.

Geometry:



Given:

Dimensions $R1 = 1$ cm, $R2 = 2$ cm;
 Relative permeability of air and coil $\mu = 1$;
 Current density $j = 10^5$ A/m²;
 Young's modulus $E = 1.075 \cdot 10^{11}$ N/m²;
 Poisson's ratio $\nu = 0.33$.

Problem:

Calculate the magnetic flux density and stress distribution.

Solution:

Since none of physical quantities varies along z-axis, a thin slice of the solenoid could be modeled. The axial length of the model is arbitrarily chosen to be 0.2 cm. Radial component of the flux density is set equal to zero at the outward surface of the solenoid. Axial displacement is set equal to zero at the side edges of the model to reflect the infinite length of the solenoid.

Comparison of Results

Magnetic flux density and circumferential stress at $r = 1.3$ cm:

	B_z (T)	σ_θ (N/m)
Reference	$8.796 \cdot 10^{-3}$	97.407
QuickField	$8.798 \cdot 10^{-3}$	96.71

Reference

F.A. Moon, "Magneto-Solid Mechanics", John Wiley & Sons, N.Y., 1984, Chapter 4.

See the Coupl1MS.pbm and Coupl1SA.pbm problems in the [Coupl1.zip](#) for magnetic and structural parts of this problem respectively.

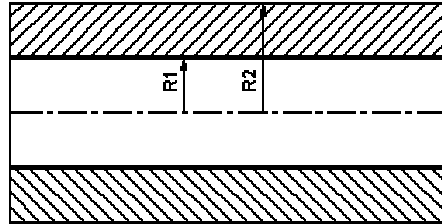
Coupl2: Cylinder subject to temperature and pressure

A very long, thick-walled cylinder is subjected to an internal pressure and a steady state temperature distribution with T_i and T_o temperatures at inner and outer surfaces respectively. Calculate the stress distribution in the cylinder.

Problem Type:

An axisymmetric problem of thermal-structural coupling.

Geometry:



Given:

Dimensions $R1 = 1$ cm, $R2 = 2$ cm;
 Inner surface temperature $T_i = 100$ °C;
 Outer surface temperature $T_o = 0$ °C;
 Coefficient of thermal expansion $\alpha = 10^{-6}$ 1/K;
 Internal pressure $P = 10^6$ N/m²;
 Young's modulus $E = 3 \cdot 10^{11}$ N/m²;
 Poisson's ratio $\nu = 0.3$.

Problem:

Calculate the stress distribution.

Solution:

Since none of physical quantities varies along z-axis, a thin slice of the cylinder can be modeled. The axial length of the model is arbitrarily chosen to be 0.2 cm. Axial displacement is set equal to zero at the side edges of the model to reflect the infinite length of the cylinder.

Comparison of Results

Radial and circumferential stress at $r = 1.2875$ cm:

	σ_r (N/m ²)	σ_θ (N/m ²)
Theory	$-3.9834 \cdot 10^6$	$-5.9247 \cdot 10^6$
QuickField	$-3.959 \cdot 10^6$	$-5.924 \cdot 10^6$

Reference

S. P. Timoshenko and Goodier, "Theory of Elasticity", McGraw-Hill Book Co., N.Y., 1961, pp. 448-449.

See the Coupl2HT.pbm and Coupl2SA.pbm problems in [Coupl2.zip](#) for the corresponding heat transfer and structural parts of this problem

Coupl3: Temperature distribution in an electric wire

Calculate the temperature distribution in a long current carrying wire.

Problem Type:

An axisymmetric problem of electro-thermal coupling.

Geometry:



Given:

Wire diameter $d = 10$ mm;
Resistance $R = 3 \cdot 10^{-4} \Omega/\text{m}$;
Electric current $I = 1000$ A;
Thermal conductivity $\lambda = 20$ W/K·m;
Convection coefficient $\alpha = 800$ W/K·m²;
Ambient temperature $T_o = 20$ °C.

Problem:

Calculate the temperature distribution in the wire.

Solution:

We arbitrary chose a 10 mm piece of wire to be represented by the model. For data input we need the wire radius $r = 5$ mm, and the resistivity of material:

$$\rho = R \cdot (\pi d^2 / 4) \Omega \cdot \text{m}, \text{ and voltage drop for our 10 mm piece of the wire: } \Delta U = I \cdot R \cdot l = 3 \cdot 10^{-3} \text{ (V)}.$$

For the current flow problem we specify two different voltages at two sections of the wire, and a zero current condition at its surface. For heat transfer problem we specify zero flux conditions at the sections of the wire and a convection boundary condition at its surface.

Comparison of Results

Center line temperature:

	T (°C)
Theory	33.13
QuickField	33.14

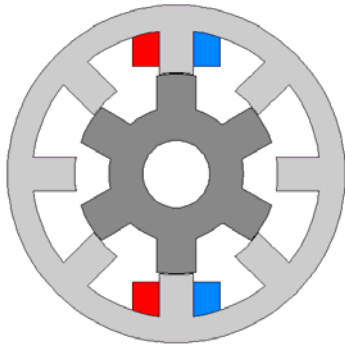
Reference

W. Rohsenow and H. Y. Choi, "*Heat, Mass, and Momentum Transfer*", Prentice-Hall, N.J., 1963.

See the Coupl3CF.pbm and Coupl3HT.pbm problems in [Coupl3.zip](#) for the corresponding current flow and heat transfer parts of this problem.

SRM Electric Motor

Last years switched reluctance motors (SRM) become a common solution in the application where deep regulation is required. Some people even says that SRM opens a new era in electrical drives. Switched reluctance motor is a combination of a simple brushless motor and a controlling electronic unit. The motor itself consists of salient pole steel rotor with no winding, and salient pole stator with a coil on each pole. Depends upon a algorithm of control system, the motor can behave in a different way according to customer needs.



Design of an SRM motor and control system rely on knowing of the torque and flux linkage as a function of the current and rotor position. The only way to obtain such dependency is numerical modeling of non-linear magnetic field with various rotor position and current in the stator coil. That work can be easily done by QuickField Workbench. The SRM sample allows to get $T = f(I, \phi)$ and $F = f(I, \phi)$ dependencies for any SRM motor, no regards the number of slots and poles and geometrical shape.

To find a torque and flux for a given rotor position and coil current we should solve a problem of magnetostatic to find magnetic field distribution. The only boundary condition needed is the zero Dirichlet condition on the outer surface of the stator. The filed sources are given current in the forward and back coil halves, marked with blue and red on the sketch above. We take into account steel saturation by defining B-H curves for stator and rotor core.

To achieve high degree of generality, we build the SRM.dll rely upon the geometric model prepared in advance by interactive QuickField model editor and stored to the `..\SRM_Files\SRM_Basic.mod` file. Also the physical data (boundary conditions, B-H curves for rotor and stator core, magnetic permeability of air and copper) are also prepared in advance and stored to the `..\SRM_Files\SRM_Basic.dms` file. Therefore, writing the SRM.dll code we can concentrate on getting output parameters.

The only geometrical manipulation we have to do programmatically is rotation of the rotor to the desired position. When needing to model another motor, say with different pole number, we only have to replace the geometrical model `..\SRM_Files\SRM4_Basic.mod` to another one with the same name.

Below we first discuss how to use the SRM model supplied with QuickField in the Workbench environment, and then briefly describe creating of such a model by Workbench application wizard and its programming.

Using the SRM model

To try the SRM model supplied with QuickField, do the following steps:

1. Run Workbench (Start->Programs->Tera Analysis->Tools->Workbench)
2. Only once: register the SRM as an exploring object if you do not do that before.
To register the new object, press the **Register New ExploringObject** button and find the name and location of the SRM.dll. QuickField installation program puts it to the `..\ActiveField\Examples\SRM` folder.

- Open new modeling session by pressing the **New Session** button. If the SRM.dll was properly registered, its icon appears in the list of registered exploring objects. When you click it, the **All Parameters** pages appears with SRM sketch and list of parameters.

Description	Notation	Value	Unit	Variable
Rotor Position	Phi	0	deg	Yes
Stator Coil Current	Ia	200	A	Yes
Air Gap Diameter	Da	177.775	mm	No

According to the SRM design the list contains 3 parameters:

- Rotor Position (Phi);
- Stator Coil Current (Ia)
- Air Gap Diameter (Da)

The first two parameters intended to be variable, and the last one is used by postprocessor when building a contour for calculation torque.

Click on the desired item in the **Variable** column to declare the parameter to be variable or not.

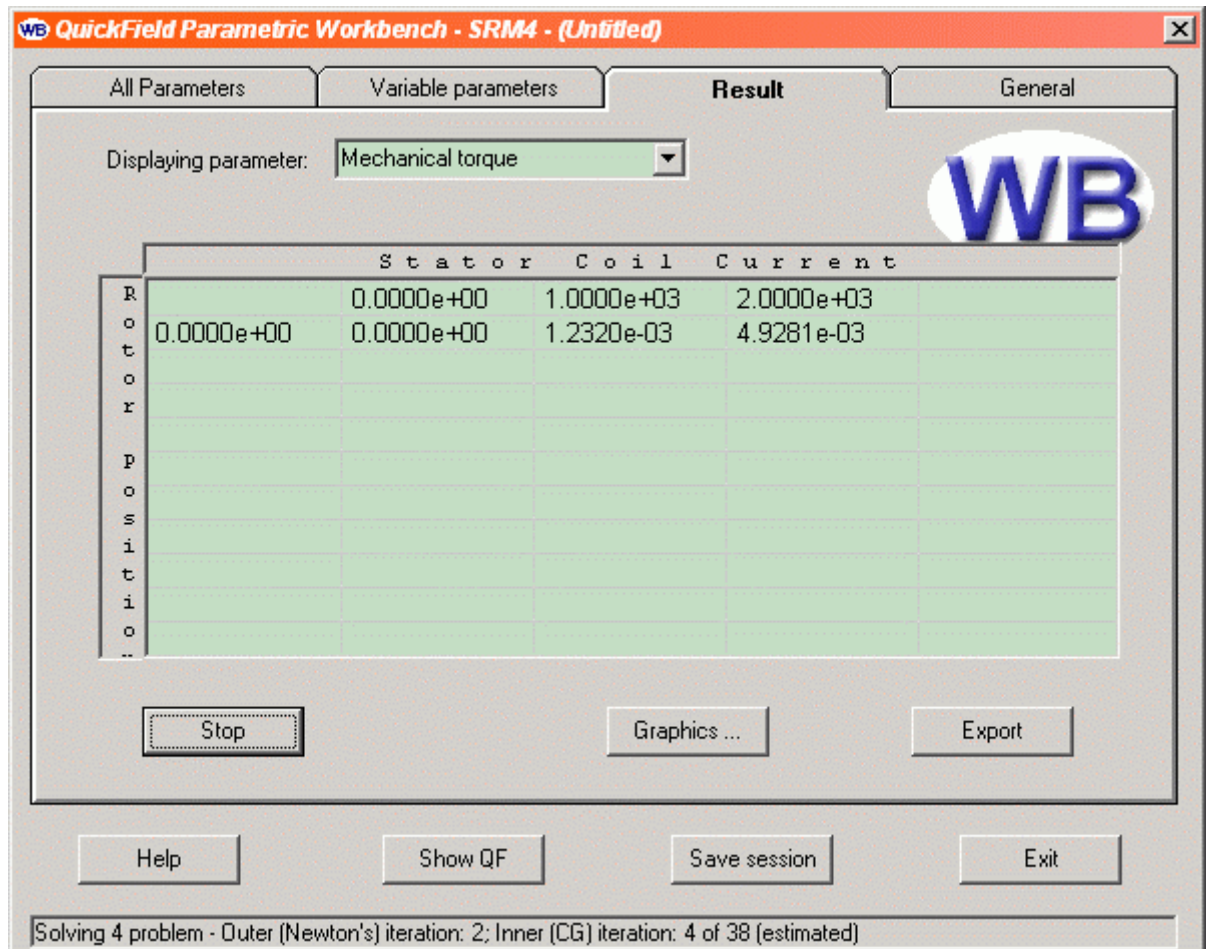
- Switch to the Variable Parameters page. If you have chosen both rotor position and stator coil current to be variable on previous step, you see the following:

The screenshot shows a software interface for defining parameter ranges and iteration types. It contains two main sections:

- Rotor Position:**
 - From: 0 deg, To: 360 deg, Min: 0, Max: 360
 - Iteration type: Linear (selected from a dropdown)
 - Step: 36 deg
- Stator Coil Current:**
 - From: 0 A, To: 10000 A, Min: 0, Max: 10000
 - Iteration type: Linear (selected from a dropdown)
 - Step: 1000 A

For each parameter you can choose the **Iteration type** from the list. Now two iterators are available: the linear iterator divides given range into equal parts whereas the random one allows to distribute each point individually.

- When you are ready with input parameter and iteration data, switch to the **Result** tab and press the **Solve** button. The results will appear in the table when calculated.



During calculation you can show and hide QuickField by **Show QF** button, select the output quantity to display in the table, display xy-plot in a separate window. Also, the calculation could be aborted at any time by the **Stop** button.

- When calculation finishes it is good time to save current modeling session to be able review input and calculated data next time. If you have Microsoft Excel installed, you can export the result table into an Excel spreadsheet.
- When you need to model another SRM machine, prepare its geometry model with QuickField model editor interactively, and put its copy into the SRM_Files directory under your folder where the SRM.dll lives. Every SRM model should have a block labeled as "**Rotor**" that will be rotated on each iteration and a pair of block labeled as "**Winding+**" and "**Winding-**". The last represent forth and back sides of a stator coil on each pole. All these coils are considered as connected in parallel.

How the SRM model was created

In the rest of this topic we discuss how to create an exploring object for Workbench such as SRM.dll. To do that you should be familiar with programming in Visual Basic and with QuickField object model principles. You also have Microsoft Visual Basic 6.0 installed on your computer before installing QuickField.

Creating of a new exploring object consists of two main steps: creating the skeleton of code with the QuickField Exploring Object Wizard and customization the automatically generated code.

Creating a skeleton of code using QuickField Exploring Object Wizard.

That process is described in full details in the [Lesson 3](#) of the ActiveField tutorial. Below we describe only the things, that are specific for the SRM model.

The input parameters are:

Description	Notation	Unit	Value		
			Min	Max	Default
Rotor Position	Phi	deg	0	360	0
Stator Coil Current	Ia	A	0	10000	5000
Air Gap Middle Diameter	Da	mm	0	1000	177.75

The first parameter - rotor position - is of geometrical type. That means that the geometry model should be rebuild and remeshed each time the parameter value changes. The second parameter is of physical type. When its value changes, the problem is solved again using the same geometry. The last parameter - air gap middle diameter - is of the postprocessor type. When it changes by Workbench (if we want that), the QuickField will neither generate new model nor solve another problem. Such parameter is using only for analyzing results.

We also declare two output parameters:

Name	Notation	Unit	Value
Mechanical Torque	M	N*m	Torque of the motor
Pole Flux	F	Wb	The magnetic flux trough one pole

Customization the code written by the wizard.

In the code modules created by wizard the subroutines that are most likely candidates to modification are separated in a special module named Custom. In our case it is stored in the SRM.bas file. There are four procedures defined:

- **ModifyModel** - the place for code modifying the geometry model according to current values of input parameters;
- **SetLabel** - called by framework each time one of the physical parameter changes its value. Its primary goal is setting values for labels of blocks, edges, and vertices.
- **Calculations** - good place for writing code calculating output parameters.
- **BuildContour** - an auxiliary subroutine that can be used for creating a contour, if the integral values used for calculation of output parameters.

The main task of our **ModifyModel** subroutine is selecting the rotor and rotation it on the desired position. The following code does that:

```
''' Local variables for all input parameters
Dim Phi As Double
Phi = theParameters("Rotor Position").Value

''' -----
''' TODO: Modify QuickField model (Mdl) here
Const PI As Double = 3.1415926
Dim rotor As ShapeRange
Set rotor = Mdl.Shapes.LabeledAs(Block:="Rotor")
If Not rotor Is Nothing Then
```



```

    rotor.Move qfRotation, PointXY(0, 0), Phi / 180 * PI
End If

```

Please note that we do not need rebuild the mesh and save modified model - the framework does it for us automatically.

The **SetLabel** function is called each time when one of the "physical" parameter changes. This subroutine have not to set all properties to all labels. Instead, it changes only the value of total current for block labels "**Winding+**" and "**Winding-**"

```

Case "Stator Coil Current"
''' -----
    Dim      Ia As Double
    Ia = theParameters("Stator Coil Current").Value

    ''' TODO: Edit QuickField label corresponding
        'Stator Coil Current' parameter
    ''' Probable code for Block label:
    ''' - uncomment code below
    ''' - for Vertex and Edges use 'qfVertex' or 'qfEdge'
constants
    ''' - replace 'Air' with your QuickField label name
    '''

    Set Lbs = Prb.DataDoc.Labels(qfBlock) 'Select block labels
collection
    Set Lab = Lbs("Winding+") 'Get label
    Set LabCnt = Lab.Content 'Get label content
    LabCnt.Loading = Ia
    LabCnt.TotalCurrent = True
    Lab.Content = LabCnt 'Update label content

    Set Lab = Lbs("Winding-") 'Get label
    Set LabCnt = Lab.Content 'Get label content
    LabCnt.Loading = -Ia
    LabCnt.TotalCurrent = True
    Lab.Content = LabCnt 'Update label content
    ''' -----

```

The two subroutines above organize model creation, modification and solving. Now we modify the routines extracting output parameters. The key subroutine doing that is **Calculations**. As distinction from the code generated by wizard, we need three different contours for calculating three integral values: the torque and the flux linkages with left and right halves of stator coil. Let us put the code for creating each contour in a separate subroutine: **BuildContourTorque**, **BuildContourWplus**, **BuildContourWminus**.

The **Calculation** routine

```

''' -----
''' TODO:
''' - if you have point output parameters:
''' Replace 'PointXY(0, 0)' by a Point you need accordingly input
parameters
''' - if you have no point output parameters:
''' Remove these code linesDim Cnt As QuickField.Contour

' Mechanical torque
Set Cnt = BuildContourTorque(Res)
Pt.Value(1) = Res.GetIntegral(qfInt_MaxwellTorque, Cnt).Abs
' Pole Flux
Set Cnt = BuildContourWplus(Res)
Pt.Value(2) = Res.GetIntegral(qfInt_FluxLinkage, Cnt).Abs

```

```

Set Cnt = BuildContourWminus(Res)
Pt.Value(2) = Abs(Pt.Value(2) - Res.GetIntegral(qfInt_FluxLinkage,
Cnt).Abs)
''' -----

```

Each subroutine that builds a contour is very simple:

1. The contour surrounding the rotor for calculation of the torque:

```

Private Function BuildContourTorque(Res As QuickField.Result)
    Dim Wnd As QuickField.FieldWindow 'Result field window object
    ' Get FieldWindow object
    Set Wnd = Res.Windows(1)
    ' Get new Contour object
    Dim Cnt As QuickField.Contour
    Set Cnt = Wnd.Contour

    ''' -----
    ''' TODO: Build Contour here
    Dim Ra As Double
    Ra = theParameters("Air Gap Diameter").Value / 2#
    Cnt.AddLineTo PointXY(Ra, 0), 0
    Cnt.AddLineTo PointXY(-Ra, 0), 3.1415926
    Cnt.AddLineTo PointXY(Ra, 0), 3.1415926
    ''' -----
    Set BuildContourTorque = Cnt
End Function

```

2. The next two functions builds contours for flux calculation:

```

Private Function BuildContourWplus(Res As QuickField.Result) As
QuickField.Contour
    Dim Wnd As QuickField.FieldWindow 'Result field window object
    ' Get FieldWindow object
    Set Wnd = Res.Windows(1)
    ' Get new Contour object
    Dim Cnt As QuickField.Contour
    Set Cnt = Wnd.Contour
    Cnt.Delete True
    Cnt.AddBlock "Winding+"
    Set BuildContourWplus = Cnt
End Function

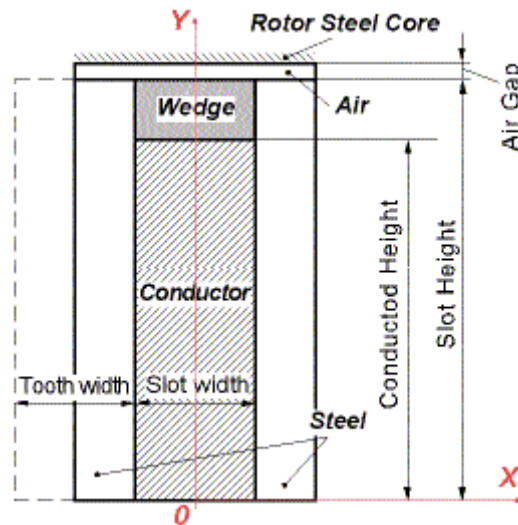
Private Function BuildContourWminus(Res As QuickField.Result)
    Dim Wnd As QuickField.FieldWindow 'Result field window object
    ' Get FieldWindow object
    Set Wnd = Res.Windows(1)
    ' Get new Contour object
    Dim Cnt As QuickField.Contour
    Set Cnt = Wnd.Contour
    Cnt.Delete True
    Cnt.AddBlock "Winding-"
    Set BuildContourWminus = Cnt
End Function

```

Now we can compile our SRM project as SRM.dll file (**File->Make SRM.dll..** command) and use it for calculation.

Tooth-Slot and Air Gap Model

In this sample we investigate magnetic field and current distribution in the simplified model of a slot of electric machine.



The solid rectangular conductor made from copper lies in the open rectangular slot. The opposite armature core is considered to be toothless.

On the main screen you can enter the geometric dimensions of the tooth, slot, air gap and conductor, as well as a few physical parameters. You can change values or accept default ones. Once you are ready with data editing, press the **Calculate** button. The QuickField window appears or not depending on the **Show QuickField** flag.

The calculation consists of following stages:

1. First the geometry model Slot.mod and the data for DC magnetic problem are created.
2. Then the main module starts solving of DC magnetic problem and analyze it result. It calculate the entire flux linked with the conductor, the magnetic flux crossing the air gap (a "payload" flux) and the flux leakage. It also calculate the Ohmic resistance and inductance of the conductor per 1 meter of axial length.
3. Then the geometric model for an AC magnetic problem is created. To take the tooth saturation into account, we divide the tooth into 7 sub-regions. The permeability value achieved in the center of each sub region in the DC problem is set to the AC magnetic problem.
4. Than the sample program solves the AC magnetic problem and determinates resistance and inductance of the conductor by AC current of specified frequency.

All the calculation results are displayed in the report window. You can save the report to a text file using the **Save** button.

The Tooth example program employs the COMDLG32 component of MS Visual Basic that can be or can be not installed on your computer. To be sure that all modules needed are installed, use the Setup.exe program for installing the Tooth sample on your computer.

Source codes of the Tooth samples are written in Visual Basic. The program is designed as a set of objects and classes to isolate the calculation and presentation layers. The code that communicates with QuickField is located in the Solver class (Solver.cls file).

Cable: ActiveField Example

QuickField, enforced by ActiveField technology may be effectively used for multi-physics analysis of various engineering tasks. This analysis could be highly automated. It even can be implemented as a Microsoft Word document equipped by the set of VBA macros for automatic creation of QuickField problem, solving, postprocessing and report generation. Rather complicated example - analysis of tetra-core cable - is available as [ActiveField Cable Example](#). If you have working knowledge of Visual Basic, and understanding of QuickField Object model - you are welcome to analyze source code of these macros.

This document displays the results of cable analysis based on specific modeling parameters. Pictures, tables and graphs below have been automatically calculated by Professional version of QuickField, controlled by VBA code implemented as MS Word macros. [Corresponding QuickField problems](#) can be analyzed by the Students version.

1. [Model description](#)
2. [Input parameters](#)
3. [Calculated cable parameters](#)
4. [Field pictures](#)

1. Model description.

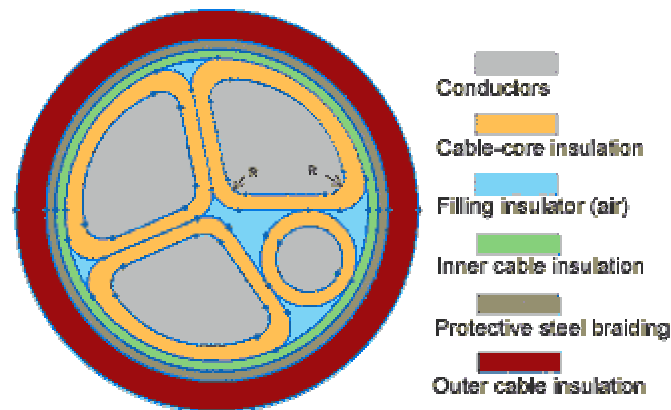


Figure1. Cable sketch.

This high-voltage tetra-core cable has three triangle sectors with phase conductors and round neutral conductor in the lesser area of the cross-section above. All the conductors are made of aluminum. Each conductor is insulated and the cable as a whole has a three-layered insulation. The cable insulation consists of inner and outer insulators and a protective braiding (steel tape). The sharp corners of the phase conductors are chamfered to reduce the field crown. The corners of the conductors are rounded. Empty space between conductors is filled with some insulator, possibly with an air.

It is often required to design a cable according to parameters of the conductor section areas. Conductor section areas are defined in the Table 1. The tables 2 to 7 describe other input parameters.

2. Input parameters.

Table 1. Conductors' geometric parameters.

Phase conductor area	120	Mm ²
Neutral conductor area	35	Mm ²
Thread rounding radius (R)	2	Mm

Table 2. Insulator geometric parameters.

Cable-core insulation thickness	2	Mm
Inner cable insulation thickness	1	Mm
Protective steel braiding thickness	1	Mm
Outer cable isolation thickness	3	Mm

Table 3. The precision.

Areas calculation reasonable error	0.001	Mm ² .
------------------------------------	-------	-------------------

Table 4. Conductors' loading.

Current amplitude	200	A.
Voltage amplitude (electrostatics)	6500	V.
Frequency	50	Hz.
Current phase (for static problems)	0	Deg.

Table 5. Conductors' physical properties.

Relative permeability	1	
Conductivity	36000000	S/m
Thermal conductivity	140	W/K·m
Young's modulo	6.9e+10	N/m ²
Poisson's ratio	0.33	
Coefficient of thermal expansion	2.33e-5	1/K
Specific density	2700	Kg/m ³

Table 6. Steel braiding physical properties.

Relative permeability	1000	
Conductivity	6000000	S/m.
Thermal conductivity	85	W/K·m
Young's modulo	2e+11	N/m ²
Poisson's ratio	0.3	
Coefficient of thermal expansion	0.000012	1/K
Specific density	7870	Kg/m ³

Table 7. Insulator physical properties.

	Core	Inner	Outer	
Relative permeability	1	1	1	
Conductivity	0	0	0	S/m
Relative electric permittivity	2.5	2.5	2.5	
Thermal conductivity	0.04	0.04	0.04	W/K·m
Young's modulo	10000000	10000000	10000000	N/m ²
Poisson's ratio	0.3	0.3	0.3	
Coefficient of thermal expansion	0.0001	0.0001	0.0001	1/K
Specific density	900	900	1050	Kg/m ³

3. Calculated cable parameters.

Cable physical parameters are presented in the next table.

Cable outer diameter is calculated using conductor and insulator geometrical parameters put into Table 1 and Table 2. Cable linear weight per meter is calculated from geometrical parameters and specific densities of the cable components. The whole cable specific density is a total density calculated by taking into account all cable components.

Table 8. Cable physical parameters

Cable outer diameter	4.28e+01	Mm
Weight (per meter)	2.74e+00	Kg
Cable specific density	1.90e+03	Kg/m ²

"Conductors' capacitance" table holds self- and mutual-capacitances of the cable conductors. These values are calculated in the QuickField electrostatics problem using the charge approach. For each table row the separate QuickField problem is solved. One of two conductors' surfaces carries a unit charge and the other conductor's potential is evaluated. The mutual capacitance is equal to: $C_{ij} = U_j / Q_i$. Self-capacitance is calculated by the measurement of the potential at the same charged conductor.

Table 9. Conductors' capacitance, F

	Conductor1	Conductor2	Conductor3	Null-cord
Conductor1	2.53e-10	1.02e-09	1.95e-09	8.43e-10
Conductor2	1.02e-09	2.67e-10	1.02e-09	1.88e-09
Conductor3	1.95e-09	1.02e-09	2.53e-10	8.42e-10
Neutral cord	8.43e-10	1.88e-09	8.42e-10	1.28e-10

Conductors' inductances are represented in the Table 10. Values in the columns 2–5 are calculated in the magnetostatic problem at the phase defined in the Table 4. Values in the columns 6–9 are calculated in AC magnetic problem. All values are got using the flux linkage approach by the formula: $L_{ij} = \Phi_j / I_i$. The table diagonal elements represent the self-inductance values.

Table 10. Conductors' inductance

	In magnetostatic problem				In AC magnetic problem			
	C-1	C-2	C-3	0-cord	C-1	C-2	C-3	0-cord
Conductor1	1.15e-05	1.12e-05	1.11e-05	1.13e-05	6.17e-06	5.99e-06	5.94e-06	6.02e-06
Conductor2	1.12e-05	1.15e-05	1.12e-05	1.11e-05	5.99e-06	6.17e-06	5.99e-06	5.93e-06
Conductor3	1.11e-05	1.12e-05	1.15e-05	1.13e-05	5.94e-06	5.99e-06	6.17e-06	6.02e-06
Neutral cord	3.89e-10	3.84e-10	3.89e-10	4.04e-10	6.02e-06	5.93e-06	6.02e-06	6.27e-06

Table 11 includes the impedance and impedance-like values. In the magnetostatics problem the conductor's impedance (equal to the resistance) per meter is calculated by the formula: $R = l / (\rho \cdot S)$ Joule heat per meter in magnetostatics problem is calculated by the formula: $P = I_A^2 \cdot R$, where I_A is the root-mean-square current and R is the conductor impedance.

The conductors' impedances in AC magnetics problem are calculated using the Ohm's law as a complex ratio of the conductor's average potential divided by the conductor total current density. The real part of this ratio represents the resistance, imaginary part — reactance and the modulus — impedance. The Joule heat in the AC magnetic problem is calculated using the corresponding QuickField integral.

Table 11. Conductors' impedance.

	In electrostatics problem		In AC magnetic problem		
	Conductors	Null cord	Conductor1	Conductor2	Conductor3
Impedance, Ω	2.31e-04	7.94e-04	2.40e-04	2.55e-04	2.80e-04
Resistance, Ω	2.31e-04	7.94e-04	2.15e-04	2.37e-04	2.59e-04
Reactance, Ω	0.00e+00	0.00e+00	1.08e-04	9.41e-05	1.06e-04
Joule heat, W	4.63e+00	0.00e+00	4.71e+00	4.74e+00	4.71e+00

The generated heat field is exported from the AC magnetics problem into the heat transfer problem. As a result of QuickField simulation you can see the cable exterior surface average temperature, heat flow from the cable surface and the average temperatures of all conductors. Average temperatures are relative numbers presented in Celsius assumed that ambient space temperature is 20 °C.

Table 12. Cable heat parameters

Exterior surface average temperature	2.35e+01	°C
Heat flow	1.42e+01	W
Conductors average temperature, °C		
Conductor1	Conductor2	Conductor3
4.59e+01	4.68e+01	4.59e+01
Null-cord		3.93e+01

Stress analysis problem is the utmost one, that imports the temperature field from the heat transfer problem and the magnetic forces from the AC magnetic problem. Due to this magnetic and thermal loading the cable components become deformed. The numerical values of these deformations are presented in the next table.

Table 13. Stress analysis problem results.

Maximal displacement	5.14e-02	Mm
Maximal Mohr criteria value	8.16e+07	N/m ²

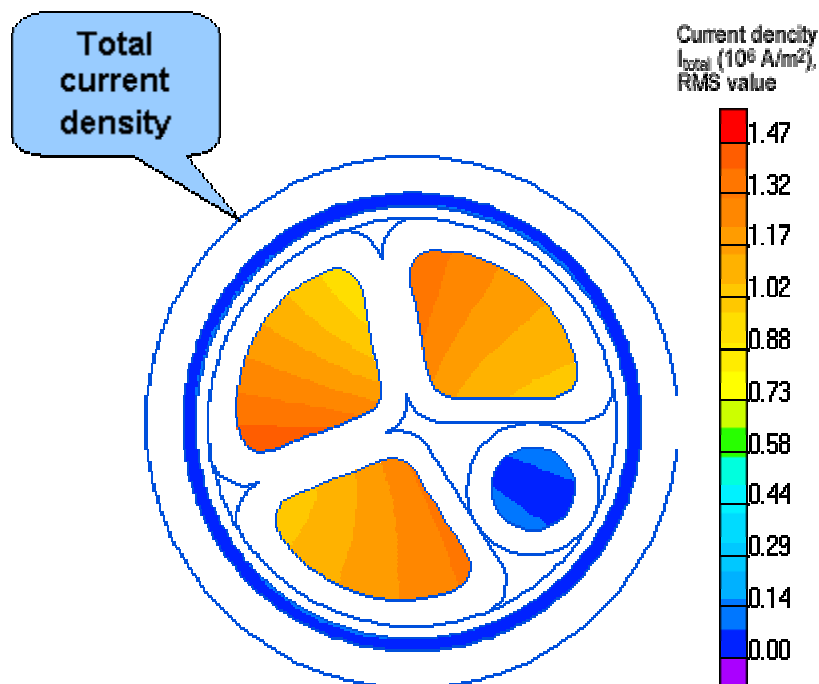
The strength value is important for the cable fault analysis.

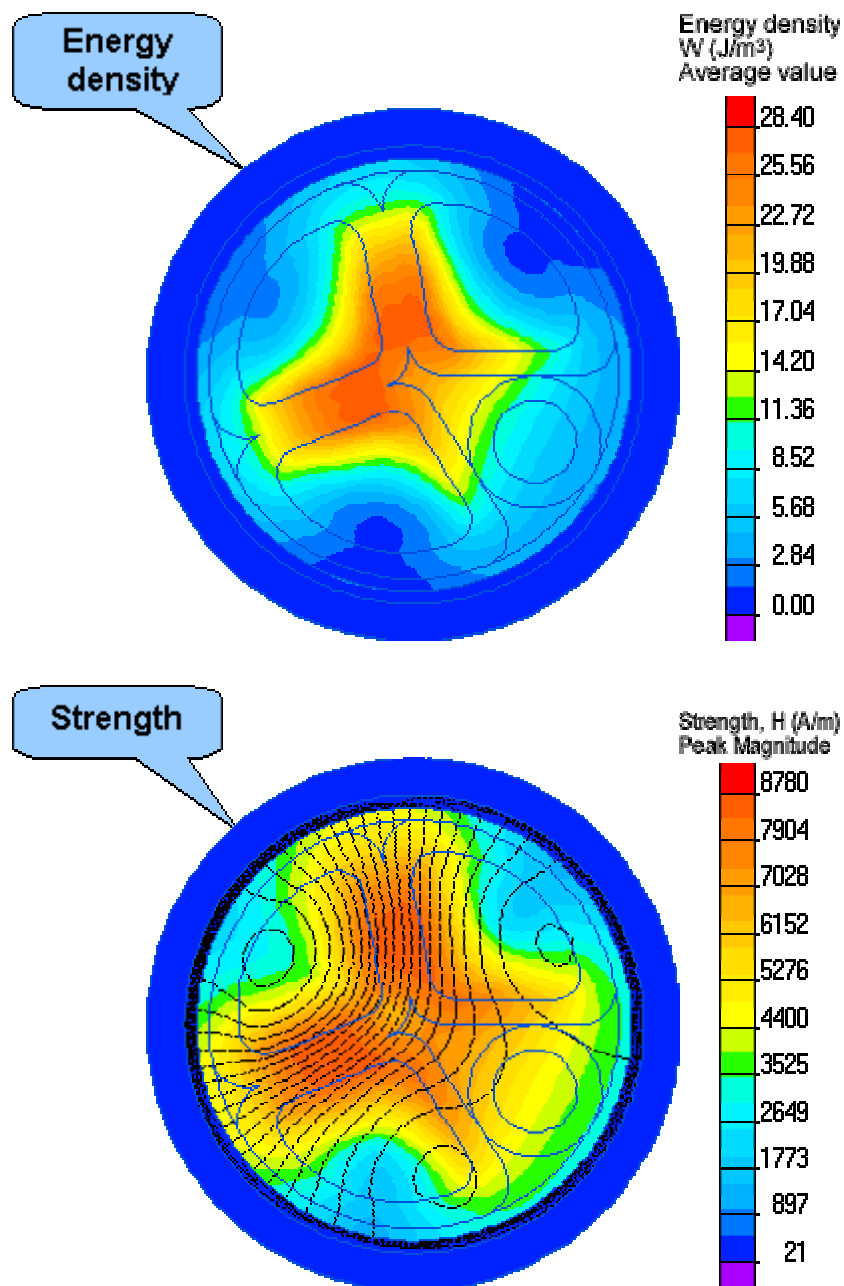
Table 14. The strength.

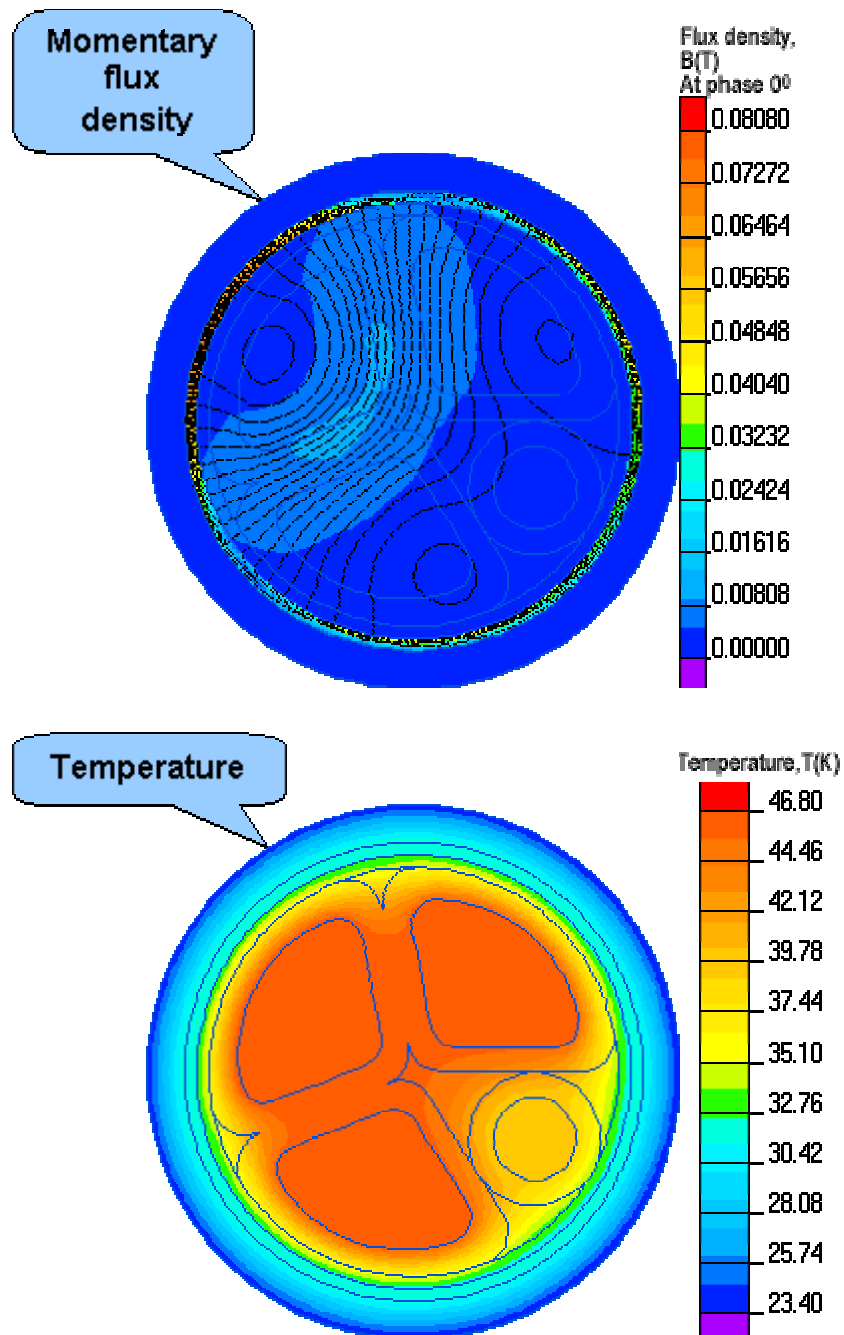
Maximal peak strength value	8.78e+03	A/m
-----------------------------	----------	-----

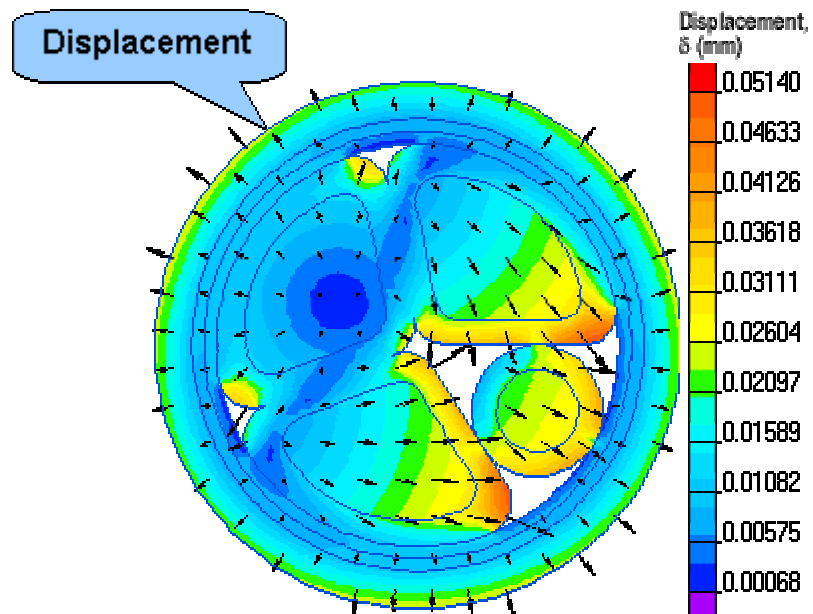
The "Strength" field is shown on a figure below as well as the "Total current density", "Energy density", "Momentary flux density", "Temperature" and "Displacement" field pictures.

Section 5. Field pictures.









Main inductance determination in rotating machines. Analytical and Numerical calculation: A didactical approach

Bargallo, R. ⁽¹⁾, Llaverias, J. ⁽¹⁾, De Blas, A. ⁽¹⁾., Martín, H. ⁽¹⁾, Piqué, R. ⁽²⁾

(1) Electrical Engineering Department.

(2) Electronic Engineering Department

EUETIB, Politechnical University of Catalonia (UPC)

c/Urgell, 187, 08036 Barcelona (Spain)

Tel. (34) 934137411, fax: (34) 934137401, ramon.bargallo@upc.edu

Abstract.

The accurate determination of saturated magnetizing inductances has been the subject of much research over a long time. These results are necessary for the appropriate adjustment of control regulation loops and for the improvement of transient response and stability of electric drives. Traditionally the analytical calculation involves the determination of some empirical factors, such as the d-axis and q-axis reactance factors. In references [1] to [3] there are many expressions for salient and non-salient pole machines, but these are valid only for the considered pole shape.

If possible we should use an expression, or method, independent of the pole shape. Analytical formulation is not adequate for this reason. Now we can use the FE method to calculate this and other parameters.

In addition the time devoted today to the design of electrical machines has been reduced and this makes it impossible to use a lot of empirical or graphical methods. The use of FEM provides a way to quickly and accurately calculate the size of an electrical machine and its parameters. This paper has been written to describe this methodology in an educational environment.

Keywords.

Main inductance determination, FE method, cylindrical and salient pole machines.

1. Analytical calculation of magnetizing inductances.

In the following paragraphs we describe how obtain an analytical expression for the main inductances. This methodology shows how these are function of the pole shape and how explain this in an educational environment.

A. Uniform air gap machine

The magnetizing inductance of a uniform air gap machine can calculated according to the following procedure:

Calculation of:

- A. MMF created to the 3-phase equilibrate current system
- B. Air gap induction B_1 (only considers the fundamental component)
- C. Total flux per phase Φ
- D. Main inductance determination: $L_m = \Phi/I$

The following expression is the result of this process.

$$L_m = \frac{\mu_0}{\pi} \cdot m \cdot \frac{D \cdot L}{g_{eq}} \cdot \left(\frac{N \cdot \xi}{p} \right)^2 \quad (1)$$

with: m – number of phases, D – air gap diameter, L – length of the machine, g_{eq} – equivalent air gap (with Carter's and saturation correction), N – number of turns per phase, p – pole pairs.

B. Salient pole machines

The calculation is similar, but we found some differences:

- We calculate the MMF projection over two axis: direct and quadrature axis.
- Thus we determine the induction create for these two components and determine the fundamental component.
- Thus we can calculate the flux and the main inductance for every component:

$$L_{md} = \Phi_d / I; L_{mq} = \Phi_q / I \quad (2)$$

These process leads to the following expressions:

$$L_{md} = k_d \cdot L_m; \quad L_{mq} = k_q \cdot L_m \quad (3)$$

Where L_m is the magnetizing inductance calculate supposing that the air gap is uniform and k_d and k_q are coefficients that depended on pole shape.

The following table shows these coefficients for different pole shape configuration; the first row is for a classical salient pole synchronous machine and the others are for permanent magnet machines.

Table I. direct and quadrature correction factors.

Salient pole synchronous machine	$k_d = \frac{1}{\pi} \cdot (\psi \cdot \pi + \sin(\psi \cdot \pi))$ $k_q = \frac{1}{\pi} \cdot \left(\psi \cdot \pi - \sin(\psi \cdot \pi) + \frac{2}{3} \cdot \cos(\psi \cdot \frac{\pi}{2}) \right)$
PMSM. Surface magnets	$k_d = 1; \quad k_q = 1$
PMSM. Inset magnets	$k_d = \frac{1}{\pi} \cdot [\psi \cdot \pi + \sin(\psi \cdot \pi) + c_g \cdot (\pi - \psi \cdot \pi - \sin(\psi \cdot \pi))]$ $k_q = \frac{1}{\pi} \cdot \left[\frac{1}{c_g} \cdot (\psi \cdot \pi - \sin(\psi \cdot \pi)) + (\pi - \psi \cdot \pi + \sin(\psi \cdot \pi)) \right]$ $c_g \approx 1 + \frac{h}{g}$
PMSM. Buried magnets	$k_d = \frac{4}{\pi} \cdot \frac{\psi}{1 - \psi^2} \cdot \cos\left(\frac{\psi \cdot \pi}{2}\right)$ $k_q = \frac{1}{\pi} \cdot (\psi \cdot \pi - \sin(\psi \cdot \pi))$ $\psi = \frac{\beta}{\tau_p} = \frac{D - 2 \cdot p \cdot h}{D}$

With: τ_p - pole pitch, ψ = pole arc/ pole pitch, h - permanent magnet height.

2. Numerical determination of magnetizing inductance.

The numerical determination of magnetizing inductance involves the realization of Finite Element Analysis (FEA) and the determination of the magnetic energy stored in the air gap. The following paragraphs describe the relations between this and the magnetic inductance. In addition we describe two ways for the calculation of stored energy; the first is by integration of density of energy and the second is by circuit modelling.

A. Magnetic energy stores in the air gap (uniform air gap machine).

If we consider an ideal machine with sinusoidal distribution of the induction along the air gap, that is,

$$B = \hat{B} \cdot \sin\left(\frac{\pi \cdot x}{\tau_p}\right) \quad (4)$$

and we calculate the magnetic energy stored in the airgap, we obtain:

$$W = \mu_0 \cdot \frac{m^2}{2 \cdot \pi} \cdot \left(\frac{N \cdot \xi}{p} \right)^2 \cdot \frac{D \cdot L}{g_{eq}} \cdot I_m^2 \quad (5)$$

If we combine (5) with (1) we can write:

$$W = \frac{m}{2} \cdot L_m \cdot I_m^2 \quad (6)$$

usually $m = 3$. You can obtain the same expression if you consider the electrical circuit model with coupled coils.

For example for the induction machine model with 3 coils in the stator and 3 coils in the rotor, that is:

$$[L] = \begin{bmatrix} L_s & L_{sr} \\ L_{rs} & L_r \end{bmatrix}; [L_s] = \begin{bmatrix} L_{as} & L_{abs} & L_{acs} \\ L_{bas} & L_{bs} & L_{bcs} \\ L_{cas} & L_{cbs} & L_{cs} \end{bmatrix}; [L_r] = \begin{bmatrix} L_{ar} & L_{abr} & L_{acr} \\ L_{bar} & L_{br} & L_{bcr} \\ L_{car} & L_{cbr} & L_{cr} \end{bmatrix} \quad (7)$$

$$[L_{sr}] = [L_{rs}]^t = \begin{bmatrix} L_{asar} \cdot \cos \theta_r & L_{asbr} \cdot \cos(\theta_r + \frac{2 \cdot \pi}{3}) & L_{ascr} \cdot \cos(\theta_r + \frac{4 \cdot \pi}{3}) \\ L_{bsar} \cdot \cos(\theta_r + \frac{4 \cdot \pi}{3}) & L_{bsbr} \cdot \cos \theta_r & L_{bscr} \cdot \cos(\theta_r + \frac{2 \cdot \pi}{3}) \\ L_{csar} \cdot \cos(\theta_r + \frac{2 \cdot \pi}{3}) & L_{csbr} \cdot \cos(\theta_r + \frac{4 \cdot \pi}{3}) & L_{cscr} \cdot \cos \theta_r \end{bmatrix}$$

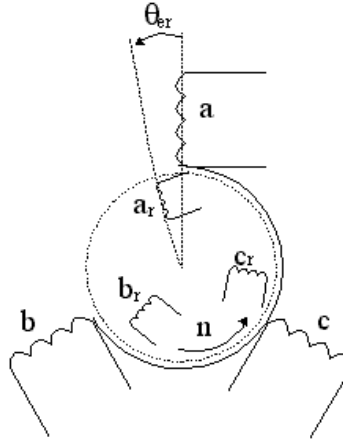


Figure 1. simplified machine.

We obtain:

$$W = \frac{1}{2} \sum L_{ij} \cdot I_i \cdot I_j$$

$$W = \frac{1}{2} \cdot \left[\begin{aligned} &L_{as} \cdot i_{as}^2 + L_{bs} \cdot i_{bs}^2 + L_{cs} \cdot i_{cs}^2 + L_{ar} \cdot i_{ar}^2 + L_{br} \cdot i_{br}^2 + L_{cr} \cdot i_{cr}^2 + \\ &\left(\begin{aligned} &L_{abs} \cdot i_{as} \cdot i_{bs} + L_{bcs} \cdot i_{bs} \cdot i_{cs} + L_{cas} \cdot i_{cs} \cdot i_{as} + \\ &L_{abr} \cdot i_{ar} \cdot i_{br} + L_{bcr} \cdot i_{br} \cdot i_{cr} + L_{car} \cdot i_{cr} \cdot i_{ar} + \\ &+ L_{asar} \cdot i_{as} \cdot i_{ar} + L_{asbr} \cdot i_{as} \cdot i_{br} + L_{ascr} \cdot i_{as} \cdot i_{cr} + \\ &L_{bsar} \cdot i_{bs} \cdot i_{ar} + L_{bsbr} \cdot i_{bs} \cdot i_{br} + L_{bscr} \cdot i_{bs} \cdot i_{cr} + \\ &+ L_{csar} \cdot i_{cs} \cdot i_{ar} + L_{csbr} \cdot i_{cs} \cdot i_{br} + L_{cscr} \cdot i_{cs} \cdot i_{cr} \end{aligned} \right) \end{aligned} \right] \quad (8)$$

(We omitted the terms with $\cos()$ to simplify the expression). If we consider the following values, corresponding to an instant with:

$$\begin{aligned} i_{as} &= \hat{I}; & i_{bs} &= i_{cs} = -\frac{1}{2} \hat{I} \\ i_{ar} &= i_{br} = i_{cr} = 0 \end{aligned} \quad (9)$$

we obtain:

$$W = \frac{3}{2} \cdot L_m \cdot I^2 + \frac{3}{2} L_{\sigma s} \cdot I^2 \quad (10)$$

Except for the last term, this is the same expression (6). This term is a result to the dispersion effect and will be not considered for the main inductance calculation.

B. Magnetic energy stores in the salient pole machine.

We can obtain an expression for the magnetic energy stored in the case of the salient pole machine, but this takes longer to determine. We develop an expression based on circuit model approximation. In the salient pole machine we consider the first harmonic approximation for the inductance variation, i.e.,

$$L \approx L_0 + L_2 \cos 2\theta_{er} \quad (11)$$

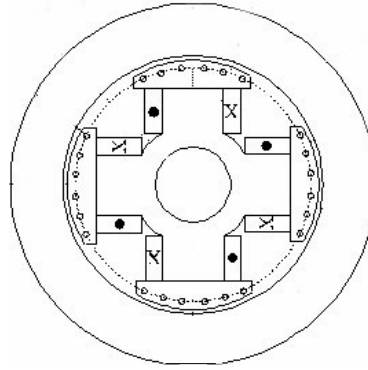


Figure 2. Salient pole machine

for the 3-phase synchronous machine we can write:

$$\begin{aligned} L_{aa} &= L_{\sigma s} + L_0 + L_2 \cos 2\theta_{er} \\ L_{bb} &= L_{\sigma s} + L_0 + L_2 \cos(2\theta_{er} + 2\pi/3) \\ L_{cc} &= L_{\sigma s} + L_0 + L_2 \cos(2\theta_{er} - 2\pi/3) \\ L_{bc} &= -L_0/2 + L_2 \cos 2\theta_{er} \\ L_{ac} &= -L_0/2 + L_2 \cos(2\theta_{er} + 2\pi/3) \\ L_{ab} &= -L_0/2 + L_2 \cos(2\theta_{er} - 2\pi/3) \\ L_{af} &= L_{sf} \cos \theta_{er}, L_{bf} = L_{sf} \cos(\theta_{er} - 2\pi/3), \\ L_{cf} &= L_{sf} \cos(\theta_{er} + 2\pi/3) \end{aligned} \quad (12)$$

The energy stored is:

$$W = \frac{1}{2} \cdot \left[L_{aa} \cdot i_a^2 + L_{bb} \cdot i_b^2 + L_{cc} \cdot i_c^2 + L_{ff} \cdot i_f^2 + 2 \cdot \left[L_{bc} \cdot i_b \cdot i_c + L_{ac} \cdot i_a \cdot i_c + L_{ab} \cdot i_a \cdot i_b + L_{af} \cdot i_a \cdot i_f + L_{bf} \cdot i_b \cdot i_f + L_{cf} \cdot i_c \cdot i_f \right] \right] \quad (13)$$

(We omitted the terms with $\cos()$ to simplify the expression). If we consider the following values, corresponding to an instant with:

$$\begin{aligned} i_a &= \hat{I} \\ i_b &= i_c = -\frac{\hat{I}}{2} \\ i_f &= 0 \quad (\text{without field current}) \end{aligned} \quad (14)$$

We obtain the following expression:

$$W = \frac{3}{2} \cdot I^2 \cdot \left[\frac{3}{2} \cdot L_0 + \frac{3}{2} \cdot L_2 \cdot \cos(2 \cdot \theta_{er}) \right] + \frac{3}{2} L_{\sigma} \cdot I^2 \quad (15)$$

The last term is a result to the dispersion effect and will be not considered for the main inductance calculation.

If we consider two selected positions for the rotor, i.e.

- $\cos(2 \cdot \theta_{er}) = 1 \Rightarrow$ *Direct field orientation*
- $\cos(2 \cdot \theta_{er}) = -1 \Rightarrow$ *quadrature field orientation*

Some after algebraic manipulations, we obtain:

$$\cos(2 \cdot \theta_{er}) = 1 \Rightarrow \begin{cases} W = \frac{3}{2} \cdot I^2 \cdot \left[\frac{3}{2} \cdot L_0 + \frac{3}{2} \cdot L_2 \right] + \frac{3}{2} L_{\sigma} \cdot I^2 \\ L_{md} = \frac{3}{2} \cdot [L_0 + L_2] \\ W = \frac{3}{2} \cdot I^2 \cdot L_{md} + \frac{3}{2} L_{\sigma} \cdot I^2 \end{cases} \quad (16)$$

$$\cos(2 \cdot \theta_{er}) = -1 \Rightarrow \begin{cases} W = \frac{3}{2} \cdot I^2 \cdot \left[\frac{3}{2} \cdot L_0 - \frac{3}{2} \cdot L_2 \right] + \frac{3}{2} L_{\sigma} \cdot I^2 \\ L_{mq} = \frac{3}{2} \cdot [L_0 - L_2] \\ W = \frac{3}{2} \cdot I^2 \cdot L_{mq} + \frac{3}{2} L_{\sigma} \cdot I^2 \end{cases} \quad (17)$$

C. Inductance determination by means of flux concatenation

Another technique for the calculation of inductance is by the use of flux concatenation by a coil. If we consider a magnetic field distribution along the air gap, and its first harmonic, we can calculate the flux concatenation and the main inductance:

$$L = \frac{\Phi}{I} = N \cdot \frac{\int \nabla \times \vec{A} \cdot d\vec{S}}{I} = N \cdot \frac{\oint \vec{A} \cdot d\vec{l}}{I} \quad (18)$$

If we consider a salient pole machine, we use a flux oriented over the direct and quadrature axis respectively, for the determination of direct and quadrature inductances.

3. Practical Applications

The following paragraphs show three examples of determination of main inductance. Two of them are compared with experimental results.

A. Asynchronous machine: 1.5 kW; 50 Hz; 220 / 380 V; 6.4 / 3.7 A; $\cos\phi = 0.85$; 1420 min⁻¹; F class; $J = 0.0105$ kgm²; Δ Connexion.

Geometric and electrical data: 36/28 slots; 44 conductors/slot; $D = 80$ mm; $g = 0.375$ mm; $L = 100$ mm. We considered that $k_c \cdot k_{sat} = 1.3$ and $\xi = 0.955$.

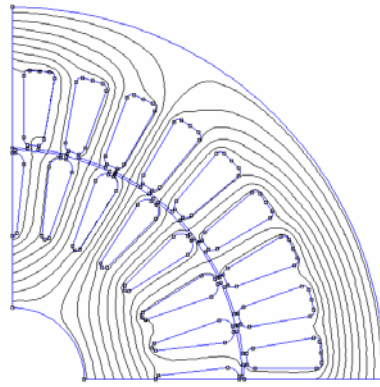


Figure 3. FEM model for asynchronous machine. Only $\frac{1}{4}$ of the machine has been modeled.

Table II. Main inductance for asynchronous machine.

Method	L_m (H)
Analytical calculation	0.310
FEA	0.313
Experimental results	0.255

B. Synchronous machine: 6 kVA; 220 V; 15.8 A; 50 Hz; 1500 min^{-1} ; Y connexion.

Geometric and electrical data: salient pole with uniform airgap (under the pole) $g = 2$ mm; $D = 304$ mm; $L = 100$ mm; $\psi = 0.55$; 36 slots; double layer lap winding; 5 conductors per slot and layer. We considered that $k_c \cdot k_{sat} = 1.3$ and $\xi = 0.955$.

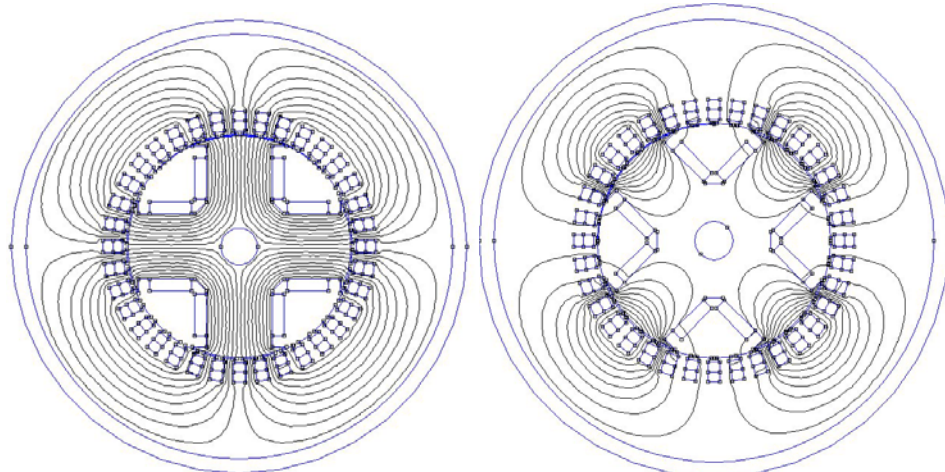


Figure 4. FEM model for synchronous machine. Direct field orientation. Figure 5. Quadrature field orientation

Table III. Main inductance for synchronous machine.

Method	L_d (mH)	L_q (mH)
Analytical calculation	9.84	4.25
FEA	10.7	4.23
Experimental results (reduced slip test)	7.42	5.30

C. Synchronous machine with permanent magnets. 5.1 Nm; 3500 min^{-1} ; $I_N = 2.56$ A; F class

Geometrical data: $D = 80$ mm; $L = 68.9$ mm; 36 slots; 6 pole; 35 conductors per slot; single layer lap winding; $\zeta = 0.96$; permanent magnet height $h = 3$ mm; $g = 0.5$ mm; $\psi = 0.65$; $k_c \cdot k_{sat} = 1.3$; surface permanent magnet.

In this case to impose $i_f = 0$ we change the PM characteristic from a non-magnetic material with the same magnetic permeability of the PM. This machine is considered as uniform air gap machine due to the value of recoil permeability of the PM (near to 1.0)

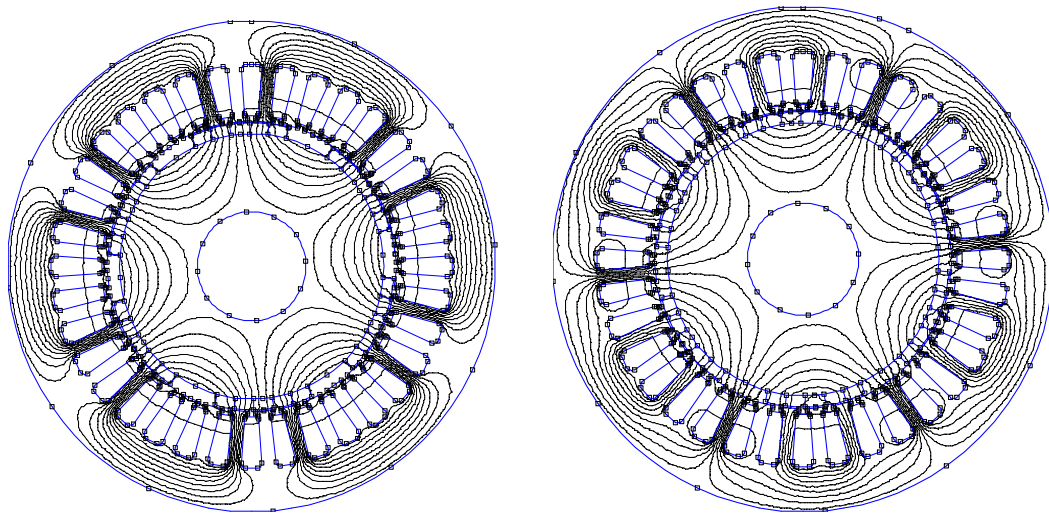


Figure 6 and 7. FEM model for synchronous machine. Direct field orientation. Quadrature field orientation

For this machine we determined the inductance by the method of flux concatenation. We obtain the magnetic field distribution and harmonic components showed in the figures 8 and 9.

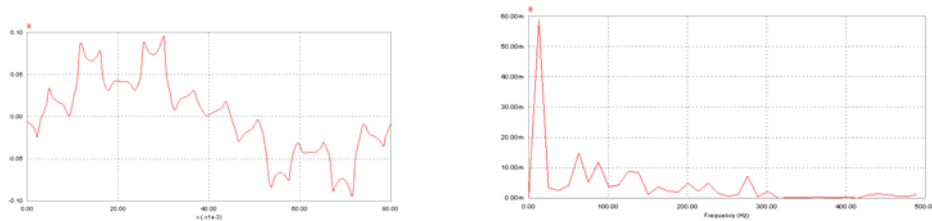


Figure 8. Magnetic field distribution along the airgap. Figure 9. Harmonic distribution of magnetic field.

The following table (IV) shows the calculated values.

Table IV. Main inductance for synchronous machine with PM.

Method	L (mH)
Analytical calculation	6.55
FEA (energy)	5.15
Flux method (FEA)	6.0

3. Conclusions.

- We explained some methods to determine the main inductances for alternating current machines in an educational environment.
- We considered correction factors that are dependents on the pole-shape configuration.
- FEM is more precise than analytical calculation and is not dependent on an empirical or geometrical factors.
- Some of these experimental results are discordant with theoretical results due to estimation of some geometrical measures and magnetic characterization.

Bibliography

- [1] J. Corrales Martín. Cálculo Industrial de Máquinas Eléctricas. Tomo 1. Ed. Marcombo. 1982
- [2] B. Chalmers, A. Williamson. AC Machines. Electromagnetics and Design. Ed. Research Studies Press Ltd. 1992.
- [3] J.F. Gieras, E. Santini, M. Wing. Calculation of synchronous machines of small permanent magnet alternating current motors: comparison of analytical approach and FEM with measurements. IEEE Transactions of Magnetics, vol 34, nº 5, September 1988.
- [4] M.R. Hassanzadeh, A. Kiyomarsi. Analytical calculation of magnetizing inductances in interior permanent magnet motors. ICEM, Cracow, September 2004.
- [5] R. Bargalló. Diseño de Máquinas Eléctricas. Tema 8. Determinación de parámetros. EUETIB. 2004.

Steady State Performance Evaluation of a Permanent Magnet Synchronous Motor Based on FEA

Lidija Petkovska, Senior Member IEEE and Goga Cvetkovski, Member IEEE

Ss. Cyril and Methodius University
Faculty of Electrical Engineering
Karpos II b.b., P.O.Box 574, 1000 Skopje (Macedonia)

phone: + 389 2 30 99 145, fax: + 389 2 30 64 262, e-mail: lidijap@etf.ukim.edu.mk ; gogacvet@etf.ukim.edu.mk

Abstract. The paper deals with the determination and an evaluation of steady state performance characteristics of a synchronous motor with surface mounted permanent magnets. At the beginning, a numerical calculation of the magnetic field distribution of permanent magnet synchronous motor (PMSM), under consideration is carried out. For this purpose, the Finite Element Method (FEM) is applied. By using output data from the field computation, all relevant characteristics of the motor are determined. The results of the numerical calculations are presented by diagrams. When possible, calculated steady state characteristics are compared with experimentally obtained ones; they show a very good agreement. An evaluation of the steady state behaviour of a permanent magnet synchronous motor, based on the Finite Element Analysis (FEA) is presented.

Key Words

Permanent Magnet Synchronous motor, FEM, FEA, Magnetic flux density, Coenergy, Electromagnetic torque.

1. Introduction

The 3-phase permanent magnet AC motor, acting as conventional synchronous type motor, has found renewed interest in the last two decades [1], [2]. The recent development of high energy magnets has enhanced their application in wide range of areas. The built-in of permanent magnets in the rotor core of synchronous motors as an excitation, and in particular the use of samarium-cobalt or neodymium-boron-iron magnets has challenged innovations in the permanent magnet synchronous motor (PMSM) design and analysis. In the paper, parameters and steady state performance characteristics of a PMSM are determined and analysed.

The main task is always to calculate steady state characteristics, as exact as possible. It has been found as rather complicated issue. It is obvious that the stress should be put on the exact determination of the parameters, as they are "playing" an important role in the accuracy with which all the characteristics of the PM synchronous motor under consideration will be derived.

2. Object of Study

The object of investigation is a Koncar motor type EKM 90M-6, with rated data: 18 A, 10 Nm, 1000 rpm. The motor is supplied from an AC source at 50 Hz, by current sine waves. Six permanent magnet poles made of SmCo5 are surface mounted on the rotor. The side view of the motor and its geometrical cross section are presented in Fig. 1 and Fig. 2, respectively.

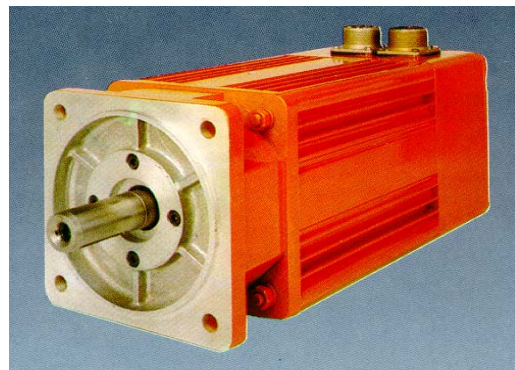


Fig. 1. Side view of a PMSM type EKM 90M-6

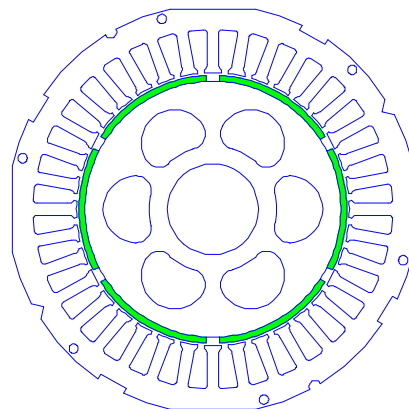


Fig. 2. Cross-section of the motor EKM 90M-6

3. FEM Calculation of PMSM

The Finite Element Method (FEM) has been used extensively in the numerical calculation of the magnetic field in electrical machines, in general. The output results, and a possibility to use them for calculation of both electromagnetic and electromechanical characteristics, are an excellent basis for carrying out Finite Element Analysis (FEA). Many researchers all over the world, including the authors of this paper, have done a lot of work in this area. Many papers in this topic have been published [3]-[11]. Different software packages exist in use. The presented results in the paper are computed by using an user friendly software package FEMM [12].

In the first step, usually considered as a pre-processing stage, depending on the user choice the mesh of finite elements with an appropriate density is generated fully automatically. In the FEA of the PMSM it is consisted of 17,190 nodes and 34,041 elements. For the purposes of FEM calculations of the magnetic field in the motor under consideration, the mesh is spread over the whole cross-section of the motor, as can be seen in Fig. 3.

In the pre-processor, named *femm.exe* all requested input data are included: • the exact geometrical cross section of stator and rotor magnetic core; • current density in the excited stator windings; • all boundary conditions of the region which is going to be analysed; • all material characteristics of the motor (permanent magnets, copper wire, B-H magnetising curve). The numerical FEM model of the PMSM, being completed, is ready for practical use.

When applying the software package FEMM for analysis of the permanent magnet synchronous motor, the magnetic problem is considered to be the time dependent harmonic problem. Hence, the calculations of the magnetic field are performed at rated frequency $f_n=50\text{Hz}$.

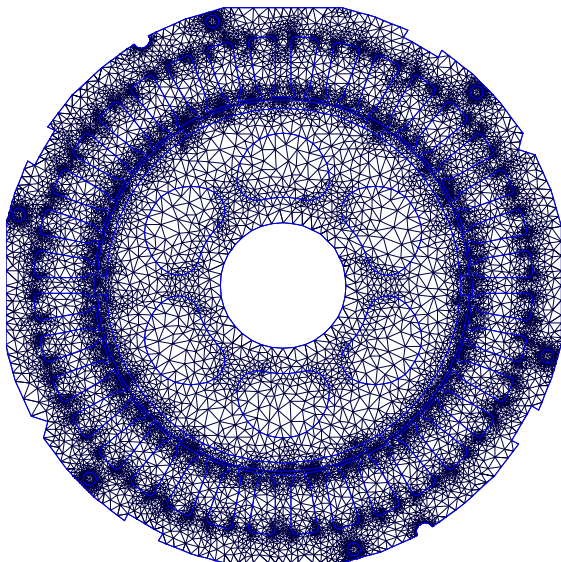


Fig. 3. Finite elements mesh of the PMSM

The field solutions are obtained by running the FEMM solver, called *fkern.exe*. As the whole cross section of the motor is used, only the first order Dirichlet's boundary conditions are applied; on the outer stator line and the inner rotor line it is set to be $A=0$.

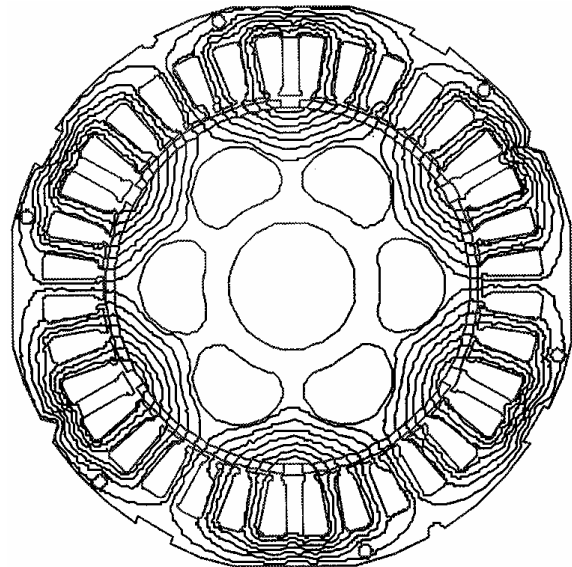
Armature currents in the stator windings are varied from $I=0$ to the rated value $I_n=18\text{A}$. Rotor is freely moving (rotating) in the air-gap, continuously changing position, and the d-axis of the rotor is continuously taking different angles θ against the referential axis of the stator, firmly linked with one of the winding axes.

After the processing step is executed, the values of magnetic vector potential in every node of the motor domain are obtained. Later, one can use them for many purposes. The unit *femview.exe* in the FEMM package is offering user friendly calculations and graphical presentations of the most important electromagnetic and electromechanical quantities.

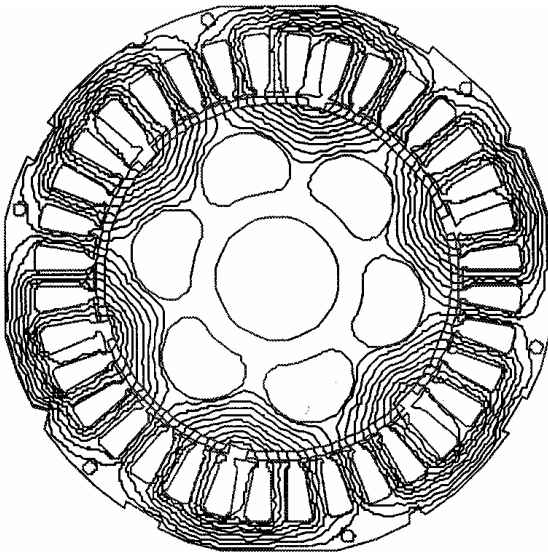
A. Magnetic Field Distribution

The best way to understand the phenomena in any investigated motor is "to get inside and to see" the magnetic field distribution. Graphical presentation and visualization of the FEM results give the magnetic flux distribution in the cross-section of permanent magnet synchronous motor. A part of the most interesting results of the calculations are given in continuation.

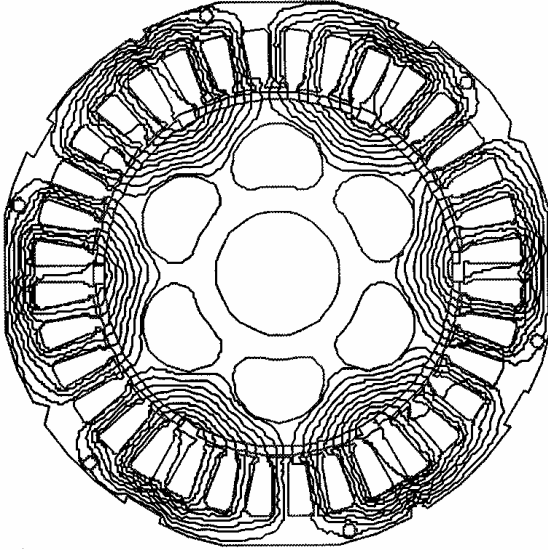
The magnetic field distribution in PMSM is presented in Fig. 4, at following regimes: • (a) no-load condition, i.e. zero armature current, meaning magnetic field obtained by the permanent magnets only; • (b) rated-load with rated stator winding current $I_n=18\text{A}$ and rated load angle $\delta_n=39^\circ$ [deg.el.], i.e. $\theta=13^\circ$ [deg.mech.]; • (c) loading condition at pull-out (maximum value) torque, meaning load angle $\delta_{\max}=90^\circ$ [deg.el.], i.e. $\theta=30^\circ$ [deg.mech.].



(a) no-load at $I=0$ and $\theta=0^\circ$ deg.



(b) rated load at $I_n=18$ A and $\theta=13$ deg.

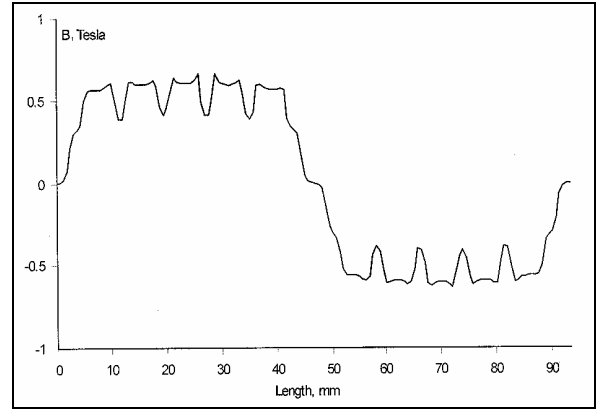


(b) pull-out load at $I_n=18$ A and $\theta=30$ deg.

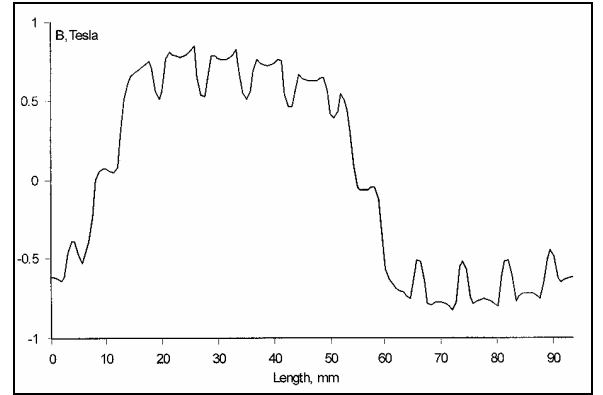
Fig. 4. Magnetic flux plots in the middle cross-section of PMSM under typical operating conditions

The FEMM software package enables comprehensive presentation of the spatial distribution of magnetic flux density along an arbitrary selected line, as well. The distribution along the mid-gap line is presented in Fig. 5 (a), (b) and (c), in the same way as precedent, at the same operating regimes and loading conditions of the PMSM. The following diagrams are spanned to one pole pitch.

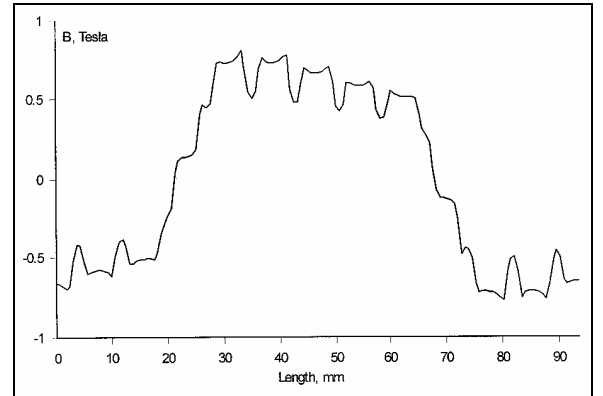
These diagrams can be used for carrying out a profound analysis of the air-gap magnetic field properties regarding both intensity and shape. When the permanent magnet synchronous motor is loaded, the influence of armature reaction magnetic field is clearly shown, in the figures. The influence of stator core teeth, on the air-gap field distribution is also clearly indicated in the figures.



(a) no-load at $I=0$ and $\theta=0$ deg.



(b) rated load at $I_n=18$ A and $\theta=13$ deg. ($\delta_n=39$ deg.el.)



(c) pull-out load at $I_n=18$ A and $\theta=30$ deg. ($\delta_{\max}=90$ deg.el.)

Fig. 5. Mid-gap magnetic flux density spatial distribution

B. Air-gap Flux Linkage

The numerical calculation of fluxes is based on the field theory, applied on a bounded and closed systems. If the calculations are performed per pair of excited poles, it is:

$$\Phi_g = \int_{\Sigma} \text{rot} \mathbf{A} \cdot d\mathbf{S} = \oint_C \mathbf{A} \cdot d\mathbf{r} = \int_{\Sigma} \mathbf{B} \cdot d\mathbf{S} \quad (1)$$

For N excited turns, the air-gap flux linkage is:

$$\Psi_g = N \cdot \Phi_g = \iint_S (\mathbf{B} \cdot \mathbf{n}) dS \quad (2)$$

C. Computation of Inductances

It is very important matter to calculate as accurate as possible the values of the parameters of the PMSM. Of the most important significance are the direct- and the quadrature- axis inductances, as they are determining corresponding synchronous reactances [13]; it is well known that they are the most significant parameters when dealing with steady state and/or dynamic performance analysis of PMSM.

The numerical calculation of inductances is based on FEM results. It is performed separately for d- and q- axis. In this case, it is found to be sufficient to calculate magnetic field only along one pole pitch. Neumann's boundary conditions of the second order, are imposed on the side lines of the cut [14].

The field should not be excited; it means that permanent magnets have to be replaced with finite elements related only with a correspondent permeability ($\mu_r=1.05$), but not carrying the magnetic remanence ($B_r=0.95$ T). Only the armature winding is energized in an appropriate way [15], [16], as explained below:

1) *d-axis*: When calculating the direct axis inductance L_d , currents in the armature winding are distributed to peak at a quadrature axis, producing field with a peak at direct axis. The magnetic field distribution is presented in Fig. 6.

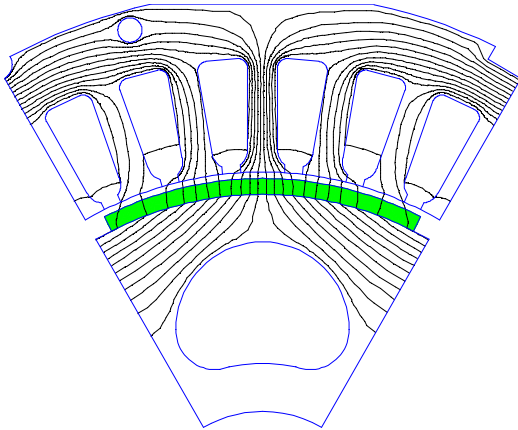


Fig. 6. Magnetic flux distribution for L_d calculation

2) *q-axis*: The quadrature axis inductance L_q , is calculated in similar way as L_d . In this case, the armature field is moved forward in space for 90° el. and produces peak at a quadrature axis. It means that armature currents of the stator windings peak at the direct axis. In this case, the magnetic flux distribution for one pole pitch, and with the same boundary conditions when calculating d-axis magnetic field, is presented in Fig. 7.

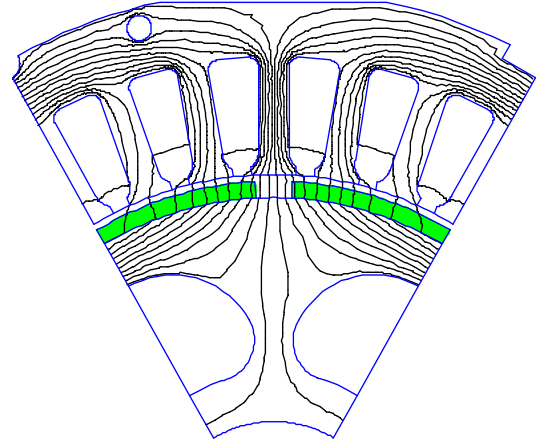


Fig. 7. Magnetic flux distribution for L_q calculation

In general, the inductance is calculated as a ratio of the flux linkage to the armature current, leading to:

$$L = \frac{\Psi}{I} \quad (3)$$

The previous equation is applied for the computation of the *d*-axis and *q*-axis inductance. The corresponding flux linkage Ψ , for each studied case is calculated by applying respective results FEM in Eq. (3); the magnetic field calculations are carried out in a way as previously has been explained, in accordance with Fig. 6 and Fig. 7.

As it was assumed the fictitious direct/quadrature winding to have the same number of turns as the real stator phase winding, it is requested to introduce another factor to find the direct- and quadrature- axis inductance, respectively [14]. For a 3-phase AC machine, the armature current in the direct/quadrature axis would have to be $3/2$ times as great as the phase current to produce the same magneto-motive force along the respective axis as the three phase winding. Hence,

$$L_{d,q} = \frac{L}{3/2} \quad (4)$$

The calculations yield to results:

$$L_d = 5.816 \text{ mH} \quad \text{and} \quad L_q = 5.803 \text{ mH} \quad (5)$$

4. Motor Parameters Determination

The two-axes model of the synchronous machines is well established classical approach for an analytic-graphic investigation of their behaviour [13]. Many researchers widely use this method for fast prediction of the initial data for further more detailed and deepened analysis [17]. The basic idea is to develop and to use a set of equations, describing the motor performance in *d,q* reference frame and in terms of the loading angle δ . The only request is to have available the motor parameters. The accuracy, with which the performance characteristics of the PMSM will be determined, is in the direct dependence of the accuracy with which the motor parameters are calculated.

Some of the motor parameters could be easily measured; some are available from the producer's data; but very often their values are unknown, and it is requested an experience and skill to apply in the best way existing and well known numerical, experimental or analytical calculation methods. Different approaches are possible.

Starting with the numerical procedure, the d, q parameters of the PMSM under consideration are determined. By using the FEM results computed for L_d and L_q given in the previous heading with Eq. (5), one can determine the values for d, q reactance of PMSM, at 50 Hz as:

$$X_d = 1.827 [\Omega] \quad \text{and} \quad X_q = 1.823 [\Omega]$$

The already known fact that, that in synchronous motors with surface mounted permanent magnets, there is almost no difference between reactance along d - and q -axis has been also proved in this case.

Armature winding resistance R_a and a leakage inductance L_{sa} per phase are determined from an experimental testing investigation of the permanent magnet synchronous motor type EKM 90M-6 [2]. Their measured values are given below:

$$R_a = 0.1242 [\Omega]$$

$$L_{sa} = 2.2 [\text{mH}] \quad \Rightarrow \quad X_{sa} = 0.691 [\Omega]$$

Having available the parameters of the PMSM, the phasor diagram at rated operating conditions is constructed [17], and is found the rated loading angle to be:

$$\delta_n = 39.2 [\text{deg. el.}]$$

This value of the loading angle of the considered motor at rated operating conditions, will be determined by using numerical calculation of the steady-state characteristics via Finite Element Method.

5. Steady-State Characteristics

In the engineering practice, the intention of researchers, producers and users is always focussed to an estimation, analysis and evaluation of the electric machine behaviour. For that purpose, it is requested to have available performance characteristics, as accurate as possible.

The armature currents I and rotor positions θ along one pole pitch, are arbitrary selected. The rotation is supposed to be counter clockwise. The reference axis is selected to be the A -phase axis of the stator windings; the initial rotor position and $\theta=0$ deg. mech. is defined when stator A -axis and rotor N -pole axis (d -axis) are in accordance.

The PMSM is analysed at different operating conditions. Numerical calculations of the most relevant electro-magnetic and electromechanical quantities, based on the FEM post-processing results, are presented in the following subsections.

A. Magnetic Flux Density

The flux density \mathbf{B} is calculated from the basic relation used in the definition and introduction of the magnetic vector potential \mathbf{A} , in the computations of the magnetic field with Finite Element Method. The equation defining the link between A and B is:

$$\nabla \times \mathbf{A} = \mathbf{B} \quad (6)$$

Applying the numerical procedure for its solution in the air-gap domain, magnetic flux density B_g per pair of poles is computed. In Fig. 8, characteristics of the flux density, for three typical armature currents I (zero, half of the rated and rated) and different rotor positions θ along one pole pitch (0–60 deg. mech.) of the motor are presented.

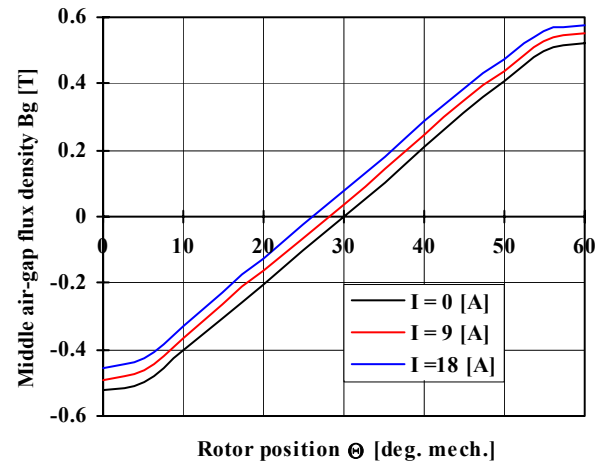


Fig. 8. Magnetic flux density characteristics $B_g = f(\theta, I)$

B. Magnetic Field Coenergy

In linear magnetic field problems, the magnetic energy W and the coenergy W' are equal. But, in the most cases, the problem is non-linear, so the coenergy is computed by using:

$$W' = \frac{1}{2} \int_V \mathbf{J} \cdot \mathbf{A} \, dV \quad (7)$$

In fact, this quantity has no physical explanation, but it is very useful for calculation of the electro-magneto-mechanical quantities when an energy concept is applied.

For the quasi static model of the PMSM, electromagnetic coenergy W' is calculated numerically from the following expression:

$$W'(\theta, I) = \int_0^I \psi(I, \theta) dI \quad | \quad \theta = \text{const} \quad (8)$$

The magnetic coenergy is calculated in dependence of the position of moving parts in the domain (the rotor) at arbitrary selected armature current. The calculated characteristics are presented in Fig. 9.

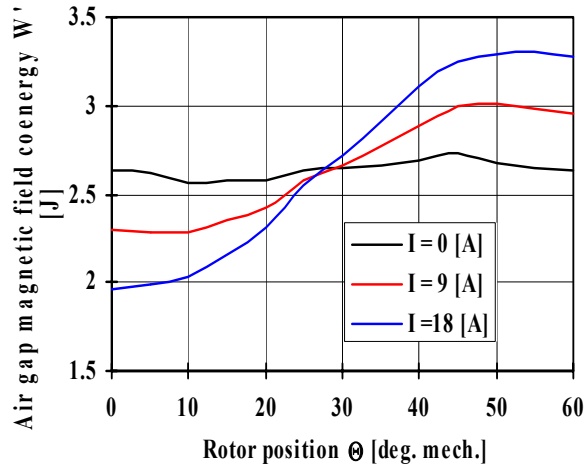


Fig. 9. Magnetic coenergy characteristics $W' = f(\theta, I)$

C. Electromagnetic Torque

The knowledge of the static torque characteristics is very important issue for carrying out analysis and evaluation of behaviour of electric motors. For calculation, various approaches exist. In theory, the torque is computed from the field solution in a number of various ways. Three approaches for calculation are in practical use: Flux-Current Method, the Maxwell Stress Method and Virtual Work Method. In this paper, the energy concept for numerical calculation of torque in the PMSM is applied.

The electromagnetic torque T_{em} is effected by the variation of the magnetic field coenergy in the air-gap domain, at virtual displacement of the rotor, while the armature current is forced to be constant.

The equation for calculation is derived in the form:

$$T_{em}(\theta, I) = \left. \frac{\partial W'(\theta, I)}{\partial \theta} \right|_{I=\text{cons.}} \quad (9)$$

The results of calculations, performed for rated current $I_n = 18$ A and $I_n/2 = 9$ A, are presented in Fig. 10.

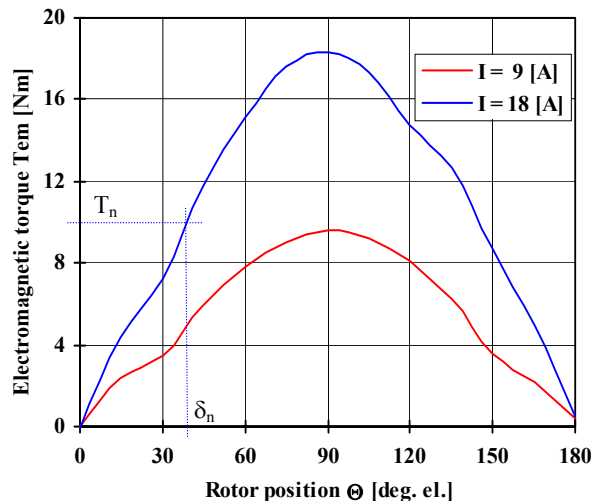


Fig. 10. Electromagnetic torque characteristics $T_{em} = f(\theta, I)$

7. Performance Evaluation of PMSM

The proposed methodology by implementing different methods for calculation of steady-state characteristics under different operating conditions, enables to carry out a deepened performance analysis of the permanent magnet synchronous motor, and an evaluation of its behaviour at various loads.

The Finite Element Analysis (FEA), based on the computations performed by using FEM, enables to evaluate the magnetic field properties in the whole investigated domain of the PMSM. The Figures 5. where the spatial distribution of the magnetic flux density is presented are showing the effect of the armature reaction field on the main PM excitation field, in the most natural and evident way. The same phenomenon is also recognised in Fig. 8., presented by the points where the magnetic flux density characteristics $B_g = f(\theta, I)$ are passing through zero values.

The particular FEM calculation is performed, and the inductances, i.e. the reactances along the d, q axes are determined. By using them, the phasor diagram of the PMSM under rated operating conditions is constructed; the rated loading angle is found to be $\delta_n = 39.2$ [deg.el.]. At the same time, the FEM results for the electromagnetic torque calculations, and the corresponding characteristics $T_{em} = f(\theta, I)$ presented in Figure 10., allow to determine numerically the rated loading angle, too. From the characteristic calculated at the rated armature current $I_n = 18$ [A], for the rated value of torque $T_{em} = 10$ [Nm] one can easily find almost the same value for $\delta_n = 39$ [deg.el.].

The performance characteristics of the considered PMSM are verified in two ways, depending on the available data. Some of the computed results are compared with the data obtained directly from the producer, and the others, with the experimentally obtained ones.

The armature windings' parameters are calculated in two ways: the resistance per phase R_a is calculated analytically; the leakage inductance L_{sa} per phase is determined by using three-dimensional magnetic field calculations in the whole investigated domain of the PMSM [2]. These parameters are also measured. Showing a very good agreement, they prove the applied methodologies as accurate and reliable.

As a verification of this work, here below is presented only a brief comparison of armature current I , at rated load torque 10 [Nm], determined by different methods:

$$\text{Calculated: } I_{calc} = 18 \text{ [A]}$$

$$\text{Measured: } I_{meas} = 17.6 \text{ [A]}$$

The above presented analysis is justifying the applied methodology for calculation performance characteristics of the PMSM type EKM 90M-6, as accurate and correct. Consequently, it can be recommended for similar calculations of any type of synchronous motors.

Conclusion

Finite Element Analysis is the best way for performance evaluation of the electrical machines in general. Presented approach, when applied on a surface mounted permanent magnet synchronous motor is proving the statement. Obviously, the phenomena outside of the magnetic core (i.e. end regions) are not showing an important influence, so the steady state characteristics, calculated by using Finite Element Method, in the 2D domain, are with the satisfactory accuracy.

This fact that the rated loading angle, determined with two different approaches is with the almost same value, is proving two important contributions presented in the paper: • first, the motor parameters calculated by FEM approach are quite accurate; • second, the use of the phasor diagram for determining the rated loading angle is proved to be correct. Knowing that the phasor diagram is drawn with FEM calculated values of the reactance X_d and X_q , the direct conclusion is that their values can be anticipated as accurate. On the other hand, the static electromagnetic torque characteristics are also determined by using FEM, but in a quite different procedure. Both procedures giving the same results are obviously correct.

Measured values and the testing results are the best way to confirm both analytically and numerically calculated parameters and characteristics. The mutual agreement presented in the paper, is proving the proposed approach and methodology as accurate.

The authors are foreseeing the future task is transient performance and dynamic analysis of the considered PMSM. This work and in particular the presented results, showing an excellent agreement, can be used as good basis and relevant guide.

References

- [1] S. Low and W. H. Lee, "Characteristics and Performance Analysis of a Permanent Magnet motor with a Multistacked Imbricated Rotor", *IEEE Trans. on Energy Conversion*, vol. EC-2, No. 3, October 1987, pp. 450-457.
- [2] L. Petkovska: "A Contribution to Analysis of Permanent Magnet Excitation Field Influence on Characteristics of an Electronically Operated Synchronous Motor, via 3D Magnetic Field Calculation", pp. 214, *PhD Thesis*, Skopje, Macedonia, 1991.
- [3] N. Esposito, A. Musolino, B. Tellini: Nonlinear Analysis of Electromagnetic Fields in Permanent Magnet Machines via an Integral formulation", in *Journal Studies in Applied electromagnetics and Mechanics*, Vol. 10, pp. 100-104, IOS Press, Ohmsha, Amsterdam, Netherlands, 1996.
- [4] L. Susnjic, Z. Haznadar: "Electromagnetic Analysis of a Radial-Flux Synchronous Machine Excited by Surface Mounted Permanent Magnets", *International Symposium on Electromagnetic Field Computations-ISEF'01*, pp. 211-214, Cracow, Poland, 2001.
- [5] L. Petkovska, M. Cundev, G. Cvetkovski and V. Sarac, "Different Aspects of Magnetic Field Computation in Electrical Machines", in *Book of Abstracts of the 10th International Symposium on Numerical Field Calculation in Electrical Engineering - IGTE'2002*, p.p. 73; on **CD** pp. 1-6, Graz, Austria, 2002.
- [6] L. Petkovska, M. Cundev, V. Sarac: "FEM analysis of Asymmetrical Magnetic Field in Electrical Machines", *Proceedings of the Second ACOMEN'2002 International Conference*, manuscript published on **CD** pp.1-10, Liege, Belgium, 2002.
- [7] L. Petkovska, M. Cundev, G. Cvetkovski, V. Stoilkov: "Modelling the Configuration of Electrical Machines for 3D Magnetic Field Calculation", in *Journal on Applied Electromagnetics, JBMSAEM '98*, Heron Press Applied Science Series, p.p. 45-50, Sofia, Bulgaria, 2000.
- [8] G. Cvetkovski, L. Petkovska, M.Cundev, V. Stoilkov: "3D Magnetic Field Calculation in Permanent Magnet Machines", in *Journal on Applied Electromagnetics, JBMSAEM '98*, Heron Press Applied Science Series, pp. 39-44, Sofia, Bulgaria, 2000.
- [9] G. Cvetkovski, L. Petkovska, M. Cundev: "PM Disc Motor Parameters Evaluation Using FEM Data", *Proceedings on the 6th International Symposium on Electric and Magnetic Fields - EMF'2003*, Symposium Reports, p.p. 191-194, Aachen, Germany, 2003.
- [10] V. Sarac, L. Petkovska, M. Cundev, "Non-linear Time Harmonic Analysis of Shaded-Pole Micromotor" *International Symposium on Electromagnetic Field Computations-ISEF'03*, vol. 1/2, pp. 137-142, Maribor, Slovenia, 2003.
- [11] Q. Zhao, Z. An, Z. Liu, R. Tang: "Analysis of Flux Leakage Coefficient of Permanent Magnet Synchronous Motor with U-shaped Magnets Rotor", *Proceedings of the 6th International conference on Electrical Machines and Systems - ICEMS'2003*, Vol. 1/2, pp. 56-58, Beijing, China, 2003.
- [12] D. Meeker, "Finite Element Method Magnetics - FEMM", *User's Manual, Ver. 4.0*, Foster-Miller, MA, USA, 2004.
- [13] C. Krause, O. Wasynchuk and S.D. Sudhoff, "Analysis of Electrical Machinery", book, IEEE Press, 2nd Edition, New York, USA, 1994.
- [14] S. J. Salon, "Finite Element Analysis of Electrical Machines," book, Kluwer Academic Publishers, Norwell, MA, USA, 1995.
- [15] Z. Kolondzovski and L. Petkovska, "Identification of a Synchronous Generator Parameters Via Finite Element Analysis", in *Book of Abstracts of the 11th International Symposium on Numerical Field Calculation in Electrical Engineering - IGTE'2004*, p.p. 96; on **CD** pp. 1-6, Seggauberg (Graz), Austria, 2004.
- [16] K. Shima, K. Ide and M. Takahashi, "Finite-Element Calculation of Leakage Inductances of a Saturated Salient-Pole Synchronous Machine with Damper Circuits," *IEEE Trans. On Energy Conversion*, vol. 17, No. 4, December 2002, pp. 463-470.
- [17] G. Cvetkovski, L. Petkovska and S. Gair, "Performance Analysis of a Permanent Magnet Disc Motor for Direct Electric Vehicle Drive", *Journal ELECTROMOTION*, Vol. 10, No. 3, July-September 2003, pp. 353-358.

Influencia de la Geometría del Rotor en la Corriente del Estator de MSIP(s)

J.A. Güemes Alonso, A.M. Iraolagoitia Iriondo

Departamento de Ingeniería Eléctrica
E.U.I.T.I., Universidad del País Vasco
Plaza de la Casilla, 3, 48012 Bilbao (España)
Telef.: +34 946014363, 946014367, fax: +34 946014300
e-mail: joseantonio.guemes@ehu.es, ana.iraolagoitia@ehu.es

Resumen. En este trabajo, se analiza la influencia del tamaño de los imanes en el comportamiento de un motor síncrono de imanes permanentes (MSIP) de baja velocidad, con los imanes montados en la superficie del rotor. Se comparan dos motores con distintas geometrías del rotor (modificación del tamaño de los imanes) e igual estator y se observa la influencia en las características principales de la máquina. Hemos comprobado que para un motor de 5 kW, al aumentar el volumen de los imanes en un 66 %, el valor de la corriente del estator se reduce en un 49 %. El estudio del comportamiento del motor se realiza utilizando el método de elementos finitos (MEF). El método constituye una aplicación industrial al diseño y modelado de este tipo de máquinas y puede ser útil para determinar fórmulas precisas para el cálculo de la corriente del estator, par, factor de potencia y rendimiento de la máquina, cuando se modifica el tamaño de los imanes.

Palabras llave. Imanes permanentes, método de elementos finitos, modelado, motor síncrono, simulación.

1. Introducción

Los motores de imanes permanentes de ca puede dividirse en dos grandes grupos: los motores brushless dc (NLDC) que tienen forma de onda de la fuerza electromotriz trapezoidal y los motores síncronos de imanes permanentes (MSIP) que tienen forma de onda de la fuerza electromotriz senoidal.

El interés de los MSIP(s) está creciendo en un amplio abanico de aplicaciones. Las razones principales del incremento de aplicaciones de los MSIP(s) son en primer lugar, la eficiencia y las bajas pérdidas del rotor y en segundo lugar, la reducción del precio de los imanes (NdFeB).

En términos generales, los MSIP(s) son preferibles a los motores asíncronos, en todas aquellas aplicaciones que requieran una velocidad constante con arranque suave y funcionamiento silencioso.

En ingeniería eléctrica, normalmente las máquinas eléctricas son representadas por un circuito equivalente. El conocimiento de los diferentes parámetros del circuito

equivalente de la máquina, nos permite conocer su comportamiento, bajo ciertas condiciones de funcionamiento, por aplicación de las leyes de los circuitos eléctricos.

El MEF, constituye una herramienta muy importante para los ingenieros eléctricos, en el análisis del comportamiento de máquinas eléctricas, al permitir conocer con un margen de error acotado, los diferentes parámetros de la máquina, así como su comportamiento en situaciones extremas de funcionamiento.

En el análisis por elementos finitos de motores síncronos de imanes permanentes, el primer paso es simular el comportamiento de la máquina “en reposo” (sin corriente por los devanados del estator), lo que nos permite conocer el valor de la “fuerza electromotriz” y estimar el valor de la corriente por los devanados del estator para la potencia útil de la máquina. En el valor de la “fuerza electromotriz”, influye de una forma notable la geometría del rotor y el tamaño de los imanes.

La optimización de la geometría del rotor es muy importante, dado que podemos conseguir el mismo par con distintos valores de la corriente por los devanados del estator, disminuyendo en consecuencia el precio del controlador del motor.

En los últimos años, se han publicado distintos trabajos en los que se estudia la influencia de la forma y tamaño de los imanes (geometría del rotor) en el: a) diseño de circuitos magnéticos [1], b) estudio de ruidos y vibraciones de motores [2], y c) comportamiento de motores eléctricos [3] – [6].

En este trabajo se comparan dos motores con distintas geometrías de rotor e igual estator y comprobamos su influencia en las características principales de la máquina.

De acuerdo con lo anterior, el objetivo del trabajo es observar cómo influye el tamaño de los imanes (modificación de la geometría del rotor) en las

características del motor. La simulación y el estudio del comportamiento de la máquina, se realiza utilizando el MEF..

El método propuesto, puede ser muy útil para determinar fórmulas precisas, de aplicación industrial, que permitan calcular la corriente del estator, par, factor de potencia y rendimiento de la máquina, cuando se modifica el tamaño de los imanes.

2. Método

La “fuerza electromotriz en reposo” y por fase, en los devanados del estator, puede determinarse por medio de la expresión:

$$E_q = \pi\sqrt{2}NfK_w\phi \quad (1)$$

Donde:

- E_q fuerza electromotriz inducida por el flujo de excitación del rotor (sin considerar la reacción de inducido);
- N número de espiras en serie por fase del devanado del estator;
- f frecuencia;
- K_w factor de devanado del estator;
- ϕ flujo máximo.

Considerando la relación existente entre el flujo y el vector potencial magnético A .

$$\phi = \oint A dl \quad (2)$$

Para modelos planos en dos dimensiones, la ecuación (1) puede ponerse en la forma:

$$E_q = 2\pi\sqrt{2}NfAP \quad (3)$$

Donde P es la profundidad del modelo (longitud del paquete de chapas).

Por otra parte, como es conocido, el par electromagnético de un motor síncrono trifásico de polos salientes puede determinarse por la ecuación:

$$T_e = \frac{3p}{\omega} [E_q I_q + (X_d - X_q) I_d I_q] \quad (4)$$

Donde:

- p número de pares de polos;
- ω velocidad angular;
- X_d reactancia directa;
- X_q reactancia en cuadratura;
- I_d intensidad directa;
- I_q intensidad en cuadratura.

Al primer término de la ecuación (4), se denomina “par alineado con los imanes” y al segundo “par de reluctancia”.

En los motores síncronos de imanes permanentes, con los imanes montados en la superficie del rotor, las reactancias directa y en cuadratura pueden admitirse iguales.

$$X_d = X_q = X_s \quad (5)$$

En estas condiciones el par de reluctancia es nulo y la ecuación (4) puede escribirse:

$$T_e = \frac{3p}{\omega} E_q I_q \quad (6)$$

De acuerdo con lo anterior, la potencia electromagnética de la máquina puede determinarse por medio de la expresión:

$$P_e = T_e \frac{2\pi n}{60} = 3E_q I_q \quad (7)$$

Donde n es la velocidad del motor en rpm.

Finalmente la potencia útil se calcula, restando a la potencia electromagnética, las pérdidas en el hierro y las pérdidas mecánicas.

Las pérdidas mecánicas se calculan en función de la velocidad del rotor y las pérdidas en el hierro a partir de la densidad de flujo magnético en los elementos del modelo de elementos finitos [7].

De la ecuación (7) observamos que la potencia de un motor síncrono de imanes permanentes, con los imanes montados en la superficie, la potencia útil depende de la corriente y la “fuerza electromotriz en reposo”. En consecuencia para conseguir un determinado valor de potencia/par de la máquina, puede ser interesante diseñar máquinas que tengan un alto valor de la “fuerza electromotriz en reposo”, disminuyendo de esta forma la corriente por los devanados del estator y en consecuencia reduciendo, previsiblemente la potencia y, el costo del dispositivo controlador del motor.

Los factores que influyen en el valor de la “fuerza electromotriz en reposo” (1), son el número de espiras, la frecuencia y el flujo. La frecuencia viene determinada por la velocidad de la máquina. A su vez, en el valor del flujo influye la geometría del estator, la longitud de entrehierro, la geometría del rotor y, la forma, tamaño y dirección de imantación de los imanes.

En este trabajo estudiamos como influye en las características de la máquina, el valor del flujo (modificando el volumen de los imanes) permaneciendo constante el número de espiras.

Respecto a la forma de los imanes es aconsejable que tengan la cara interior y, principalmente la exterior de forma circular (radio similar al del rotor), pero esto encarece notablemente su precio, por lo que utilizaremos imanes de sección rectangular.

3. Motor

Las características principales del motor objeto de estudio son:

- Motor trifásico
- Tensión de entrada del controlador: 400 V
- Frecuencia de la tensión del controlador: 50 Hz
- Frecuencia de la tensión del motor: 12.5 Hz
- Velocidad nominal (referida a 12.5 Hz): 125 rpm
- Número de imanes permanentes: 12; $p = 6$
- Número de ranuras del estator: 72
- Potencia útil: 5 kW
- Tipo de imanes: NdFeB.

La figura 1 muestra un cuarto de la geometría del motor.

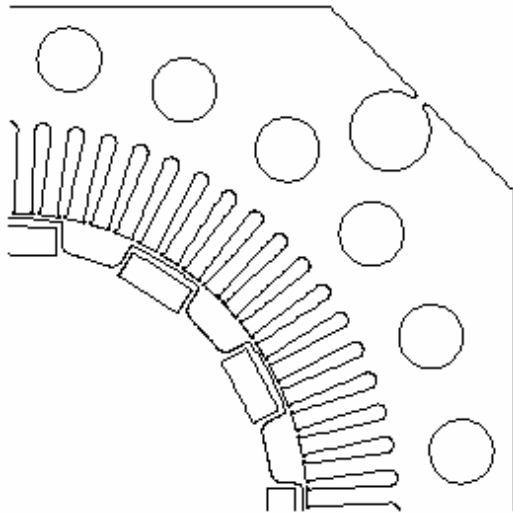


Fig. 1. Motor (rotor A)

Las características de par, potencia, rendimiento y factor de potencia del motor indicado, son comparadas con las del motor que se obtiene al sustituir el rotor por el mostrado en la figura 2 (permaneciendo constante la longitud de entrehierro). El volumen de los imanes se incrementa en un 66 %, (permaneciendo constante la altura y longitud de los imanes; el sentido de imantación y, el tipo de imanes).

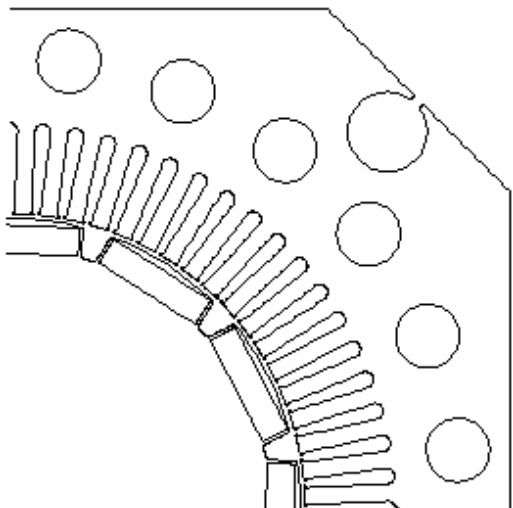


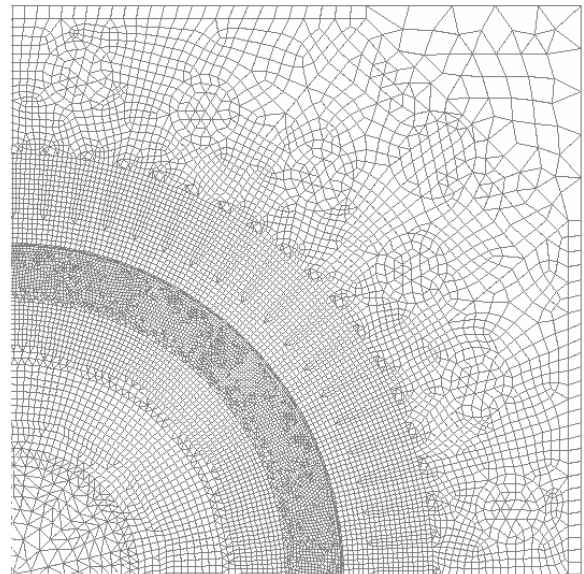
Fig. 2. Motor (rotor B)

La simulación y estudio del comportamiento de los motores (rotor A y rotor B), se realizan mediante el método de elementos finitos utilizando modelos en dos dimensiones.

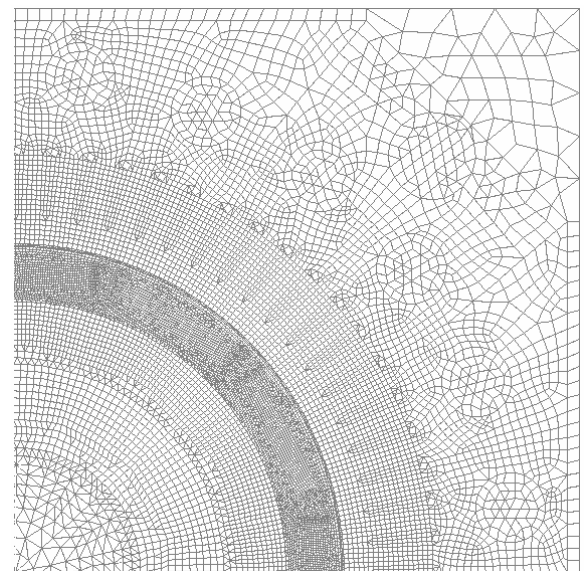
4. Modelo

El modelo de elementos finitos está constituido por una sección recta del motor y un espacio de aire que lo rodea.

La figura 3, muestra el mallado utilizado.



a) Rotor A



b) Rotor B

Fig. 3. Malla de elementos finitos (cuarto del modelo)

Las propiedades de los materiales se definen como sigue:

- Para el aire (entrehierro, comienzo ranuras del rotor y aire exterior) y el cobre (bobinado del estator) por medio de la permeabilidad magnética.

- Para el núcleo magnético del estator y rotor por medio de la curva BH, a la frecuencia de trabajo, del material con el que están construidas las chapas magnéticas.
- Los imanes por medio de su permeabilidad magnética y campo coercitivo en sus dos componentes (H_{CX} y H_{CY}).

Las excitaciones se definen por medio de las densidades de corriente en los devanados del estator.

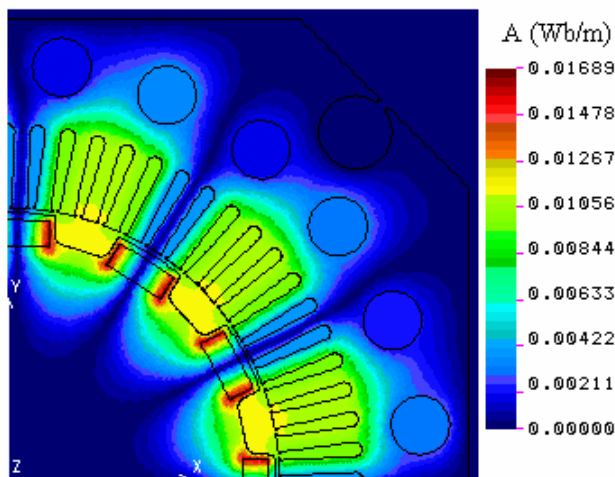
La condición de contorno es vector potencial magnético nulo en la periferia del modelo.

El tipo de análisis realizado es magnetostático.

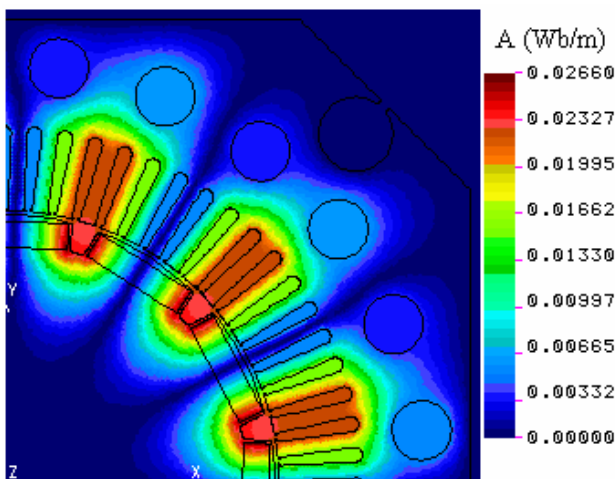
5. Análisis

En primer lugar se determina la “fuerza electromotriz” por fase, inducida en los bobinados del estator por los imanes (E_q), para lo cual se realiza la simulación del comportamiento de la máquina “en reposo”.

Una vez realizado el análisis se tiene los mapas de vector potencial magnético mostrados en la figura 4.



a) Rotor A



b) Rotor B

Fig. 4. Vector potencial magnético “en reposo”

Podemos observar que el vector potencial magnético, se incrementa de una forma importante en el motor con el rotor B respecto al motor con el rotor A. El valor de la “fuerza electromotriz” por fase, calculada por medio de la ecuación (3), es 110 V para el primer motor y 224 V para el segundo motor (incremento del 204 %).

La potencia electromagnética esperada de cada uno de los motores, para valores de $0 < I_q < 20$ A, calculada de acuerdo con la expresión (7), se muestra en la figura 5.

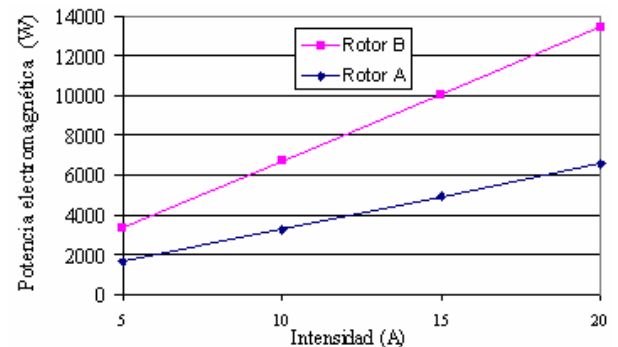


Fig. 5. Potencia electromagnética

Del gráfico anterior, se deduce que para una potencia útil de 5 kW y una vez estimadas las pérdidas mecánicas y en el hierro, la intensidad esperada es de 15,6 A para el primer motor y de 7,6 A para el segundo motor (reducción en el valor de la corriente del 49 %).

La figura 6, muestra el par electromagnético calculado de acuerdo con la expresión (6), para valores $0 < I_q < 20$ A.

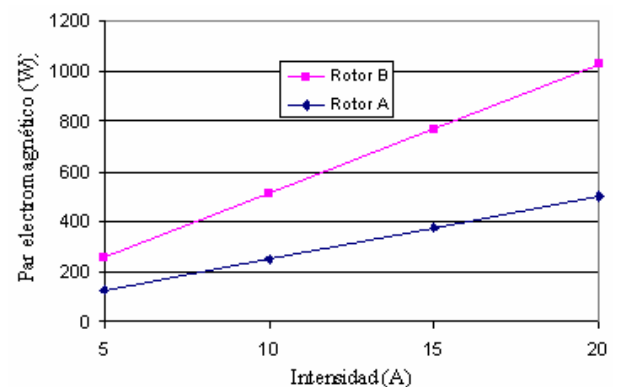


Fig. 6. Par electromagnético

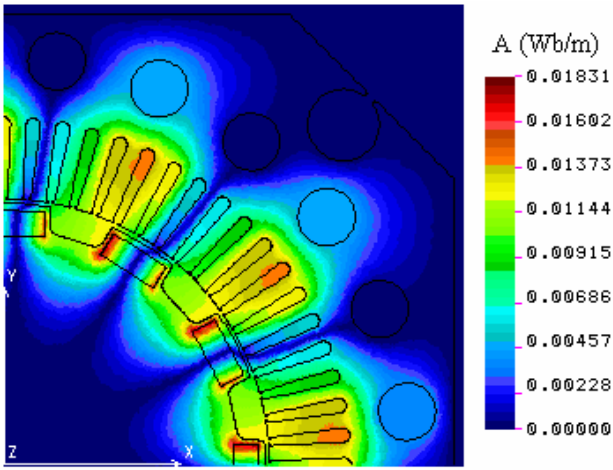
En segundo lugar, se ha simulado el comportamiento del motor (rotor A y B) para valores I_q de 5, 10, 15 y 20 A.

Una vez realizados los análisis para los valores de corriente indicados, se determina la fuerza electromotriz resultante en carga, por medio de la ecuación:

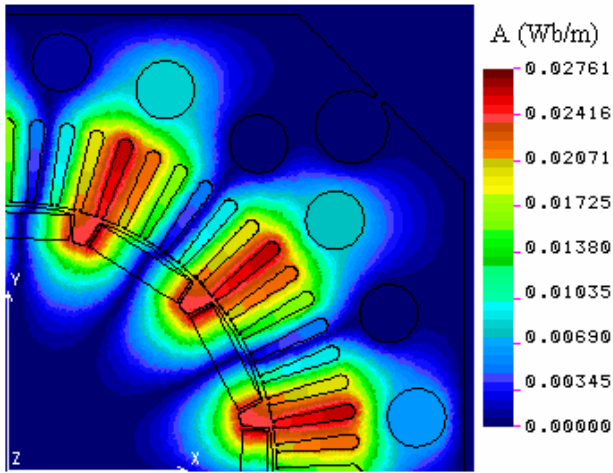
$$E_R = 2\pi\sqrt{2} N f A_R P \quad (8)$$

Donde A_R es el valor máximo del vector potencial magnético resultante (debido a los imanes y corriente por el estator).

La figura 7 muestra la distribución del vector potencial magnético, en ambos motores, para 15 A.



a) Rotor A



b) Rotor B

Fig. 7. Vector potencial magnético en carga ($I_q = 15$ A)

El ángulo de retraso del rotor respecto del campo resultante, se determina por medio de la ecuación:

$$\delta_\phi = \arccos \frac{\phi_q}{\phi_R} \quad (9)$$

Donde ϕ_R es el flujo resultante (debido a los imanes y corrientes).

La figura 8 muestra la variación del ángulo de retraso del rotor respecto del campo magnético resultante, en función de la corriente, para los dos motores analizados.

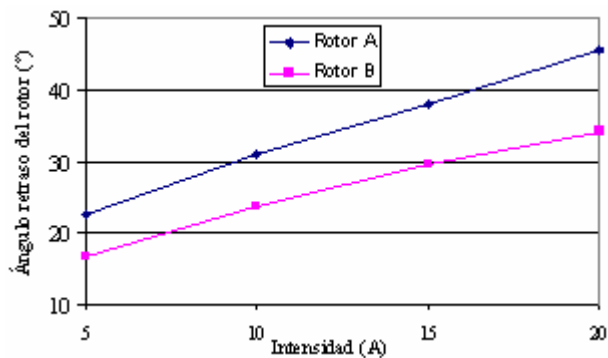


Fig. 8. Ángulo de retraso del rotor.

La reactancia síncrona, se determina por medio de la expresión:

$$X_s = X + X_{cb} \quad (10)$$

Donde:

- X reactancia de reacción de inducido más la reactancia de dispersión del paquete de chapas;
- X_{cb} reactancia de dispersión de cabezas de bobina.

La reactancia de dispersión de cabezas de bobina, puede calcularse por medio de la expresión [8]:

$$X_{cb} = 4\pi f \cdot p \cdot n_{pf} \cdot Z_n^2 \cdot \lambda_{cb} \cdot L \quad (11)$$

Donde:

- f frecuencia;
- p número de pares de polos;
- n_{pf} número de ranuras por fase y polo;
- Z_n número de conductores por ranura;
- λ_{cb} permeancia por unidad de longitud;
- L longitud del inducido.

Finalmente el factor de potencia se determina por la ecuación:

$$\cos \phi = \frac{E_q + RI_q}{U} \quad (12)$$

La figura 9 muestra la variación del factor de potencia, en función de la corriente, para cada uno de los motores estudiados.

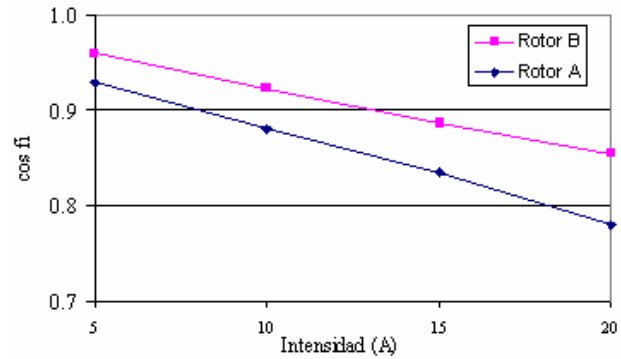


Fig. 9. Factor de potencia

Podemos observar que para la potencia deseada, el factor de potencia es 0,82 (muy bajo) para el primer motor (rotor A) y de 0,93 para el segundo motor (rotor B).

La tensión de alimentación por fase, es de 180 V para el primer motor y de 270 V para el segundo.

De acuerdo con lo indicado anteriormente podemos afirmar que para el mismo valor de potencia (5 kW), la intensidad esperada por los bobinados del estator en el motor con el rotor B es un 49,7 % menor que en el motor con el rotor A, mientras que el factor de potencia con el rotor B es un 13,5 % superior que con el rotor A.

6. Conclusiones

En este trabajo se ha simulado el comportamiento de un motor síncrono de imanes permanentes, observando como se modifican las características del motor al modificar el tamaño de los imanes.

Hemos verificado que en el prototipo inicial y para una potencia de 5 kW, el factor de potencia es muy bajo y la tensión de alimentación es inferior a los 400V.

Al incrementar el volumen de los imanes en un 66 % respecto de su tamaño en el prototipo inicial, la corriente del estator se reduce para la misma potencia en un 49 %.

El método expuesto en este trabajo puede ser muy útil para determinar fórmulas fiables al cálculo de la corriente del estator, factor de potencia y rendimiento de la máquina, cuando se modifica el tamaño de los imanes, la longitud de entrehierro o el número de espiras.

Referencias

- [1] T. Nakata y N. Takahashi, "New design method of permanent magnets by using finite element method", IEEE Trans. Magnetics, vol. 6, no. 6, pp. 2494-2497, noviembre 1983.
- [2] G.H. Jang y D.K. Lieu, "The effect of magnet geometry on electric motor vibration", IEEE Trans. Magnetics, vol. 27, no. 6, pp. 5202-5204, noviembre 1991.
- [3] D. Pavlik, V.K. Garg, J.R. Repp y J. Weiss, "A finite element technique for calculating the magnet sizes and inductances of permanent magnet machines", IEEE Trans. Energy Conversion, vol. 3, no. 1, pp. 116-122, marzo 1988.
- [4] Seong-Pyo Hong, Han-Sam Cho, Hae-Seok Lee y Hyun-Rae Cho, "Effect of the magnetization direction in permanent magnet on motor characteristics", IEEE Trans. Magnetics, vol. 35, no. 3, pp. 1321-1324, mayo 1999.
- [5] Maxime R. Dubois, Henk Polider y Jan A. Ferreira, "Magnet shaping for minimal magnet volume in machines", IEEE Trans. Magnetics, vol. 38, no. 5, pp. 2985-2987, septiembre 2002.
- [6] Yong Li, Jibin Zou, y Yongping Lu, "Optimum design of magnet shape in permanent-magnet synchronous motors", IEEE Trans. Magnetics, vol. 39, no. 6, pp. 3523-3526, noviembre 2003.
- [7] Jacek F. Gieras y Mitchell Wing, Permanent Magnet Motor Technology, Ed. Marcel Dekker, New York 2002, pp. 551-556.
- [8] J. Corrales Martín, Cálculo industrial de máquinas eléctricas. Tomo I, Marcombo Buxareu Editores. Barcelona 1982.

Determinación de la Reactancia de Dispersión de Cabezas de Bobina en MSIP(s)

J.A. Güemes Alonso, A.M. Iraolagoitia Iriondo

Departamento de Ingeniería Eléctrica
E.U.I.T.I., Universidad del País Vasco
Plaza de la Casilla, 3, 48012 Bilbao (España)
Telef.: +34 946014363, 946014367, fax: +34 946014300
e-mail: joseantonio.guemes@ehu.es, ana.iraolagoitia@ehu.es

Resumen. En este trabajo, se presenta un método de aproximación práctica para la determinación de la reactancia de dispersión de cabezas de bobina, aplicado a un motor síncrono de imanes permanentes (MSIP). El análisis del comportamiento del motor se realiza utilizando el método de elementos finitos (MEF) mediante modelos en tres dimensiones (3D). El flujo de cabezas de bobina puede ser calculado mediante modelos en dos dimensiones (2D), pero es necesario resolver un gran número de modelos. En el trabajo se describe un método para calcular la reactancia de dispersión de cabezas de bobina comparando la energía calculada en un modelo en 3D completo (incluye a las cabezas de bobina), con la energía calculada en un modelo en 3D sin cabezas de bobina y, con la energía calculada en un modelo en 2D. El método propuesto puede utilizarse para determinar ecuaciones de uso industrial aplicadas al cálculo de la reactancia de dispersión de cabezas de bobina. Los resultados obtenidos indican que los valores de las reactancias de dispersión de las cabezas de bobina son algo mayores que los obtenidos por un cálculo analítico.

Palabras llave. Imanes permanentes, método de elementos finitos, modelado, motor síncrono, reactancia de cabezas de bobina, simulación.

1. Introducción

El gran desarrollo de las aleaciones de alto magnetismo ha hecho posible que los motores de imanes permanentes (MIP) sean hoy día una alternativa muy interesante.

En los últimos años se han desarrollado varias familias de imanes permanentes, con propiedades magnéticas y físicas muy destacables. Los tipos de imanes permanentes más utilizados en la actualidad para el caso de máquinas eléctricas, son los imanes de tierras raras de Neodimio Hierro Boro (NdFeB).

Los MIP de corriente alterna son semejantes a los motores síncronos convencionales en los que el devanado de campo giratorio se sustituye por imanes permanentes. Si la forma de la onda de la tensión inducida es senoidal se denominan “motores síncronos de imanes permanentes” (MSIP), cuando la forma de la onda es trapezoidal son conocidos como “motores cc sin

escobillas o brushless dc” [1], esta terminología es debida a la semejanza con las características de los motores de corriente continua.

El interés de los MSIP(s) está creciendo en un amplio abanico de aplicaciones. Las razones principales de este incremento son en primer lugar la eficiencia y en segundo lugar la reducción del precio de los imanes (NdFeB).

En términos generales, los MSIP(s) son preferibles a los motores asíncronos, en todas aquellas aplicaciones que requieran una velocidad constante, arranque suave y funcionamiento silencioso.

El MEF es un procedimiento de análisis matemático que aproxima los valores de las magnitudes físicas, que pueden describirse con ecuaciones diferenciales válidas en una determinada región. Inicialmente se aplicó sobre todo al análisis mecánico, pero desde hace unas décadas se viene utilizando con éxito en el área de ingeniería eléctrica, y particularmente en el estudio de máquinas eléctricas rotativas.

El uso del MEF como herramienta de cálculo y simulación durante el proceso de diseño de un motor eléctrico, permite por una parte, conocer su comportamiento y, por otra, modelarlo por medio de un circuito equivalente.

En ingeniería eléctrica, normalmente las máquinas eléctricas son representadas por un circuito equivalente. El conocimiento de los diferentes parámetros del circuito equivalente de la máquina, nos permite conocer su comportamiento, bajo ciertas condiciones de funcionamiento, por aplicación de las leyes de los circuitos eléctricos.

Un parámetro importante del circuito equivalente de un MSIP es la reactancia síncrona. Como es conocido, dicha reactancia es la suma de la reactancia de reacción de inducido, la reactancia de dispersión del núcleo y la reactancia de dispersión de cabezas de bobina

La reactancia de reacción de inducido y la reactancia de dispersión del núcleo pueden calcularse simulando el comportamiento del motor mediante modelos en 2D (en vacío y en carga)

Considerando que en las zonas de cabezas de bobina, el flujo magnético se canaliza principalmente por el aire, armadura y carcasa del motor y que las cabezas de bobina están formadas por una parte recta y otra circular concéntrica con el eje, la reactancia de cabezas de bobina se podría calcular por medio de modelos en 2D. Primero se analiza la parte recta de las cabezas con un modelo plano 2D y posteriormente los tramos circulares mediante modelos 2D axisimétricos. Este método de análisis necesita simular un gran número de modelos 2D axisimétricos porque en cada tramo circular el número de conductores y corrientes es diferente.

El desarrollo de los paquetes informáticos de elementos finitos y la mayor potencia de los actuales ordenadores personales, permiten resolver sistemas con mayor número de ecuaciones y más rápidamente que hace unos pocos años. Con la técnica de modelado sólido en 3D, se pueden resolver geometrías complejas.

El objetivo fundamental de este trabajo es determinar las reactancias de dispersión de cabezas de bobina, de un motor síncrono de imanes permanentes. La simulación y estudio del comportamiento del motor se realiza mediante el MEF utilizando modelos sólidos en 3D.

La mayoría de los estudios realizados utilizando el MEF para la simulación y análisis del comportamiento de las máquinas eléctricas en general y, de los MSIP(s) en particular, son en dos dimensiones, siendo relativamente pocos los realizados en tres dimensiones. Entre las publicaciones de estos últimos años podemos citar el trabajo de Demenko [2], que calcula las inductancias de cabezas de bobina de un motor de imanes permanentes utilizando el método del “elemento lado”, mediante simulaciones en 2D y 3D y el trabajo de Engström [3], que examina el efecto de la dispersión en máquinas de imanes permanentes con especial atención a la producción del par, para el caso de máquinas sin ranuras, comparando los resultados obtenidos en simulaciones mediante modelos en 3D y en 2D.

El método propuesto, se basa en comparar la energía obtenida para un modelo completo en 3D (incluye las cabezas de bobina), con la energía calculada, por una parte, para un modelo sin cabezas de bobina en 3D y, por otra, para un modelo en 2D. Los resultados de la reactancia de cabezas de bobina calculados a partir de las energías anteriormente citadas, se comparan con el valor determinado a partir de la energía para un modelo en 3D, donde sólo se simula el comportamiento de las cabezas de bobina, y también con el valor obtenido por un cálculo analítico.

El método presentado en este trabajo, puede ser muy útil para determinar fórmulas precisas, de aplicación industrial, al cálculo de la reactancia de cabezas de

bobina, en función de la geometría de las cabezas de bobina.

2. Descripción del motor

Las características principales del motor objeto de estudio son:

- Motor trifásico
- Tensión de alimentación del controlador: 400 V
- Frecuencia de la tensión del controlador: 50 Hz
- Frecuencia de la tensión del motor: 12.5 Hz
- Velocidad nominal (referida a 12.5 Hz): 125 rpm
- Número de imanes permanentes: 12; $p = 6$
- Número de ranuras del estator: 72
- Potencia útil: 5 kW
- Tipo de imanes; NdFeB.

La figura 1 muestra un cuarto de la geometría del motor.

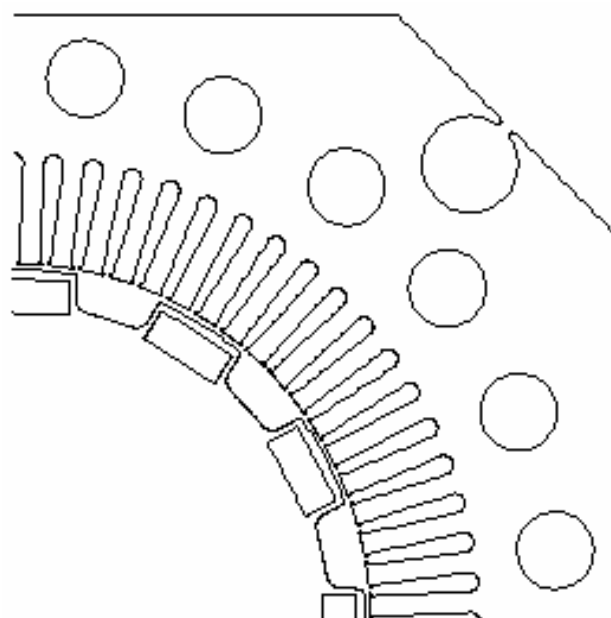


Fig. 1. Motor

3. Modelos

Se utilizan dos tipos de modelos de elementos finitos, en 3D y en 2D.

A. Modelos en 3D

Dada las simetrías existentes, los modelos están constituidos por 120° de la mitad del motor y un espacio de aire rodeando a las cabezas de bobina.

Se utilizan tres modelos: completo, sin cabezas de bobina y sólo cabezas de bobina.

En las figuras 2, 3 y 4, se muestran respectivamente los tres modelos citados.

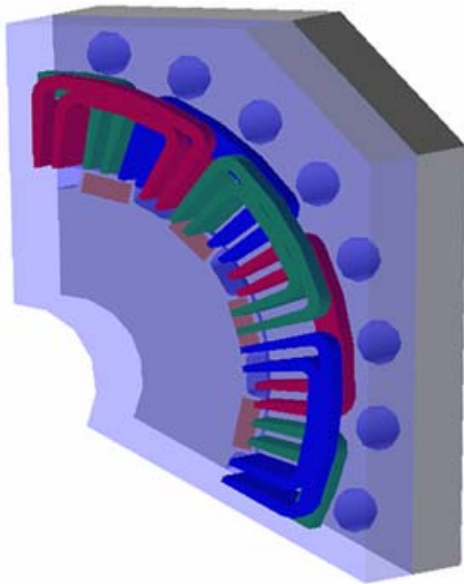


Fig. 2. Modelo completo

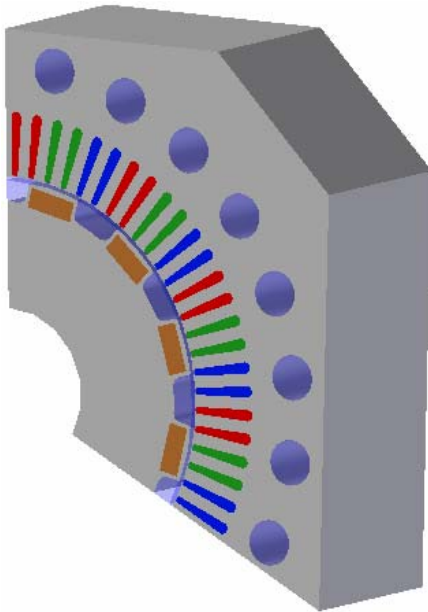


Fig. 3. Modelo sin cabezas de bobina

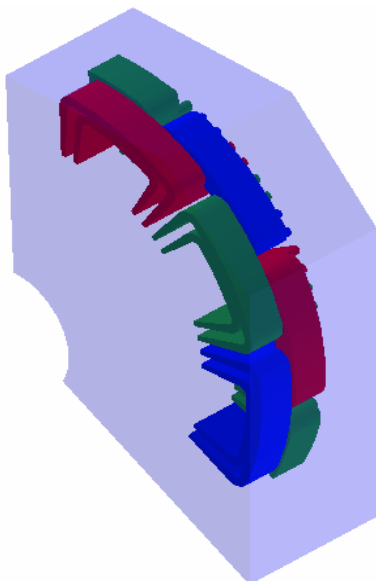


Fig. 4. Modelo sólo cabezas de bobina

El mallado se ha realizado con elementos tetraedros de 4 nodos, prestando especial atención a las zonas críticas (entrehierro y zonas próximas). En la figura 5 se muestra, a modo de ejemplo, el mallado utilizado para el modelo completo.

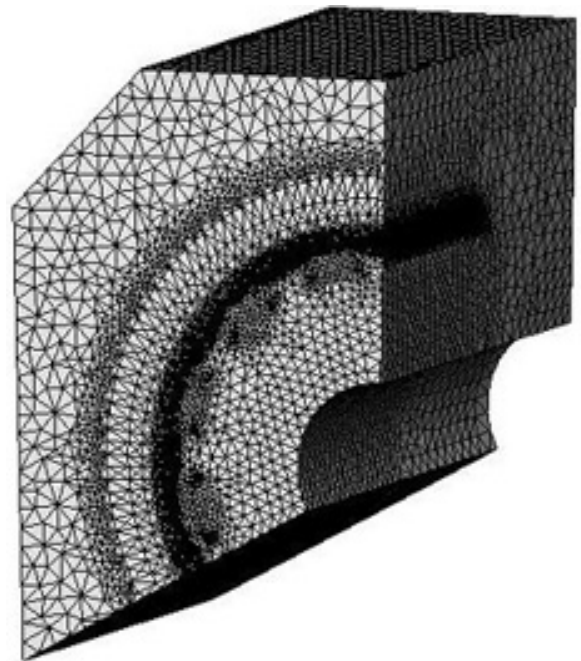


Fig. 5. Malla de elementos finitos en 3D

Las propiedades de los materiales se definen como sigue:

- Para el aire (entrehierro, comienzo ranuras del rotor y aire exterior) y el cobre (bobinado del estator) por medio de la permeabilidad magnética.
- Para el núcleo magnético del estator y rotor por medio de la curva BH, a la frecuencia de trabajo, del material con el que están construidas las chapas magnéticas.
- Los imanes por medio de su permeabilidad magnética y campo coercitivo en sus dos componentes (H_{CX} y H_{CY}).

Las excitaciones se definen por medio de la corriente en cada uno de los devanados del estator.

La condición de contorno es flujo tangencial en el exterior del motor.

B. Modelo en 2D

El modelo de elementos finitos está constituido por una sección recta transversal del motor y un espacio de aire que lo rodea.

Las excitaciones se definen por medio de las densidades de corriente en los devanados del estator.

Las propiedades de los materiales se definen igual que en el modelo en 3D.

La condición de contorno es vector potencial magnético nulo en la periferia del modelo.

La figura 6, muestra el mallado utilizado.

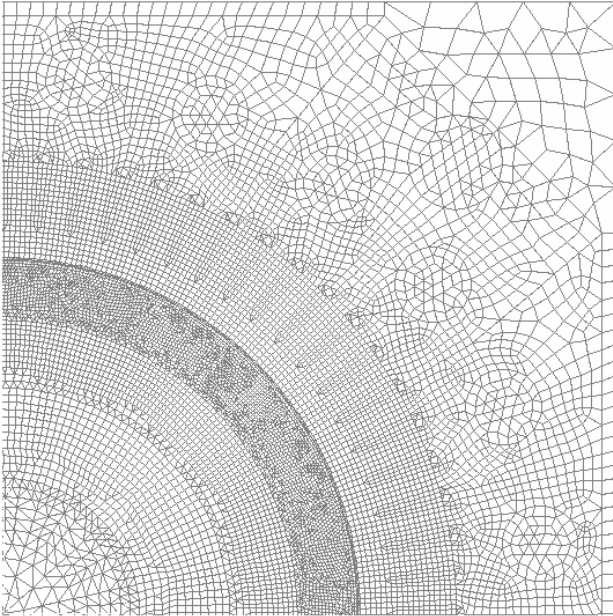


Fig. 6. Malla de elementos finitos en 2D (cuarto del modelo)

4. Metodología y análisis

Los pasos seguidos en el estudio que se presenta en este trabajo, son los siguientes:

- 1) Simular el comportamiento del motor mediante los cuatro modelos descritos anteriormente (completo en 3D, sin cabezas de bobina en 3D, sin cabezas en 2D y sólo cabezas de bobina en 3D). Cálculo de la energía magnética de cada uno de los modelos.
- 2) Determinar la energía de dispersión de las cabezas de bobina por medio de las energías obtenidas en los distintos modelos.
- 3) Calcular la reactancia de dispersión de cabezas de bobina a partir de las energías de dispersión de las cabezas obtenidas en el paso anterior.
- 4) Determinar la reactancia de dispersión de cabezas de bobina por un método analítico.
- 5) Comparar los resultados.

A. Método de elementos finitos

En todos los modelos, el análisis del comportamiento del motor se ha realizado para la situación correspondiente al funcionamiento de plena carga y considerando corriente por el estator transversal.

Las figuras 7 y 8 muestran respectivamente la distribución de la densidad de flujo magnético obtenida en la simulación del modelo completo en 3D, y en el modelo sin cabezas de bobina 2D.

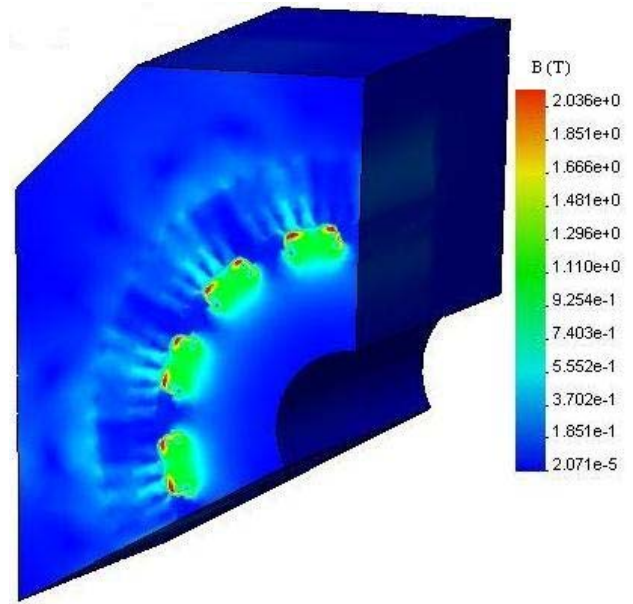


Fig. 7. Modelo completo en 3D

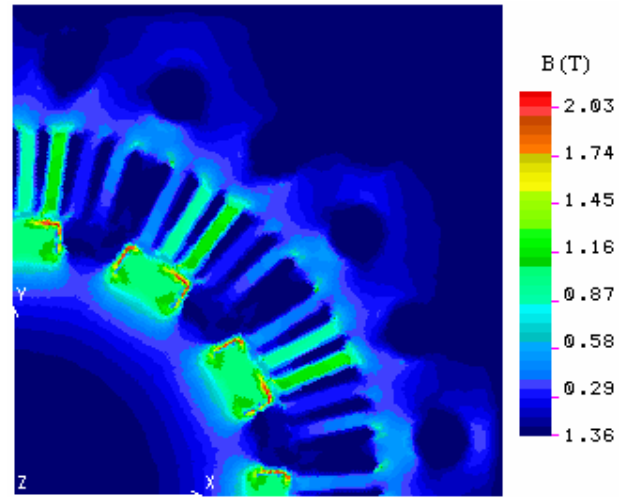


Fig. 8. Modelo en 2D

La energía de cabezas de bobina, teniendo en cuenta que los modelos en 3D analizados representan 1/6 del motor, se calcula con las siguientes ecuaciones:

$$W_{cb1} = 6(W_{c3D} - W_{n3D}) \quad (1)$$

$$W_{cb2} = 6W_{c3D} - W_{n2D} \cdot P \quad (2)$$

$$W_{cb3} = 6W_{s3D} \quad (3)$$

Donde:

- W_{cb1} energía de cabezas de bobina calculada por el primer procedimiento;
- W_{cb2} energía de cabezas de bobina calculada por el segundo procedimiento;
- W_{cb1} energía de cabezas de bobina calculada por el tercer procedimiento;
- W_{c3D} energía calculada en el modelo completo en 3D;
- W_{n3D} energía calculada en el modelo sin cabezas en 3D;
- W_{n2D} energía calculada en el modelo en 2D;

- P Profundidad del modelo (longitud del paquete de chapas).
- W_{s3D} energía calculada en el modelo en 3D de sólo cabezas de bobina.

La reactancia de dispersión por fase de las cabezas de bobina, se determina por medio de la siguiente expresión:

$$X_{cb} = \frac{4\pi f W_{cb}}{3I^2} \quad (4)$$

Donde:

- f frecuencia;
- I Corriente por fase.

B. Método analítico

Con el propósito de comparar los resultados obtenidos por el método propuesto, se ha calculado la reactancia de dispersión de las cabezas de bobina utilizando un cálculo analítico [4].

Para ello, primeramente se determina la permeancia por unidad de longitud de las cabezas de bobina a partir de ecuación:

$$\lambda_{cb} = 4\pi 10^{-7} n_{pf} \left(0,6 \frac{L_{cb}}{L} - 0,3 \frac{\gamma n \tau_m}{L} \right) \quad (5)$$

Donde:

- λ_{cb} permeancia por unidad de longitud;
- n_{pf} número de ranuras por polo y fase
- L_{cb} longitud media de una cabeza de bobina;
- L longitud del inducido;
- γn paso de bobina en ranuras;
- τ_m paso medio de ranura;

La reactancia de cabezas de bobina, puede calcularse por medio de la expresión:

$$X_{cb} = 4\pi f \cdot p \cdot n_{pf} \cdot Z_n^2 \cdot \lambda_{cb} \cdot L \quad (6)$$

Donde:

- p número de pares de polos;
- Z_n número de conductores por ranura;

5. Resultados

Una vez realizados los análisis para los distintos modelos, se tienen los resultados mostrados en la tabla I

TABLA I.- Energía magnética de los modelos

Modelo	Energía (J)
Completo en 3D (W_{c3D})	85,2798
Sin cabezas en 3D (W_{n3D})	85,1338
Sin cabezas en 2D (W_{n2D})	2025,2342
Sólo cabezas de bobina en 3D (W_{s3D})	0,042776

La tabla II muestra la energía de dispersión de cabezas de bobina calculada por cada uno de los procedimientos previamente descritos (1), (2), (3).

TABLA II.- Energía de cabezas de bobina

Procedimiento	Energía (J)
1) Modelo completo y sin cabezas de bobina (W_{cb1})	0,8762
2) Modelo completo y en 2D (W_{cb2})	5,3704
3) Modelo sólo cabezas (W_{cb3})	0,2566

Finalmente, la tabla III muestra el valor de la reactancia de dispersión de cabezas, calculada por medio de la energía (4) y la calculada por el método analítico (6).

TABLA III.- Reactancia de dispersión de cabezas de bobina

Procedimiento	X_{cb} (Ω)
1) Modelo completo y sin cabezas de bobina (1) y (4)	0,569
2) Modelo completo y en 2D (2) y (4)	3,487
3) Modelo sólo cabezas (3) y (4)	0,166
4) Cálculo analítico (6)	0,439

De los resultados obtenidos podemos indicar que:

- 1) El primer procedimiento de cálculo, ofrece un valor superior (30%) al calculado por el método analítico. Dado que no se pudo contrastar los resultados experimentalmente no podemos afirmar cual de estos valores es la mejor aproximación.
- 2) Con el segundo procedimiento se obtienen valores muy altos, por lo que no parece apropiado. La causa puede ser como consecuencia de comparar dos modelos con formas y tamaños de elementos muy distintas.
- 3) El valor obtenido con los resultados de la simulación del modelo que solamente recoge las cabezas de bobina, es muy pequeño, ya que no tiene en cuenta que parte del flujo de dispersión de las cabezas se cierra a través del núcleo. De lo que se deduce que este tercer procedimiento, a pesar de que sería el más sencillo de aplicar y tener un tiempo de resolución menor, tampoco sería válido al cometer importantes errores.

6. Conclusiones

En este trabajo se ha simulado el comportamiento de un MSIP mediante un modelo de elementos finitos en 3D.

Se han propuesto distintos procedimientos para el cálculo de la reactancia de dispersión de cabezas de bobina.

El procedimiento más adecuado es el primero, obteniendo la reactancia de cabezas de bobina a partir del modelo completo y el modelo sin cabezas de bobina en 3D.

El cálculo de la reactancia de dispersión de cabezas de bobina a partir del modelo de sólo cabezas de bobina, no es adecuado dado que conduce a errores importantes.

El método puede ser útil para determinar formulas precisas que permitan calcular la reactancia de dispersión de cabezas de bobina en función de la forma del bobinado.

Referencias

- [1] J. Gieras and M. Wing, "Permanent magnet motor technology". Ed. Marcel Dekker, Inc. New York, 2002.
- [2] A. Demenko, L. Nowak and W. Pietrwski, "Calculation of end-turn leakage inductances of electrical machines using the edge element method". The International Journal for Computation and Mathematics in Electrical and Electronic Engineering, vol 20, no 1, pp 132-139, 2001.
- [3] J. Engström, "Effects of axial Leakage on torque performance in PM machines", Proceedings of the International Conference on Electrical Machines, ICEM 2002, Brugge - Belgium, 2002
- [4] J. Corrales Martín, "Cálculo industrial de máquinas eléctricas, ed. Marcombo Buxareu Editores, Barcelona 1982.
- [5] Chang-Chou Hwang and Y. H. Cho, "Effects of leakage flux on magnetic fields on interior permanent magnet synchronous motors". IEEE Trans. Magnetics, vol 37, pp. 3021-3024, 2001.

Anàlisi d'Elements Finites Aplicat a un Motor Síncron d'Imants Permanents

D. Saltiveri
UNIVERSITAT POLITÈCNICA DE CATALUNYA
DEPARTAMENT D'ELECTRÒNICA
E-Mail: saltive@eel.upc.es

Abstracte

Aquest treball estudia la determinació de les característiques en regim permanent d'un motor síncron amb imants permanents superficials, mitjançant el mètode dels elements finits (FEM). Primerament, es presenta la distribució del camp magnètic del motor síncron d'imants permanents (PMSM) en estudi, treballant en buit i en condicions nominals. A partir del càlcul de l'energia magnètica emmagatzemada es calculen les inductàncies als eixos directe i en quadratura. Finalment, es representen gràficament el parell electromagnètic i el parell de "cogging" del motor respecte l'angle de càrrega. Quan es comparen els resultats calculats respecte als obtinguts experimentalment, es demostra que aquest mètode de càlcul es fiable.

1. Introducció

El motor trifàsic d'alterna d'imants permanents, funcionant com un motor síncron convencional, ha tingut un interès creixent en les darreres dues dècades. El recent desenvolupament d'imants d'alta energia, ha ampliat significativament els seus camps d'aplicació. La inserció d'imants permanents de SmCo o NdFeB al rotor dels motors síncrons per crear l'excitació, ha suposat innovacions en el disseny i anàlisis dels PMSM. En aquest treball, es determinen i analitzen els paràmetres i les característiques d'un motor síncron d'imants permanents superficials.

Així doncs, la tasca principal és determinar amb la màxima precisió les característiques en regim permanent del PMSM, i per això s'han de calcular els seus paràmetres de la manera més exacta possible, mitjançant el mètode dels elements finits.

El programa utilitzat per realitzar l'anàlisi d'elements finits (FEA) és el FEMM 3.4 del Dr. David Meeker. Aquest és un software de lliure distribució i es pot trobar a la pàgina web: <http://femm.foster-miller.net>.

2. Motor síncron d'imants permanents

El PMSM estudiat és un motor comercial tipus 142UMC30 de Control Techniques, les seves característiques es presenten a les Taules I i II. El motor s'alimenta a partir de tres corrents sinusoidals i al rotor es troben sis pols d'imants permanents de NdFeB muntats superficialment. A la Fig. 1 es pot veure una vista alçada d'aquest motor instal·lat en una bancada experimental.

Taula I: Especificacions constructives del PMSM

Inèrcia	0,00205 kg·m ²
Longitud del rotor	92,5 mm
Ranures al estator	18
Conductors per ranura	40
Material magnètic	NdFeB
Remanència magnètica	1,23 T
Coercivitat magnètica	915 kA/m

Taula II: Especificacions elèctriques del PMSM

Tipus de connexió	Estrella
Número de pols	6
Potència nominal	3,83 kW
Constant de voltatge (K _e)	0,098 V(rms)/rpm
Constant de parell (K _t)	1,6 N·m/A(rms)
Corrent nominal	7,625 A(rms)
Velocitat nominal	3000 rpm
Parell nominal	12,2 N·m



Fig. 1. Vista alçada del PMSM Control Techniques 142UMC30

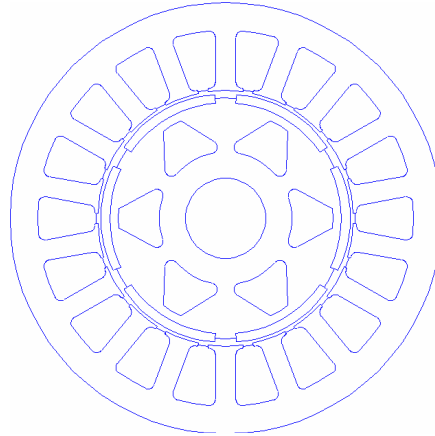


Fig. 2. Secció transversal del PMSM Control Techniques 142UMC30

3. Càlcul del PMSM amb el mètode d'elements finits

El mètode d'elements finits s'ha utilitzat extensivament en el càlcul numèric del camp magnètic de màquines elèctriques en general. La possibilitat de calcular les característiques electromagnètiques i electromecàniques a partir dels resultats obtinguts, justifica la utilització de l'anàlisi d'elements finits. Molts investigadors d'arreu del món treballen en aquest camp i han publicat molts papers amb aquest topic. Existeixen molts paquets de software per realitzar el FEA, alguns són generals i altres estan més orientats a màquines elèctriques. Els resultats presentats en aquest treball han estat obtinguts utilitzant el programa FEMM.

En el primer pas, considerat com etapa de preprocés, es dibuixa la secció transversal del PMSM i es defineix la malla d'elements finits amb una densitat apropiada. Normalment, la mida dels triangles de la malla es deixa escollir automàticament pel programa, encara que en alguns casos ens interessa seleccionar manualment una mida més petita per obtenir uns resultats més acurats, com en el cas de l'entreferro de la màquina. En el FEA realitzat per obtenir la distribució del camp magnètic, la malla esta formada per 32482 nodes i 64808 elements, distribuïts per tota la secció transversal del PMSM, com es pot veure a la Fig. 3.

En el preprocessador, anomenat *femm editor*, s'introdueixen totes les dades requerides per realitzar l'anàlisi: la secció transversal exacta del nucli magnètic de l'estator i del rotor, els materials del PMSM (imants permanents, coure, aire, acer) i les seves característiques (corba de magnetització, permeabilitat magnètica, coercivitat magnètica, conductivitat elèctrica), les condicions de contorn de la regió a analitzar i el corrent que circula pels bobinats de la màquina. Com s'ha dibuixat la secció transversal completa del motor, només s'aplica la condició de contorn de primer ordre de Dirichlet ($A=0$) al cercle més extern de l'estator.

Una vegada acabada l'etapa de preprocés, el model del PMSM es troba a punt per ser analitzat. La solució del problema s'aconsegueix executant el "solver" del FEMM, així

s'obtenen els valors del potencial vector magnètic a cada node. Després es poden fer servir aquests resultats per diferents propòsits. Mitjançant el postprocessador del FEMM, anomenat *femm viewer*, es possible realitzar els càlculs i les representacions gràfiques de les variables electromagnètiques i electromecàniques més importants.

A. Distribució del camp magnètic

Una de les millors maneres d'entendre el funcionament de qualsevol motor es veure la distribució del seu camp magnètic. La representació gràfica dels resultats obtinguts mitjançant FEM, ens proporciona la distribució del flux magnètic a la secció transversal del motor síncron d'imants permanents estudiat. Una part dels resultats més interessants es presenten a continuació.

La distribució del camp magnètic al PMSM es presenta a la Fig. 3, pels dos següents règims: (a) treballant en buit, és a dir, corrent d'armadura zero, per tant el camp magnètic obtingut és el que prové únicament dels imants; (b) treballant en condicions nominals, és a dir, parell nominal ($T_N = 12,2 \text{ N}\cdot\text{m}$) amb corrent nominal als bobinats de l'estator ($I_N = 7,625 \text{ A}$).

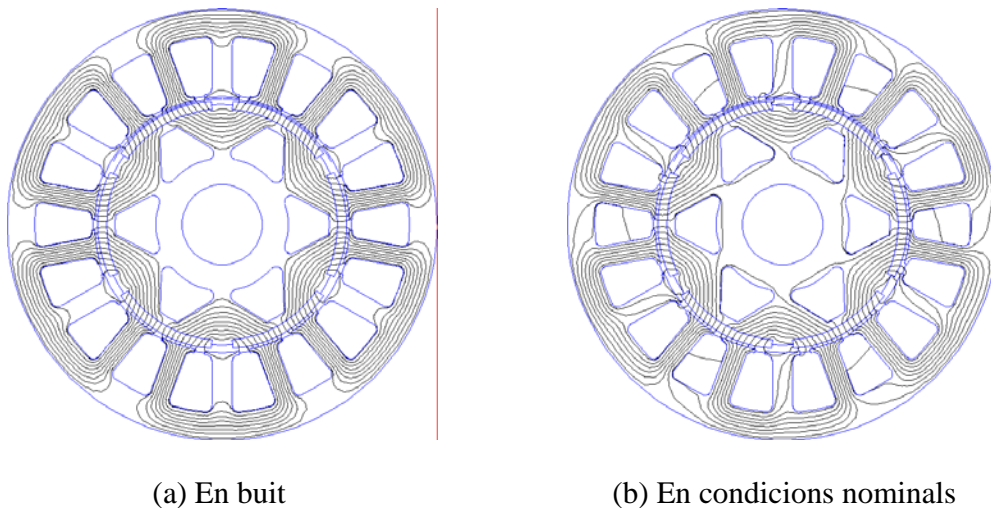


Fig. 3. Representació del flux magnètic a la secció transversal del PMSM

El postprocessador del FEMM també ens permet dibuixar la distribució espacial de la densitat de flux magnètic al llarg d'una línia escollida. A la Fig. 4. es representa la seva distribució al llarg de 120° mecànics (360° elèctrics) d'entreferro.

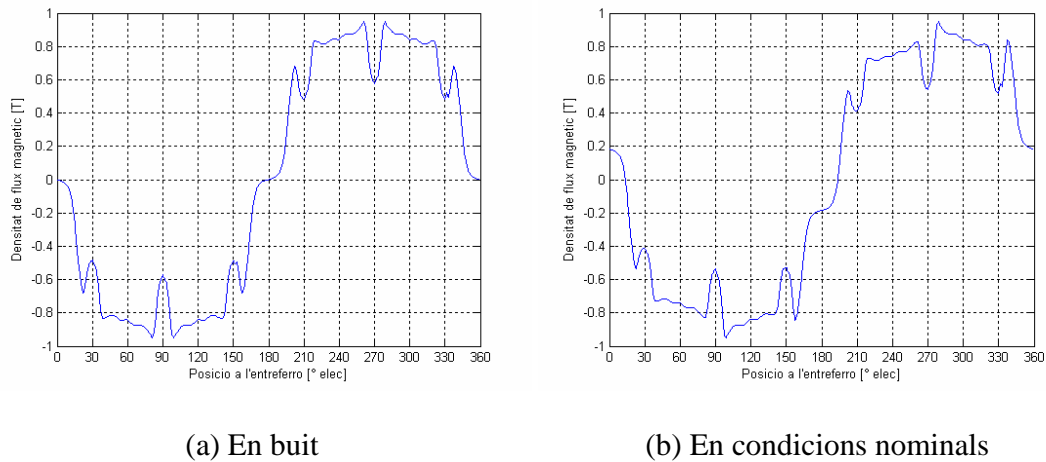


Fig. 4. Representació del flux magnètic a la secció transversal del PMSM

Mitjançant aquests diagrames es poden analitzar en profunditat les propietats del camp magnètic a l'entreferro de la màquina, tenint en compte la seva intensitat i forma. A la Fig. 4b es pot apreciar l'efecte de la reacció d'armadura, quan el motor síncron d'imants permanents treballa amb càrrega. A les figures també es pot apreciar l'efecte de les dents de l'estator sobre la distribució del camp magnètic.

B. Càlcul de les inductàncies

És molt important calcular el més acuradament possible els valors dels paràmetres del PMSM. Els més significatius són les inductàncies en l'eix directe (L_d) i en l'eix en quadratura (L_q), ja que d'elles depenen les reactàncies síncrones (X_d i X_q). Aquests són els paràmetres més importants per analitzar la performance en règim permanent i/o dinàmic del PMSM.

El càlcul numèric de les inductàncies es basa en els resultats obtinguts amb FEM i és fa per separat pels eixos directe i en quadratura. El camp no ha d'estar excitat, això suposa que els imants permanents s'han de substituir per elements finits associats a la seva corresponen permeabilitat relativa ($\mu_r = 1.048$), però sense coercivitat magnètica ($H_c = 0$). Només els bobinats del estator han d'estar excitats d'una manera apropiada, com s'explica en els següents paràgrafs.

1) Eix d: Quan es calcula la inductància en l'eix directe L_d , els corrents estatòrics han d'estar distribuïts per tenir el seu màxim a l'eix en quadratura, produint el màxim de camp d'armadura a l'eix directe. La distribució del camp magnètic es presenta a la Fig. 5.

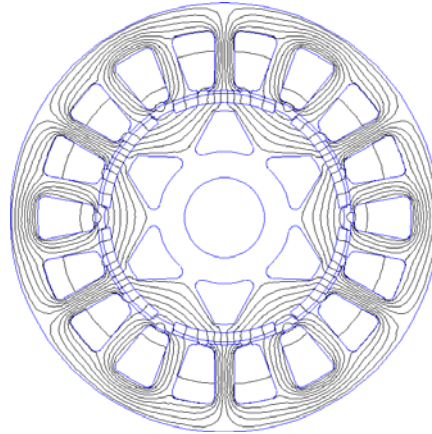


Fig. 5. Distribució del camp magnètic pel càlcul de L_d

2) Eix q: La inductància en l'eix en quadratura L_q , es calcula d'una manera similar a L_d . En aquest cas, el camp d'armadura es desplaça 90° elèctrics, produint el seu màxim a l'eix en quadratura. Això suposa que el màxim dels corrents estatòrics tenen el seu màxim a l'eix directe. La distribució del camp magnètic en aquest cas es presenta a la Fig. 6.

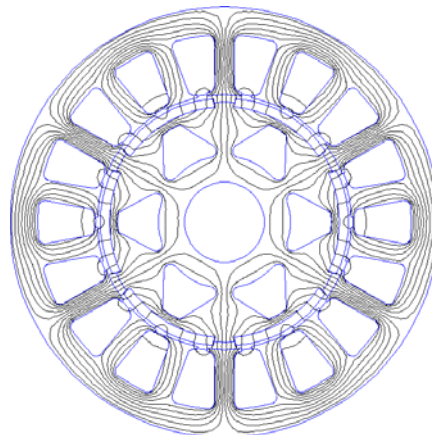


Fig. 6. Distribució del camp magnètic pel càlcul de L_q

Les inductàncies es calculen a partir de l'energia magnètica a l'entreferro i el corrent estatòric, mitjançant la següent formula:

$$L = \frac{W}{\frac{3}{2} \cdot I^2} \quad (1)$$

Com que s'assumeix que els bobinats ficticis dels eixos directe i en quadratura tenen el mateix número de voltes que el bobinat real per fase, per una màquina trifàsica d'alterna,

el corrent estatòric en els eixos directe i en quadratura ha de ser 3/2 vegades més gran que el corrent estatòric per fase, per produir la mateixa força electromotriu.

La corresponent energia magnètica W a l'entreferro, s'obté en cada cas a partir dels resultats de l'anàlisi d'elements finits del PMSM, d'acord amb la Fig. 5 i la Fig. 6. Els resultats finals són:

$$L_d = \frac{W}{\frac{3}{2} \cdot I^2} = \frac{0,377}{\frac{3}{2} \cdot 7,625^2} = 4,32 \text{ mH} \quad (2)$$

$$L_q = \frac{W}{\frac{3}{2} \cdot I^2} = \frac{0,449}{\frac{3}{2} \cdot 7,625^2} = 5,15 \text{ mH} \quad (3)$$

4. Determinació dels paràmetres del PMSM

El model en dos eixos de les màquines síncrones és l'aproximació més clàssica per analitzar i investigar el seu comportament. Molts investigadors utilitzen aquest mètode com a primera aproximació, per després realitzar un anàlisi més detallat i en profunditat de la màquina. La idea bàsica és desenvolupar i utilitzar una sèrie d'equacions que descriguin el comportament del motor als eixos d i q . L'únic requeriment és disposar dels seus paràmetres. La precisió de les característiques de funcionament del PMSM obtingudes utilitzant aquest mètode, depèn de manera directa de l'exactitud en el càlcul dels paràmetres del motor.

Alguns dels paràmetres del motor els dona el fabricant a la fulla de característiques, però molt sovint els seus valors són desconeguts. Per tant, normalment s'ha de buscar la millor opció per poder calcular-los mitjançant mètodes numèrics, analítics o experimentals.

En aquest treball les inductàncies principals del PMSM, s'han calculat aplicant procediments numèrics. A partir dels resultats obtinguts a les equacions (2) i (3), es poden calcular les reactàncies X_d i X_q del PMSM treballant a 50 Hz.

$$X_d = 2 \cdot \pi \cdot f \cdot L_d = 2 \cdot \pi \cdot 50 \cdot 4,32 \cdot 10^{-3} = 1,357 \Omega \quad (4)$$

$$X_q = 2 \cdot \pi \cdot f \cdot L_q = 2 \cdot \pi \cdot 50 \cdot 5,15 \cdot 10^{-3} = 1,618 \Omega \quad (5)$$

El fet de que en un motor síncron d'imants permanents superficials, no hi ha gaire diferència entre les reactàncies als eixos directe i en quadratura, es demostra en aquest cas.

Les reactàncies principals també s'han obtingut mitjançant assaig. Els resultats són els següents:

$$X_d = 2 \cdot \pi \cdot f \cdot L_d = 2 \cdot \pi \cdot 50 \cdot 4,35 \cdot 10^{-3} = 1,366 \Omega \quad (6)$$

$$X_q = 2 \cdot \pi \cdot f \cdot L_q = 2 \cdot \pi \cdot 50 \cdot 5,90 \cdot 10^{-3} = 1,853 \Omega \quad (7)$$

Comparant els resultats calculats (4) (5) i els experimentals (6) (7), podem observar que la discrepància és mínima.

5. Característiques del PMSM en regim permanent

En el sector de l'enginyeria de màquines elèctriques, l'objectiu d'investigadors i constructors, està sempre centrat en estimar, analitzar i avaluar el comportament de la màquina. Per tal propòsit, es necessita disposar d'unes característiques de funcionament, el més acurades possible.

En aquest apartat, el PMSM s'analitza per diferents condicions de funcionament i es presenten les característiques de parell electromagnètic i parell de "cogging".

A. Parell electromagnètic

El coneixement de la característica de parell estàtic és molt important per poder realitzar l'anàlisi i l'avaluació del comportament dels motor elèctrics. Per calcular-la es poden fer servir diferents aproximacions. En teoria, el parell es calcula a partir de la solució del camp magnètic de diferents formes. Tres aproximacions s'utilitzen habitualment: el mètode de flux-corrent, el mètode del tensor de Maxwell i el mètode de treball virtual.

En aquest treball, s'ha utilitzat el mètode del tensor de força per calcular el parell electromagnètic al voltant de l'entreferro, mitjançant el post-processor del FEMM. Per obtenir la característica de parell completa, s'ha anat desplaçant el fasor espacial de corrent estatòric de 0° a 180° elèctrics, en increments de 3° elèctrics, mantenint l'eix directe del rotor alineat amb l'eix de la fase A de l'estator. Aquest càlcul ha estat realitzat pel corrent nominal de la màquina i per tant la característica que es mostra a la Fig. 7, és la nominal.

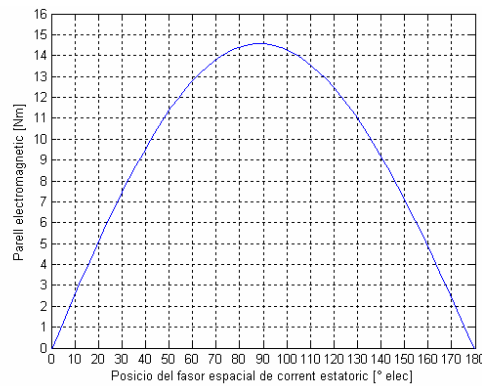


Fig. 7. Característica nominal de parell electromagnètic del PMSM

A partir de la gràfica de la Fig. 7 i sabent el parell nominal ($T_N = 12,2 \text{ N}\cdot\text{m}$), es pot obtenir l'angle de càrrega nominal ($\delta_N = 57^\circ \text{ elec}$) del motor.

B. Parell de “cogging”

Es pot obtenir el parell de “cogging” anul·lant el corrent d'armadura i fent girar el rotor, utilitzant el mateix mètode de càlcul de l'apartat anterior. En aquest cas, s'ha seleccionat l'eix de la fase *A* de l'estator com a eix de referència, la posició inicial és quan l'eix *A* de l'estator i l'eix *d* del rotor es troben en fase, i per tant el parell de “cogging” és zero.

Per obtenir una bona característica, s'ha anat girant el rotor en increments de $0,1^\circ$ mecànics, de 0° a 20° mecànics, és a dir, d'una ranura a una altra. El parell màxim de “cogging” obtingut és $2,3 \text{ N}\cdot\text{m}$ aproximadament i la seva forma és fonamentalment sinusoidal, com es pot observar a la Fig. 8.

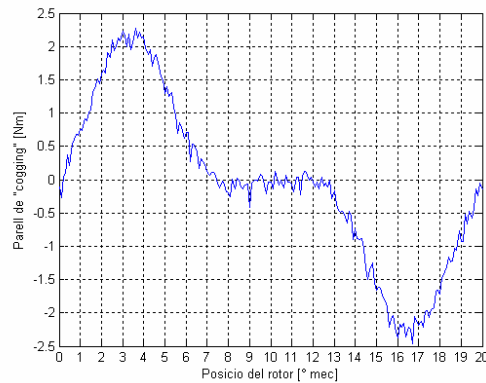


Fig. 8. Parell de “cogging” del PMSM

Conclusions

L'anàlisi d'elements finits és una de les millors solucions per avaluar el comportament de màquines elèctriques en general. L'aproximació presentada, aplicada a un motor síncron d'imants permanents superficials, demostra aquesta afirmació. En aquest cas, els elements constructius fora del nucli magnètic, no són de gran influència. Per tant, les característiques en regim permanent calculades a partir del mètode dels elements finits, en dos dimensions, tenen suficient precisió.

Els resultats calculats i experimentals són la millor manera de confirmar els paràmetres i les característiques obtingudes. La concordança entre ells, presentada en aquest treball, prova que la metodologia utilitzada és correcta i fiable.

Magnetic field reduction screening system for a magnetic field source used in industrial applications

H.Beltran, V.Fuster, M.García

Institut de Tecnologia Elèctrica.

Avda. Juan de la Cierva, 24 – Parc Tecnològic Paterna

46980 Paterna (Valencia). Spain

Phone: +34961366670 Fax: +34961366680 E-mail: Hector.Beltran@itenergia.com

Vicente.Fuster@itenergia.com, Marta.Garcia@itenergia.com

Abstract. This paper presents the description of the design and solution given as magnetic screen for a 50Hz industrial application, combining different materials to obtain the optimum reduction of the field. Important ideas are presented on the magnetic field behaviour, the response of the different materials subjected to magnetic fields, the effects and variations (in the shape and intensity of the field), introduced by the screen, and also, the differences in these influences produced by the screen as a function of their material properties, dimensions or positions. Keeping the magnetic field within a certain region of the space without disturbing the field in the other regions is not an easy task. That is why simulation and real measurements have to be combined. With the digital model, a large number of simulations are carried out modifying the screen step by step to obtain the optimal field reduction. The final measurements have validated the improvements performed by the screen.

Keywords

Magnetic shielding, low frequency electromagnetic fields, human exposure, screen parameters, industrial application.

1. Introduction

During the last years, electromagnetic fields have been a permanent point of conflict due to the growing awareness of the health risks by the general public. Although lots of biomedical studies have been carried out on this domain, none of them has been able to establish a clear relation confirming electromagnetic fields as a cause of any kind of illness. However, it is clear there has to be limits in order to control possible exposures. European authorities have regulated these aspects fixing limits for the radiated emissions produced by different kind of electromagnetic sources [1]. These limits vary as a function of the frequency and, for the case of the industrial applications (50Hz) they are:

- For occupational exposure: 500 μ T
- For general public exposure: 100 μ T

The application introduced in this paper deals with the magnetic screening performed in an industrial process trying to reduce the magnetic field emitted by one of the components below the established limits.

2. Problem description

Placed in an industrial environment, as a part of the productive process, an industrial coil is used to demagnetize the workpieces being fabricated which could keep a remanent magnetic fields on its inside as a result of the productive process manipulation and transformation. These fields existing in the workpieces are not useful at all, resulting even damaging for the correct functioning of the pieces once they are installed and have to start working. Therefore, they have to be eliminated.

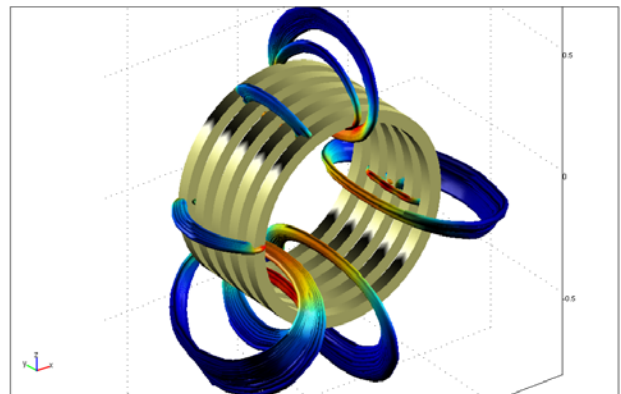


Figure 1 - Coil with workpiece and magnetic flux lines.

Demagnetization is the reduction of a magnetic field from its maximum magnetization intensity to almost zero, achieved by a repeated polarity reversal at a given frequency.

For demagnetization, the amplitude of an applied alternating field must be continuously reduced as shown in figure 2. The initial demagnetization field strength must be at least equal to the magnetization field strength existing in the sample. The reduction of field strength within the workpiece can be achieved electrically by reducing the magnetic field progressively while it circulates through the coil, or mechanically by slowly withdrawing the workpiece from the field of a constantly energized demagnetization coil. The figure below can give an idea of the procedure.

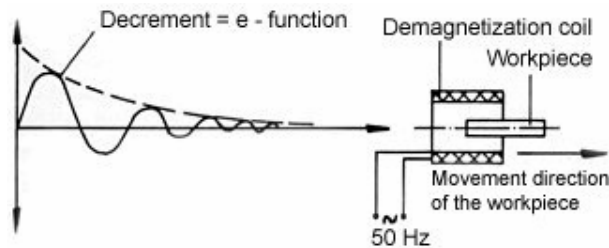


Figure 2 - Demagnetization process.

The dimensions of the coil which has been shielded are:

- Length = 300mm.
- Internal diameter = 450mm.
- External diameter = 500mm.

The coil is connected to the low voltage electric network with a 400V supply establishing a value for the field strength on its centre around 10kA/m. The elevated field strength implies the existence of high field levels not only in the centre of the coil but in all the surroundings. These levels are to be checked and reduced in those zones considered necessary. This will be done through the installation of a magnetic screen which has as main requirement, apart from shielding the magnetic flux in the outside, not to alter the field strength in the centre of the coil since it could damage the functioning of the coil, therefore preventing the goal it has in the industrial process, which is, the removal of remanent magnetic field inside the workpieces.

3. Procedure

A. Initial measurements.

These measurements allow determining the initial situation under normal conditions, in situ. For the registration of the magnetic field values a total number of 13 points were controlled. The representation of the magnetic field in these points could give an idea of the shape and aspect of the field. The scheme of measurements is displayed in figure 3. All the measurements were submitted at the coil's axle height, since they were included like that in the same plane, and the one where the values of magnetic field are maximum referred to the centre of the coil.

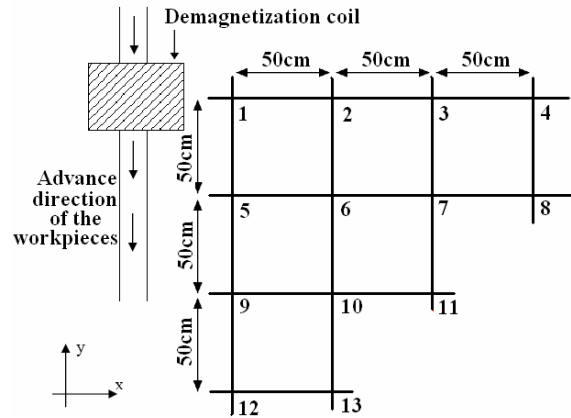


Figure 3 - Map of measurements around the coil.

The values registered are (values of magnetic field density in μT and position in meters being the (0,0) reference point the centre of the coil):

Point	1	2	3	4	5	6
Position X	0.5	1	1.5	2	0.5	1
Position Y	0	0	0	0	-0.5	-0.5
Field (B)	763	85	30	13	456	92

Point	7	8	9	10	11	12	13
Position X	1.5	2	0.5	1	1.5	0.5	1
Position Y	-0.5	-0.5	-1	-1	-1	-1.5	-1.5
Field (B)	26	11	127	46	18	38	24

Table 1 - Values of magnetic field density without screen.

These initial measurements made it possible to characterize the field created by the coil. Once this field was known, a digital model was established. The magnetic field created by this model has the aspect depicted in figure 4 and was developed to correspond exactly with that created by the real coil. This was obtained by the comparison of magnetic field values in the 13 points controlled in situ and the field simulated by the model in those 13 points.

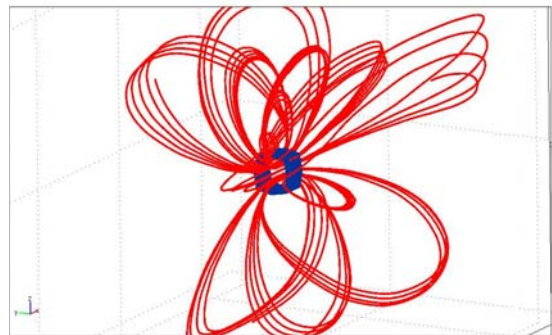


Figure 4 - 3D view of the digital model with the magnetic field flux lines generated by the coil.

The values of magnetic field are useful not only to develop the model but also to have an idea of the initial situation. With this knowledge it is easier to project the type of screen which is going to be necessary in order to fix the magnetic field in the surroundings under the limits.

B. Design of the screen.

In view of the magnetic behaviour of the different materials ([3]-[4]) iron and aluminium were selected as the optimal materials to employ in the construction of the screen. Another important decision to take was the thickness of the plates to install [5], from ([2],[6]), 2mm were selected for both aluminium and iron, trying with this size to optimize the field reduction and the structure weight. Apart from that, the shape for the screen as well as the position had to be chosen, other studies ([2],[7]) helped to decide it should be placed as close to the coil as possible, trying to enclose it inside the screen. There were space limitations due to the industrial environment where the demagnetizing coil was place, though the width of the screen could not be large.

The first option was to introduce 2 iron plates, one on each side of the coil, to analyze the absorption level of magnetic field they were able to perform. The election of iron located on the sides of the coil where the field is parallel to the surface of the plate is because of its good behaviour in that position [2]. The aspect of the field with this first screen was:

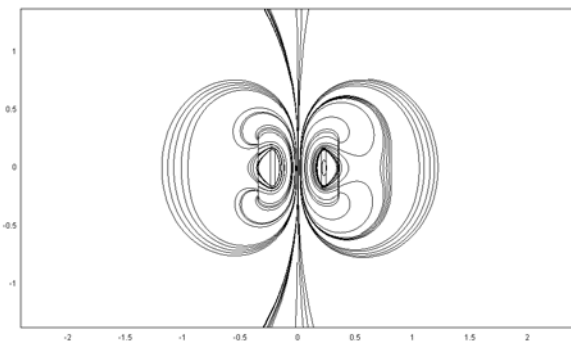


Figure 5 – Flux lines distributions with the first screen.

Results from this redistribution of the magnetic field were not successful, even increasing the width of the iron from the initial 0.5m to nearly 2m the reduction was not enough.

The second option was then the introduction of a second iron plate on each lateral. Different simulations were performed, varying the width of the plates as well as the distance between them. The optimal distance was concluded to be 5cm. With this new disposition, a great reduction was obtained on the x direction but it was still poor in the y direction. The aspect of the field distribution can be observed in figure 6.

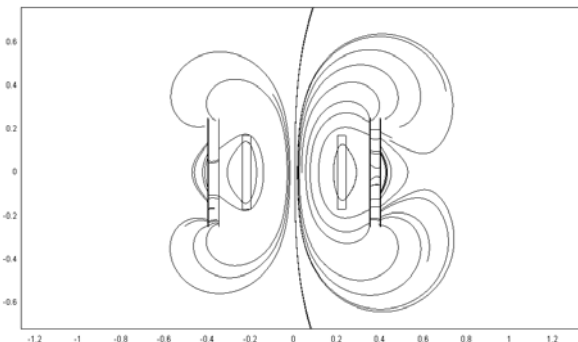


Figure 6 - Flux lines distributions with a second screen.

It was decided, instead of incrementing the lateral volume of the screen, and due to problems of space, to install other parts of the screen in the y direction. So, aluminium was used to close the screen around the coil placing 2 wings of this material, with an angle of 60°, on each of the exterior iron plates. The resulting structure was as follows:

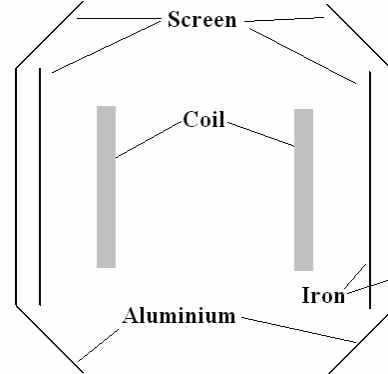


Figure 7 - Section of the final design of the screen surrounding the coil.

Various angles for the wings were simulated. Equally, fixing them to the interior iron plate was tried too. Form all the possibilities, the previous distribution was found to be the best. This solution adopted as definitive creates a distortion of the magnetic field as is visualized below.

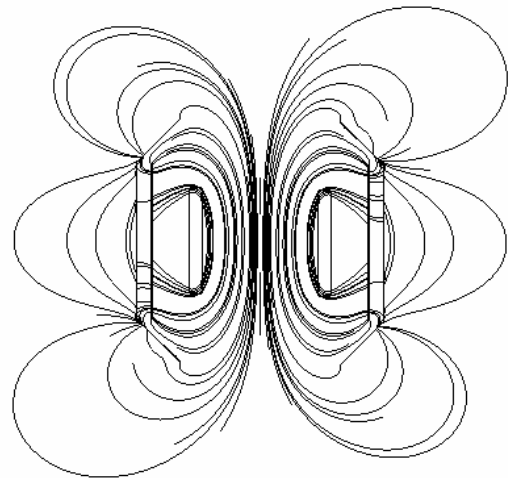


Figure 8 - Magnetic flux lines simulated with the coil shielded.

Once simulated and the designed values obtained under the limits and with a certain security margin, the screen was constructed and installed.

C. Final measurements.

After the design, construction and installation of the screen, new measurements were performed in order to check the efficiency of the shielding and verify the calculations and simulations carried out during the design. The results are summarized in table 2. Once again the magnetic field density is expressed in μT and the position in meters having as the (0,0) reference the centre of the coil.

Point	1	2	3	4	5	6
Position X	0.5	1	1.5	2	0.5	1
Position Y	0	0	0	0	-0.5	-0.5
Field (B)	91	36	14	6	88	34

Point	7	8	9	10	11	12	13
Position X	1.5	2	0.5	1	1.5	0.5	1
Position Y	-0.5	-0.5	-1	-1	-1	-1.5	-1.5
Field (B)	12	4	45	21	14	20	11

Table 2 - Values of magnetic field density with screen.

By comparing tables 1 and 2, it is clearly observed that the values of magnetic field have registered a big reduction in all the point, except point number 9. This is due to the fact that the screen reduces the field absorbing magnetic flux lines and confining this energy into the material, but also deflects the unabsorbed flux lines. This phenomenon makes it possible to increase the magnetic field in some regions of the space due to the concentration of magnetic lines of higher field intensity. This is the case of point 9 as has been seen during the design. It is located close of the axe of the coil were magnetic field lines are concentred.

Apart from that, the goal of the reduction of magnetic flux density under the limits has been accomplished for all the points. None of them rests above $100\mu\text{T}$ which was the requirement. The percentage of reduction varies from the 88% obtained in point 1 to the 20% of point 11. The smaller the field was at the beginning, the smaller the reduction obtained. Anyway, for the rest of the points the reductions are all important but different, due to the deformation registered by the screen.

4. Conclusions

The whole design of a magnetic screen has been performed throughout measurements and simulations.

The magnetic field reduction achieved by means of the installation of the screen goes beyond the 88% in the most critical points referred to the initial situation. The combination of two kinds of materials as well as the good selection of the relative position has been fundamental in order to obtain such a large reduction.

References

- [1] Directiva 2004/40/CE del parlamento europeo y del consejo de 29 de abril de 2004 sobre las disposiciones mínimas de seguridad y de salud relativas a la exposición de los trabajadores a los riesgos derivados de los agentes físicos (campos electromagnéticos)
- [2] "Estudio y diseño de sistemas de apantallamiento para centros de transformación frente a los campos electromagnéticos". Internal document published by UNION FENOSA in collaboration with the Instituto de Tecnología Eléctrica. January 2005.
- [3] L.Hasselgren, J.Luomi, "Geometrical Aspects of Magnetic Shielding at Extremely Low Frequencies", IEEE transaction on electromagnetic compatibility, Vol.37, N.3, August 1995.
- [4] O.Bottauscio, M.Chiampi, D. Chiarabaglio, F. Fiorillo, L. Rocchino, and M. Zucca, "Role of magnetic materials in power frequency shielding: numerical analysis and experiments,". Proc.Inst.Elect.Eng., vol.148,pp. 104-110, Mar.2001.
- [5] U.Adriano, O.Bottauscio, M.Zucca, "Material Efficiency in Magnetic Shielding at low and intermediate frequency", IEEE transaction on magnetics. Vol.39. N.5, September 2003.
- [6] H.Beltran, V.Fuster, A.Quijano, "Optimal Shielding Thickness of Low Frequency Magnetic Fields" XII International Symposium on Electromagnetic Fields, in mechatronics, electric and electronic engineering. Baiona (Spain) 2005.
- [7] E.Salinas, "Conductive and ferromagnetic screening of 50Hz magnetic fields from a three phase system busbars" Journal of Magnetism and Magnetic Materials. 226-230 (2001) 1239-1241.

Análisis del campo magnético en una línea eléctrica de AT

R. Moreno, J.A. Güemes y I. Pico

Departamento de Ingeniería Eléctrica
E.U.I.T.I., Universidad del País Vasco
Plaza de la Casilla, 3, 48012 Bilbao (España)
Telef.: +34 946014363, fax: +34 946014300
e-mail: iepgualj@lg.ehu.es

Resumen. El incremento en los últimos años de la preocupación por los posibles efectos que pudieran tener los campos magnéticos, producidos por las líneas eléctricas de alta tensión en los seres vivos, ha originado multitud de estudios e informes para esclarecer esta posible fuente “productora” de enfermedades. Creemos que puede resultar de utilidad, para futuros diseños de líneas de transporte de energía eléctrica, emplear una herramienta de cálculo como es el método de elementos finitos, para el cálculo de la distribución y magnitud del campo magnético generado por las líneas eléctricas. De esta forma, se puede conocer con antelación si la línea produce un campo magnético superior al estimado por la Recomendación del Consejo Europeo 1999/519/CE, que establece el límite de tolerabilidad para el campo magnético en $100 \mu\text{T}$ y, en caso necesario tomar las medidas correctoras oportunas. En este trabajo utilizando el método de elementos finitos, se calcula la densidad de flujo magnético generado por una línea de 30 kV de doble circuito y se comparan los resultados con los medidos experimentalmente (en la línea). Igualmente se simula el comportamiento de diferentes configuraciones geométricas de líneas eléctricas con el fin de determinar cuales producen una menor “contaminación magnética”.

Palabras llave. Campo magnético, contaminación magnética, método de elementos finitos, líneas eléctricas,

1. Introducción

Algunos experimentos de laboratorio han detectado que, bajo determinadas condiciones, y en algunos modelos en animales, los campos magnéticos pueden tener efectos biológicos. Sin embargo, ni las investigaciones “in vitro”, ni las realizadas a animales y personas han demostrado que dichos campos sean nocivos para la salud. Tampoco han permitido establecer el mecanismo mediante el cual, los campos magnéticos podría actuar sobre los seres vivos ni, lo que es más importante, a partir de qué dosis podría hablarse de riesgo para las personas.

El Ministerio de Sanidad y Consumo de España en Julio de 2001 establece: “No puede afirmarse que la exposición a campos electromagnéticos dentro de los límites establecidos en la Recomendación del Consejo Europeo (1999/519/CE) produzca efectos adversos para

la salud humana. Por tanto, el comité concluye que el cumplimiento de la citada recomendación es suficiente para garantizar la protección de la población”

La recomendación de la Unión Europea, de 12 de Julio de 1999, fija el límite de tolerabilidad en $100 \mu\text{T}$, la cual ha tenido en cuenta el principio de precaución. Esta recomendación es ratificada por multitud de organismos, instituciones, informes científicos, médicos, etc. Entre ellos destacamos:

- La Asociación Internacional para la Protección radiológica (IRPA).
- El Instituto Nacional de Normativa de Estados Unidos (ANSI).
- La Comisión Internacional para la Protección contra la Radiación no Ionizante (ICNIRP).
- El Consejo Nacional de Protección Radiológica del Reino Unido (NRPB).
- El Consejo Nacional de Protección Radiológica y Medidas de Estados Unidos (NCRP).
- El Comité Europeo de Normalización Electrotécnica (CENELEC).

En los últimos años, se han publicado distintos trabajos en los que se estudia el campo magnético producido por líneas de transporte de energía eléctrica [1] – [5] y la forma de reducirlo [6] – [7].

El primer y principal objetivo del trabajo, es simular el comportamiento magnético de una línea de alta tensión, utilizando el método de elementos finitos mediante modelos en dos dimensiones, y comparar los resultados obtenidos con las medidas experimentales realizadas en la línea.

El segundo objetivo es simular y analizar la distribución de la densidad de flujo magnético en función de la configuración geométrica de los conductores de la línea, la secuencia de fase y el desfase de corrientes entre circuitos, con el fin de determinar que configuraciones producen una menor “contaminación magnética”.

2. Línea de alta tensión

El método presentado en este trabajo, se ha aplicado a la determinación y medida de la distribución de la densidad de flujo magnético de una línea eléctrica de alta tensión de 2ª categoría, de 30 kV y doble circuito con un conductor por fase de aluminio acero LA-180. La configuración de la línea es tipo barril, siendo la altura del conductor más bajo en el centro del vano de 12 m.

En la figura 1, puede verse la configuración de la línea.



Fig. 1. Línea eléctrica de alta tensión.

3. Metodología

Los pasos seguidos en la comunicación para validar el método propuesto son los siguientes:

- 1) Medir la densidad del flujo magnético en una recta situada perpendicular a la línea de alta tensión, en el centro del vano y a un metro del plano del terreno. Las medidas se realizan a ambos lados del centro de la línea con un mínimo de 10 puntos de medida y hasta una distancia de 25 m del eje de la línea.
- 2) Conocer el histórico de corrientes y potencias en el tiempo de las medidas.
- 3) Utilizando el método de elementos finitos, simular el comportamiento de la línea para la corriente, en el momento de realizar las medidas, facilitada por la compañía suministradora en el histórico de potencias.
- 4) Medir el valor de la densidad de flujo magnético en el modelo de elementos finitos en los mismos puntos indicados en el punto 1.
- 5) Verificar que la magnitud y distribución del campo magnético obtenido de la simulación están acordes con las leyes físicas fundamentales para el cálculo del campo magnético.

- 6) Comparar los valores obtenidos en las mediciones de campo con los medidos en la simulación del comportamiento de la línea utilizando el método de elementos finitos.
- 7) Simular el comportamiento de distintas configuraciones de líneas con el fin de determinar que configuraciones producen una menor “contaminación magnética”.

4. Modelo

El modelo de elementos finitos utilizado es plano 2D y esta constituido por una sección recta de los 6 conductores y el espacio de aire que los rodea. El espacio de aire tomado a la izquierda, arriba y derecha de los conductores es de 25 m (debe ser suficientemente amplio para admitir que en el contorno del modelo, la densidad de flujo magnético sea despreciable).

En la figura 2, se muestra el modelo utilizado.

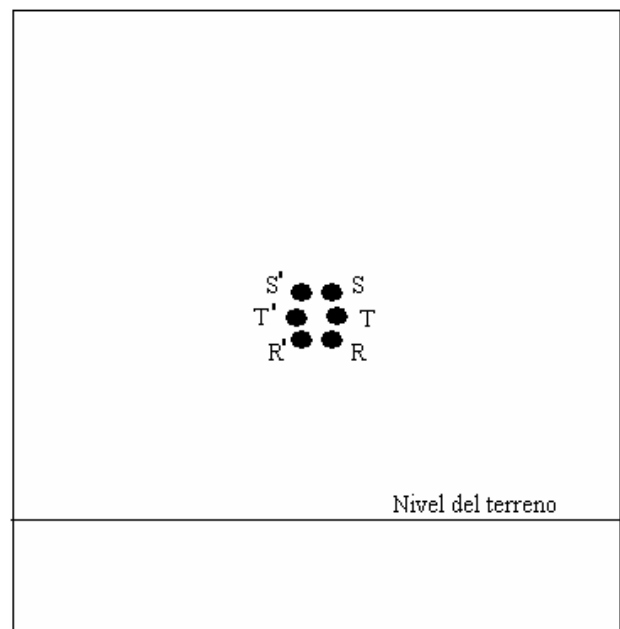


Fig. 2. “Modelo”

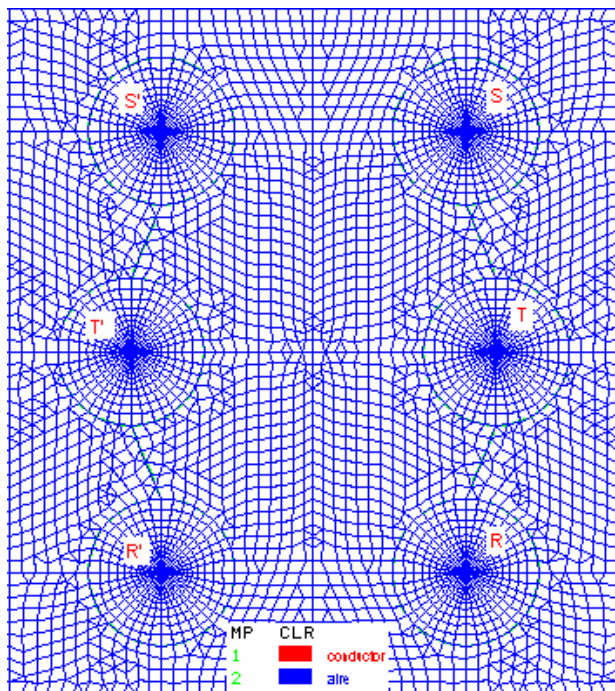
Los elementos utilizados son planos de 4 nodos. En la figura 3, se muestra el mallado utilizado en la zona de los conductores.

Las excitaciones se definen por medio de la densidad de corriente en cada uno de los conductores. La densidad de corriente se calcula a partir del histórico de potencias, en el periodo en el que se realizaron las medidas de campo.

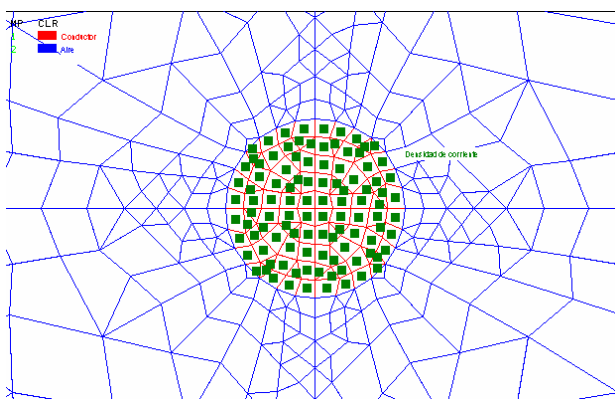
Las propiedades se definen por medio de la permeabilidad magnética del aire, conductores eléctricos y la tierra.

La condición de contorno es vector potencial magnético nulo en la periferia del modelo.

El tipo de análisis realizado es magnetostático.



a) zona próxima a los conductores



b) zoom de un conductor

Fig. 3. Mallado

La simulación del comportamiento de la línea, se ha realizado para instantes de tiempo de 0; 2,5; 5; 7,5; 10; 12,5; 15; 17,5 y 20 ms (cada 45° durante un periodo) de la forma de onda correspondiente a la corriente por la fase R.

En la figura 4, se muestra la forma de onda de la densidad de flujo magnético en el centro de la línea y centro del vano, a un metro de altura de la superficie del terreno, obtenida de la simulación del comportamiento de la línea utilizando el método de elementos finitos (50 A por circuito).

Podemos observar que, para la corriente de ensayo, la forma de onda de la densidad de flujo magnético está desfasada 24,5° respecto de la forma de onda de la corriente por la fase R.

En las figuras 5 y 6 se muestra respectivamente, la distribución del vector potencial magnético y densidad de flujo magnético, en la zona de los conductores, para el instante en el que la corriente es máxima en la fase R.

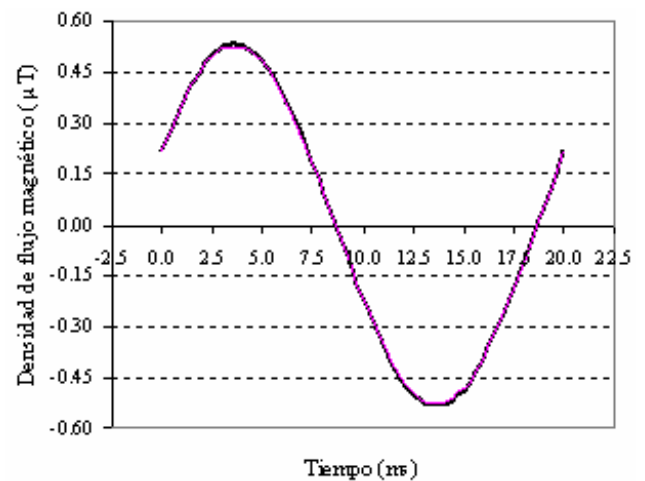


Fig. 4. Densidad de flujo magnético

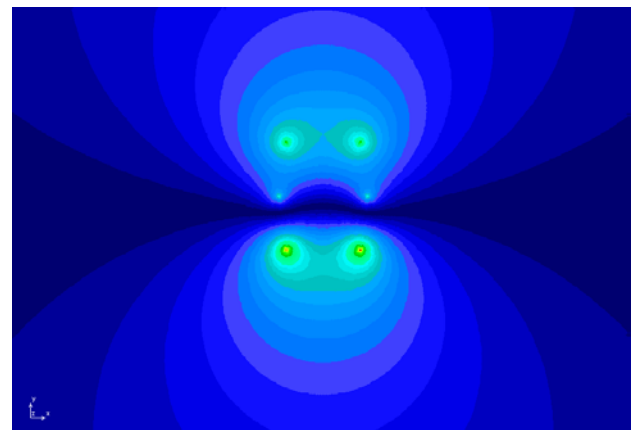


Figura 5. Vector potencial magnético

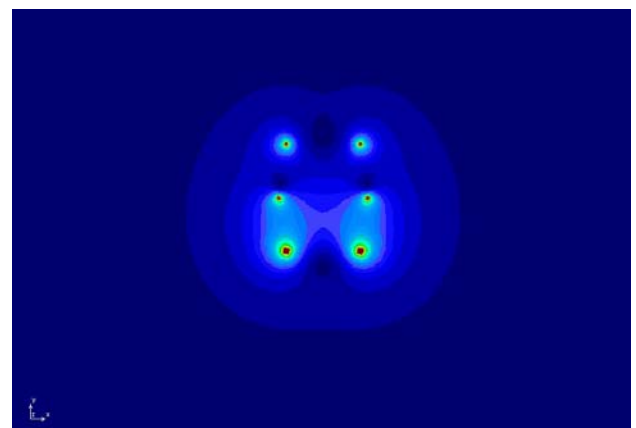


Fig. 6. Densidad de flujo magnético

5. Comparación de resultados

Una vez realizada la medida de campo y la simulación del comportamiento de la línea para las corrientes calculadas (50 A por circuito), se tienen los valores de densidad de flujo magnético mostrados en la figura 7.

Podemos observar como los resultados obtenidos por simulación se asemejan a los medidos experimentalmente. Únicamente en los puntos situados bajo la eléctrica línea, se obtiene por medición un valor

de la densidad de flujo magnético ligeramente superior al obtenido por simulación.

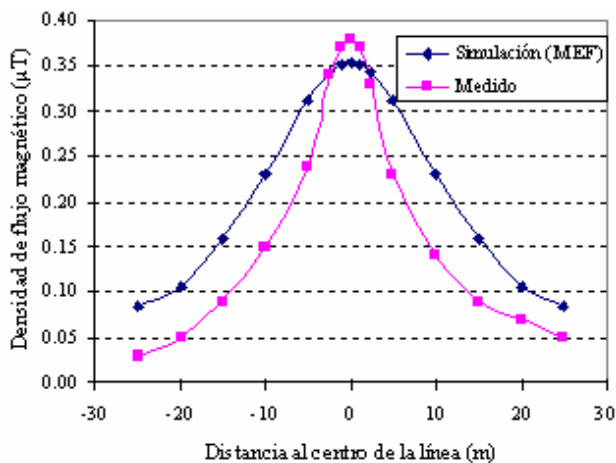


Fig. 7. Densidad de flujo magnético

La diferencia existente entre los valores medidos en las prácticas de campo con los obtenidos por simulación, pueden ser debido principalmente a que la corriente real, en el periodo de medición, fuera ligeramente inferior a la calculada por el histograma de potencias facilitado por la compañía suministradora y también a la precisión del instrumento de medida.

En la curva de medidas de las prácticas de campo (Fig 7), se observa que los valores de densidad de flujo magnético en el lado derecho son algo superiores a la misma distancia en el lado izquierdo, lo que demuestra que la corriente real por el circuito 1, en el momento de realizar las medidas, era superior a la corriente por el circuito 2.

El campo magnético en cada uno de los ejes se ha medido con un gaussímetro con un rango de medida de 0,01 μT a 2000 μT (2 mT), con una precisión de ±10 % y un ancho de banda de 30 a 300 Hz.

Las medidas de densidad de flujo magnético, se realizaron en puntos separados dos metros entre sí y situados en una recta localizada perpendicular a la línea de alta tensión, en el centro del vano y a un metro del plano del terreno. En cada uno de los puntos se realizan tres medidas (B_x , B_y , B_z), calculando el valor resultante de la densidad de flujo magnético en ese punto, por medio de la ecuación:

$$B = \sqrt{B_x^2 + B_y^2 + B_z^2} \quad (1)$$

Realizado nuevamente la simulación del comportamiento magnético de la línea, para el valor máximo de corriente, (400 A por circuito), se tiene un valor máximo de la densidad de flujo magnético de 3 μT (medio en el centro del vano y a un metro de altura sobre el plano del terreno). El valor obtenido es muy inferior a los 100 μT establecidos por la recomendación de la Unión Europea 1999/519/CE.

6. Simulación del campo magnético con distintas configuraciones y/o secuencias de fase.

En vista de los resultados obtenidos anteriormente, en este apartado simulamos el comportamiento magnético de: a) distintas configuraciones de líneas y, b) distintas secuencia o desfases de las corrientes entre circuitos. En ambos casos el estudio se realiza para el valor máximo de la corriente por la línea (400 A por circuito).

A. Distintas configuraciones

En la figura 8, se muestran las distintas configuraciones de líneas estudiadas.

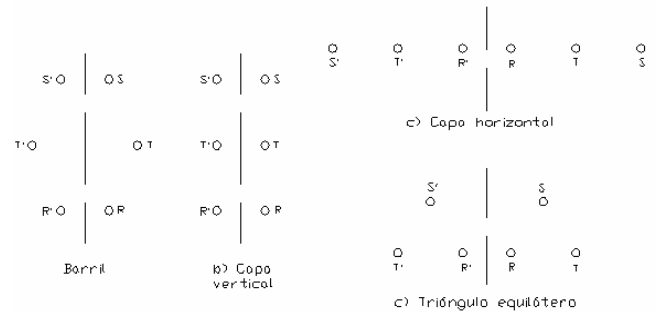


Fig. 8. Distintas configuraciones

Una vez realizada la simulación del comportamiento de las distintas configuraciones, se tiene el resultado mostrado en la figura 9.

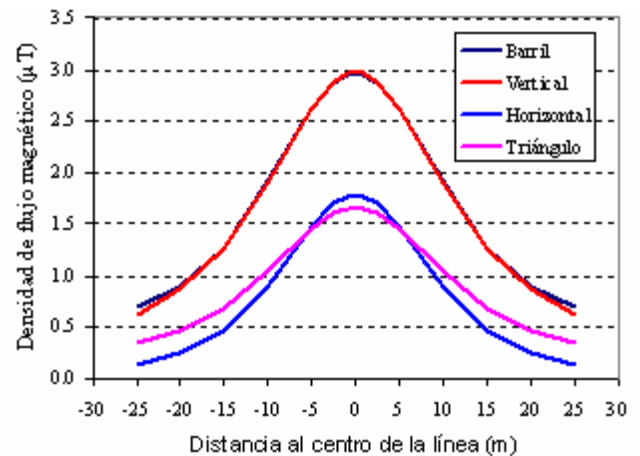


Fig. 9 Densidad de flujo magnético en distintas configuraciones de los conductores de la línea

Se puede observar que el valor de la densidad de flujo magnético disminuye aproximadamente a la mitad, utilizando las configuraciones en triángulo y horizontal, mientras que, como era esperado, la configuración en doble capa vertical da resultados muy similares a la configuración barril.

En la figura 10, se muestra como varía la distribución de la densidad de flujo magnético en función de la configuración geométrica de los conductores de la línea, para el instante en el que la corriente es máxima en la fase R.

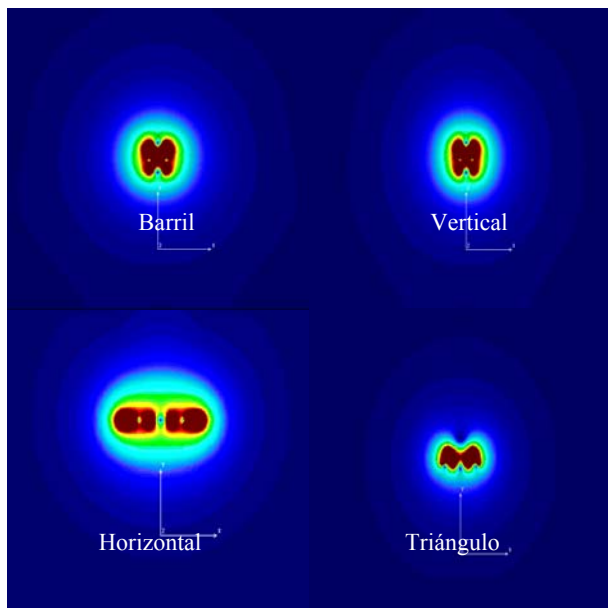


Fig. 10. Distribución de la densidad de flujo magnético

B. Modificación de la secuencia de fases o desfase de corrientes entre circuitos.

Finalmente se han estudiado como afecta en la distribución de la densidad de flujo magnético, los siguientes factores:

- Cambio del orden de secuencia de fases del circuito 2 (configuración 1 – véase figura 11a).
- Cambio del orden de secuencia de fases y adelanto de 30° de las corrientes del circuito 2 con respecto a las corrientes del circuito 1 (configuración 2 - véase figura 11b)
- Adelanto de 30° de las corrientes del circuito 2 respecto del circuito 1 (configuración 3 - véase figura 11c).

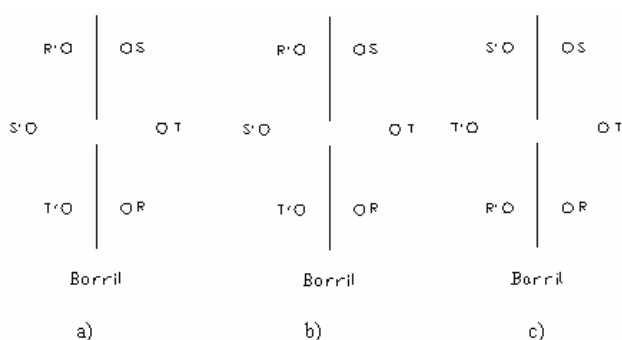


Fig. 11. Distintas secuencias y/o desfases de corrientes entre circuitos

Una vez realizado el análisis se tienen los resultados mostrados en la figura 11.

Se puede apreciar como al cambiar el orden de secuencia de fases en uno de los circuitos (configuración 1), se reduce el campo magnético de una forma importante (66 %). Si además de esto, las corrientes entre a ambos circuitos están desfasadas (configuración 2), la reducción

del campo es más acusada (74 %). En cambio si únicamente las corrientes de un circuito van desfasadas 30° respecto de las del otro (configuración 3), no se obtiene una reducción del campo magnético apreciable.

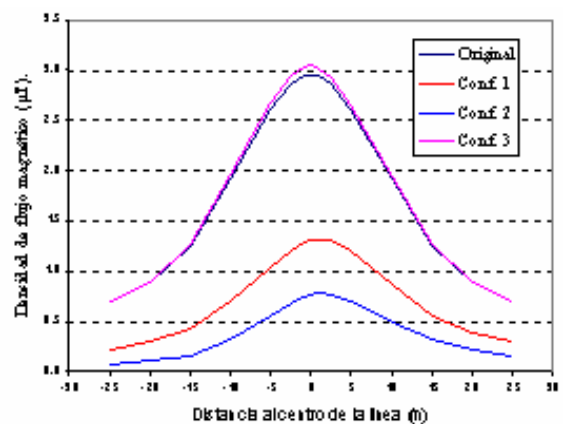


Fig. 12. Densidad de flujo magnético para distintas secuencias del orden de sucesión de fases y/o desfases de corrientes

La figura 13, muestra la distribución de la densidad de flujo magnético para cada una de las configuraciones anteriormente indicadas para el instante en que la corriente es máxima en la fase R.

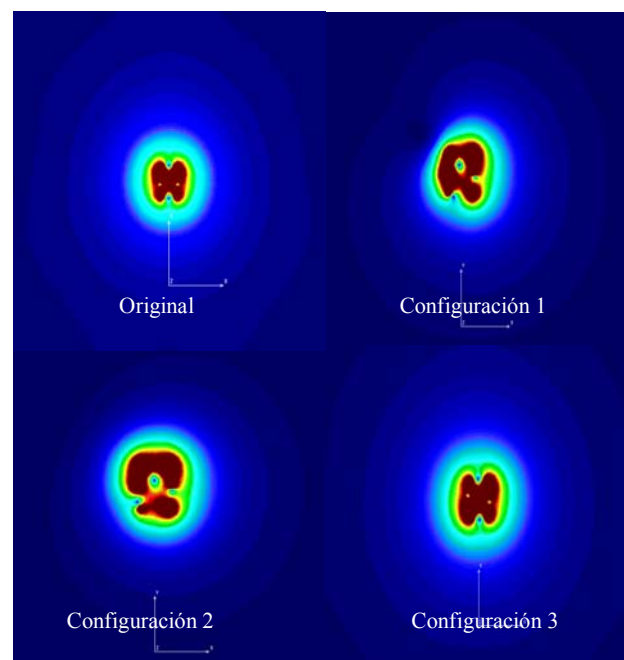


Fig. 13. Distribución de la densidad de flujo magnético

De los resultados anteriores, podemos indicar que con un adecuado replanteo del orden de secuencia de fases y del “desfase de corrientes entre los dos circuitos” se puede reducir los niveles de densidad de flujo magnético de forma importante.

En este trabajo se han estudiado distintas configuraciones de líneas y se ha indicado cual es la más aconsejable respecto de la mínima “contaminación magnética”. No obstante en el diseño de una línea, influyen otros factores como la capacidad entre conductores o entre estos y tierra, el tamaño de las torres, etc.

El método presentado en este trabajo es de gran ayuda para los ingenieros eléctricos que se dedican al cálculo de líneas eléctricas, pues permite incluir en sus proyectos además de los datos habituales, la curva de densidad de flujo magnético esperada.

Otra aplicación importante que puede tener el método es el cálculo de la capacidad entre conductores y a tierra de la línea propuesta.

7. Conclusiones

Según los resultados de las medidas realizadas “in situ”, se constata que el campo magnético producido por esta línea de 30 kV de doble circuito, está por debajo del límite de tolerabilidad establecido por la recomendación de la Unión Europea, 1999/519/CE.

La simulación a través de método de elementos finitos, da resultados aceptables y resulta una herramienta muy útil para la realización de estudios de campo magnético.

El método presentado en este trabajo permite realizar comparaciones entre los “mapas” de densidad de flujo magnético, generados por distintos tipos de configuraciones geométricas de los conductores de la línea, con o sin cambio de la secuencias de fase y/o desfase de las corrientes entre circuitos.

Se ha constatado que la configuración triángulo y horizontal ofrecen un mejor resultado que la configuración barril y vertical.

Con una correcta redistribución de las fases se consigue reducir de una forma importante el valor del campo. No obstante en el diseño de una línea han de considerarse otros factores tales como las capacidades entre conductores, las pérdidas por efecto corona, el costo de la línea, etc.

El método expuesto pueda utilizarse para determinar formulas de aplicación industrial, para calcular el valor del campo magnético “producido” para distintas configuraciones de líneas en función de la corriente y la secuencia de fases.

Referencias

- [1] W.T. Kaune and L.E. Zaffanella, “Analysis of magnetic fields produced far from electric power lines”, IEEE Trans. Power Delivery, vol. 7, no. 4, pp. 2082-2091, 1992.
- [2] R.G. Olsen, “Electromagnetic fields from power lines”, IEEE International Symposium on Electromagnetic Compatibility, pp. 138-143, 1993.
- [3] A.V. Manishev and B.D. Russell, “Measurement of Magnetic fields in the direct proximity of power line conductors”, IEEE Trans. Power Delivery, vol. 10, no. 3, pp. 1211-1216, 1995.
- [4] C. Garrido, A.F. Otero and J. Cidrás, “Low-frequency magnetic fields from electrical appliances and power lines”, IEEE Trans. Power Delivery, vol. 18, no. 4, pp. 1310-1319, 2003.
- [5] P. Sarma Maruvada, A. Turgeon, D.L. Goulet and C. Cardinal, “An experimental of residential magnetic fields in the vicinity of transmission lines”, vol. 13, no. 4, pp. 1328-1334, 1998.
- [6] A.R. Memari and W. Janischewskyj, “Mitigation of magnetic field near power lines”, IEEE Trans. Power Delivery, vol. 11, no. 3, pp. 1577-1586, 1996.
- [7] V.S. Rashkes and R. Jordan, “Magnetic field reduction methods: efficiency and cost”, vol. 13, no. 2, pp. 552-559, 1998.
- [8] “IEEE Standard procedures for measurement of power frequency electric and magnetic fields from AC Power line”, IEEE Std 644-1994.
- [9] Varios, “Magnetic fields from electric power lines theory and comparison to measurements”, IEEE Trans. Power Delivery, vol. 3, no. 4, pp. 2127-2136, 1988.
- [10] P.P. Silvestre, R.L. Ferrari, “Elementos Finitos para Ingeniería Eléctrica”.
- [11] Recomendación del consejo Europeo sobre los límites de exposición del público a campos electromagnéticos (0 Hz a 300 GHz). 1999/519/CE.
- [12] Campos eléctricos y magnéticos de 50hz. Análisis del estado actual de conocimientos” REE y UNESA, 2001.